論文 / 著書情報
Article / Book Information

題目(和文)	ホットワイヤーセル法による微結晶Si薄膜太陽電池の高効率化に関する研究
Title(English)	Study of high efficiency microcrystalline silicon thin film solar cells prepared by hot wire cell method
著者(和文)	井出吉紀
Author(English)	
出典(和文)	学位:博士(工学), 学位授与機関:東京工業大学, 報告番号:甲第5725号, 授与年月日:2004年3月26日, 学位の種別:課程博士, 審査員:
Citation(English)	Degree:Doctor (Engineering), Conferring organization: Tokyo Institute of Technology, Report number:甲第5725号, Conferred date:2004/3/26, Degree Type:Course doctor, Examiner:
学位種別(和文)	博士論文
Type(English)	Doctoral Thesis

DOCTORAL THESIS

Study of High Efficiency Microcrystalline Silicon Thin Film Solar Cells Prepared by Hot Wire Cell Method

A THESIS SUBMITTED IN PARTIAL FULFILLMENT OF
THE REQUIREMENTS FOR THE DEGREE OF
DOCTOR OF ENGINEERING

December, 2003

Directed by **Professor Makoto Konagai**

Presented by **Yoshinori Ide**

Department of Physical Electronics
Graduate School of Science and Engineering
Tokyo Institute of Technology

Preface

The demand for new energy resources is steadily increasing with growth of worldwide economy. Unexpected environmental destruction such as greenhouse effects, air pollution and acid rain has become a serious problem all over the world. The destruction has resulted from the today's energy consumption system based on an outrageous consumption of fossil fuels such as petroleum, coal and natural gas. In order to solve these problems, we should concentrate on new energy resources in parallel with development of the energy-saving technology.

Compared to other wide variety of renewable energy projects such as hydropower and wind power, photovoltaic technology has recently attracted a great deal of attention as the most advanced of the alternative energy resources, because it is free and inexhaustible and brings no by-products to harm the environment. Solar energy radiated on the earth for a year is more than 10,000 times of the total energy consumption in the world. Therefore, supply of sufficient energy for the world can be guaranteed even by a portion of this energy, if it is utilized directly and effectively. The use of this technology to generate electric power is now almost exclusively based on single crystalline silicon solar cells. Although solar cells have already been used as an energy source for household use, they have not been widely spread and used yet. This is simply because it is expensive. To become economically competitive with the conventional fossil fuels and nuclear energy, it is necessary to develop highly efficient solar cells that guarantee long-term stability and are cheap to manufacture. To achieve

these goals, major research efforts have recently shifted from bulk to thin film grown on cheap glass substrates.

Silicon thin film solar cells are classified structurally into amorphous silicon (a-Si:H) solar cells and microcrystalline silicon (μc-Si:H) solar cells. Thin film solar cells based on μc-Si:H solar cells have been becoming very important due to their stability and potentially high conversion efficiency. Recently, tandem (hybrid) solar cells which have a-Si:H solar cell for the top cell and μc-Si:H solar cell for the bottom cell have been intensively investigated due to their high cost performance. Until now, the growth of the μc-Si:H films at low substrate temperature has been realized by photochemical vapor deposition (photo-CVD) and plasma enhanced CVD (PECVD). However, the growth rate of these processes is still low. For further cost-down, new process which can deposit μc-Si:H films at high deposition rate of over 2 nm/s is highly required.

In this thesis, new process "Hot Wire Cell method" to prepare high efficiency μc-Si:H thin film solar cells have been intensively investigated. In this method, high deposition rate can be achieved due to the high dissociation efficiency of the reactant gases. High efficiency a-Si:H thin film solar cells have also been investigated for fabrication of a-Si:H/μc-Si:H tandem cells. In order to obtain high efficiency μc-Si:H thin film solar cells, first, many efforts have been made for improvement of intrinsic μc-Si:H film quality. Second, for improvement of p/i interface of the solar cell, 2-step growth method was proposed and carried out. Furthermore, high rate depositions were also investigated. Finally, a-Si:H/μc-Si:H tandem cells were fabricated.

Contents

Chapter 1. Overview and Objectives of This Research 1

Chapter 2. Characteristics and Principles of Hot Wire Cell Method 16

2-1 Introduction 16

2-2 Fabrication of Hot Wire Cell System 17

2-3 Principles of Hot Wire Cell Method 21

2-4 Advantages of Hot Wire Cell Method 23

References 25

Chapter 3. Fabrication and Characterization of Amorphous Silicon Thin Films and Solar Cells 27

3-1 Introduction 27

3-2 Experimental Details 28

3-3 Results and Discussion 30

3-3-1 Characterization of Amorphous Silicon Thin Films and Improvement of Film Quality 30

3-3-2 Characterization of Amorphous Silicon Solar Cells 40

3-3-3 High Rate Deposition of Amorphous Silicon Thin Films and Solar Cells 42

3-4 Summary 46

References 47

Chapter 4. Theoretical Analysis of Microcrystalline Silicon Thin Film Solar Cells 48

4-1 Introduction 48

4-2 Calculation for Solar Cell Performances by Using AMPS-1D 49

4-3 Results of Calculation 57

4-3-1 Effects of p-layer materials 57
4-3-2 Effects of n-layer materials 62
4-3-3 Effects of i-layer film properties 64
4-4 Summary 76
References 78

Chapter 5. Fabrication and Characterization of Microcrystalline Silicon Thin Films and Solar Cells 79
5-1 Introduction 79
5-2 Experimental Details 80
5-2-1 Experimental Setup 80
5-2-2 Deposition Conditions 82
5-3 Deposition and Characterization of Microcrystalline Silicon Thin Films and Solar Cells 87
5-3-1 Dependence on Hydrogen Flow Rate 87
5-3-2 Dependence on Deposition Pressure 92
5-3-3 Dependence on Substrate Temperature 96
5-3-4 Dependence on Filament Temperature 98
5-3-5 Fabrication and Characterization of Solar Cells 100
5-4 Examination of Tantalum Filament and 2-Step Growth Method 106
5-4-1 Examination of Tantalum Filament 106
5-4-2 Study of Initial Growth of Films and 2-Step Growth Method 115
5-4-3 Application of 2-Step Growth Method to Solar Cells 117
5-4-4 Comparison of Tungsten and Tantalum Filament in Solar Cell Performances 122
5-4-5 Optimization in Fabrication of Solar Cells 124
5-5 Optimization of Deposition Parameters and Degradation Properties of Microcrystalline Silicon Thin Films and Solar Cells 131
5-5-1 Optimization of Deposition Parameters 131
5-5-2 Degradation Properties of Films and Solar Cells 148

5-5-3 Post-oxidation of Microcrystalline Silicon Thin Films 153
5-6 Theoretical Analysis and Fabrication of Amorphous Silicon /Microcrystalline Silicon Tandem Solar Cells 158
5-6-1 Theoretical Analysis of Amorphous Silicon/ Microcrystalline Silicon Tandem Solar Cells 160
5-6-2 Fabrication and Characterization of Amorphous Silicon/Microcrystalline Silicon Tandem Solar Cells 164
5-7 Summary 166
References 169

Chapter 6. Approaches for High Rate Deposition of Microcrystalline Silicon Thin Films 173
6-1 Introduction 173
6-2 Experimental Details 174
6-3 High Rate Deposition and Solar Cell Properties 176
6-3-1 Dependence on Mono-silane Flow Rate 176
6-3-2 Dependence on Filament-Substrate Distance 178
6-3-3 Effects of Filament Length on Film Properties 184
6-3-4 Fabrication and Characterization of Solar Cells 189
6-4 Summary 197
References 198

Chapter 7. General Conclusions and Future Prospects 199
7-1 General Conclusions 199
7-2 Future Prospects 206

Acknowledgements 207
List of Publications 209

Chapter1

Overview and Objectives of This Research

Role of renewable energy in the foreseeable future

Energy is essential to industry, promotes global economics growth and helps to create the wealth and support the technology needed to combat environmental degradation. Energy also provides the amenities that make human life comfortable but the secure supply of energy at affordable prices is necessary.

For more than a century, the world's commercial energy needs have been met predominantly by fossil fuels including oil, coal and natural gas. Fossil fuels have sizeable proven reserves with the prospect of future discovery and better extraction rate through advanced technology. At this time, there is no single or group of substitutes, which offer a commercial alternative to fossil fuels.

Nonetheless, fossil fuels are finite and development of other energy sources for the longer term is both inevitable and prudent. From historical point of view, future energy systems may comprise an even greater mix of energy sources, with the higher visibility of renewable sources becoming a new transition. The place those new sources hold in the future energy mix will depend upon their technical development and price, as well as safety and environmental impact. Nuclear are already in use, but in the recent years, development of nuclear has been held black by political and public concerns about safety, no doubt heightened by Chernobyl and Tokai village disaster.

Several technologies which exploit the energy potential of wind, modern biomass and solar photovoltaic are established in the marketplace. Modern renewable energy technologies are progressing quickly down their "cost learning curves" and gaining from the economics already achieved by more mature energy technologies. Some of the more promising renewable technologies may well become commercially competitive and start to make a measurable contribution to energy supply by 2020. Renewable energy offers some environmental benefits over fossil fuels. The greater use of fossil energy results in serious emissions of nitrogen oxides (NO_x), sulfur oxides (SO_x) and volatile organic compounds that are directly correlated to "acid rain" and photochemical smog, destroying the ecological balance. Fossil fuels also emit carbon dioxide (CO_2), which is one of the "greenhouse gases". There is strong concern that increased concentration of CO_2 in the atmosphere and could lead to an excessive "greenhouse effect" and possible global warning.

Therefore, the exploitation of adequate, environmentally responsible and economical energy is one of the fundamental preconditions for the survival of the world's steadily increasing population. Although the energy resources to maintain our civilization in the 20th century has been supplied mostly by fossil fuels, toxic emissions and CO_2 must be reduced to ward off ecological damage and climate changes. Oil, natural gas, coal and nuclear energy will make an important contribution for many years to come, but renewable sources of energy will have to play an increasingly important role in the foreseeable future.

Photovoltaic – electricity from the Sun

Solar energy is one of the renewable sources and generally recognized to be

environmentally benign and inexhaustible. We have dreamed of harnessing the power of the sun and are trying to utilize this solar radiation in various ways. Examples of direct utilize of this solar radiation as light or heat on comparatively large-scale includes photovoltaic power generation and solar heat power generation. Wind power generation, hydroelectric power generation and wave power generation can be considered as examples of indirect utilization of solar radiation.

Among a wide variety of these technologies developed to exploit the renewable sun's power, the simplest and most elegant technology is solar photovoltaic. Based on solid-state physics, photovoltaic cells convert sunlight energy directly into electricity without the need for an intermediate electrical generator. The technology is simple, dependable and can be used on any scale from milliwatts to megawatts. Photovoltaic systems have no moving parts, thus maintenance is minimal. Above all, the technology is environmentally friendly, silent and emission free. It is elegant and easy to install.

The solar cell is the key feature of photovoltaic technology; the light is absorbed in it by semiconductor material, generating pairs of activated charged particles that must be split by the cell's internal electric field (apace charge region of the diode) during their lifetime and passed to the metal contacts at the cell surface. Conversion efficiency, i.e. the ratio of maximum extractable electricity to the amount of the incident light power, is the most important physical parameter for characterizing a solar cell. Mass-produced solar cells of single-crystalline silicon currently achieved efficiencies of around 18-20%.

In spite of various advantages in photovoltaic power generation as above mentioned, before "oil-shock" in 1973, solar cells had been used for a limited application area such as apace power sources. A big barrier impeding the expansion of

large-scale power source application was the high price of solar cell modules, which were more than \$50/W_p (peak watts) by 1974. That is because the cost of the electrical energy generated by solar cells was very high compared with that generated by fossil fuels and nuclear power generation. Therefore, the cost reduction of solar cells is the main focus of considerable research worldwide. Photovoltaic manufacturers in R&D and market development activities have benefited from two decades of support of their respective government organizations, such as the New Energy and Industrial technology Development Organization (NEDO) and Photovoltaic Power Generation Technology Research Association (PVTEC) in Japan as a part of the New Sunshine Program under the Ministry of Economy, Trade and Industry, Department of Energy (DOE) in USA as a part of the U.S. National Photovoltaic Program and the Commission of the European Communities (CEC) in Europe as a part of JOULE program. These considerable efforts have been strongly encouraged to accelerate remarkably the pace of technology development.

Microcrystalline Silicon thin films and solar cells

The history of microcrystalline silicon film started since Veprek et al. deposited it by using the method named "Chemical Hydrogen Plasma Transport" for the first time in 1968.[1)] In this method, crystalline silicon with a room temperature was etched by atomic hydrogen produced by remote plasma, as a result, radicals were generated and they were transported to the substrate heated at a temperature over 200^{o}C. Then, microcrystalline silicon film was deposited on the substrate. After 1968, Ovshinsky et al. in Energy Conversion Device Co. reported they could obtain amorphous silicon films with high conductivity in 1979.[2)] However, they

experimentally confirmed the existence of crystalline phase in amorphous silicon films in 1980.[3] They are the origin of the material that we recently called microcrystalline silicon. Since then, Usui et al. in Sony Co. deposited microcrystalline silicon films for the first time using hydrogen based silane gas.[4] At the almost same time, Hirose (Hiroshima univ.)[5] and Matsuda (AIST) et al.[6] succeeded in obtaining microcrystalline silicon films at a low temperature. From the systematic researches of Matsuda, it was found that the formation of microcrystalline silicon film has relationship with hydrogen and ion bombardment from plasma prevents the growth of crystalline.[7] Although microcrystalline silicon films could be deposited around 30 years ago, they couldn't attract much attention to solar cell applications. Because microcrystalline silicon film has many defects and impurities, the large carrier recombination at the grain boundary is a serious problem, and it is very difficult to overcome these problems. Therefore, microcrystalline silicon films have been thought to be not useful for intrinsic absorber layer of silicon based thin film solar cells. Thus, amorphous silicon solar cells have been intensively and widely investigated for such a long period until now. In this situation, Neuchatel univ. in Switzerland reported pin solar cell properties for the first time in 1994. They could achieve a conversion efficiency of 7.7%.[8, 9] Beside, their microcrystalline silicon thin film solar cells didn't show any light soaked degradation properties like amorphous silicon solar cells. Therefore, since 1994, microcrystalline silicon thin film solar cells have attracted much attention as a next generation high efficiency thin film solar cell. Figs. 1-1 and 1-2 shows status of microcrystalline silicon thin film solar cells. The maximum conversion efficiency of 10.7% was recently achieved by KANEKA Corp. using PECVD for microcrystalline silicon single cells and amorphous Si/microcrystalline Si tandem cells, respectively.[10] Besides, recently, a conversion efficiency of 9.4% was

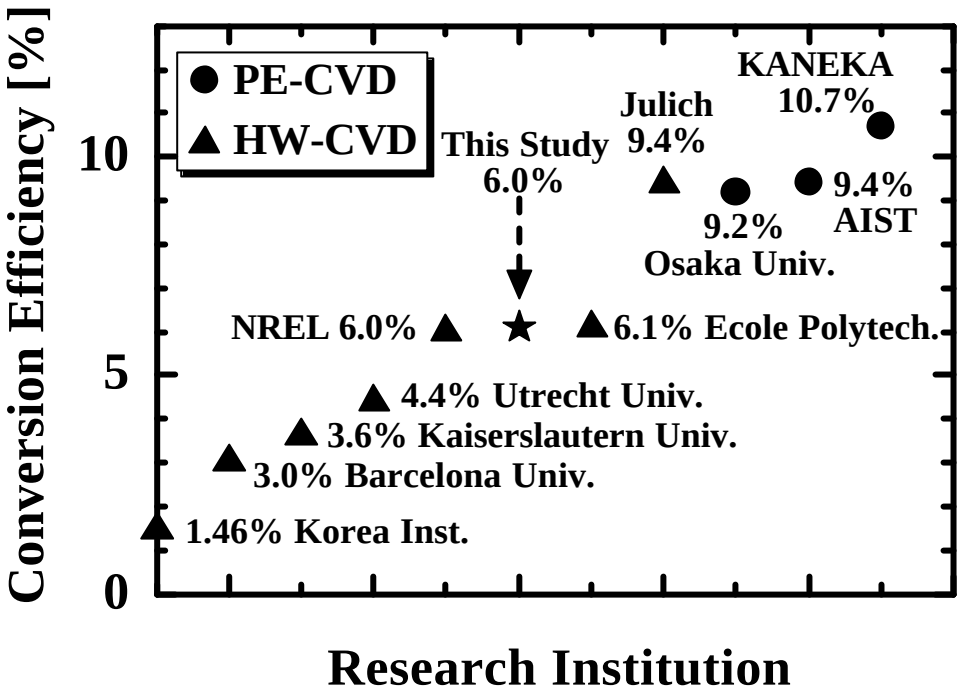

Fig. 1-1: Status of microcrystalline silicon thin film solar cells

FZ Julich	mc-Si:H(0.1nm/s)	9.4%
Ecole Polytech.	mc-Si:H	6.1%
Tokyo Tech. (This Study)	***mc-Si:H (0.3-0.4 nm/s)***	***6.0%***
NREL	mc-Si:H	6.0%
Utrecht Univ.	mc-Si:H	4.4%
Kaiserslautern Univ.	mc-Si:H	3.6%
Barcelona Univ.	mc-Si:H	3.0%
Korea Inst. of Energy Research	mc-Si:H	1.46%

Fig. 1-2: Status of microcrystalline silicon thin film solar cells prepared by HW-CVD

also achieved by IP-Julich using Hot Wire CVD.[11] at a deposition rate of 0.1 nm/s.

In silicon based thin film solar cells, the active absorber layer is amorphous or microcrystalline thin film that has been deposited on a supporting substrate made of glass, ceramic, metal, plastic, or another semiconductor. The main advantage of thin film solar cells is their promise of lower costs, since less energy for processing and lower costs for the materials are required, and large-scale production is feasible. The deposition of semiconductors on foreign substrates usually results in microcrystalline or amorphous silicon films with optical and electrical properties that can be substantially different from the single crystal behavior. However, one of the major problems in thin film solar cells is that higher defect density reduces the efficiency and stability compared to the single crystal silicon solar cells in many cases. Therefore, great efforts have been made to understand the influence of lattice defects on the photovoltaic properties of films. Though remarkable improvements have been obtained in particular cases, many fundamental problems still remain.

The progress in the development of amorphous silicon based thin film solar cells have been impressive in recent years, and its application is successfully established in small consumer products like desk calculators and wristwatches. Research and development of cost reduction technologies for large area and thin film module production are now concentrated on further understanding of the long-term stability problems and further improvements in stabilized conversion efficiencies.

Recently, the research activities have shifted towards thin film solar cells using microcrystalline silicon that have a great potential to attain high conversion efficiency and high stability compared to amorphous silicon solar cells. Among them, microcrystalline silicon has attracted the most attention. The advantage of using silicon is the possibility of mass production. There are rich silicon resources in the

earth and long succession of the study of the silicon technology. Besides, silicon is toxic free. However, microcrystalline silicon is indirect semiconductor like single crystalline silicon, therefore, it has low absorption coefficient within the visible light wavelength region. The band gap of microcrystalline silicon is as same as that of single crystalline silicon and the value is 1.1eV. The absorption coefficient of microcrystalline silicon is described with that of amorphous and single crystalline silicon in Fig. 1-3. The absorption coefficient of microcrystalline silicon is similar to that of single crystalline silicon in low photon energy region less than 1.5 eV and also similar to that of amorphous silicon in high photon energy region over 2.0 eV. Because of these optical properties, the thickness of at least 2.0 μm is required for intrinsic absorber layer of microcrystalline silicon solar cells even with a good light trapping. This thickness is much thicker than the thickness of 0.3 μm for amorphous silicon. Therefore, for further cost-reduction, high deposition rate of 2-5 nm/s is highly required for microcrystalline silicon solar cells. For high efficiency and low cost, recently, amorphous silicon/microcrystalline silicon tandem (hybrid) solar cells have been intensively investigated, and these tandem cell modules already started to be sold.

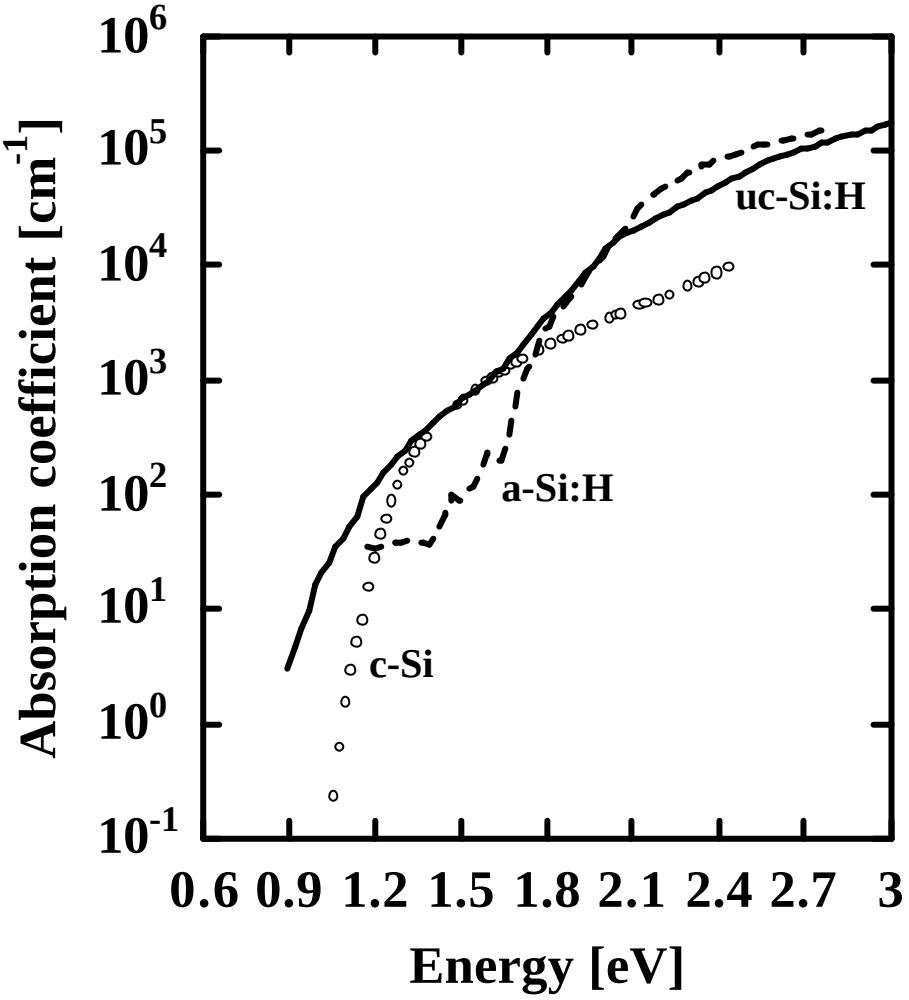

Fig. 1-3: Absorption coefficient of microcrystalline silicon compared with amorphous silicon and single crystalline silicon

Objectives of this study

The overall objective of this study is to contribute towards developing new technologies for high efficiency and low cost thin film solar cells. Until now, various deposition techniques of chemical vapor deposition (CVD) such as plasma-CVD[7, 9] and photo-CVD[12] are developed to fabricate silicon based thin film solar cells. However, the deposition rate of these techniques is still low and the apparatus of these techniques is complicated. In order to achieve mass production of solar cells, novel deposition techniques which have simple apparatus and high deposition rate are required. For this purpose, Hot Wire Cell method is proposed as a novel technique for the growth of microcrystalline silicon thin films.

As above mentioned, Hot Wire Cell method is newly proposed to achieve high efficiency and low cost microcrystalline thin film solar cells. Since the fabrication method of Hot Wire Cell method have not been established yet, that is first investigated and established to prepare device quality intrinsic microcrystalline silicon films. The solar cell performances mainly depend on the properties of intrinsic absorber layer because intrinsic absorber layer acts as active layer in the solar cell. From these points of view, several approaches in this study are attempted to achieve device quality microcrystalline silicon thin films with moderate deposition rate at a low substrate temperature, which enable depositing on the cheap glass substrate. In case of photo-CVD, it was demonstrated that radical flux ratio ($[SiH_3]/[H]$) on the growing surface is the key factor in the growth of high quality amorphous and crystalline silicon at a low substrate temperature.[13] However, the deposition conditions and mechanism of Hot Wire Cell method are very different from those of photo-CVD or plasma-CVD, and they have not been well known and established.

Therefore, one of the objectives of this study is to establish deposition technique for achieving high quality microcrystalline silicon thin films by Hot Wire Cell method. For this purpose, the apparatus of the Hot Wire Cell system was fabricated and various approaches to obtain high quality microcrystalline silicon thin films have been examined. For example, the influence of various deposition parameters such as filament temperature, substrate temperature, pressure, gas flow rate and filament-substrate distance on the structural and electrical properties of films were evaluated. Since the solar cell performances largely depends on p/i interface properties, the investigations and improvements of p/i interface were also carried out. Furthermore, for cost reduction, several approaches for high rate deposition of microcrystalline silicon thin films were attempted.

Outline of this study

This thesis consists of eight chapters as shown in the last part prior to references' page of this chapter 1 (Fig. 1-4).

Chapter 1 refers to an overview and objectives of this study. First, an informed look ahead at the future of photovoltaic technologies as one of renewable sources is indicated. Second, in spite of a wide range of solar cells that is currently explored for their potential use in photovoltaic applications, the increasing demand to develop thin film solar cells as a suitable energy source economically and environmentally is demonstrated. Then, among various kinds of thin film solar cells, the advantage of low cost solar cells based on microcrystalline silicon thin film are given. The last part in this chapter propose the novel deposition process, Hot Wire Cell method, for achieving high deposition rate.

Chapter 2 reviews the configurations and features of the Hot Wire Cell system. The fundamental principle of Hot Wire Cell method including the dissociation reactions of reactant gases at the surface of filament and gas phase reactions of radicals produced at the filament is also described in the first half chapter.

Chapter 3 demonstrates the results of amorphous silicon thin films and solar cells prepared by Hot Wire Cell method. To find the good deposition conditions for amorphous silicon films might be also very useful for the investigation of microcrystalline silicon films. The electrical and structural characterization of amorphous silicon films and improvement of their film quality were carried out. Then, amorphous silicon thin film solar cells were fabricated and characterized. Furthermore, high rate deposition of amorphous silicon thin films and solar cells are attempted.

Chapter 4 demonstrates the results of theoretical analysis for microcrystalline silicon solar cells. Calculation for solar cell performances were carried out by using AMPS-1D BETA Version 1.00 (A one-dimensional device simulation program for the Analysis of Microelectronic and Photonic Structures) that was developed by the electronic materials and processing research laboratory in Penn. State University with the support of the Electric Power Research Institute and equipment support by IBM. In the initial stage of this research, the ideal device structure for microcrystalline silicon thin film solar cells was not established. Therefore, silicon materials such as amorphous silicon and microcrystalline silicon were theoretically examined if they were suitable for p-layer and n-layer of microcrystalline silicon solar cell. Then, the influence of i-layer film properties on solar cell performances was also theoretically investigated.

Chapter 5 demonstrates the results of microcrystalline silicon thin films and solar cells prepared Hot Wire Cell method. The electrical and structural

characterization of microcrystalline silicon films and improvement of their film quality were carried out. Then, microcrystalline silicon thin film solar cells were fabricated and characterized. Furthermore, p/i interface properties of microcrystalline silicon thin film solar cells was also investigated and improvement of p/i interface properties was attempted.

Chapter 6 demonstrates the results of approaches for high rate deposition of microcrystalline silicon thin films and solar cells. First, high rate deposition was attempted by increasing gas flow rate and decreasing filament-substrate distance. Then, in order to male up the reduction of gas dissociation efficiency caused by the increase of reactant gas flow rate, long filament was examined for high rate deposition.

Chapter 7 summarizes the results obtained in this study. Subjects to accomplish further improvement of conversion efficiency of microcrystalline silicon thin film solar cells prepared Hot Wire Cell method are discussed.

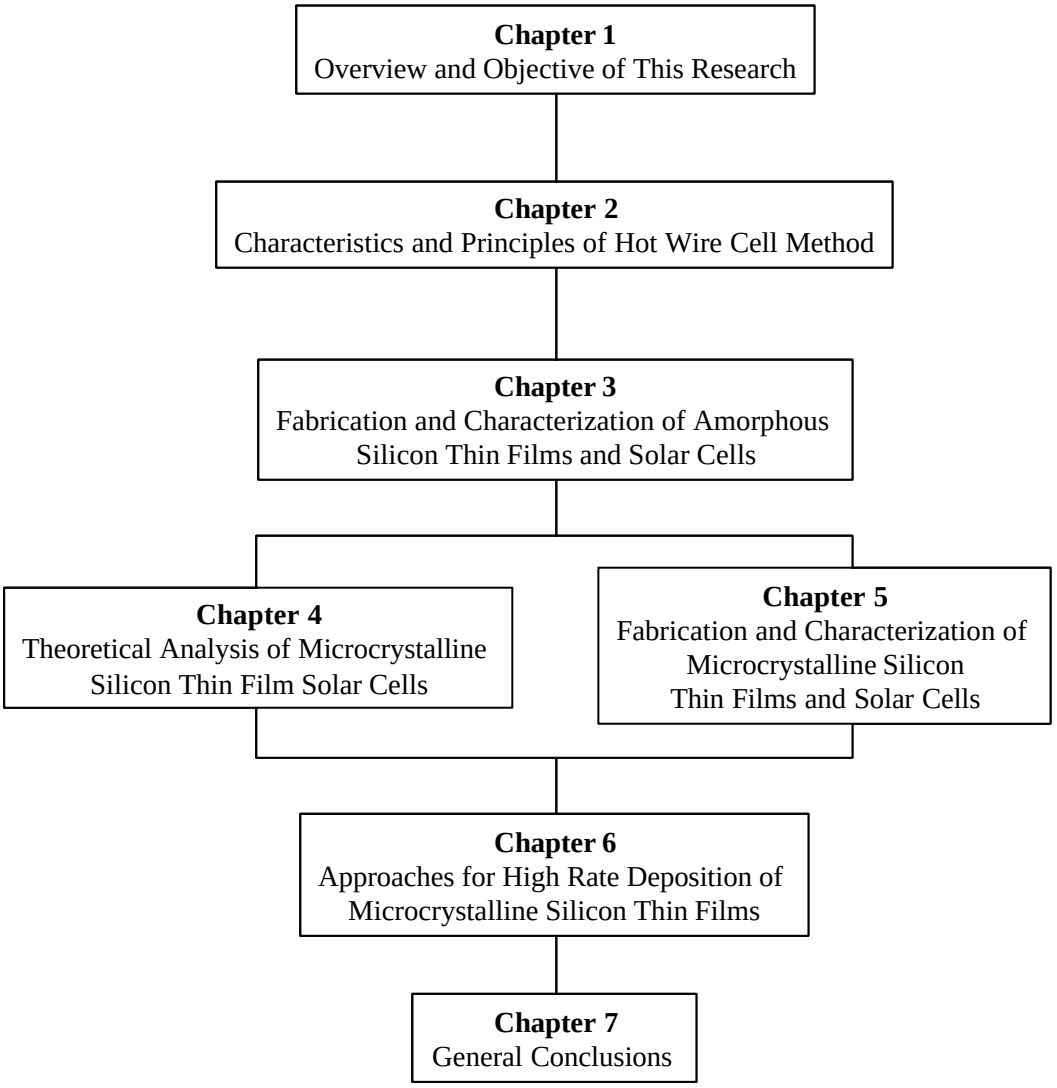

Fig. 1-4: Overview of this study

References

[1] S. Veprek and V. Marecek: Solid State Electron **11** (1968) 683.

[2] A. Madan, S. R. Ovshinsky and E. Benn: Phil. Mag. **B, 40** (1979) 259.

[3] R. Tsu, M. Izu, S. R. Ovshinsky and F. H. Pollak: Solid State Commun. **36** (1980) 817.

[4] S. Usui and M. Kikuchi: J. Non-Cryst. Solids **34** (1979) 1.

[5] T. Hamasaki, H. Kurata, M. Hirose and Y. Osaka: Appl. Phys. Lett. 37 (1980) 1084.

[6] A. Matsuda et al.: Jpn. J. Appl. Phys. **20** (1980) L183.

[7] A. Matsuda: J. Non-Cryst. Solids **59&60** (1983) 767

[8] J. Meier, R. Flueckiger, H. Keppner and A. Shah: Appl. Phys. Lett. **65** (1994) 860.

[9] J. Meier, P. Torres, R. Platz, S. Dubail, U. Kroll, J. A. Anna Selvan, N. Pellaton Vaucher, C. Hof, D. Fischer, H. Keppner, A. Shah, K. D. Ufert, P. Giannoules and J. Koehler: Mat. Res. Soc. Symp. Proc. **420** (1996) 3.

[10] Y. Tawada, H. Yamagishi and K. Yamamoto: Solar Energy Materials & Solar Cells **78** (2003) 647.

[11] S. Klein, F. Finger, R. Carius, T. Dylla, B. Rech, M. Grimm, L. Houben and M. Stutzmann: Thin Solid Films **430** (2003) 202.

[12] P. Siamchai, A. Yamada and M. Konagai: Jpn. J. Appl. Phys. **33** (1994) 6099.

[13] T. Oshima, A. Yamada and M. Konagai: Jpn. J. Appl. Phys. **36** (1997) 6481.

Chapter2

Characteristics and Principles of Hot Wire Cell Method

2-1 Introduction

Low-temperature deposition of silicon based thin films, such as amorphous silicon (a-Si:H) and microcrystalline silicon (μc-Si:H), is one of the most important technological requirements in the semiconductor industry for thin film solar cells. These films are usually prepared by plasma enhanced chemical vapor deposition (PECVD) method, since PECVD is the only method to satisfy the industrial requirements so far, although there are some exceptional cases of using low-temperature thermal CVD or photo CVD. However, the PECVD method is not perfect for the deposition rate and there is the problem in the influence of plasma damage, such as ion bombardment damage in various devices.

On the other hand, the Hot Wire Cell method was developed to overcome these problems arising in the PECVD processes. In this process, a heated tungsten filament is used to induce the catalytic and/or pyrolytic dissociation of reactant gases[1)] and produce atomic hydrogen as a reaction by-product, which reacts with silane molecules to produce SiH_3 radicals. Recently similar processes named catalytic chemical vapor deposition (Cat-CVD)[2-4)] and Hot Wire CVD[5-7)] have been studied intensively. A wide variety of materials, including a-Si:H,[8-12)] μc-Si:H,[13-17)]

silicon-nitride,[18, 19] epitaxial silicon[20, 21] and epitaxial $Si_{1-y}C_y$[22, 23] films have been achieved by Hot Wire CVD.

This chapter first describes the physical characteristics and dissociation efficiency of the Hot Wire Cell. Then, the fundamental principles of Hot Wire Cell method are reviewed. Finally, some advantages of Hot Wire Cell method are discussed briefly.

2-2 Fabrication of Hot Wire Cell System

The Hot Wire Cell apparatus used in this study was shown in Fig. 2-1. The apparatus consists mainly of three parts: the parts for gas inlet into the low-pressure deposition chamber, for gas decomposition via catalytic and/or pyrolytic cracking reactions at the surface of a heated filament and the substrate for film formation using decomposed species transported from the filament. A tungsten wire is used as a filament, because the melting point of tungsten is as high as 3382°C, and also because it remains as high as 2165°C[24] even when the surface of tungsten is covered to silicide by the reaction with mono-silane (SiH_4) gas.

The apparatus of Hot Wire Cell system is almost the same as Cat-CVD[25] and Hot Wire CVD. The significant difference between our Hot Wire Cell method and these works is the layout of the filament. In this work, we used the integrated combination of gas inlet and the filament, which is called "Hot Wire Cell unit". The name of the Hot Wire Cell is derived from the Knudsen cell or plasma cell used in the molecular beam epitaxy system. The Hot Wire Cell unit consists of a gas inlet pipe, a hot wire filament and current-introduction terminals. A coiled tungsten wire is used as a hot wire filament. Tungsten wire with a diameter of 0.5 mm was used as a hot wire

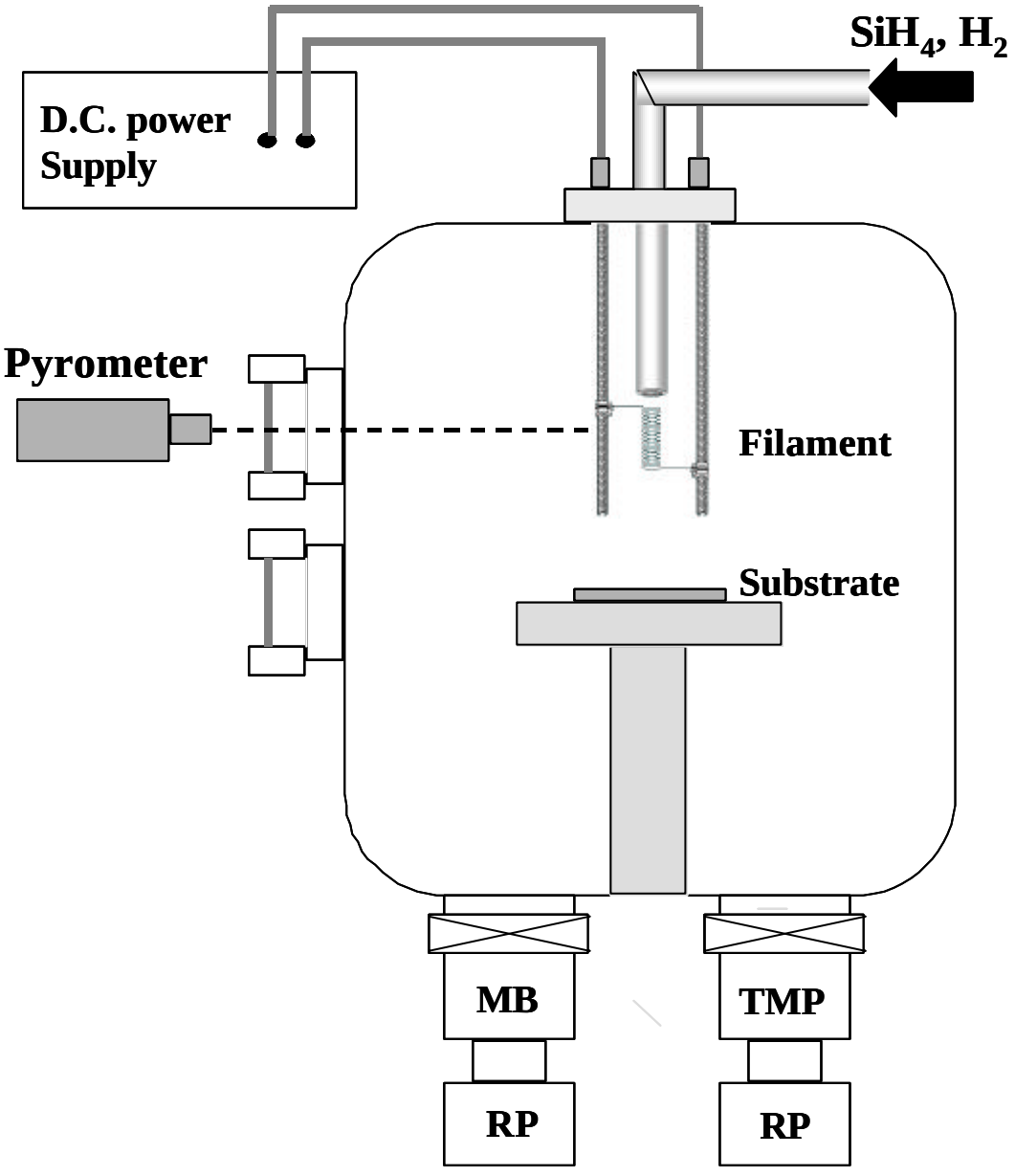

Fig. 2-1: Schematic view of the deposition chamber

filament. The axis of the coiled filament in the chamber was parallel to the gas flow. The filament was heated by supplying DC electric power directly to it and the temperature was kept constant throughout the experiment by controlling the power.

The schematic view of the Hot Wire Cell unit is shown in Fig. 2-2. The Hot Wire Cell unit is consisted of the 114 mmϕ flange, the copper and molybdenum rods that are used for the current terminals, stainless pipe which is used for gas inlet and tungsten filament. The distance of each rod is about 3.5 cm, the filament coiled with a diameter of 4 mm and the length of 1.5 cm is arranged near the gas inlet pipe. The distance between the filament and the gas inlet pipe is about 2-2.5 cm. The molybdenum rods and gas inlet pipe can be replaced by new one, when they become old.

A stainless steel chamber with a diameter of 56cm and a height of 60cm is used for the deposition of intrinsic μc-Si:H films and is ordinarily pumped by a turbo molecular pump (TMP). The base pressure of this chamber is around $2x10^{-7}$ Torr. While deposition, a mechanical booster pump (MB) or TMP is used for evacuation. In the case of the deposition at a pressure of less than 50 mTorr, the TMP is ordinarily used. The gas pressure is controlled by adjusting the valve between the chamber and MB or TMP. The apparatus is a hybrid multi chamber system (Hot Wire chamber and photo-CVD chamber) and have a load-lock chamber. Corning 7059 glass, Asahi U-type TCO glass and single crystalline Si wafer used as substrates were placed on a substrate holder. The substrate holder was placed on the stage that has a heater block inside. The temperature of the substrate was measured by a calibrated thermocouple placed inside of the stage. The calibration for real substrate temperature was previously carried out by using a second thermocouple attached directly onto the glass substrate. The distance between the substrate holder and the filament is varied form 15

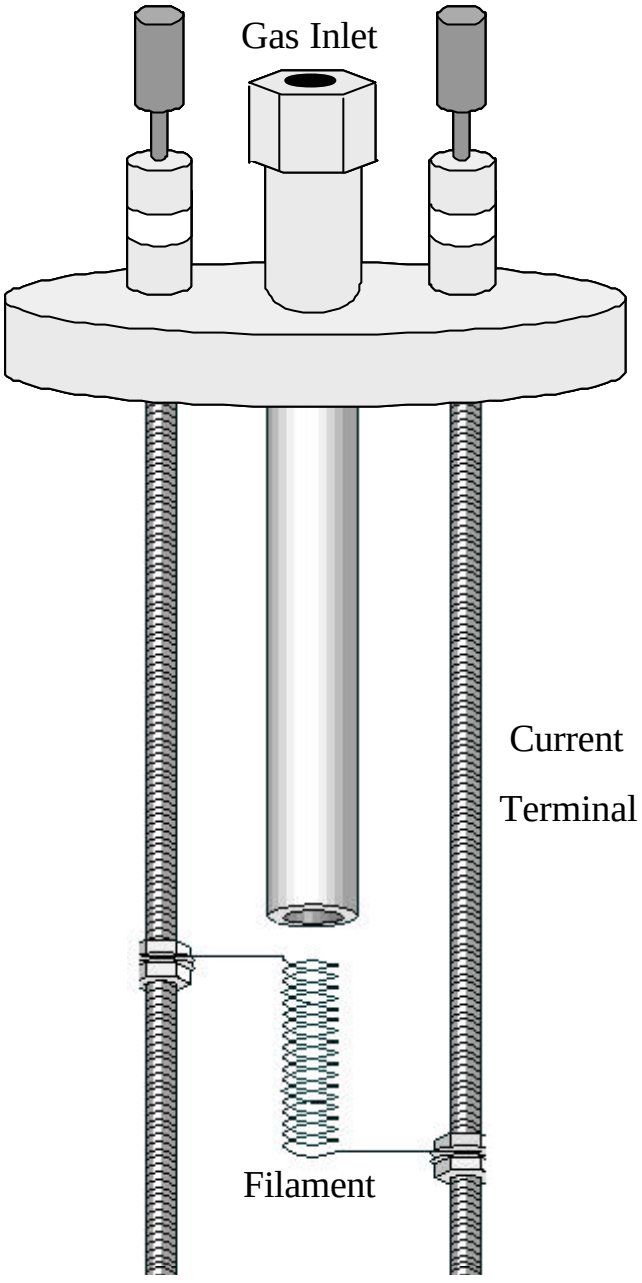

Fig. 2-2: Schematic view of the Hot Wire Cell unit

cm to 1.5 cm by changing the stage height.

The value of the filament temperature is essentially important in the Hot Wire Cell method. However, the precise estimation of the real filament temperature is difficult. The filament temperature is measured by using an optical pyrometer through a quartz window of the chamber. The filament temperature is also estimated from the temperature dependence of the electric current applied to the filament. The value obtained from the pyrometer includes ambiguity due to the emissivity of tungsten observed through the quartz window. The emissivity of the tungsten surface is believed to be about 0.4.[26] The temperature estimation appears to have some errors of around several tens ^{o}C, because the temperature is not constant along the entire wire.

2-3 Principles of Hot Wire Cell Method

In photo-CVD, gas molecules are decomposed by photon energy from an UV lamp or exited mercury atoms that are exited by an UV lamp. Such decomposed species are transported to the substrate through the gas phase reactions and form a film. In thermal CVD, reactant gases are decomposed on the growing surface and the decomposed species contribute to the film deposition immediately. On the other hand, in case of the Hot Wire Cell method, reactant gas molecules are decomposed via catalytic and/or pyrolytic cracking reactions on a heated filament. The exact reactions of SiH_4 molecules occurred on the surface of the heated tungsten are not clear. Matsumura implied that SiH_4 molecules are decomposed to SiH_2 or SiH_3.[1] However, recently, the reactions of SiH_4 molecules on the surface of the filament have been investigated both experimentally and theoretically by several researchers[27-30], and similar results have been reported as follows:

The decomposition reactions on the filament

$$SiH_4 \rightarrow Si + 4H \quad (2\text{-}1)$$

$$\rightarrow Si + 2H_2 \quad (2\text{-}2)$$

$$H_2 \rightarrow 2H \quad (2\text{-}3)$$

The primary gas phase reactions

$$H + SiH_4 \rightarrow H_2 + SiH_3 \quad (2\text{-}4)$$

$$Si + SiH_4 \rightarrow Si_2H_4^* \rightarrow 2SiH_2 \quad (2\text{-}5)$$

$$\rightarrow SiH + SiH_3 \quad (2\text{-}6)$$

$$\rightarrow Si_2H_2 + H_2 \quad (2\text{-}7)$$

$$\rightarrow Si_2H_4 \quad (2\text{-}8)$$

The secondary gas phase reactions

$$H + SiH_3 \rightarrow H_2 + SiH_2 \quad (2\text{-}9)$$

$$SiH_2 + SiH_4 \rightarrow Si_2H_6 \quad (2\text{-}10)$$

$$SiH + SiH_4 \rightarrow Si_2H_5 \quad (2\text{-}11)$$

$$Si_2H_2 + SiH_4 \rightarrow Si_3H_6 \quad (2\text{-}12)$$

$$H + Si_2H_{2(4)} \rightarrow H_2 + Si_2H_{1(3)} \quad (2\text{-}13)$$

$$Si_2H_4 + SiH_4 \rightarrow Si_3H_8 \quad (2\text{-}14)$$

$$\rightarrow SiH_2 + Si_2H_6 \quad (2\text{-}15)$$

$$SiH_3 + SiH_3 \rightarrow SiH_2 + SiH_4 \quad (2\text{-}16)$$

$$\rightarrow Si_2H_4 + H_2 \quad (2\text{-}17)$$

$$\rightarrow Si_2H_5 + H \quad (2\text{-}18)$$

$$\rightarrow Si_2H_2 + 2H_2 \quad (2\text{-}19)$$

$$\rightarrow Si_2H_6 \quad (2\text{-}20)$$

In the recent researches, it is reported that the reactant gas molecules such as SiH_4 and H_2 are decomposed on the surface of a filament as shown in Eqs. 2-1, 2-2 and 2-3. SiH_4 molecules are completely decomposed into bare silicon atoms, generating atomic hydrogen and/or H_2 molecules. And H_2 molecules are decomposed into atomic hydrogen. The probability of these dissociation reactions largely depends on the filament temperature. In case of low temperature deposition of silicon, atomic hydrogen plays very important role especially in the formation of μc-Si:H film. In Hot Wire Cell method, atomic hydrogen can be sufficiently generated from a dissociation of SiH_4 gas, since the gas decomposition efficiency is very high. As a result, in some deposition conditions, μc-Si:H films can be obtained by using only SiH_4 gas. Eqs. from 2-4 to 2-8 show the primary gas phase reactions. In these reactions, bare silicon atoms and atomic hydrogen are consumed by SiH_4 molecules that are not decomposed on the filament, newly generating radicals such as SiH_3, SiH_2, SiH, Si_2H_2 and Si_2H_4. These radicals are commonly generated in other CVD methods and it is reported that they are experimentally detected in Hot Wire CVD. In the secondary gas phase reactions, as shown in Eqs. from 2-9 to 2-20, there are probabilities that higher silane radicals such as Si_2H_6 and Si_3H_8 can be generated. These higher silane radicals are undesirable radicals for obtaining high quality silicon films. On the other hand, these secondary gas phase reactions largely depend on the gas pressure. Therefore, for obtaining high quality silicon films, it is very important for controlling the deposition pressure.

2-4 Advantages of Hot Wire Cell Method

The advantages of Hot Wire Cell method are summarized as follows:

1. Soft process

   Hot Wire Cell method is considered to be a process without ion bombardment damages caused by energetic charged particles. Therefore, it can be expected the interfaces and properties of silicon films are quite improved compared with that of prepared by PECVD.

2. Low substrate temperature process

   In the Hot Wire Cell method, filament temperature is set to high temperature around 2000^{o}C. Since the deposition species such as radicals are generated not by substrate surface but by filament, the film can be grown at low substrate temperatures around 100-200^{o}C. Low substrate temperature process is very important factor not only because the film can be deposited on glass substrates, but also because the impurity distribution of semiconductor devices is not destroyed.

3. High deposition rate

   In the Hot Wire Cell method, since the filament is placed perpendicular to the substrate, the reactant gases are efficiently decomposed during passing through the filament, thus high deposition rate can be obtained. Atomic hydrogen is sufficiently produced as a result of the decomposition of SiH_4 gas. Atomic hydrogen introduces the crystallization of the silicon films at low substrate temperature. Therefore, Hot Wire Cell method is useful process for high rate deposition of μc-Si:H films.

References

[1] H. Matsumura: Jpn. J. Appl. Phys. **37** (1998) 3175.

[2] H. Matsumura: Jpn. J. Appl. Phys. **25** (1986) L949.

[3] H. Matsumura and H. Tachibana: Appl. Phys. Lett. **47** (1985) 833.

[4] H. Matsumura, H. Umemoto, A. Izumi and A. Masuda: Thin Solid Films **430** (2003) 7.

[5] A. H. Mahan, J. Carapella, B. P. Nelson, R. S. Crandall and I. Balberg: J. Appl. Phys. **69** (1991) 6728.

[6] S. Klein, F. Finger, R. Carius, T. Dylla, B. Rech, M. Grimm, L. Houben and M. Stutzmann: Thin Solid Films **430** (2003) 202.

[7] J. K. Rath, H. Meiling and R. E. I. Schropp: Solar Energy Materials & Solar Cells **48** (1997) 269.

[8] K. Ishibashi, M. Karasawa, G. Xu, N. Yokokawa, M. Ikemoto, A. Masuda and H. Matsumura: Thin Solid Films **430** (2003) 7.

[9] N. Tsuji, T. Akiyama and H. Komiyama: J. Non-Cryst. Solid **198-200** (1996) 1054.

[10] E. C. Molenbroek, A. H. Mahan, E. J. Johnson and A. C. Gallagher: J. Appl. Phys. **79** (1996) 7278.

[11] J. Doyle, R. Robertson, G. H. Lin, M. Z. He and A. C. Gallagher: J. Appl. Phys. **64** (1988) 3215.

[12] P. Papadopulos, A. Scholz, S. Bauer, B. Schroeder and H. Oechsner: J. Non-Cryst. Solid **164-166** (1993) 87.

[13] R. Iiduka, A. Heya and H. Matsumura: Solar Energy Materials & Solar Cells **48** (1997) 279.

[14] J. E. Bouree, J. Guillet, C. Grattepain and J. Chaumont: Thin Solid Films **430**

(2003) 110.

[15] S. Kasouit, P. R. Cabarrocas and R. Vanderhaghen: Thin Solid Films **427** (2003) 335.

[16] O. Vetterl, M. Hulsbeck, J. Wolff, R. Carius and F. Finger: Thin Solid Films **427** (2003) 46.

[17] B. Schroeder: Thin Solid Films **430** (2003) 1.

[18] H. Matsumura: J. Appl. Phys. **66** (1989) 3612.

[19] S. Okada and H. Matsumura: Jpn. J. Appl. Phys. **36** (1997) 7035.

[20] J. Thiesen, E. Iwaniczko, K. M. Jones, A. Mahan and R. Crandall: Appl. Phys Lett. **75** (1999) 992.

[21] T. Watahiki, A. Yamada and M. Konagai: J. Crystal Growth **209** (2000) 335.

[22] T. Watahiki, K. Abe, H. Tamura, S. Miyajima, A. Yamada and M. Konagai: Thin Solid Films **395** (2001) 221.

[23] T. Watahiki, K. Abe, H. Tamura, S. Miyajima, A. Yamada and M. Konagai: Material Science & Engineering **B89** (2002) 328.

[24] K. N. Tu and J. W. Mayer: *Silicide Formation in Thin Films Reactions and Diffusion,* eds. J. M. Poat et al. (John Wiley and Sons, New York, 1978) p.359.

[25] H. Matsumura: Jpn. J. Appl. Phys. **30** (1991) L1522.

[26] Y. S. Touloukian and D. P. DeWitt: *Thermal Radiative Properties, Metallic Elements and Alloys*, The TPRC Data Serikes (IFI/Plenum Press, 1970) Vol. 7.

[27] A. Gallagher: Thin Solid Films **395** (2001) 25.

[28] J. K. Holt, M. Swiatek, D. G. Goodwin, R. P. Muller, W. A. Goddard III and H. A. Atwater: Thin Solid Films **395** (2001) 29.

[29] S. Tange, K. Inoue, K. Tonokura and M. Koshi: Thin Solid Films **395** (2001) 42.

[30] J. E. Bouree: Thin Solid Films **395** (2001) 157.

Chapter3

Fabrication and Characterization of Amorphous Silicon Thin Films and Solar Cells

3-1 Introduction

Recently, a-Si:H/μc-Si:H tandem solar cells have attracted much attentions,[1-3] because both of low cost and high conversion efficiency can be expected. However, for tandem cells, around 65% of cell performances largely depends on a-Si:H top cell, therefore, high efficiency and high stability of a-Si:H top cell is strongly required for tandem solar cell. Besides, for the mass production and the further reduction of the cost of solar cells, the deposition rate should be increased to 1-2nm/s. From these points of view, the HW-Cell method is one of the promising methods for obtaining a-Si:H and μc-Si:H thin films, since high deposition rate, low substrate temperature and high efficiency of gas usage can be expected.[4] Furthermore, in HW-Cell method, the film structure can be easily controlled from amorphous to microcrystalline by changing filament temperature,[5, 6] therefore, there is an advantage that a-Si:H/μc-Si:H tandem solar cells can be fabricated in the same system. Our group already had enough knowledge and technique for fabricating a-Si:H single solar cells since many researches of a-Si:H materials and solar cells have been done for around 20 years and a stabilized conversion efficiency of 9.0% has been achieved by using photo-CVD method.[7] Therefore, we thought that the study of a-Si:H solar cells

prepared by HW-Cell method is necessary for the development of high cost performance tandem solar cells, the deep understanding of HW-Cell method and it can be also useful for the study of μc-Si:H solar cells prepared by HW-Cell method.

In this work, we have investigated the structural and electrical properties of a-Si:H thin films deposited by the Hot Wire Cell method using SiH_4 gas without hydrogen dilution. Furthermore, the superstrate pin a-Si:H solar cells with these intrinsic a-Si:H thin films deposited by the Hot Wire Cell method were fabricated in order to investigate the film quality.

3-2 Experimental Details

Intrinsic a-Si:H thin films were deposited on Corning7059 glass and single crystal Si wafers by Hot Wire Cell method in a hybrid multichamber system (Hot Wire Cell method and photo-CVD). The chamber was evacuated by a turbomolecular pump, and the base pressure was around 10^{-7} Torr. Only SiH_4 gas was used for intrinsic a-Si:H film deposition. The filament in the shape of a coil that had a diameter of 4 mm and a length of 1.5 cm was used and it was placed parallel to the gas inlet. The filament temperature was monitored by an infrared pyrometer through a quartz window.

The deposition conditions are shown in Table 3-1. In order to characterize the quality of a-Si:H thin films, Fourier transform infrared absorption spectroscopy (FT-IR) measurement, dark (σ_d) and photoconductivity (σ_{ph}) measurements and secondary ion mass spectroscopy (SIMS) measurements were carried out. For SIMS measurements, stacked thin film layers deposited on single crystal Si wafers as a function of the deposition pressure were prepared.

In order to investigate the application of these a-Si:H films to Si-based thin film solar cells, superstrate pin solar cells were prepared with the deposition rate of 0.4-1.0 nm/s. The structure of the superstrate pin solar cell was as follows: glass/TCO(SnO_2)/p-a-SiC:H/buffer-a-SiC:H/i-a-Si:H/n-a-Si:H/ZnO/Ag/Al. The p-type, buffer and n-type layers were prepared by the photo-CVD method.

Table 3-1: Deposition parameters.

Filament temperature	1900^{o}C
Substrate temperature	150-270^{o}C
Deposition gas pressure	1-200 mTorr
SiH_4 gas flow rate	5 sccm
Filament-substrate distance	1.5-6.0 cm

3-3 Results and Discussion

3-3-1 Characterization of Amorphous Silicon Thin Films and Improvement of Film Quality

In the first step of this research, Jsc and F.F. in an a-Si:H solar cell deposited at a high deposition pressure of 0.1 Torr were as low as 5.78 mA/cm^2 and 0.52, respectively, therefore, a conversion efficiency of only 2.3% could be obtained, as shown in Fig. 3-1. In order to investigate the reason for this low conversion efficiency, we measured O and C concentrations of the a-Si:H solar cell by SIMS analysis, as shown in Fig. 3-2. The sample was grown on a TCO(SnO_2) substrate. It was found from this result that very high O and C concentrations of $2x10^{21}$ cm^{-3} and $4x10^{20}$ cm^{-3} were incorporated into the a-Si:H solar cell, respectively. Furthermore, we measured the FT-IR spectrum of a-Si:H film deposited at a pressure of 0.1 Torr, as shown in Fig. 3-3. It was found from this result that the peak at 2100 cm^{-1} was a dominant peak in this a-Si:H film. The peak at 2100 cm^{-1} which originates from Si-H_2 bonding is undesirable for the high quality a-Si:H film.[8, 9] Therefore, such a high concentration of impurities and/or Si-H_2 bonding might be the reasons for the low conversion efficiency of the solar cell. On the other hand, Jsc and F.F. in the a-Si solar cell deposited at a lower deposition pressure of 22 mTorr were 8.4 mA/cm^2 and 0.58, respectively. As the result, the conversion efficiency increased to 4.3%, as shown in Fig. 3-4. We measured the FT-IR spectrum of a-Si:H film deposited at a pressure of 22 mTorr, as shown in Fig. 3-3. It was found from this result that the peak at 2000 cm^{-1} was a dominant peak in this a-Si:H film.

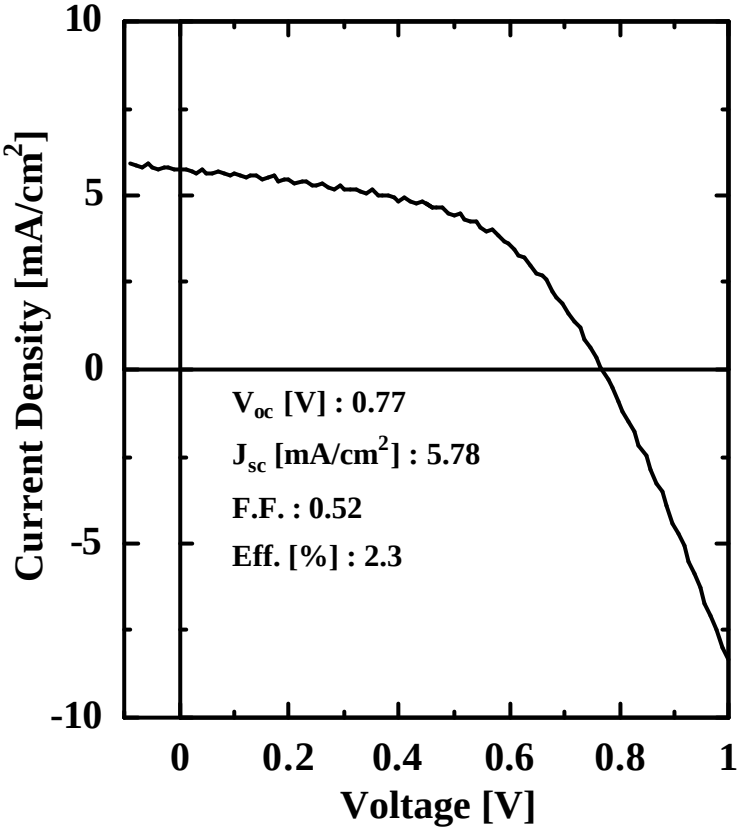

Fig. 3-1 I-V characteristics of a-Si:H solar cell deposited at a pressure of 0.1 Torr.

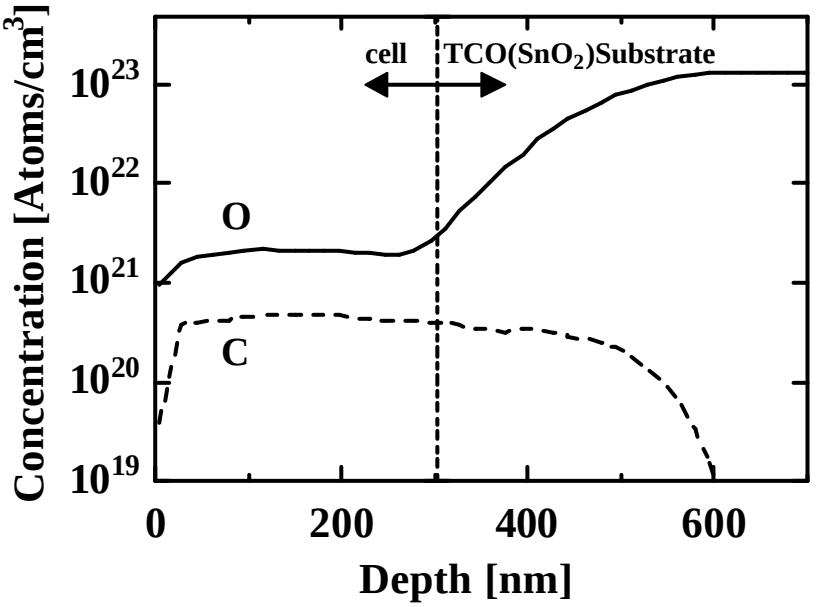

Fig. 3-2 Oxygen (O) and Carbon (C) SIMS depth profiles of a-Si:H solar cell on TCO (SnO_2) substrate.

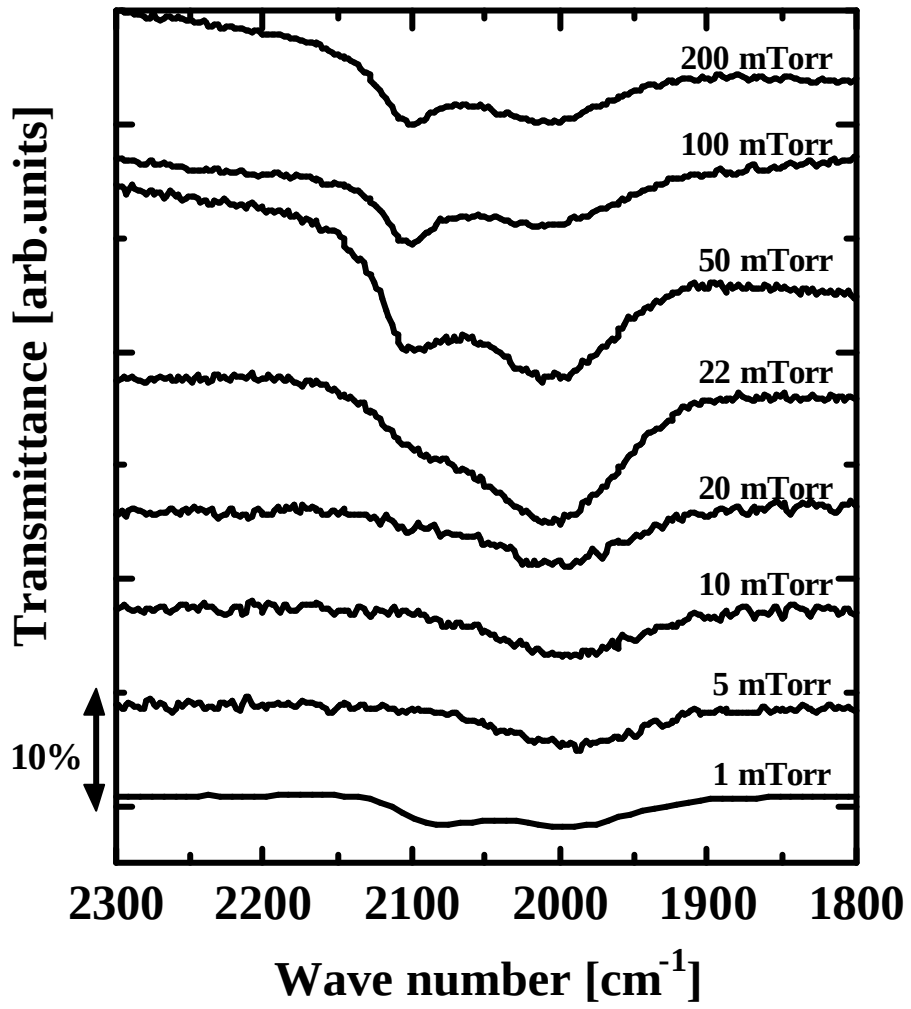

Fig. 3-3 FT-IR spectra of a-Si:H films as a function of deposition gas pressure.

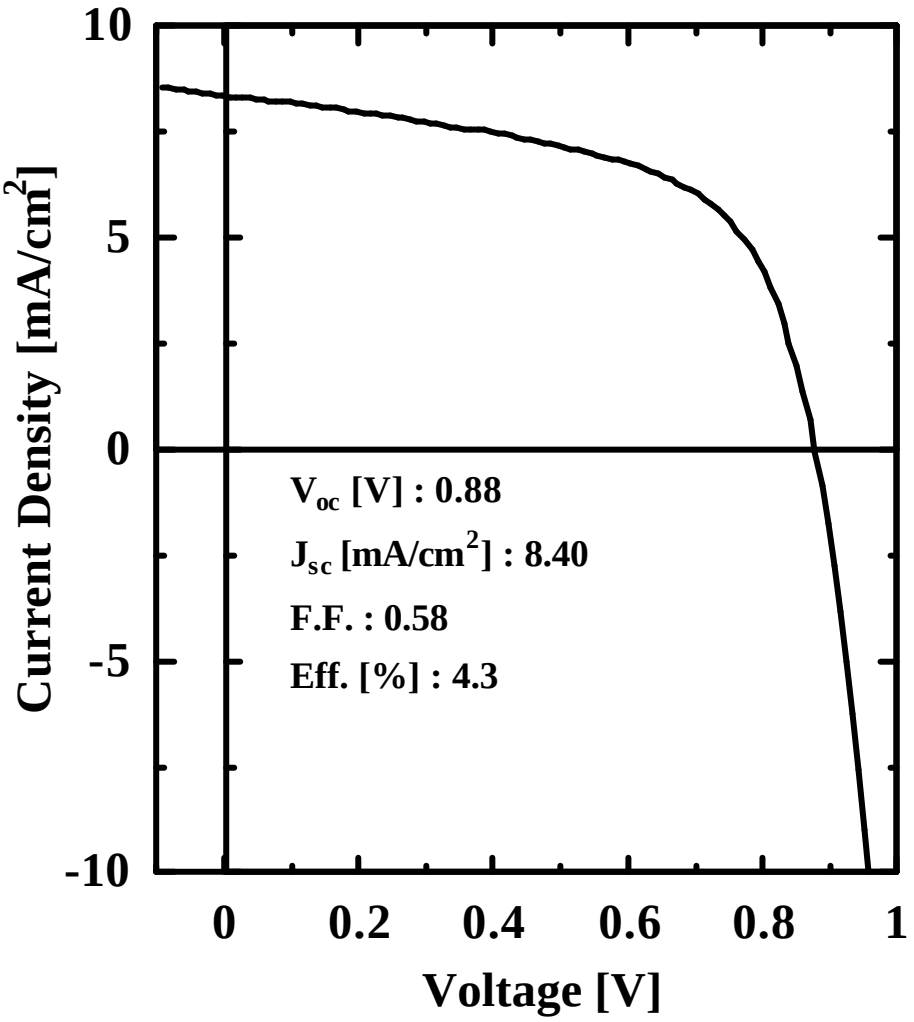

Fig. 3-4 I-V characteristics of a-Si:H solar cell deposited at a relatively low pressure of 22 mTorr.

These results imply that depositing a-Si:H films at a lower pressure can improve the film quality, therefore, we attempted to decrease the deposition pressure further, and investigate the film properties.

Figure 3-3 shows the dependence of FT-IR spectra of a-Si:H films on the deposition gas pressure. It is found from this result that the peak at 2100 cm^{-1} dramatically decreased with decreasing the deposition pressure from 200 mTorr to 5 mTorr. It is also found that the peak at 2100 cm^{-1} decreased and the Si-H stretching mode became a dominant peak when the samples were grown at the pressures of 5-20 mTorr, indicating the improvement of film quality at these pressures. The peak at 2100 cm^{-1} again increased at a low deposition pressure of 1 mTorr. First, this might be the reason that the real substrate temperature decreased because the thermal conduction between the substrate and the heater decreased at a low gas pressure. The peak at 2100 cm^{-1} increased at a low substrate temperature, as shown in Fig. 3-8. Therefore, it seems that the peak at 2100 cm^{-1} increased at a low deposition pressure. Second, atomic hydrogen generated on the filament is difficult to be consumed by the reactions with the other radicals in the gas phase, because the gas phase reaction is restrained at a low gas pressure. Therefore, atomic hydrogen was excessively supplied at a low pressure. On the other hand, in our previous works, it was already found that the peak at 2100 cm^{-1} in a-Si film increased with increasing the hydrogen dilution ratio and the peak at 2100 cm^{-1} became a dominant peak completely, when the film became μc-Si:H at a high hydrogen dilution ratio. From this result, it seems that the peak at 2100 cm^{-1} increased at a low deposition pressure of 1 mTorr because of the excess atomic hydrogen. Figure 3-5 shows the photo and dark conductivity as a function of the deposition gas pressure. The photoconductivity dramatically increased with decreasing the deposition gas pressure from 200 mTorr to 10 mTorr. As a result, the

photoconductivity of $6.5x10^{-5}$ S/cm was obtained at a low pressure of 10 mTorr. Therefore, it was found that the quality of a-Si:H could be greatly improved by decreasing the deposition gas pressure to 10 mTorr. On the other hand, the photoconductivity decreased at the deposition pressure of less than 10 mTorr. This might be the reason that the peak at 2100 cm^{-1} in the FT-IR spectra again increased at the low deposition pressure of 1 mTorr, as shown in Fig. 3-3. Then, we again measured the O and C concentrations in these films by SIMS analysis. Figure 3-6 shows the dependence of the concentrations of O and C atoms on the deposition gas pressure. For SIMS measurement, the first layer was grown at the pressure of 20 mTorr and it was decreased step by step. The lowest deposition gas pressure was 1 mTorr and then it was again increased up to 20 mTorr. The O and C concentrations of the sample were $2x10^{18}$ cm^{-3} and $1x10^{18}$ cm^{-3}, respectively. These values are comparable to those of films grown by PECVD with a super chamber system.[10] From these results, it was found that the deposition pressure should be decreased less than 20 mTorr. Since the evacuation speed is very high at a low deposition gas pressure, the concentrations of impurities such as O and C in the chamber are decreased. Therefore, the concentrations of impurities in a-Si film deposited at a pressure less than 20 mTorr are much fewer than that in a-Si film deposited at a high pressure of 0.1 Torr. Furthermore, the generation of undesirable radicals such as SiH_2, Si_2H_6, Si_3H_8 and so on, are suppressed due to the restraint of the gas phase reaction at a low deposition pressure. Therefore, the amount of $Si-H_2$ bonding and the concentration of O and C were reduced and photoconductivity increased at a low deposition pressure of 10 mTorr.

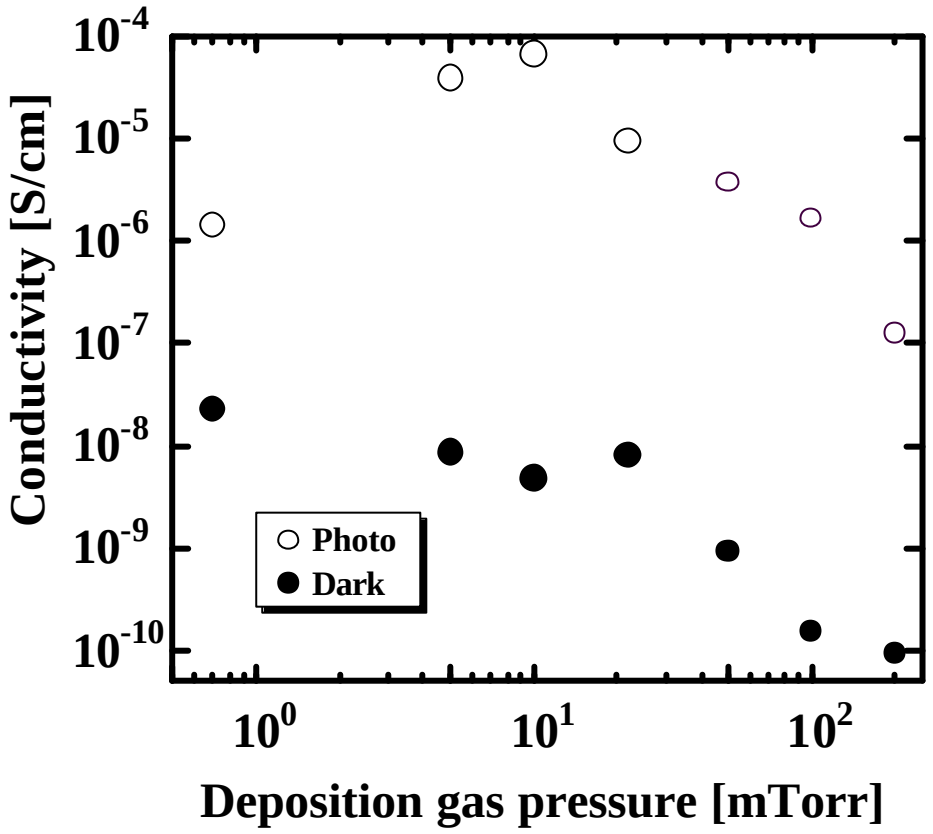

Fig. 3-5 Photo and dark conductivities of a-Si:H films as a function of deposition gas pressure.

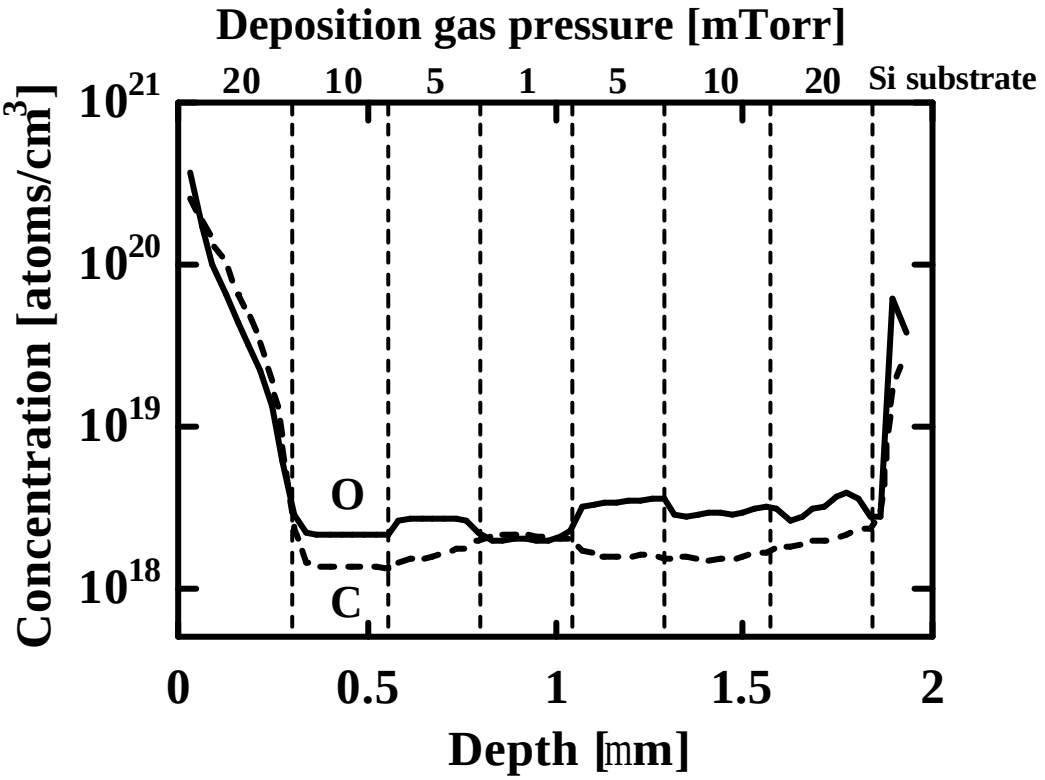

Fig. 3-6 Oxygen (O) and Carbon (C) SIMS depth profiles of a-Si:H film as a function of deposition gas pressure.

In order to find the more optimum deposition conditions, we deposited a-Si:H films at different substrate temperatures. In the experiment, the deposition pressure was fixed at 10 mTorr. Figure 3-7 shows the dependence of the photo and dark conductivity on the substrate temperature. The dark-conductivity was almost constant according to substrate temperatures. The photoconductivity of 6.5×10^{-5} S/cm was obtained at a substrate temperature of 200^{o}C. Figure 3-8 shows the dependence of FT-IR spectra on the substrate temperature. The hydrogen content of a-Si:H films decreased from 26% to 12.5% with increasing the substrate temperature from 150^{o}C to 270 ^{o}C. The peak at 2100 cm^{-1} also decreased with increasing the substrate temperature. At a low substrate temperature less than 200^{o}C, it could be speculated that the migration of film precursors was not enough on the growing surface, therefore, Si-H_2 bonding and dangling bond density increased with decreasing substrate temperature. On the other hand, at a high substrate temperature over 200^{o}C, the hydrogen content decreased and it is not enough for passivating the dangling bond. Therefore, the photoconductivity decreased with increasing the substrate temperature over 200^{o}C.

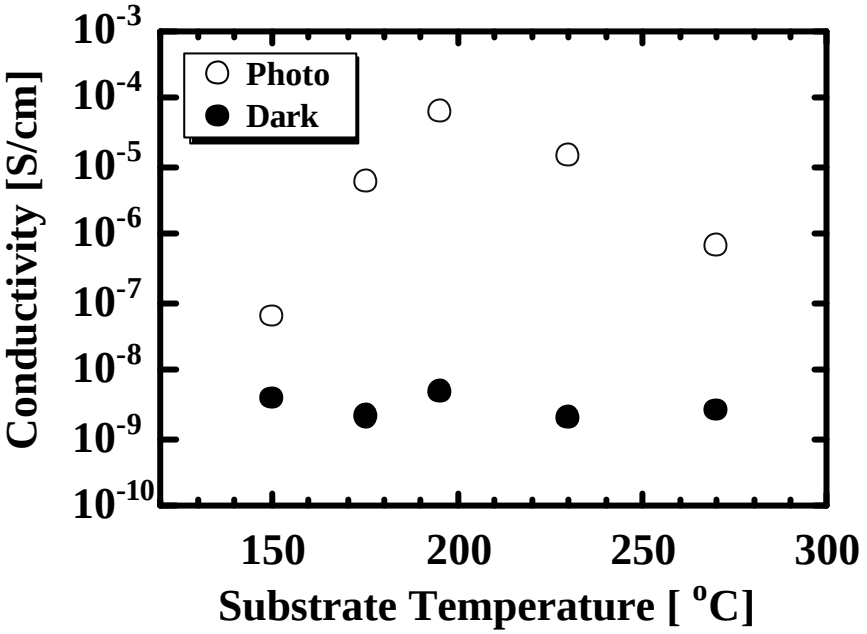

Fig. 3-7 Photo and dark conductivities of a-Si:H films as a function of substrate temperature.

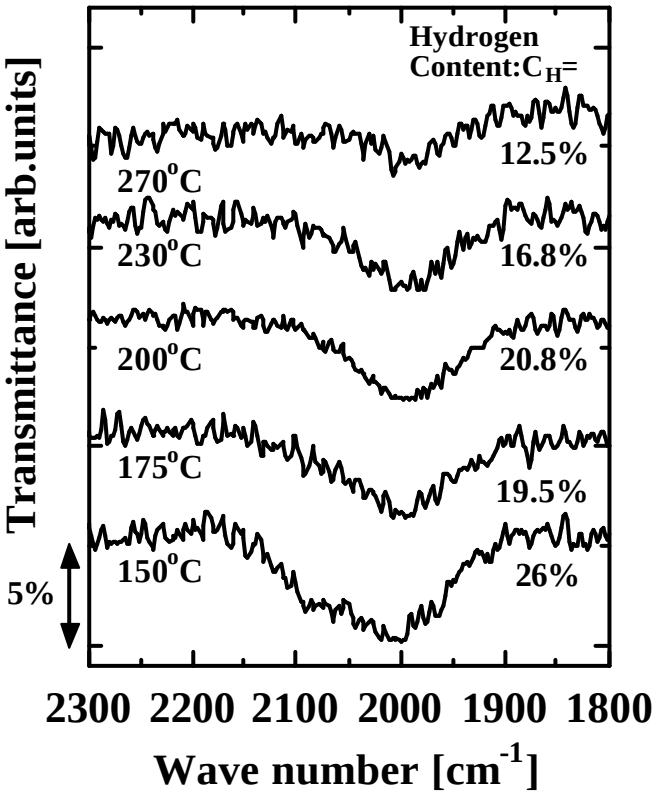

Fig. 3-8 FT-IR spectra of a-Si:H films as a function of substrate temperature.

3-3-2 Characterization of Amorphous Silicon Solar Cells

Figure 3-9 shows the initial and stabilized I-V characteristics of the a-Si:H solar cell. An intrinsic a-Si:H layer was deposited at a gas pressure of 10 mTorr, filament temperature of 1900^{o}C, substrate temperature of 200^{o}C. The thickness and the deposition rate of i-layer were 250 nm and 0.4 nm/s, respectively. The initial conversion efficiency of 7.5% could be achieved. However, Voc and FF were 0.78 V and 0.66, respectively. Therefore, in order to achieve higher conversion efficiency, it is necessary to improve the quality of intrinsic a-Si:H layer, p-layer and p/i interface. After light soaking, the stabilized conversion efficiency of 6.3% was obtained and the Voc increased from 0.78 V to 0.82 V. This kind of result is similar to that of a-Si:H solar cell deposited by photo-CVD with H_2 dilution.[11] Therefore, the phenomena seems due to the hydrogen dilution effect on the film property because of the high generation rate of atomic hydrogen in the Hot Wire Cell method. Up to now, the initial conversion efficiency of 7.75% (Voc=0.84V, Jsc=13.5mA/cm^2, F.F.=0.68) was achieved.

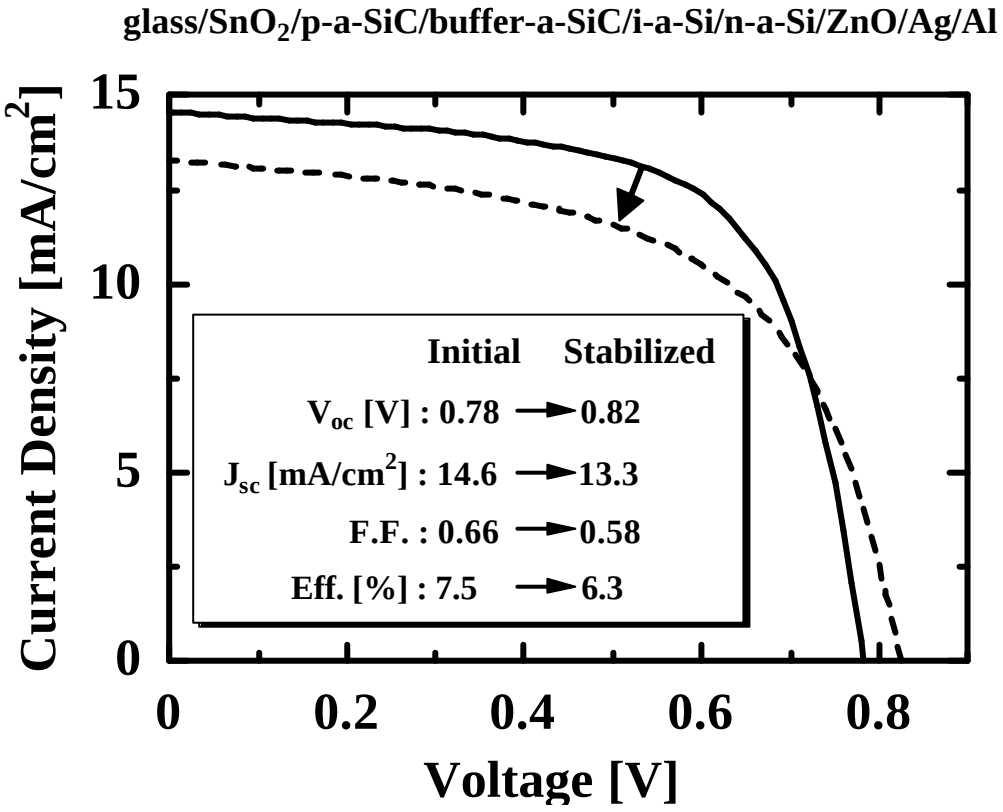

Fig. 3-9 Initial and stabilized I-V characteristics of the superstrate pin a-Si:H solar cell prepared by Hot Wire Cell method.

3-3-3 High Rate Deposition of Amorphous Silicon Thin Films and Solar Cells

Next, we tried to deposit a-Si:H films at high deposition rates. In our previous works, it was found that the deposition rate proportionally increased with increasing the flow rate of SiH_4.[12] However, from the viewpoint of gas usage, it is better to obtain high deposition rate at a low flow rate of SiH_4. Furthermore, it was found that the deposition at a low pressure was effective in improving the film quality because of the restraint of the gas phase reaction. We thought that the gas phase reaction was very important and the radicals reaching the growing surface might be much influenced by the distance between the filament and the substrate because the gas phase reaction is changed by the distance. Therefore, we changed the filament-substrate distance as another way of achieving a high deposition rate with maintaining the film quality.

Figure 3-10 shows the dependence of deposition rate of a-Si:H film on the filament-substrate distance. It was found that the deposition rate proportionally increased with decreasing the filament-substrate distance. The deposition rate of 1.5 nm/s could be achieved at the filament-substrate distance of 1.5 cm. This result is attributed to the increase of radical density by decreasing the filament-substrate distance. In order to investigate the film quality of these films, we measured photo and dark conductivity and FT-IR spectra of these a-Si:H films.

Figures 3-11 and 3-12 are dependence of photo and dark conductivity and FT-IR spectra on filament-substrate distance, respectively. From the result of conductivity measurement, the dark-conductivity was almost constant, however, the photoconductivity largely decreased with decreasing the filament-substrate distance from 3 cm to 1.5 cm.

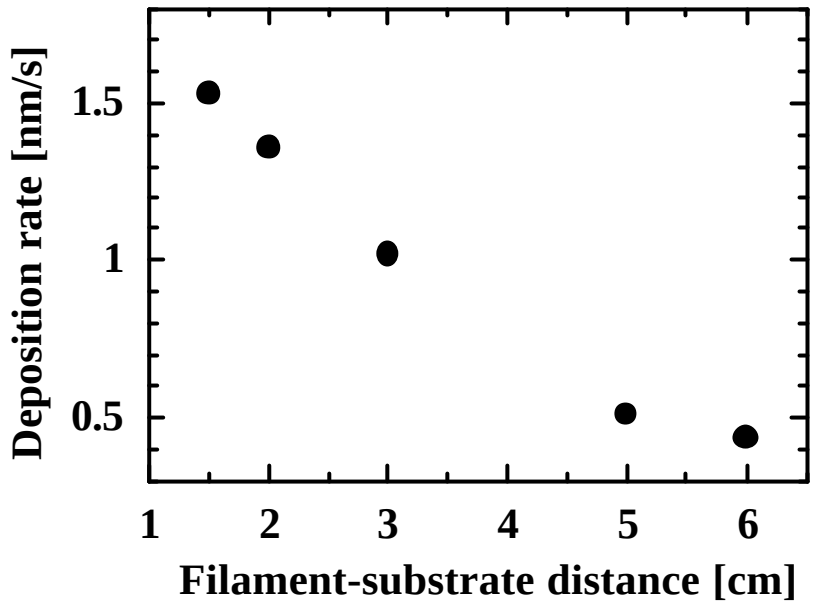

Fig. 3-10 Deposition rate of a-Si:H film as a function of filament-substrate distance.

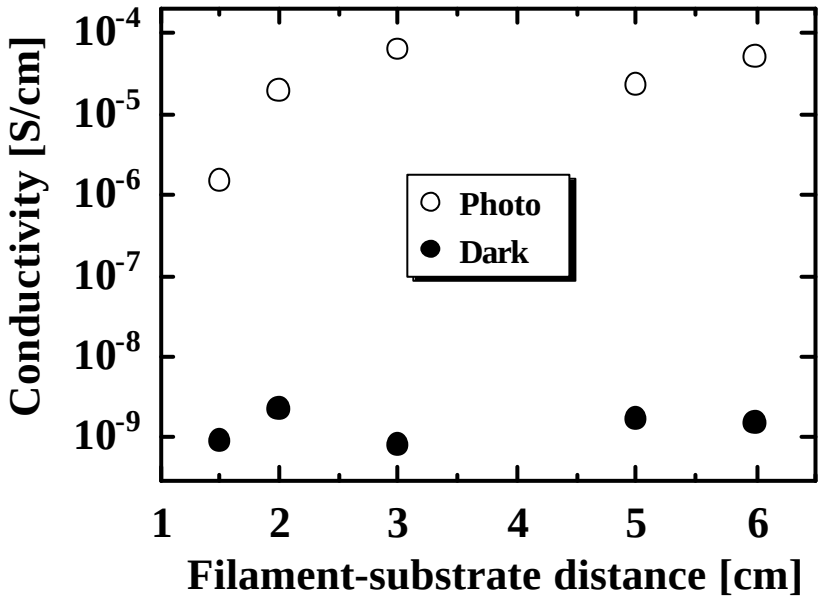

Fig. 3-11 Photo and dark conductivities of a-Si:H films as a function of filament-substrate distance.

The reason is clear in Fig. 3-12, since the peak at 2100 cm^{-1} increased with decreasing the filament-substrate distance from 3 cm to 1.5 cm. At the filament-substrate distance of 3 cm, in spite of the high deposition rate of 1 nm/s, a high photoconductivity and a dominant peak at 2000 cm^{-1} could be obtained. The reason of the degradation of film quality at the short distance might be attributed to the insufficient migration of radicals on the growing surface due to the high deposition rate and due to the undesirable radicals near the filament. In order to investigate the film quality of these a-Si:H films, solar cells were fabricated by using these films for i-layer. An intrinsic a-Si:H layer was deposited at a gas pressure of 5 mTorr and filament-substrate distance of 3 cm. The thickness and the deposition rate of i-layer were 280 nm and 1 nm/s, respectively. As a preliminary result, the initial conversion efficiency of 5.5% was achieved, as shown in Fig. 3-13. Comparing to a-Si:H solar cell deposited at a deposition rate of 0.4 nm/s, Voc and Jsc were almost same, however, F.F. was as low as 0.53. The cell performance might be much improved by optimizing the deposition conditions of p and i layer.

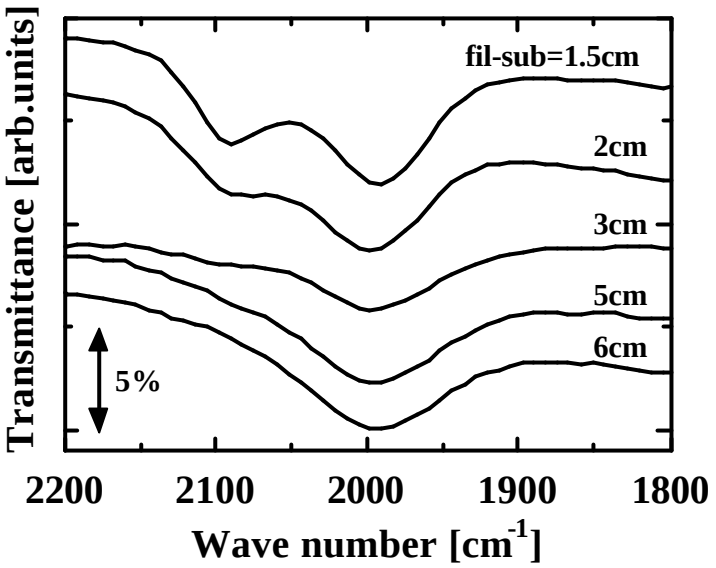

Fig. 3-12 FT-IR spectra of a-Si:H films as a function of filament-substrate distance.

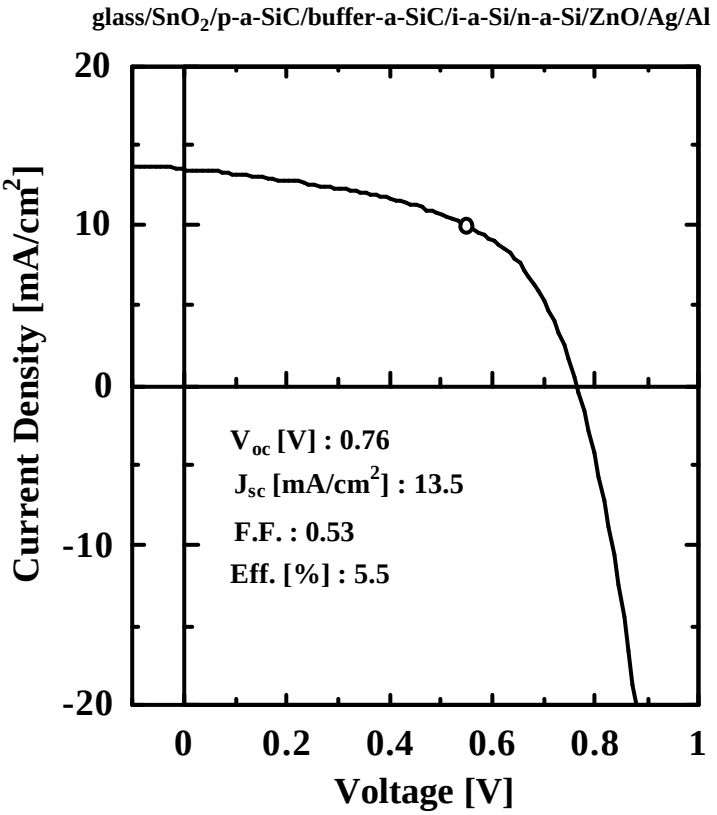

Fig. 3-13 I-V characteristics of a-Si:H solar cell deposited at a growth rate of 1 nm/s.

3-4 Summary

A-Si:H films were deposited by the Hot Wire Cell method and it was found that the deposition at a low pressure was effective in improvement of the quality of a-Si:H films. We could succeed in reducing $Si-H_2$ bonding and the concentrations of O and C atoms to the order of 10^{18} cm^{-3} at the deposition pressures of 1-10 mTorr, and the photoconductivity of $6.5x10^{-5}$ S/cm could be obtained. The initial and stabilized conversion efficiency of 7.5% and 6.3% with the deposition rate of 0.4 nm/s were achieved for superstrate pin a-Si:H solar cell. It was also found that the short filament-substrate distance was effective for the high deposition rate with maintaining film quality. We could succeed in obtaining the high photoconductivity and the dominant peak at 2000 cm^{-1} in FT-IR spectra with a high deposition rate of 1 nm/s at a pressure of 5 mTorr and a filament-substrate distance of 3 cm. The initial conversion efficiency of 5.5% with the deposition rate of 1 nm/s was achieved for superstrate pin a-Si:H solar cell.

References

[1] B. Schroeder: Thin Solid Films **430** (2003) 1.

[2] Y. Tawada, H. Yamagishi and K. Yamamoto: Solar Energy Materials & Solar Cells **78** (2003) 647.

[3] A. Shah, J. Meier, E. Vallat-Sauvain, C. Droz, U. Kroll, N. Wyrsch, J. Guillet and U. Graf: Thin Solid Films **403-404** (2002) 179.

[4] M. Ichikawa, J. Takeshita, A. Yamada and M. Konagai: Jpn. J. Appl. Phys. **38** (1999) L24.

[5] M. Ichikawa, J. Takeshita, A. Yamada and M. Konagai: Mat. Res. Soc. Symp. **557** (1999) 531.

[6] M. Konagai, T. Tsushima, M. K. Kim, K. Asakusa, A. Yamada, Y. Kudriavtsev, A. Villegas and R. Asomoza: Thin Solid Films **395** (2001) 152.

[7] K. Dairiki, A. Yamada and M. Konagai: Jpn. J. Appl. Phys. **38** (1999) 4007.

[8] T. Nishimoto, M. Takai, H. Miyahara, M. Kondo and A. Matsuda: J. Non-Cryst. Solids **299-302** (2002) 1116

[9] T. Takagi, R. Hayashi, G. Ganguly, M. Kondo and A. Matsuda: Thin Solid Films **345** (1999) 75

[10] S. Tsuda, T. Takahana, M. Isomura, H. Tarui, Y. Nakahima, Y. Hishikawa, N. Nakamura, T. Matsuoka, H. Nishiwaki, S. Nakano, M. Ohnishi and Y. Kuwano: Jpn. J. Appl. Phys. **26** (1987) 33.

[11] P. Siamchai and M. Konagai: Appl. Phys. Lett. **67** (1995) 3468

[12] M. Ichikawa, T. Tsushima, A. Yamada and M. Konagai: Sol. Energy.Mater. **66** (2001) 225.

Chapter4

Theoretical Analysis of Microcrystalline Silicon Thin Film Solar Cells

4-1 Introduction

Our group has been studied a-Si:H materials and solar cells for around 20 years and a stabilized conversion efficiency of 9.0% has been achieved by using photo-CVD method.[1)] Therefore, the fundamental technique for solar cell fabrication including p-a-SiC:H, buffer-a-SiC:H, n-a-Si:H, ZnO, Ag and Al electrode was established. However, in the initial stage of this study, we didn't have any knowledge and technique for microcrystalline silicon (μc-Si:H) solar cells. Therefore, it was required to be confirmed if p-a-SiC:H and n-a-Si:H were suitable for μc-Si:H thin film solar cells. If p-a-SiC:H and n-a-Si:H were not suitable, the other materials as p-layer and n-layer were required to be found and investigated. Thus, first, p-layer and n-layer materials such as p-a-SiC:H, p-a-Si:H, p-μc-Si:H, n-a-Si:H and n-μc-Si:H were investigated by theoretical analysis. In the theoretical analysis, these materials were applied to a μc-Si:H solar cell, their suitability was examined. For the theoretical analysis, AMPS-1D BETA 1.00 (a one-dimensional device simulation program for the Analysis of Microelectronic and Photonic Structures) was used. Next, effects of i-layer film properties on solar cell performances were also investigated by theoretical

analysis. The i-layer is an active absorber layer and it is most significant layer for solar cells and investigating the effects of i-layer film properties such as defect densities and impurity concentrations on solar cell performances are necessary for fabricating high efficiency solar cells.

4-2 Calculation for Solar Cell Performances by Using AMPS-1D

The theoretical analysis was carried out by using AMPS-1D BETA 1.00 (a one-dimensional device simulation program for the Analysis of Microelectronic and Photonic Structures). AMPS-1D was developed with the support of the Electric Power Research Institute and equipment support by IBM. AMPS-1D is the creation of Professor Stephen J. Fonash and his students. AMPS-1D is one-dimensional computer program for simulating transport physics in solid-state devices. It uses the first-principles and Poisson's equations approach to analyze the transport behavior of semiconductor electronic and opt electronic device structures. These device structures can be composed of crystalline, polycrystalline, or amorphous materials or combinations thereof. AMPS-1D numerically solves the three governing semiconductor device equations (the Poisson equation and the electron and hole continuity equations) without making any a-priori assumptions about the mechanisms controlling transport in these devices. With this general and exact numerical treatment, AMPS-1D may be used to examine a variety of device structures including homojunction and heterojunction p-n and p-i-n solar cells and detectors. Fundamental formulas of AMPS-1D are described as follows:

Poisson's equation is given by

$$\frac{d}{dx}\left(e(x)\frac{dy}{dx}\right)=q\cdot\left[p(x)-n(x)+N_D^+(x)-N_A^-(x)+p_t(x)-n_t(x)\right] \quad (4\text{-}1)$$

where the electrostatic potential y and the free electron n, free hole p, trapped electron n_t, and trapped hole p_t, as well as the ionized donor-like doping N_D^+ and ionized acceptor-like N_A^- doping concentrations are all functions of the position of the position coordinate x. Here, e is the permittivity and q is the magnitude of the charge of an electron. The free electron n, free hole p concentrations are given by

$$n=N_C\cdot F_{1/2}\exp\left(\frac{E_F-E_C}{kT}\right) \quad (4\text{-}2a)$$

$$p=N_V\cdot F_{1/2}\exp\left(\frac{E_V-E_F}{kT}\right) \quad (4\text{-}2b)$$

In these equations, N_C and N_V are the band effective densities of states for the conduction and valence bands, respectively. The Fermi integral of order one-half appearing in Equation 4-2a and b is defined as

$$F_{1/2}(h)=\frac{2}{\sqrt{p}}\int_0^\infty\frac{E^{1/2}dE}{1+\exp(E-h)} \quad (4\text{-}3)$$

where h - the Fermi integral argument – is expressed as

$$h_n=\left(\frac{E_F-E_C}{kT}\right) \quad (4\text{-}4a)$$

for free electrons and

$$h_p=\left(\frac{E_V-E_F}{kT}\right) \quad (4\text{-}4b)$$

for free holes.

The total charge arising in localized doping levels including gap states can be represented by

$$N_D^+ = N_{dD}^+ + N_{bD}^+ \tag{4-5a}$$

for the donor-dopant levels and

$$N_A^- = N_{dA}^- + N_{bA}^- \tag{4-5b}$$

for the acceptor-dopant levels. Here, N_D^+ and N_A^- seen in Poisson's equation (Equation 4-1), are the total charges arising from both the discrete and banded dopant energy levels. In these equations, N_{dD}^+ and N_{dA}^- represent the total charge originating from discrete donor and acceptor concentrations, respectively, while N_{bD}^+ and N_{bA}^- represent the total charge developed by any banded donor and acceptor levels, respectively.

The total charge arising in defect levels can be represented by

$$p_t = p_{d_t} + p_{b_t} + p_{c_t} \tag{4-6a}$$

for the donor-like states and

$$n_t = n_{d_t} + n_{b_t} + n_{c_t} \tag{4-6b}$$

for the acceptor-like states. Here, the p_t and n_t seen in Poisson's equation (Equation 4-1), are the total charges arising from the discrete, banded and continuous defect (structural or impurity) energy levels. In these equations, n_{d_t} and p_{d_t} represent the total charge, originating respectively from discrete acceptor and donor concentrations, while n_{b_t} and p_{b_t}, respectively, represent the total charge developed by any banded acceptor and donor concentrations. Finally, n_{c_t} and p_{c_t}, respectively represent the total charge developed by any continuous (exponential, Gaussian, or constant) acceptor and donor concentrations.

Above formulas has provided expressions for all the quantities contributing to the charge in Poisson's equation. A close inspection of these expressions shows that

they all are ultimately defined in terms of the free carrier populations n and p. Now, more information on n and p is required to determine how they change across a device and under different biases. The equations that keep track of the conduction band electrons and valence band holes are the continuity equations. In steady state, the time rate of change of free carrier concentrations is equal to zero. As a result, the continuity equation for the free electrons in the delocalized states of the conduction band has a form

$$\frac{1}{q}\left(\frac{dJ_n}{dx}\right) = -G_{op}(x) + R(x) \qquad \text{(4-7a)}$$

and the continuity equation for the free holes in the delocalized states of valence band has the form

$$\frac{1}{q}\left(\frac{dJ_p}{dx}\right) = G_{op}(x) - R(x) \qquad \text{(4-7b)}$$

where J_n and J_p are, respectively, the electron and hole current densities. The term $R(x)$ is the net recombination rate resulting from band-to-band (direct) recombination and S-R-H (indirect) recombination traffic through gap states. The term $G_{op}(x)$ is the optical generation rate as a function of x due to externally imposed illumination. The electron current density J_n can always be expressed as

$$J_n(x) = q\mu_n n\left(\frac{dEf_n}{dx}\right) \qquad \text{(4-8a)}$$

where μ_n is the electron mobility and n is defined in Equation 4-2a.

The hole current density J_n can always be expressed by

$$J_p(x) = q\mu_p p\left(\frac{dEf_p}{dx}\right) \qquad \text{(4-8b)}$$

where μ_p is the hole mobility and p is defined in Equation 4-2b.

There are two basic processes by which electrons and holes may recombine with each other. In the first process, electrons in the conduction band make direct transitions to vacant states in the valence band. This process is labeled as band-to-band or direct recombination R_D (also known as intrinsic recombination). In the second process, electrons and holes recombine through intermediate gap states known as recombination centers. This process, originally investigated by Shockley, Read, and Hall, is labeled indirect recombination R_I or S-R-H recombination (also known as extrinsic recombination). The net recombination term $R(x)$ in the continuity equations takes both of these processes into consideration such that

$$R(x) = R_D(x) + R_I(x) \tag{4-9}$$

The net direct recombination rate can be expressed by

$$R_D(x) = b(np - n_0 p_0) = b(np - n_i^2) \tag{4-10}$$

where b is a proportionality constant which depends on the energy-band structure of the material under analysis. The n_0 and p_0 factors are the carrier concentrations in thermodynamic equilibrium, expressed by Equations 4-2a and b.

The S-R-H net recombination can be expressed by

$$R_I(x) = \frac{(np - n_0 p_0)}{t_{p0}(n + n_t) + t_{n0}(p + p_t)} \tag{4-11}$$

where t_{p0} and t_{n0} are short hand for reciprocals of the thermal velocity-hole/electron capture cross section and Nt product. The quantities n_t and p_t depends exponentially on the position of the defects in the energy band gap.

It is assumed that a structure illuminated by a light source of frequency n_i with a photon flux of $\Phi_{0i}(n_i)$ (in units of photons per unit area per unit time) has photons obeying $hn \geq E_{gop}$. This photon flux $\Phi_{0i}(n_i)$ is impinging at $x = 0$. As the photon flux travels through the structure, the rate at which electron-hole pairs are

generated is proportional to the rate at which the photon flux decreases. Therefore, the optical generation rate can be expressed as

$$G_{op}(x) = \frac{-d}{dx}\sum_i \Phi_i^{FOR}(n_i) + \frac{d}{dx}\sum_i \Phi_i^{REV}(n_i) \quad (4\text{-}12)$$

where $\Phi_i^{FOR}(n_i)$ represents the photon flux of frequency n_i at some points x which is moving left to right (forward), and $\Phi_i^{REV}(n_i)$ represents the photon flux of frequency n_i at some points x which is moving right to left (reverse). If a device has optical properties that do not vary across the structure then, at some general points x, we have

$$\Phi_i^{FOR}(n_i) = \Phi_{0i}(n_i) \bullet \{\exp[-a(n_i)x] + R_F R_B[\exp(-a(n_i)L)]^2 \bullet \exp[-a(n_i)x] + \ldots\} \quad (4\text{-}13)$$

whereas

$$\Phi_i^{REV}(n_i) = R_B\Phi_{0i}(n_i) \bullet \{\exp[-a(n_i)L] \bullet \exp[-a(n_i)(L-x)] + R_F R_B[\exp(-a(n_i)L)]^3 \bullet \exp[-a(n_i)(L-x)] + \ldots\} \quad (4\text{-}14)$$

In these expressions, R_F is the reflection coefficient for the internal surface at $x = 0$ and R_B is the reflection coefficient for the internal surface at $x = L$ (the back surface). All of these reflection coefficients can be functions of the frequency n_i.

AMPS-1D can also take into consideration the acceptor-like, donor-like band tail states and the acceptor-like and donor-like Gaussian dangling bond states. The acceptor-like, donor-like band tail states are respectively expressed as

$$g_A(E) = g_A \cdot \exp\{-(E_C - E)/E_A\} \quad (4\text{-}15)$$

$$g_D(E) = g_D \cdot \exp\{-(E - E_V)/E_D\} \quad (4\text{-}16)$$

where E_A and E_D are the characteristic energy.

The acceptor-like and donor-like Gaussian dangling bond states are respectively expressed as

$$g_{AG}(E) = \left(\frac{N_{AG}}{\sqrt{2p}\, s_{AG}^{2}} \right) \cdot \exp\left(- \frac{(E - E_{AG})^2}{2 s_{AG}^{2}} \right) \quad (4\text{-}17)$$

$$g_{DG}(E) = \left(\frac{N_{DG}}{\sqrt{2p}\, s_{DG}^{2}} \right) \cdot \exp\left(- \frac{(E - E_{DG})^2}{2 s_{DG}^{2}} \right) \quad (4\text{-}18)$$

s_{AG} and s_{DG} are the standard deviations of the acceptor-like and donor-like Gaussian dangling bond states, respectively.

The material parameters of p-layer, i-layer and n-layer used for AMPS-1D are general parameters[2-8] for a-Si:H and μc-Si:H solar cells and shown in Tables 4-1, 4-2 and 4-3, respectively. Where N_C and N_V are effective density of states in the conduction band and valence band, respectively. f_b is $E_C - E_F$ at $x = 0$ (front-surface/p-layer interface) or at $x = L$ (n-layer/back-surface interface). g_A and g_D are prefactor in the equations 4-15and 4-16, respectively.

Table 4-1: The material parameters of p-layer used for AMPS-1D

	p-layer (p-a-SiC:H)	p-layer (p-a-Si:H)	p-layer (p-μc-Si:H)
Thickness [μm]	0.02	0.02	0.02
Carrier concentration [cm^{-3}]	$1x10^{19}$-$1x10^{21}$	$5x10^{18}$-$1x10^{20}$	$1x10^{17}$-$1x10^{20}$
N_C [cm^{-3}]	$3x10^{19}$	$3x10^{19}$	$3x10^{19}$
N_V [cm^{-3}]	$2x10^{19}$	$2x10^{19}$	$2x10^{19}$
ϕ_b [eV]	1.7	1.5	1.05
g_A/g_D [$cm^{-3}eV^{-1}$]	$5x10^{19}/5x10^{19}$	$5x10^{19}/5x10^{19}$	$5x10^{19}/5x10^{19}$
E_A/E_D [eV]	0.03/0.04	0.03/0.04	0.01/0.02
D-state density [cm^{-3}]	$5x10^{17}$	$2x10^{17}$	$1x10^{16}$
D^+-level (above E_V) [eV]	0.5	0.5	0.3
D^--level (below E_C) [eV]	0.5	0.5	0.3
Capture cross section			
$D^+ + e^- = D^o$ [cm^2]	$1x10^{-14}$	$1x10^{-14}$	$1x10^{-15}$
$D^o + h^+ = D^+$ [cm^2]	$1x10^{-15}$	$1x10^{-15}$	$1x10^{-16}$
$D^o + e^- = D^-$ [cm^2]	$1x10^{-15}$	$1x10^{-15}$	$1x10^{-16}$
$D^- + h^+ = D^o$ [cm^2]	$1x10^{-14}$	$1x10^{-14}$	$1x10^{-15}$
σ_{AG}/ σ_{DG} [eV]	0.09/0.09	0.09/0.09	0.13/0.13
Electron affinity χ [eV]	3.8	3.9	3.9
Dielectric constant	11.9	11.9	11.9
Mobility bandgap [eV]	1.95	1.7	1.1
Mobility μ_e/μ_h [$cm^2/V^{-1}/s^{-1}$]	5/0.7	10/1	50/5

Table 4-2: The material parameters of i-layer used for AMPS-1D

	i-layer (i-μc-Si:H)
Thickness [μm]	0.5-5.0
Carrier concentration [cm^{-3}]	$1x10^{10}$-$1x10^{18}$
N_C [cm^{-3}]	$3x10^{19}$
N_V [cm^{-3}]	$2x10^{19}$
ϕ_b [eV]	-
g_A/g_D [$cm^{-3}eV^{-1}$]	$5x10^{19}/5x10^{19}$
E_A/E_D [eV]	0.01/0.02
D-state density [cm^{-3}]	$1x10^{15}$-$1x10^{18}$
D^+-level (above E_V) [eV]	0.3
D^--level (below E_C) [eV]	0.3
Capture cross section	
$D^+ + e^- = D^o$ [cm^2]	$1x10^{-15}$
$D^o + h^+ = D^+$ [cm^2]	$1x10^{-16}$
$D^o + e^- = D^-$ [cm^2]	$1x10^{-16}$
$D^- + h^+ = D^o$ [cm^2]	$1x10^{-15}$
σ_{AG} / σ_{DG} [eV]	0.13/0.13
Electron affinity χ [eV]	3.9
Dielectric constant	11.9
Mobility bandgap [eV]	1.1
Mobility μ_e/μ_h [$cm^2/V^{-1}/s^{-1}$]	50/5

Table 4-3: The material parameters of n-layer used for AMPS-1D

	n-layer (n-a-Si:H)	n-layer (n-μc-Si:H)
Thickness [μm]	0.02	0.02
Carrier concentration [cm^{-3}]	$1x10^{17}$-$1x10^{19}$	$1x10^{17}$-$1x10^{20}$
N_C [cm^{-3}]	$3x10^{19}$	$3x10^{19}$
N_V [cm^{-3}]	$2x10^{19}$	$2x10^{19}$
ϕ_b [eV]	0.2	0.02
g_A/g_D [$cm^{-3}eV^{-1}$]	$5x10^{19}/5x10^{19}$	$5x10^{19}/5x10^{19}$
E_A/E_D [eV]	0.03/0.04	0.01/0.02
D-state density [cm^{-3}]	$2x10^{17}$	$1x10^{16}$
D^+-level (above E_V) [eV]	0.5	0.3
D^--level (below E_C) [eV]	0.5	0.3
Capture cross section		
$D^+ + e^- = D^o$ [cm^2]	$1x10^{-14}$	$1x10^{-15}$
$D^o + h^+ = D^+$ [cm^2]	$1x10^{-15}$	$1x10^{-16}$
$D^o + e^- = D^-$ [cm^2]	$1x10^{-15}$	$1x10^{-16}$
$D^- + h^+ = D^o$ [cm^2]	$1x10^{-14}$	$1x10^{-15}$
σ_{AG} / σ_{DG} [eV]	0.09/0.09	0.13/0.13
Electron affinity χ [eV]	3.9	3.9
Dielectric constant	11.9	11.9
Mobility bandgap [eV]	1.7	1.1
Mobility μ_e/μ_h [$cm^2/V^{-1}/s^{-1}$]	10/1	50/5

4-3 Results of Calculation

4-3-1 Effects of p-layer materials

In this section, effects of p-layer materials on solar cell performances were examined. As a n-layer, n-μc-Si:H was used, and p-a-SiC:H, p-a-Si:H and p-μc-Si:H were investigated in order to confirm if they were suitable p-layer materials for μc-Si:H thin film solar cells. As shown in Fig. 4-1, when the p-layer was p-a-SiC:H and p-a-Si:H, solar cell performances showed large dependence on the acceptor concentration of p-layer. On the other hand, when the p-layer was p-μc-Si:H, solar cell performances were constant at an acceptor concentration from $1x10^{20}$ cm^{-3} to $1x10^{17}$ cm^{-3}. In the case of p-a-SiC:H and p-a-Si:H, J_{sc} and F.F. largely decreased with decreasing the acceptor concentration less than $1x10^{19}$ cm^{-3}, as a result, conversion efficiency largely decreased at an acceptor concentration less than $1x10^{19}$ cm^{-3}. Therefore, in order not to decrease cell performances, the acceptor concentration of over $1x10^{20}$ cm^{-3} and $5x10^{19}$ cm^{-3} are required for p-a-SiC:H and p-a-Si:H, respectively. However, apart from an acceptor concentration of $5x10^{19}$ cm^{-3} for p-a-Si:H, an acceptor concentration of $1x10^{20}$ cm^{-3} is too high for p-a-SiC:H and it is not a practical value, because a general acceptor concentration for p-a-SiC:H is around $5x10^{18}$ cm^{-3}. An acceptor concentration of around $1x10^{19}$ cm^{-3} is a practical value for p-a-Si:H, however the increase of doping makes defect density increase, thus, a window of deposition parameters for obtaining high quality and high acceptor concentration at the same time is narrow. From these results, the most suitable p-layer material for μc-Si:H thin film solar cells is p-μc-Si:H. Therefore, in this study, p-μc-Si:H was used for fabrication of μc-Si:H thin film solar cells.

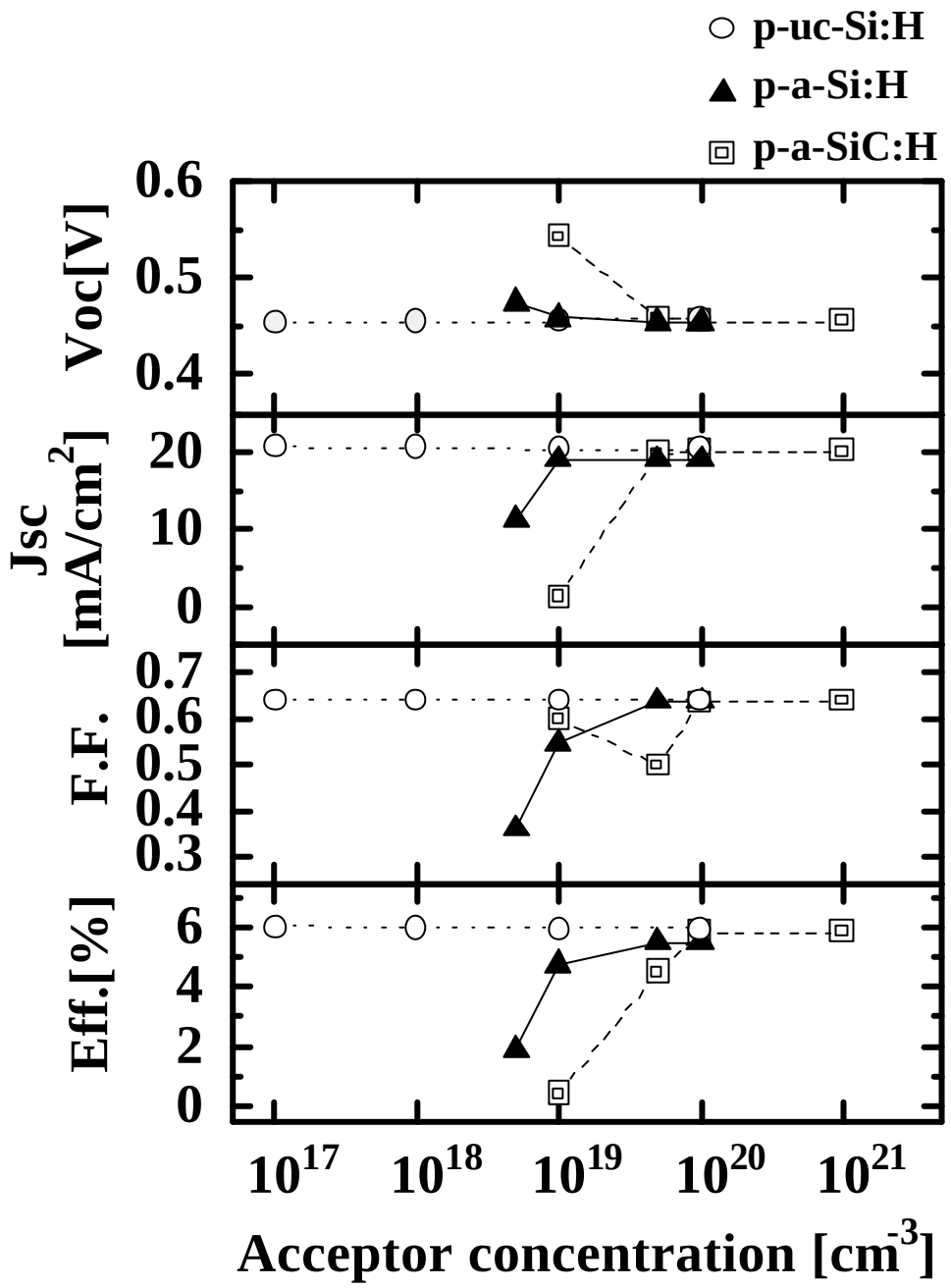

Fig. 4-1: Solar cell performances as a function of p-layer acceptor concentration in the case of p-μc-Si:H, p-a-Si:H, p-a-SiC:H

Next, in order to know the reasons for above results, band profiles and recombination rates of solar cells were investigated. As shown in Fig. 4-2, in the case of p-a-SiC:H, the electric field largely decreased with decreasing acceptor concentration less than $5x10^{19}$ cm^{-3}. One of the reasons for this decrease of the electric field might be thought that the activation energy of p-layer increased due to the low acceptor concentration. Besides, at each acceptor concentration, a band offset occurred at the valence band of the p/i interface due to the large difference of band gap, it might disturb a flow of holes. As shown in Fig. 4-3, the recombination rate in the whole i-layer region largely increased with decreasing acceptor concentration less than $5x10^{19}$ cm^{-3} due to the large decrease of the electric field in the i-layer. Especially in the region from p/i interface to the middle of i-layer, the recombination rate largely increased by 2 orders of magnitude. When the acceptor concentration was $1x10^{21}$ cm^{-3}, the recombination rate was as low as that of p-μc-Si:H in the whole i-layer region.

As shown in Fig. 4-4, in the case of p-a-Si:H, the electric field largely decreased with decreasing acceptor concentration less than $1x10^{19}$ cm^{-3}. This result is similar to that of p-a-SiC:H. A band offset also occurred at the valence band of the p/i interface due to the large difference of band gap, like in the case of p-a-SiC:H. As shown in Fig. 4-5, the recombination rate in the whole i-layer region largely increased with decreasing acceptor concentration less than $1x10^{19}$ cm^{-3} due to the large decrease of the electric field in the i-layer. Especially in the region from p/i interface to the middle of i-layer, the recombination rate largely increased by 2 orders of magnitude. When the acceptor concentration was $1x10^{20}$ cm^{-3}, the recombination rate was as low as that of p-μc-Si:H in the whole i-layer region.

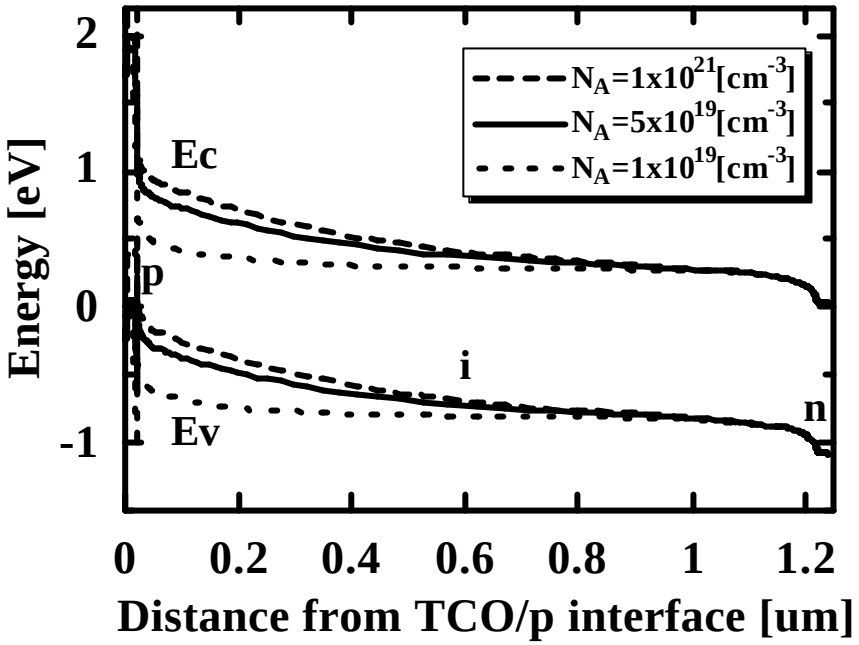

Fig. 4-2: Band profile of μc-Si:H thin film solar cell with p-a-SiC:H layer as a function of acceptor concentration

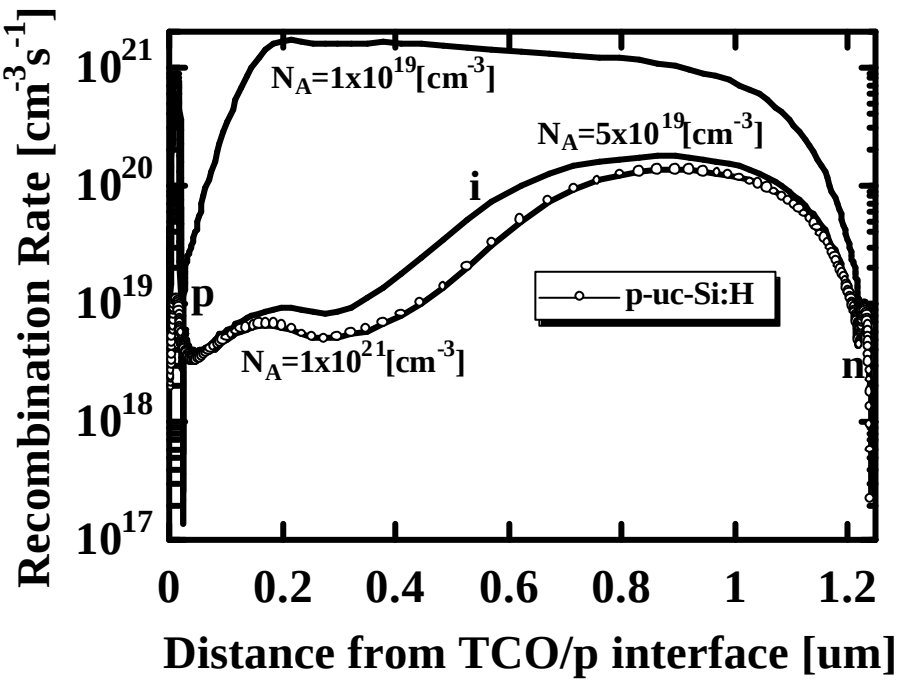

Fig. 4-3: Recombination rate of μc-Si:H thin film solar cell with p-a-SiC:H layer as a function of acceptor concentration

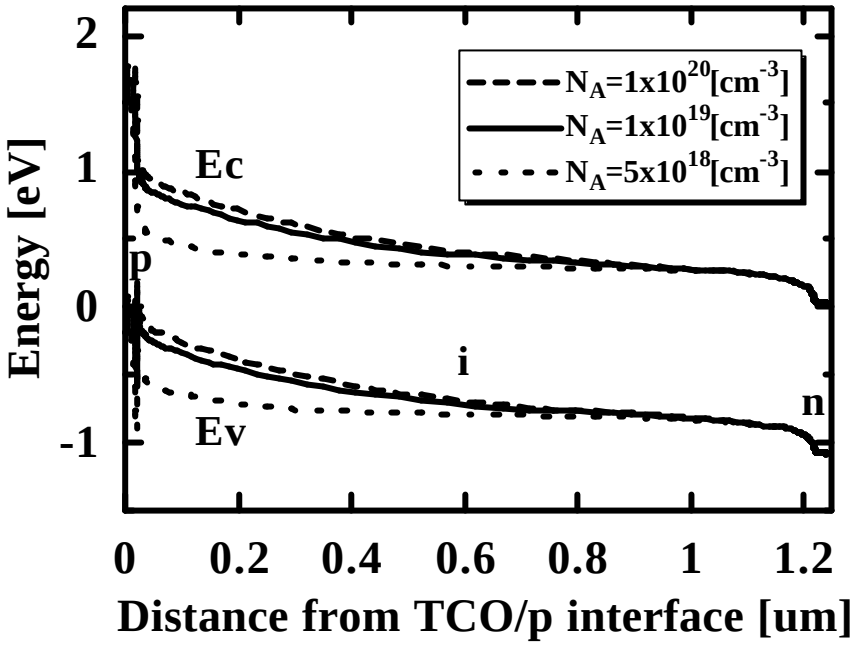

Fig. 4-4: Band profile of μc-Si:H thin film solar cell with p-a-Si:H layer as a function of acceptor concentration

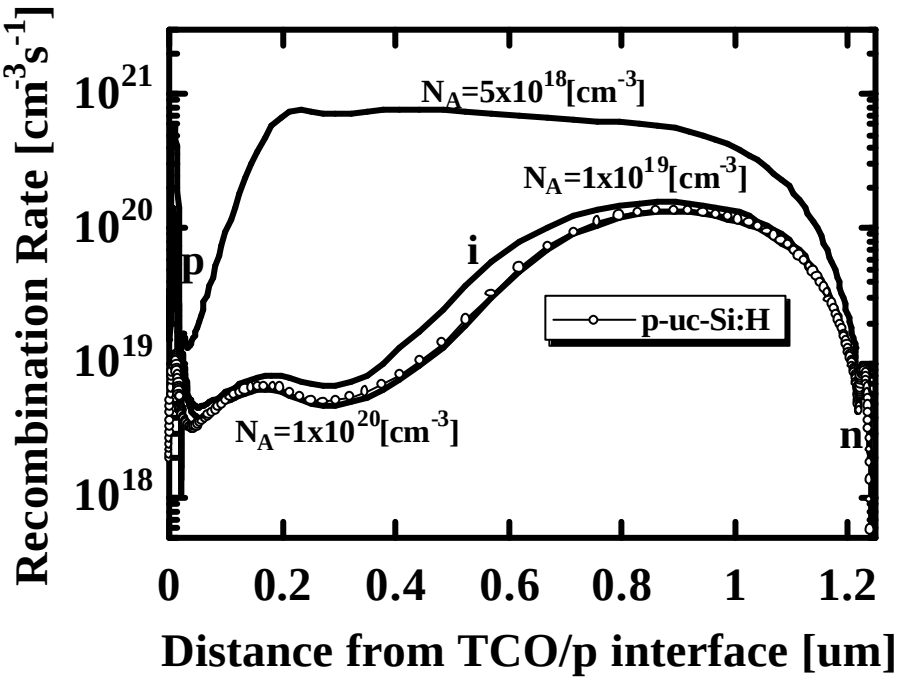

Fig. 4-5: Recombination rate of μc-Si:H thin film solar cell with p-a-Si:H layer as a function of acceptor concentration

4-3-2 Effects of n-layer materials

As above mentioned in 4-3-1, there was a large dependence of cell performances on p-layer materials. Especially when the p-layer was p-a-SiC:H and p-a-Si:H, solar cell performances showed large dependence on the acceptor concentration of p-layer. Therefore, in this section, n-a-Si:H and n-μc-Si:H were investigated in order to confirm if they were suitable n-layer materials for μc-Si:H thin film solar cells. From the results in 4-3-1, it was found that p-μc-Si:H was the most suitable material for the p-layer, thus, p-μc-Si:H was used for the theoretical analysis in this section. For both n-a-Si:H and n-μc-Si:H, donor concentration of n-layer was varied from $1x10^{17}$ cm^{-3} to $1x10^{20}$ cm^{-3}. In the case of both n-a-Si:H and n-μc-Si:H, no difference was observed in the solar cell performances at donor concentrations from $1x10^{17}$ cm^{-3} to $1x10^{20}$ cm^{-3}, as shown in Fig. 4-6. V_{oc}, J_{sc}, F.F. and conversion efficiency were constant for both n-a-Si:H and n-μc-Si:H. No difference was also observed in band profiles and recombination rates of solar cells for both n-a-Si:H and n-μc-Si:H. From these results, it is concluded that both n-a-Si:H and n-μc-Si:H can be used for μc-Si:H thin film solar cells. In our group, high quality n-a-Si:H films were already obtained by using photo-CVD method, therefore, n-a-Si:H prepared by photo-CVD was used for fabrication of μc-Si:H thin film solar cells in this study.

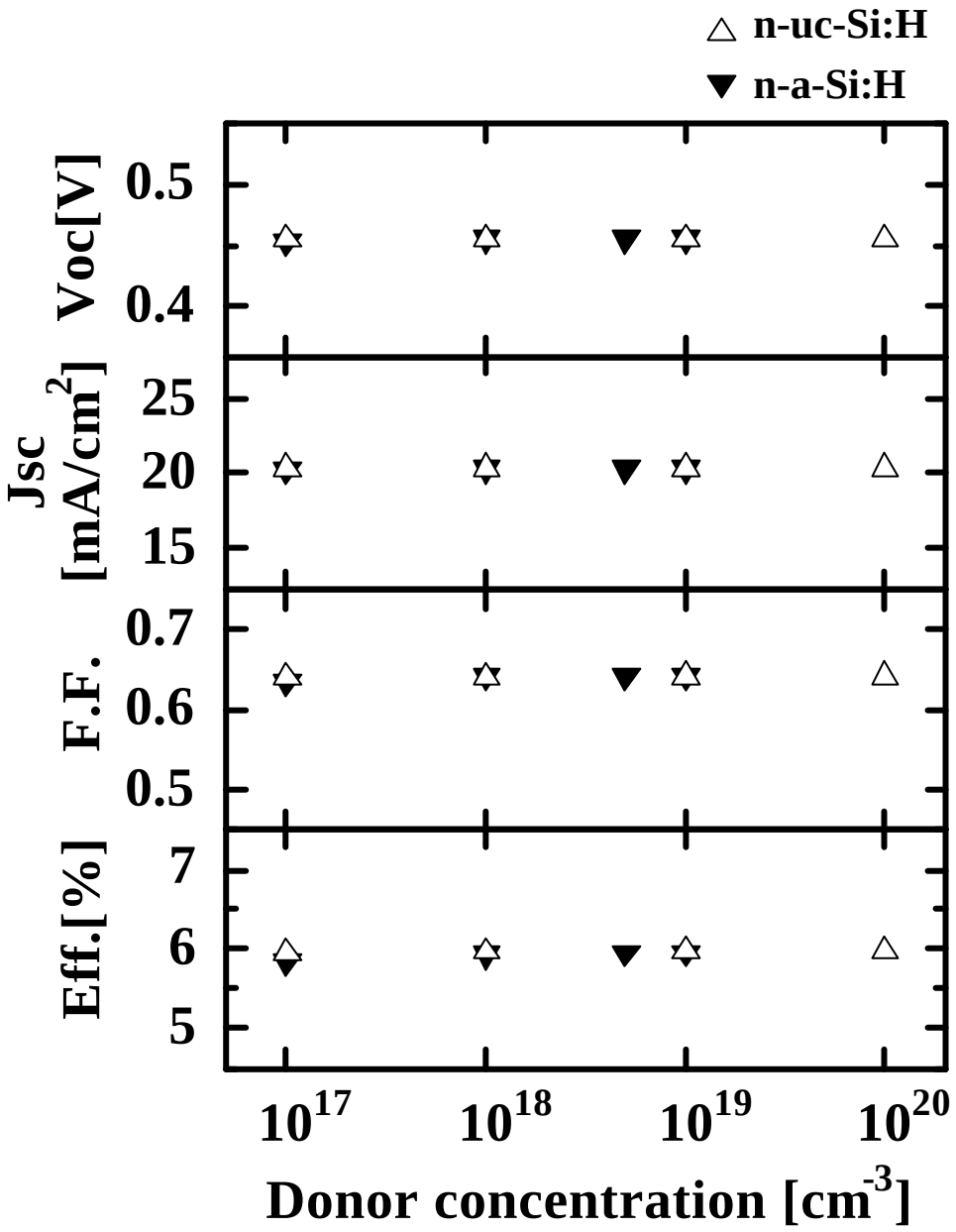

Fig. 4-6: Solar cell performances as a function of n-layer donor concentration in the case of n-μc-Si:H and n-a-Si:H

4-3-3 Effects of i-layer film properties

From the above results in 4-3-1 and 4-3-2, it was found that p-μc-Si:H is the most suitable material for p-layer and both n-a-Si:H and n-μc-Si:H can be used for μc-Si:H thin film solar cells. In this section, effects of i-layer film properties on solar cell performances were investigated. In the theoretical analysis, p-μc-Si:H and n-μc-Si:H were used for p-layer and n-layer of μc-Si:H thin film solar cells, respectively. First, effects of defect density of i-layer on cell performances were investigated. A thickness and impurity concentration of i-layer were fixed 1.2 μm and $1x10^{15}$ cm^{-3}, respectively. Defect densities were varied from $1x10^{15}$ cm^{-3} to $1x10^{18}$ cm^{-3}. As shown in Fig. 4-7, V_{oc}, F.F. and conversion efficiency largely decreased with increasing defect density from $1x10^{15}$ cm^{-3} to $1x10^{18}$ cm^{-3}. J_{sc} was almost constant at a defect density from $1x10^{15}$ cm^{-3} to $5x10^{16}$ cm^{-3}, and then it largely decreased with increasing defect density over $5x10^{16}$ cm^{-3}. The theoretical results show that if defect density can be reduced down to $1x10^{15}$ cm^{-3}, a conversion efficiency can be increased up to 9.4%. It was found that defect density is very effective in solar cell performances, and for obtaining high conversion efficiencies, defect density must be reduced less than $5x10^{15}$ cm^{-3}. In order to know the reasons for above results, band profiles and recombination rates of solar cells were investigated. As shown in Fig. 4-8, the homogeneous electric field was strongly formed in the whole i-layer region and it was almost same at defect densities of $1x10^{15}$ cm^{-3} and $1x10^{16}$ cm^{-3}, however, when the defect density increased to $1x10^{18}$ cm^{-3}, the electric field was strongly formed only at the p/i interface and it was almost zero in the whole i-layer region. Therefore, the large decrease of cell performances was caused by this weak electric field in the whole i-layer region at defect densities over $1x10^{16}$ cm^{-3}.

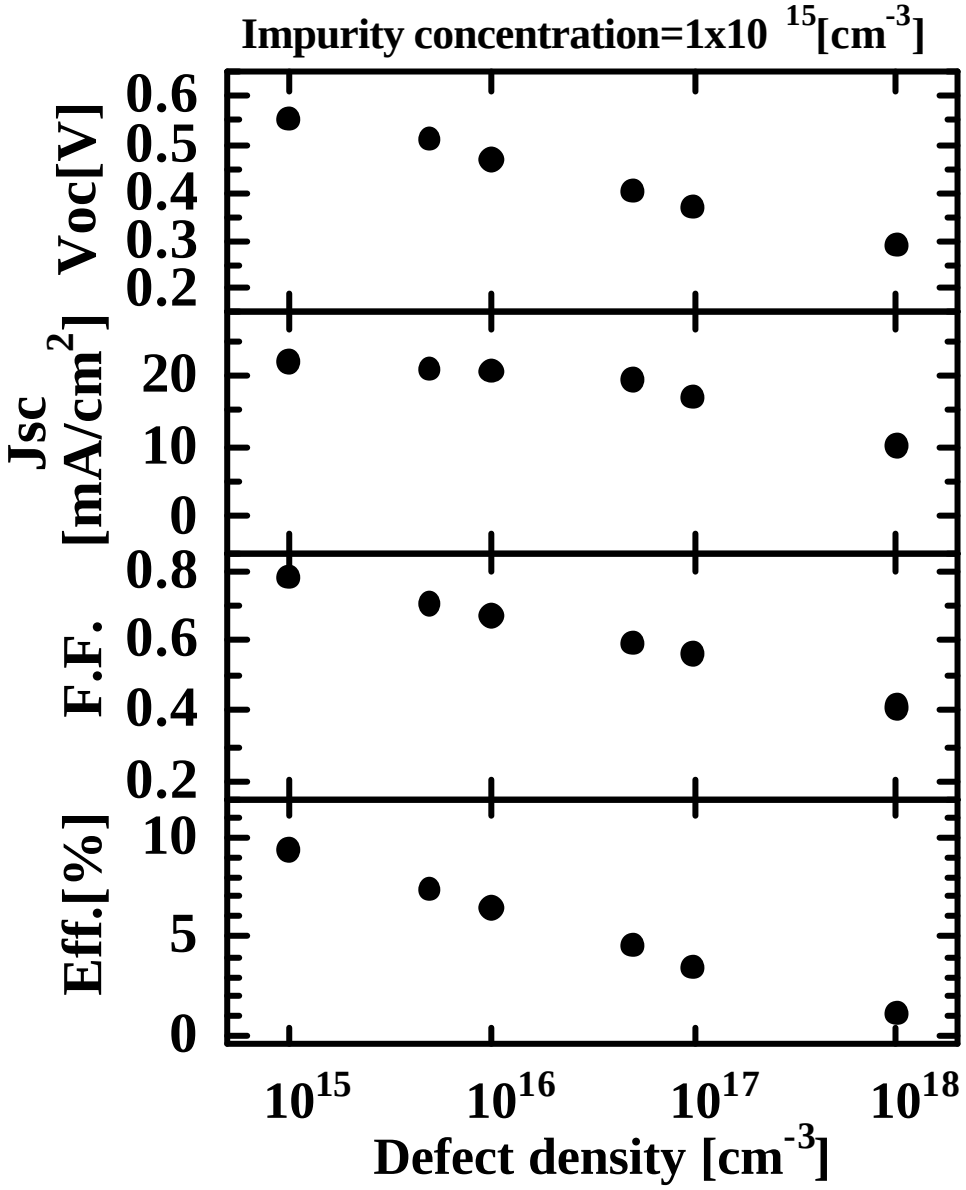

Fig. 4-7: Solar cell performances as a function of i-layer defect density

As shown in Fig. 4-9, the recombination rate was constant with a value of $1x10^{21}$ $cm^{-3}s^{-1}$ in the whole i-layer region at a defect density of $1x10^{18}$ cm^{-3} because of the weak electric field in the i-layer. The recombination rates largely decreased with decreasing defect density from $1x10^{18}$ cm^{-3} to $1x10^{15}$ cm^{-3}. Especially in the region from p/i interface to the middle of i-layer, the recombination rate largely decreased by 4 orders of magnitude with decreasing defect density from $1x10^{18}$ cm^{-3} to $1x10^{15}$ cm^{-3}. The electric field in the i-layer was almost same at defect densities of $1x10^{15}$ cm^{-3} and $1x10^{16}$ cm^{-3}, however, the recombination rate had large difference, because the rate of trapped electrons and holes in defects largely increased due to the increase of defect density.

Generally, intrinsic μc-Si:H films show n-type characteristics when impurity concentration such as oxygen concentration increases, because oxygen-related donor increases. Therefore, next, effects of impurity (donor) concentration of i-layer on cell performances were investigated. A thickness and defect density of i-layer were fixed 1.2 μm and $1x10^{15}$ cm^{-3}, respectively. Impurity concentrations were varied from $1x10^{10}$ cm^{-3} to $1x10^{18}$ cm^{-3}. As shown in Fig. 4-10, V_{oc}, J_{sc}, F.F. and conversion efficiency were constant at impurity concentrations from $1x10^{10}$ cm^{-3} to $1x10^{15}$ cm^{-3}. However, V_{oc} and F.F. slightly increased and J_{sc} largely decreased with increasing impurity concentrations over $1x10^{15}$ cm^{-3}. As a result, conversion efficiencies largely decreased at impurity concentrations over $1x10^{15}$ cm^{-3}. From the results in Figs 4-7 and 4-10, it was found that for obtaining high conversion efficiency, impurity concentration must be decreased less than $1x10^{15}$ cm^{-3}, furthermore, defect density largely limits cell performances at a impurity concentration less than $1x10^{15}$ cm^{-3}. In order to know the reasons for above results, band profiles and recombination rates of solar cells were investigated.

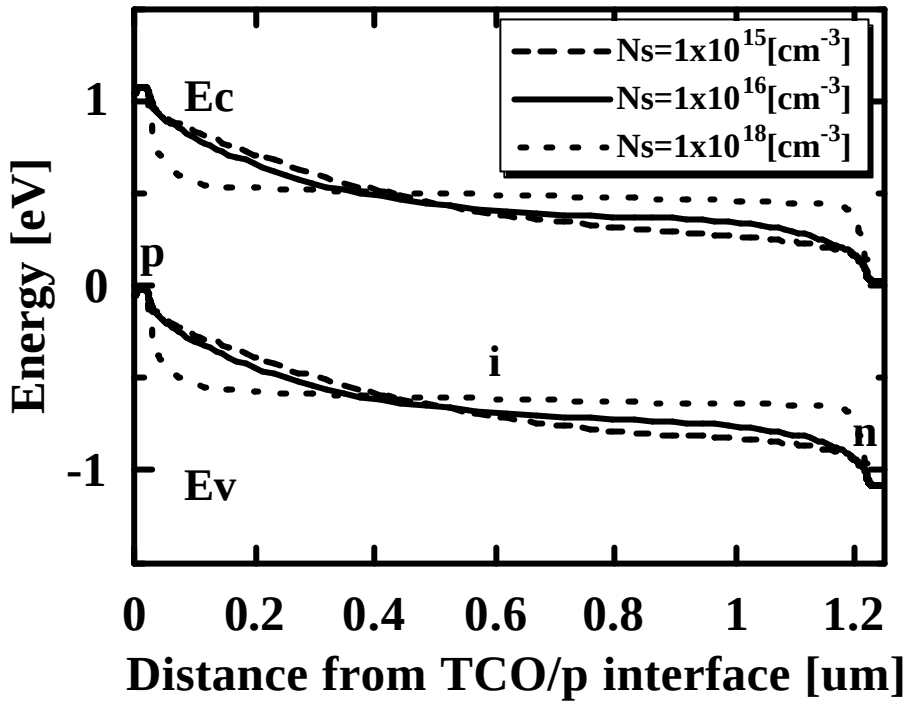

Fig. 4-8: Band profile of μc-Si:H solar cell as a function of i-layer defect density

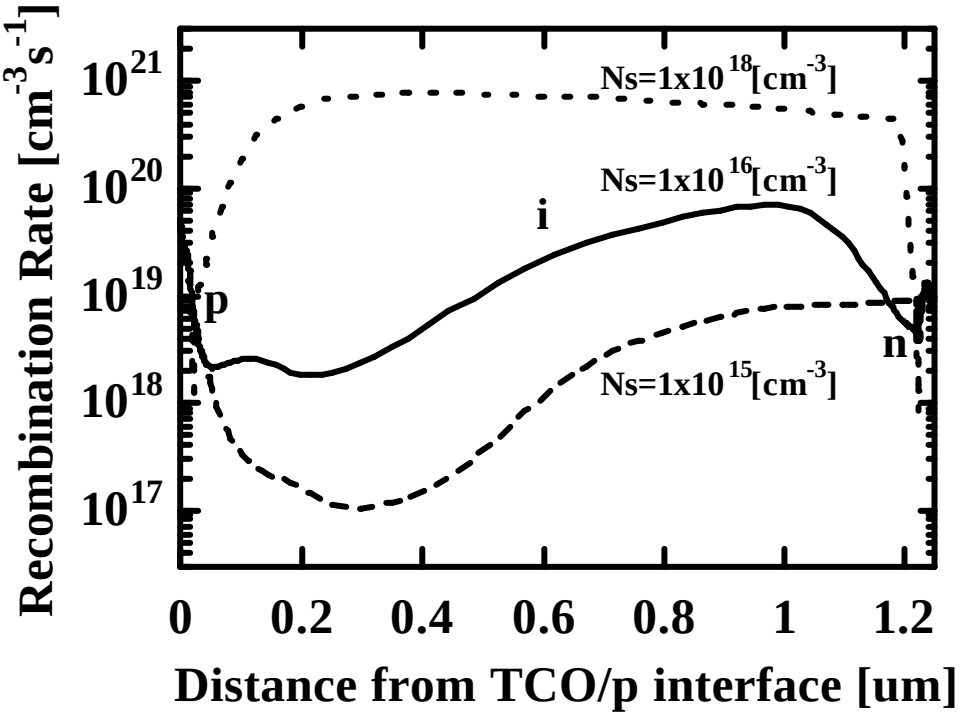

Fig. 4-9: Recombination rate of μc-Si:H solar cell as a function of i-layer defect density

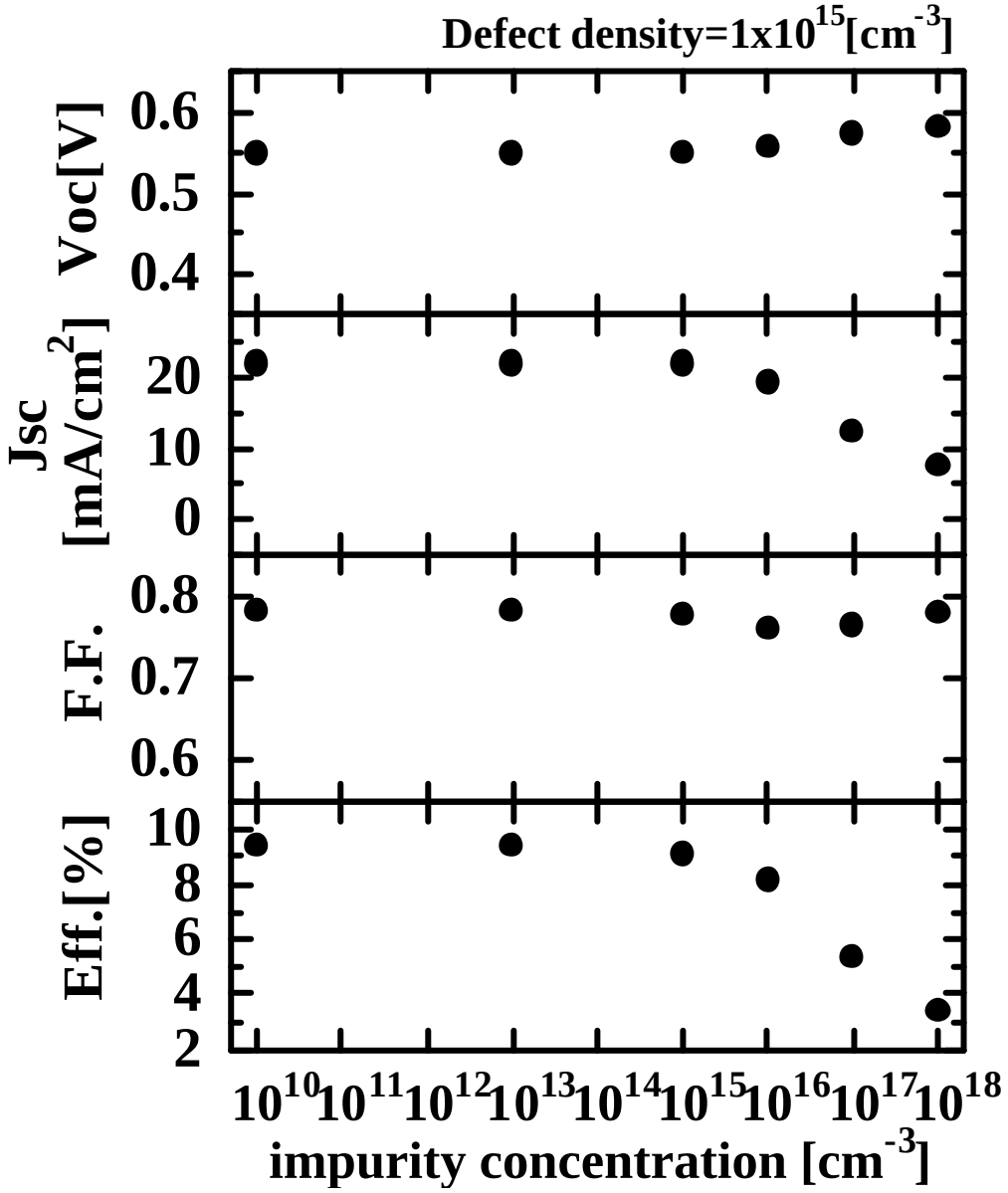

Fig. 4-10: Solar cell performances as a function of i-layer impurity concentration

As shown in Fig. 4-11, the homogeneous electric field was strongly formed in the whole i-layer region at impurity concentrations of $1x10^{10}$ cm^{-3} and $1x10^{15}$ cm^{-3}, and the electric field in the i-layer region slightly decreased with increasing impurity concentration from $1x10^{10}$ cm^{-3} to $1x10^{15}$ cm^{-3}. However, when the impurity concentration increased to $1x10^{17}$ cm^{-3}, the electric field was strongly formed only at the p/i interface and it was almost zero in the whole i-layer region. Therefore, the large decrease of cell performances was caused by this weak electric field in the whole i-layer region at impurity concentrations over $1x10^{16}$ cm^{-3}. As shown in Fig. 4-12, the recombination rate was constant with a value of $6x10^{20}$ $cm^{-3}s^{-1}$ in the whole i-layer region at a impurity concentration of $1x10^{17}$ cm^{-3} because of the weak electric field in the i-layer. The recombination rates largely decreased with decreasing impurity concentration from $1x10^{17}$ cm^{-3} to $1x10^{10}$ cm^{-3}. In the region from the middle of i-layer to the i/n interface, the recombination rate largely decreased by 3 orders of magnitude with decreasing defect density from $1x10^{17}$ cm^{-3} to $1x10^{10}$ cm^{-3}, however, around the p/i interface, the recombination rate largely decreased with increasing impurity concentration from $1x10^{10}$ cm^{-3} to $1x10^{17}$ cm^{-3}. The reason of this large decrease is because i-layer became n-type due to the high donor concentration and the electric field at the p/i interface became strong. The slight increase of V_{oc} and F.F. in Fig. 4-10 might be also caused by this reason. The difference between the recombination rates in the i-layer region from the p/i interface to the middle of i-layer and that from the middle of i-layer to n/i interface was small at impurity concentration of $1x10^{10}$ cm^{-3}, however, the difference largely increased with increasing impurity concentration to $1x10^{15}$ cm^{-3}. The reason of this result is that the electric field in the i-layer region decreased with increasing impurity concentration from $1x10^{10}$ cm^{-3} to $1x10^{15}$ cm^{-3}. Therefore, it is concluded that in order to form the homogeneous electric field strongly

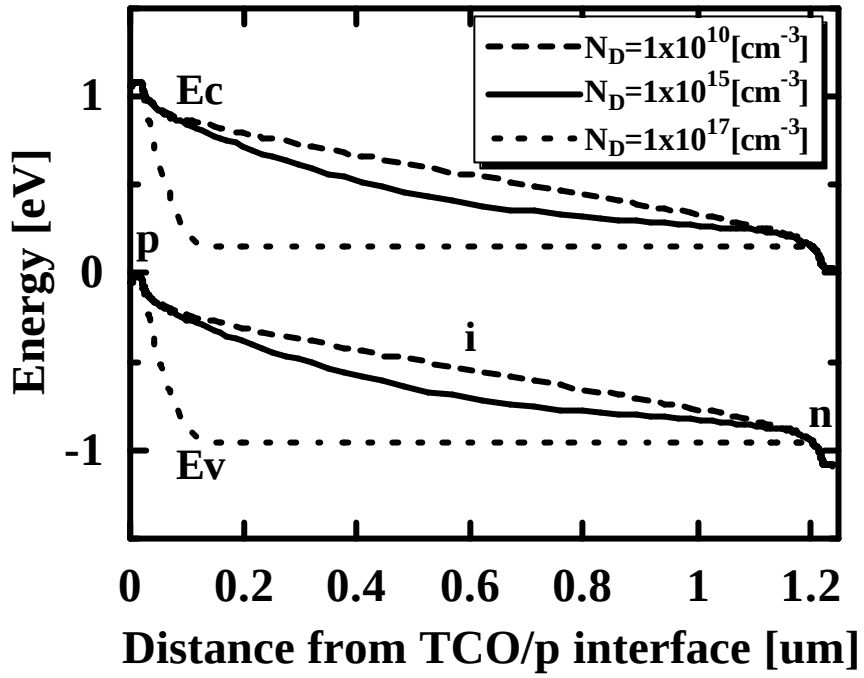

Fig. 4-11: Band profile of μc-Si:H solar cell as a function of i-layer impurity concentration

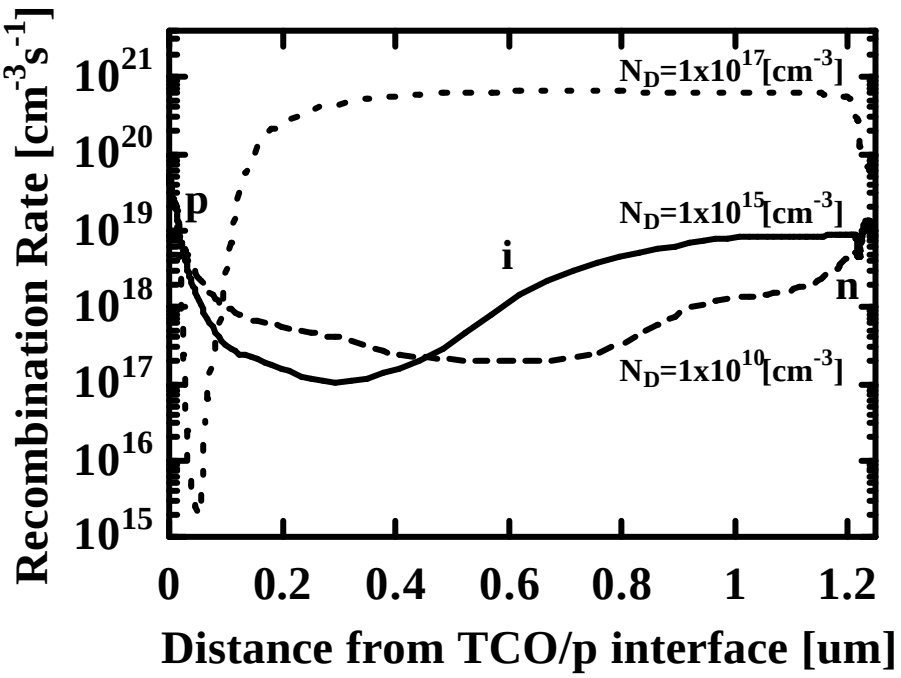

Fig. 4-12: Recombination rate of μc-Si:H solar cell as a function of i-layer impurity concentration

in the entire i-layer region and reduce the recombination rate, the i-layer must be maintained to be intrinsic and the impurity concentration must be reduced less than $1x10^{15}$ cm^{-3}.

The other important i-layer parameter is the thickness. When the i-layer thickness increases, the light absorption increases, as a result, J_{sc} increases. However, when film quality of i-layer is not good, solar cell performances are degraded with increasing the i-layer thickness, indicating that there is an optimum i-layer thickness, which depends on film quality of the i-layer. Therefore, finally, the dependence of cell performances on the i-layer thickness was investigated. The impurity concentration of the i-layer was fixed $1x10^{10}$ cm^{-3}. The thickness of the i-layer was varied from 0.5 μm to 5.0 μm for the defect densities of $1x10^{15}$ cm^{-3} and $1x10^{16}$ cm^{-3}, respectively. As shown in Fig. 4-13, V_{oc} and F.F. slightly decreased with increasing i-layer thickness at a defect density of $1x10^{15}$ cm^{-3}, and they largely decreased with increasing i-layer thickness at a defect density of $1x10^{16}$ cm^{-3}. On the other hand, when a defect density was $1x10^{15}$ cm^{-3}, J_{sc} largely increased from 15 mA/cm^2 to 30 mA/cm^2 with increasing i-layer thickness and it was saturated at a thickness of 5.0 μm. However, when a defect density was $1x10^{16}$ cm^{-3}, J_{sc} also largely increased from 15 mA/cm^2 to 22 mA/cm^2 with increasing i-layer thickness, but it was saturated at a thickness of around 2.0 μm. As the results, when a defect density was $1x10^{15}$ cm^{-3}, a conversion efficiency largely increased with increasing i-layer thickness and it had the maximum value of 11.2% at a thickness of 5.0 μm. On the other hand, when a defect density was $1x10^{16}$ cm^{-3}, a conversion efficiency had a peak value of 6% at a thickness of around 1.0-2.0 μm. In order to know the reasons for above results, band profiles and recombination rates of solar cells were investigated. As shown in Fig. 4-14, when a defect density was $1x10^{15}$ cm^{-3}, the electric field decreased with increasing i-layer thickness, however,

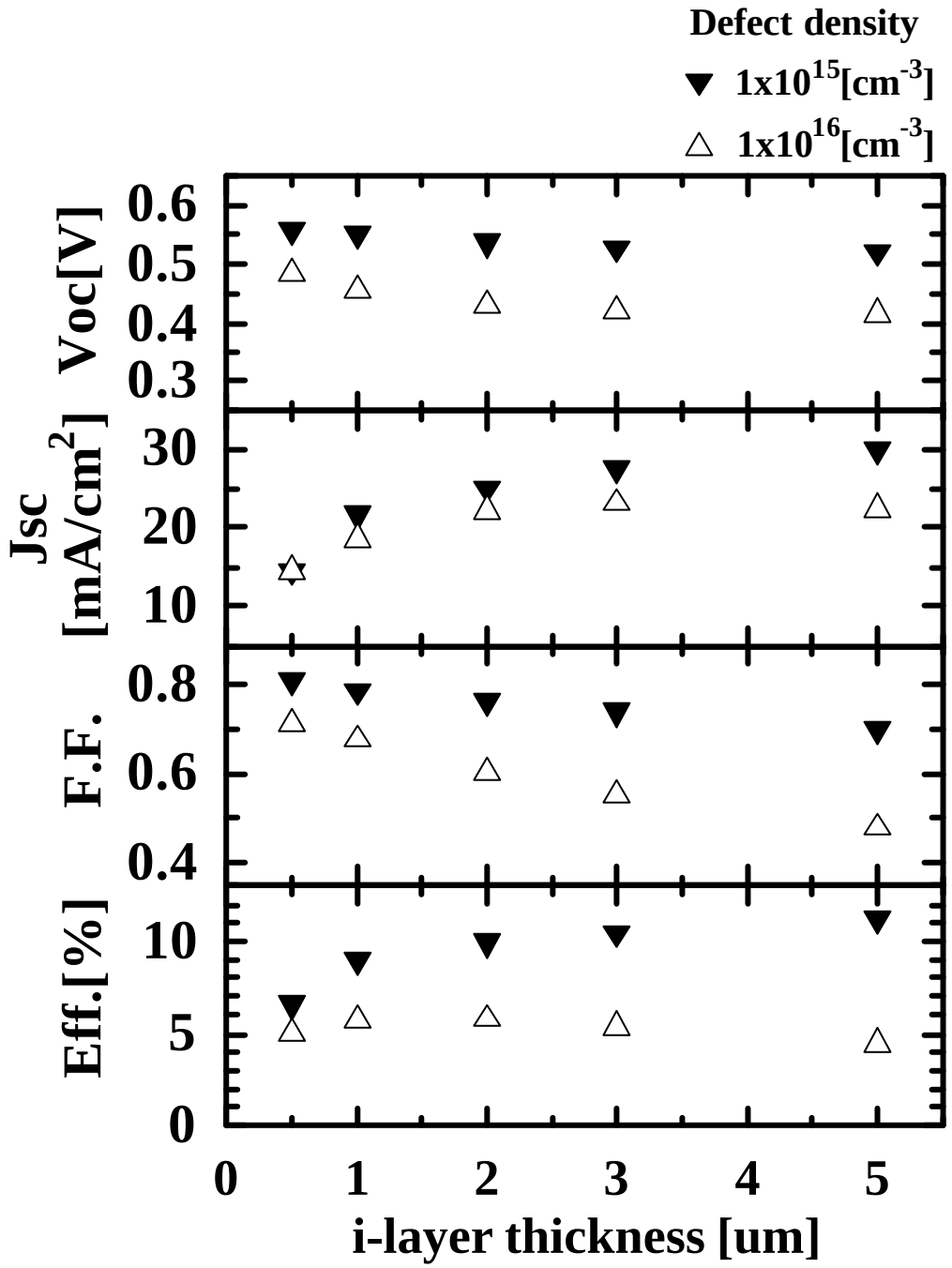

Fig. 4-13: Solar cell performances as a function of i-layer thickness at defect densities of $1x10^{15}$ cm^{-3} and $1x10^{16}$ cm^{-3}

the homogeneous electric field was strongly formed in the whole i-layer region even at a thickness of 5.0 μm. Therefore, V_{oc} and F.F. slightly decreased, but J_{sc} largely increased with increasing i-layer thickness from 0.5 μm to 5.0 μm, as a result, the maximum conversion efficiency of 11% could be obtained at a thickness of 5.0 μm, as shown in Fig. 4-13. On the other hand, when a defect density was $1x10^{16}$ cm^{-3}, the electric field in the i-layer region largely decreased with increasing i-layer thickness, and it became very weak at a thickness of 5.0 μm, as shown in Fig. 5-15. Therefore, V_{oc} and F.F. largely decreased, and J_{sc} increased with increasing i-layer thickness, but it was saturated at a thickness of around 2.0 μm, as a result, a conversion efficiency had a peak value of 6% at a thickness of around 1.0-2.0 μm. As shown in Fig. 4-16, when a defect density was $1x10^{15}$ cm^{-3}, the recombination rate increased with increasing i-layer thickness, however, the value was still as small as $1\text{-}6x10^{18}$ $cm^{-3}s^{-1}$ in the whole i-layer region because the homogeneous electric field was strongly formed in the whole i-layer region even at a thickness of 5.0 μm. On the other hand, as shown in Fig. 4-17, when a defect density was $1x10^{16}$ cm^{-3}, the recombination rate largely increased with increasing i-layer thickness, the value was as large as $1x10^{20}$ $cm^{-3}s^{-1}$ in the almost whole i-layer region. There was a large dependence of the recombination rate on the distance from the p/i interface especially at a thickness of 2.0 μm. The recombination rate largely increased with increasing the distance from the p/i interface, because the electric field was strongly formed at the p/i interface, however, it became weak in the distant region from the p/i interface. From above results, it is concluded that when the i-layer defect density is as low as $1x10^{15}$ cm^{-3}, a conversion efficiency increases with increasing i-layer thickness and the thickness can be increased around 5.0 μm, however, when the defect density is $1x10^{16}$ cm^{-3}, the optimum i-layer thickness is around 1.0-2.0 μm.

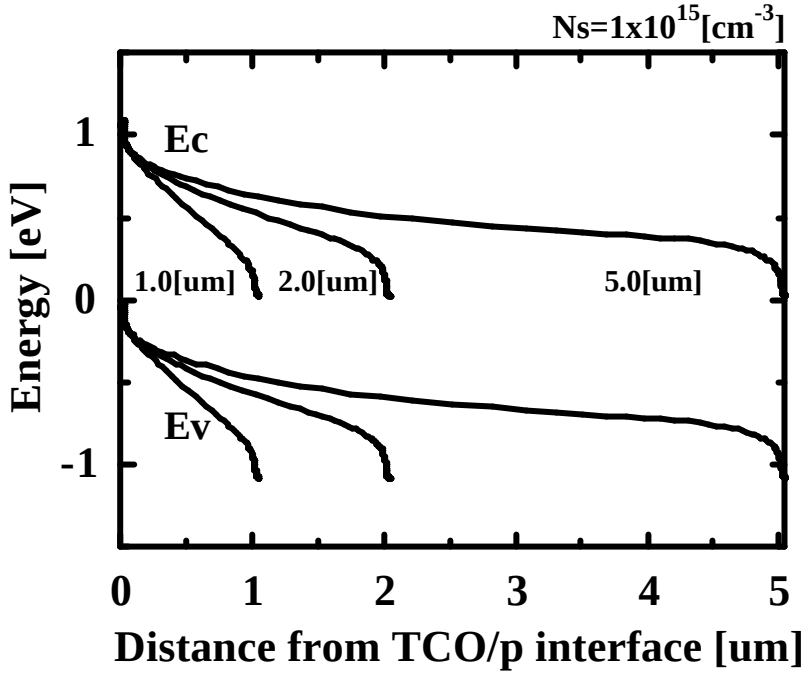

Fig. 4-14: Band profile of μc-Si:H solar cell as a function of i-layer thickness at i-layer defect density of $1x10^{15}$ cm^{-3}

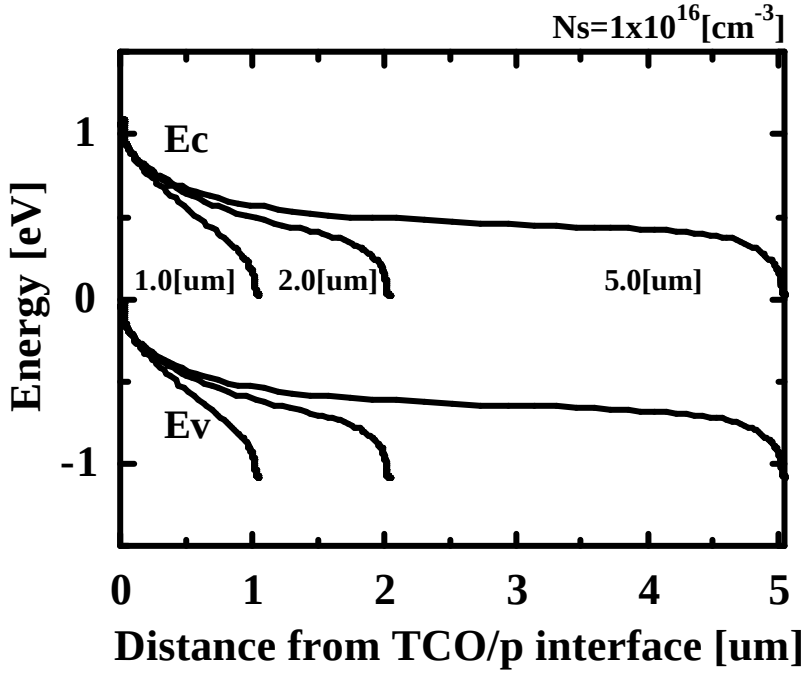

Fig. 4-15: Band profile of μc-Si:H solar cell as a function of i-layer thickness at i-layer defect density of $1x10^{16}$ cm^{-3}

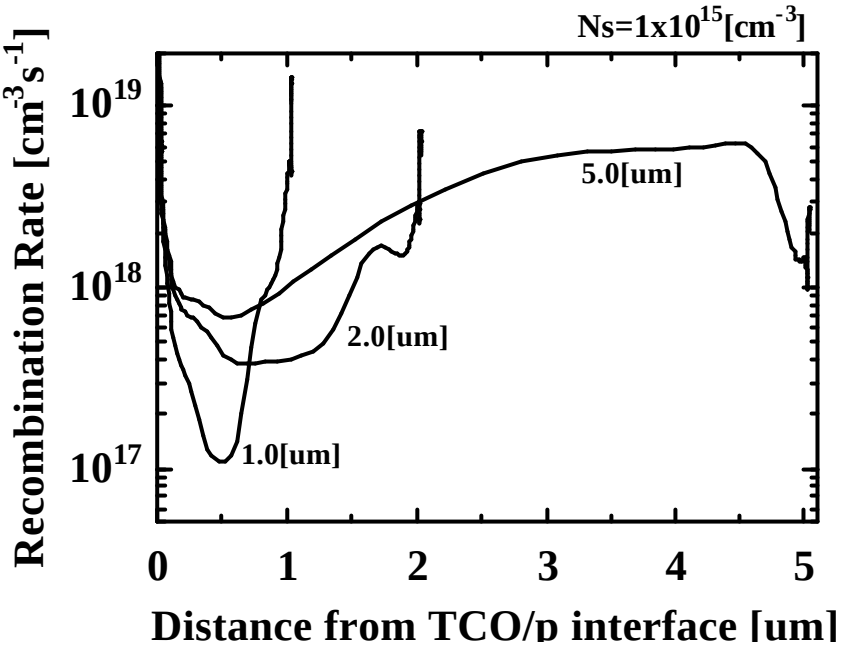

Fig. 4-16: Recombination rate of μc-Si:H solar cell as a function of i-layer thickness at i-layer defect density of $1x10^{15}$ cm^{-3}

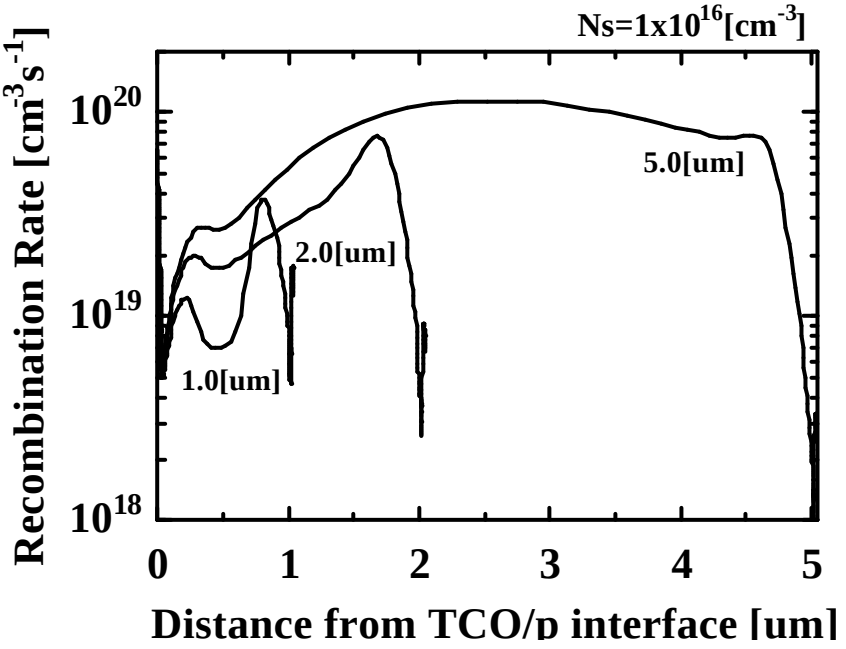

Fig. 4-17: Recombination rate of μc-Si:H solar cell as a function of i-layer thickness at i-layer defect density of $1x10^{16}$ cm^{-3}

4-4 Summary

It was investigated if p-layer and n-layer materials such as p-a-SiC:H, p-a-Si:H, p-μc-Si:H, n-a-Si:H and n-μc-Si:H were suitable for μc-Si:H thin film solar cells by theoretical analysis. For the theoretical analysis, AMPS-1D BETA 1.00 was used. First, effects of p-layer materials on solar cell performances were examined. As a result, when the p-layer was p-a-SiC:H and p-a-Si:H, solar cell performances showed large dependence on the acceptor concentration of p-layer. On the other hand, when the p-layer was p-μc-Si:H, solar cell performances were constant at an acceptor concentration from $1x10^{20}$ cm^{-3} to $1x10^{17}$ cm^{-3}. In the case of p-a-SiC:H and p-a-Si:H, cell performances largely decreased with decreasing the acceptor concentration less than $1x10^{19}$ cm^{-3}. Therefore, it is concluded that the most suitable p-layer material for μc-Si:H thin film solar cells is p-μc-Si:H. Next, n-a-Si:H and n-μc-Si:H were investigated in order to confirm if they were suitable n-layer materials for μc-Si:H thin film solar cells. In the theoretical analysis, no difference was observed in solar cell performances for both n-a-Si:H and n-μc-Si:H. Therefore, it is concluded that both n-a-Si:H and n-μc-Si:H can be used for μc-Si:H thin film solar cells. Finally, effects of i-layer film properties such as defect density, impurity concentration and film thickness on solar cell performances were investigated. Defect density was varied from $1x10^{15}$ cm^{-3} to $1x10^{18}$ cm^{-3}, as a result, it was found that defect density is very effective in solar cell performances, and for obtaining high conversion efficiencies, defect density must be reduced less than $1x10^{16}$ cm^{-3}. Impurity concentrations were varied from $1x10^{10}$ cm^{-3} to $1x10^{18}$ cm^{-3}, as a result, it was found that for obtaining high conversion efficiency, impurity concentration must be decreased less than $1x10^{15}$ cm^{-3}, besides, defect density largely limits cell performances at a impurity concentration

less than $1x10^{15}$ cm^{-3}. The thickness of the i-layer was varied from 0.5 μm to 5.0 μm for the defect densities of $1x10^{15}$ cm^{-3} and $1x10^{17}$ cm^{-3}, respectively, as the results, when a defect density was $1x10^{15}$ cm^{-3}, a conversion efficiency largely increased with increasing i-layer thickness and it had the maximum value of 11% at a thickness of 5.0 μm. On the other hand, when a defect density was $1x10^{16}$ cm^{-3}, the optimum i-layer thickness was around 1.0-2.0 μm and the maximum conversion efficiency was 6% at that thickness.

References

[1] K. Dairiki, A. Yamada and M. Konagai: Jpn. J. Appl. Phys. **38** (1999) 4007.

[2] J. P. R. Bakker, B. J. van der Horst and J. I. Dijkhuis: J. Non-Cryst. Solids **299-302** (2002) 1256.

[3] J. K. Rath, F. A. Rubinelli and R. E. I. Schropp: J. Non-Cryst. Solids **266-269** (2000) 1129.

[4] J. K. Rath, F. A. Rubinelli and R. E. I. Schropp: J. Non-Cryst. Solids **227-230** (1998) 1282.

[5] H. Liu, L. Jiao, S. Semoushkina and C. R. Wronski: J. Non-Cryst. Solids **198-200** (1996) 1168.

[6] H. Takakura and Y. Hamakawa: Solar Energy Materials & Solar Cells **74** (2002) 479.

[7] S. Yamanaka, M. Konagai and K. Takahashi: Jpn. J. Appl. Phys. **28** (1989) 1178.

[8] H. Tasaki, W. Y. Kim, M. Hallerdt, M. Konagai and K. Takahashi: J. Appl. Phys. **63** (1988) 550.

Chapter5

Fabrication and Characterization of Microcrystalline Silicon Thin Films and Solar Cells

5-1 Introduction

Recently, hydrogenated microcrystalline silicon (μc-Si:H) based thin film solar cells attracted much attention as a bottom cell of hybrid solar cells. However, for the reduction of manufacturing cost of solar cells, deposition rates should be enhanced up to 2-5 nm/s. Matsumura and Tachibana[1)] and Mahan et al.[2)] proposed Catalytic Chemical Vapor Deposition (CAT-CVD) or the Hot Wire CVD method and obtained a-Si:H films with good quality at high deposition rates of over 1 nm/s. From these points of view, HW-Cell method is one of the promising methods for obtaining a-Si:H and μc-Si:H thin films since high deposition rate, low substrate temperature and high efficiency of gas usage can be expected.[3)] In our previous works, it was demonstrated that at a high filament temperature of 2100^{o}C and relatively high deposition pressure of 0.1 Torr, μc-Si:H films with a high crystal volume fraction of 80-90% and relatively high growth rates of 0.4-3.0 nm/s could be easily obtained without hydrogen dilution.[4)] However, it was found from SIMS results that the O and C concentrations of μc-Si:H films grown at a pressure of 0.1 Torr were $5x10^{21}$ cm^{-3} and $5x10^{20}$ cm^{-3}, respectively, and the cell performances were limited critically by such a high impurity

concentration.[5] On the other hand, it was found that the O and C concentrations of a-Si:H films grown by HW-Cell method could be reduced to the order of 10^{18} cm^{-3} and Si-H/Si-H_2 ratio and electrical properties were also largely improved with decreasing deposition pressure less than 20 mTorr as above mentioned in Chapter3. Therefore, in this work, first, we tried to reduce the impurity concentration in the μc-Si:H i-layer by decreasing deposition pressure and also tried to obtain high quality films in structural and electrical properties. Second, a novel 2-step growth method was proposed in order to reduce the thickness of an incubation layer in the initial growth of i-layer. Then, deposition parameters in the 1st and 2nd layer of 2-step growth method were optimized for the further improvement of solar cell performances. Furthermore, degradation properties of films and solar cells were investigated.

5-2 Experimental Details

5-2-1 Experimental Setup

A schematic view of the hybrid multichamber system (Hot Wire Cell method and photo-CVD) used for film deposition in this study is shown in Fig. 5-1. This apparatus consists of totally 6 chambers, such as a load-lock (LD) chamber, photo-CVD-i and n chambers, HW-p chamber and HW-i chamber (for Si, SiC). In this study, HW-i chamber was used for depositions of μc-Si:H intrinsic films, besides HW-p and photo-CVD-n chambers were also used for solar cell fabrications. HW-i chamber is ordinarily evacuated by a turbo molecular pump (TMP) and is also evacuated by a TMP during deposition. The base pressure is 2-5x10^{-7} Torr. HW-p and photo-CVD-n chambers are ordinarily evacuated by a TMP and are evacuated by a

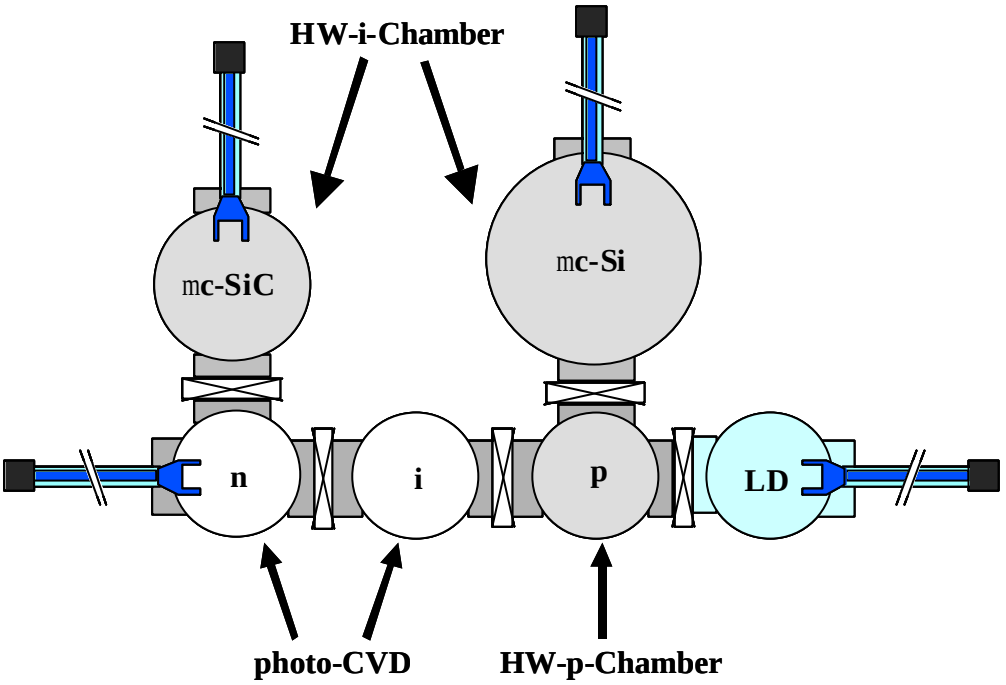

Fig. 5-1: A schematic view of the deposition system used in this study

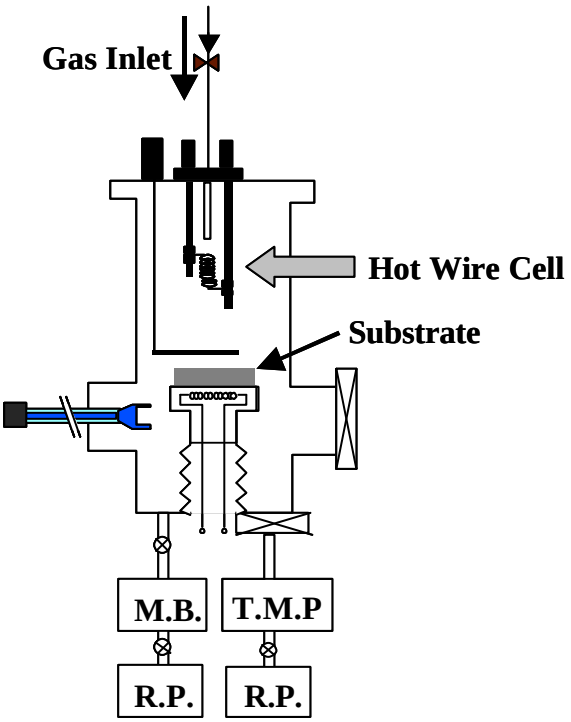

Fig. 5-2: A schematic view of the Hot Wire Cell chamber used in this study

mechanical booster pump (MB) during deposition. A schematic view of HW chamber used in this work is shown in Fig. 5-2. Gas inlet, filament, substrate and pumps are placed as shown in the Fig. 5-2.

5-2-2 Deposition conditions

Intrinsic μc-Si:H thin films were deposited on Corning7059 glasses, single crystal Si wafers and Asahi U-type TCO glasses by Hot Wire Cell method in a hybrid multichamber system. A mixture of pure SiH_4 and H_2 gases was used for the deposition of intrinsic μc-Si:H films. These gases are decomposed on the surface of the heated W (tungsten) filament as a result of the catalytic and pyrolytic dissociation.[6] The filament in the shape of a coil which had a diameter of 4 mm and a length of 1.5 cm was used and it was placed parallel to the gas inlet. The filament temperature was monitored by an infrared pyrometer through a quartz window. The structure of μc-Si:H thin films was evaluated by Raman scattering spectroscopy and scanning electron microscope (SEM) measurement. Photoconductivities (σ_{ph}) under AM1.5, 100 mW/cm^2 illumination and dark conductivities (σ_d) were measured with an Aluminum (Al) coplanar electrode configuration. Activation energy (E_a) was evaluated by the temperature dependence of σ_d. Fourier transform infrared absorption spectroscopy (FT-IR) measurement was carried our in order to evaluate hydrogen content including Si-H and Si-H_2 content. Defect density and impurity concentration of μc-Si:H thin films were measured by the electron spin resonance (ESR) measurement and the secondary ion mass spectroscopy (SIMS) measurement, respectively. For SIMS measurements, stacked thin film layers deposited on single crystal Si wafers were prepared. The ambipolar diffusion length parallel to the

substrate ($L_{\parallel}$) was evaluated by the steady-state photocarrier grating (SSPG) measurement[7-10] and that perpendicular to the substrate ($L_{\perp}$) was evaluated by the surface photovoltage (SPV) measurement.[8-11] The thickness of the films was measured with a Dektak profilometer. Raman spectra were deconvoluted in their integrated crystalline, I_c (520 cm^{-1}), amorphous, I_a (480 cm^{-1}) and intermediate, I_m (510 cm^{-1}) peaks. The crystal volume fraction, X_c, was calculated from the following equation[12]:

$$X_c = (I_c + I_m)/ (I_c + I_m + I_a) \qquad (1)$$

In order to investigate the application of these μc-Si:H films to Si based thin film solar cells, p-i-n superstrate-type solar cells were prepared on Asahi Glass Co. TCO (SnO_2) glasses with the deposition rate of around 0.3 nm/s.

The structures of solar cells fabricated was as follows: Glass/TCO(SnO_2)/p-μc-Si:H(30nm)/i-μc-Si:H(0.75-2.25μm)/n-a-Si:H(40nm)/ZnO/Ag /Al. The p-μc-Si:H and n-a-Si:H layer were prepared by HW-Cell method[13, 14] and photo-CVD method[15-17], respectively. The deposition conditions of p, i and n layers are summarized in Tables 5-1, 5-2 and 5-3, respectively. A mixture of pure SiH_4 and H_2 diluted B_2H_6 (1%) gases were used for p-μc-Si:H film deposition. p-μc-Si:H films could be obtained without H_2 dilution because of a high filament temperature of 2050°C and H_2 in H_2 diluted B_2H_6 gas. A deposition rate was about 0.2 nm/s. In order to reduce the TCO damage caused by atomic hydrogen, in the beginning of p-layer deposition, a-Si:H pre-deposition layer with a thickness of 2-3 nm was deposited on TCO substrate at a low filament temperature of 1900°C using only pure SiH_4 gas, then p-μc-Si:H film with a thickness of 25 nm was deposited. This p-μc-Si:H film has a high conductivity of 0.5-1.0 S/cm, crystal volume fraction of 40% even when the thickness was as thin as 20-30 nm. Furthermore, it was already demonstrated that a

conversion efficiency of over 7% could be obtained for μc-Si:H thin film solar cells with i-μc-Si:H prepared by photo-CVD, indicating high quality p-μc-Si:H film. A mixture of pure SiH_4 and H_2 diluted PH_3 (1%) gases were used for n-a-Si:H film deposition. This n-a-Si:H layer have been used for a-Si:H solar cells in our laboratory and the maximum stabilized conversion efficiency of 9.0% was obtained. A schematic view of the solar cell structure fabricated in this study is shown in Fig. 5-3. After the deposition of p, i, n layers on TCO(SnO_2) glass, ZnO layer with a thickness of 100 nm was deposited by MOCVD method, then Ag and Al electrodes were deposited by evaporation. RF-plasma CF_4 etching apparatus was carried out for the etching of Si films.

Table 5-1: Deposition parameters for p-μc-Si:H layer.

Substrate temperature	175^{o}C
Filament material	Tungsten (W)
Filament temperature	1900-2050^{o}C
Partial (SiH_4)/total (SiH_4+B_2H_6) pressure	7/13.5 mTorr
SiH_4 gas flow rate	0.62 sccm
B_2H_6 (H_2 diluted, 1%) gas flow rate	1.3 sccm
Filament-substrate distance	4 cm
Filament length	1.5 cm (18-turn)

Table 5-2: Deposition parameters for i-μc-Si:H layer.

Substrate temperature	120-300^{o}C
Filament material	W or Ta
Filament temperature	W: 1800-2100^{o}C, Ta: 1400-1700^{o}C
SiH_4 partial pressure	1-100 mTorr
SiH_4 gas flow rate	5 sccm
H_2 gas flow rate	5-100 sccm
Filament-substrate distance	5 cm
Filament length	1.5 cm (18-turn)

Table 5-3: Deposition parameters for n-a-Si:H layer.

Substrate temperature	175^{o}C
UV-lamp wavelength	184.9 nm
Total gas pressure	0.7 Torr
SiH_4 gas flow rate	10 sccm
PH_3 (H_2 diluted, 1%) gas flow rate	5 sccm

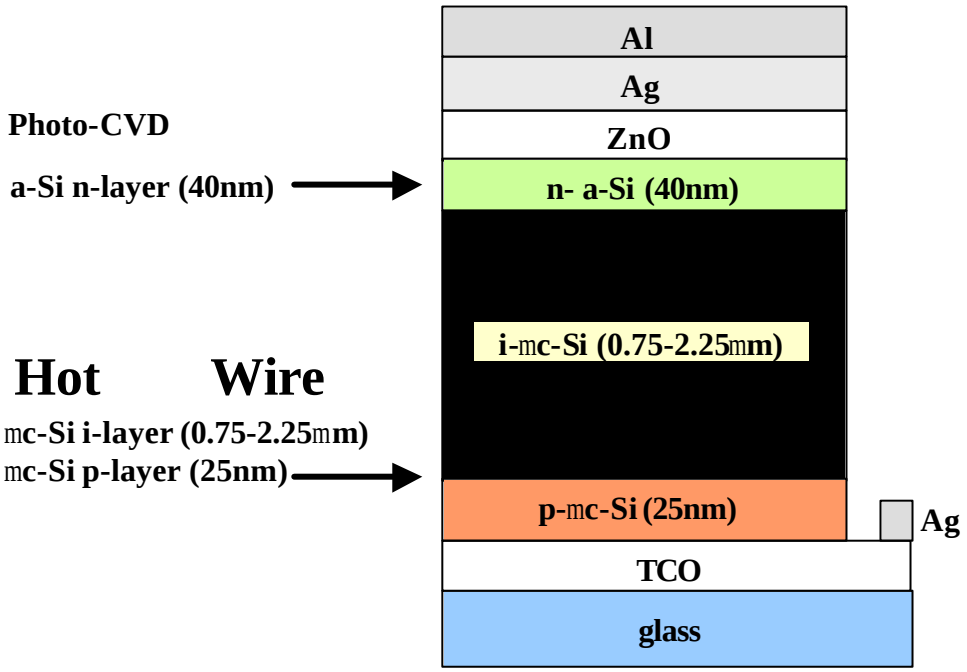

Fig. 5-3: A schematic view of the solar cell structure fabricated in this study

5-3 Deposition and Characterization of Microcrystalline Silicon Thin Films and Solar Cells

5-3-1 Dependence on Hydrogen Flow Rate

In our previous works, we attempted to obtain microcrystalline Si (μc-Si:H) films with a large grain size. As a result, it was found that films with a high crystal volume fraction (X_c) around 90% could be obtained at a relatively high deposition pressure of 100 mTorr without H_2 dilution.[3, 4, 5)] However, conversion efficiencies of solar cells with those intrinsic μc-Si:H films were as low as around 1-1.5%, as shown in Fig. 5-4. On that time, the structure of solar cells fabricated was as follows: Glass/TCO (SnO_2)/p-a-SiC:H/buffer-a-SiC:H (graded)/i-μc-Si:H/n-a-Si:H/ZnO/Ag/Al. Therefore, as demonstrated in Chapter4, one of the reasons of such a low conversion efficiency was using p-a-SiC:H. Figure 5-5 shows I-V characteristics of μc-Si:H solar cells with μc-Si:H i-layer prepared by photo-CVD. From these results, it was also demonstrated that p-a-SiC:H layer was not suitable for μc-Si:H solar cells and it largely limited cell performances. Another reason of a low conversion efficiency is low quality of μc-Si:H i-layer. From the SIMS results, it was found the O and C concentrations of μc-Si:H films grown at a pressure of 100 mTorr were $5x10^{21}$ cm^{-3} and $5x10^{20}$ cm^{-3}, respectively, as shown in Fig. 5-6. On the other hand, it was found that the O and C concentrations of a-Si:H films grown by the HW-Cell method could be reduced to the order of 10^{18} cm^{-3} with decreasing deposition pressure less than 20 mTorr, as demonstrated in Chapter3. Therefore, we thought good quality μc-Si:H films could be obtained by introducing hydrogen dilution to the deposition conditions of high quality a-Si:H films and the reduction of the O and C concentrations of μc-Si:H

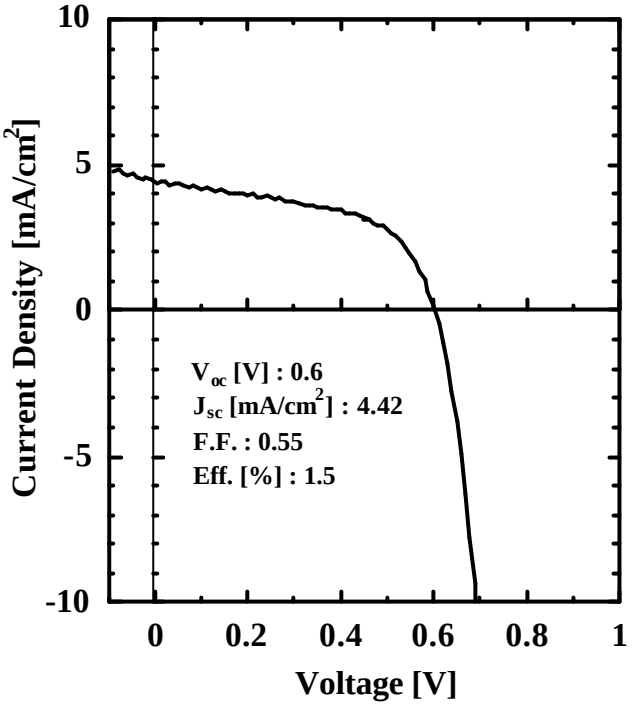

Fig. 5-4: I-V characteristics of μc-Si:H solar cell deposited at a high pressure of 100 mTorr

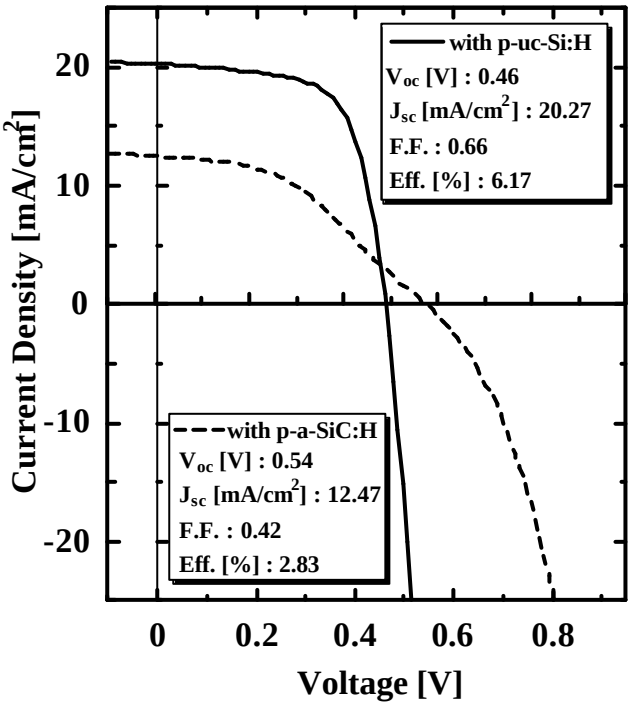

Fig. 5-5: Comparison between p-a-SiC:H and p-μc-Si:H for the cell performances The i-layer was prepared by photo-CVD

films could be done by decreasing deposition pressure. The deposition conditions of high quality amorphous silicon films are as follows: substrate temperature of 200°C, filament temperature of 1900°C, SiH_4 partial pressure (equal to total pressure) of 10 mTorr, SiH_4 flow rate of 5 sccm, filament-substrate distance of 5 cm. First, using this deposition condition, μc-Si:H films were deposited by changing only H_2 flow rate. Figure 5-7 shows Raman spectra as a function of H_2 flow rate. The film structure was amorphous at a H_2 flow rate of until 20 sccm, a film was crystallized at a H_2 flow rate of 40 sccm. The crystal volume fraction (X_c) of this μc-Si:H film was 42%. Next, conductivity and FT-IR measurement were carried out for these μc-Si:H films. As shown in Fig. 5-8, dark conductivity (σ_d) has a correlation with film structure, the value was constant and in the order of 10^{-9} at a H_2 flow rate of until 20 sccm, reflecting amorphous structure, and largely increased to the order of 10^{-7}, reflecting the crystallization. Photoconductivity (σ_{ph}) decreased with increasing a H_2 flow rate from 5 sccm to 20 sccm, but it increased with increasing a H_2 flow rate to 40 sccm. As shown in Fig. 5-9, total H content in μc-Si:H film slightly decreased from 15.5% with increasing H_2 flow rate until 20 sccm, and it largely decreased to 10% at a H_2 flow rate of 40 sccm. That is because the film structure was completely amorphous at a H_2 flow rate until 20 sccm, and at a H_2 flow rate 40 sccm, it became microcrystalline with X_c of 40%, indicating amorphous region decreased to 60%. It can be thought that H atoms of μc-Si:H film exist mainly in the amorphous region. Thus, the amorphous region decreased to 60%, total H content decreased from 15.5% to 10%, whose decrease ratio was 65%, indicating that total H content in the amorphous region was almost constant. On the other hand, Si-H bonding largely decreased, $Si-H_2$ bonding largely increased with increasing H_2 flow rate, indicating a degradation of a-Si:H film quality due to the decrease of $Si-H/Si-H_2$ ratio.

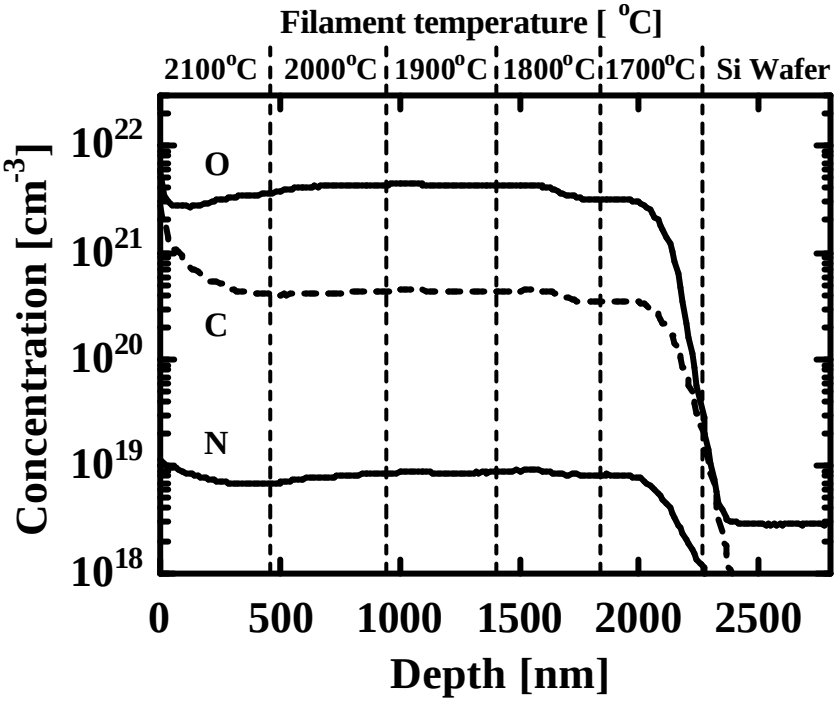

Fig. 5-6: SIMS depth profile of μc-Si:H film deposited at a pressure of 100 mTorr

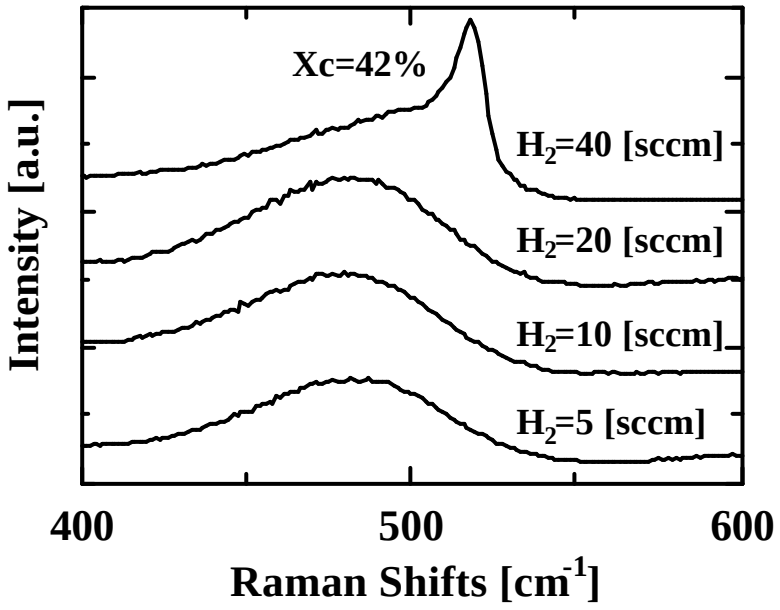

Fig. 5-7: Raman spectra as a function of H_2 flow rate

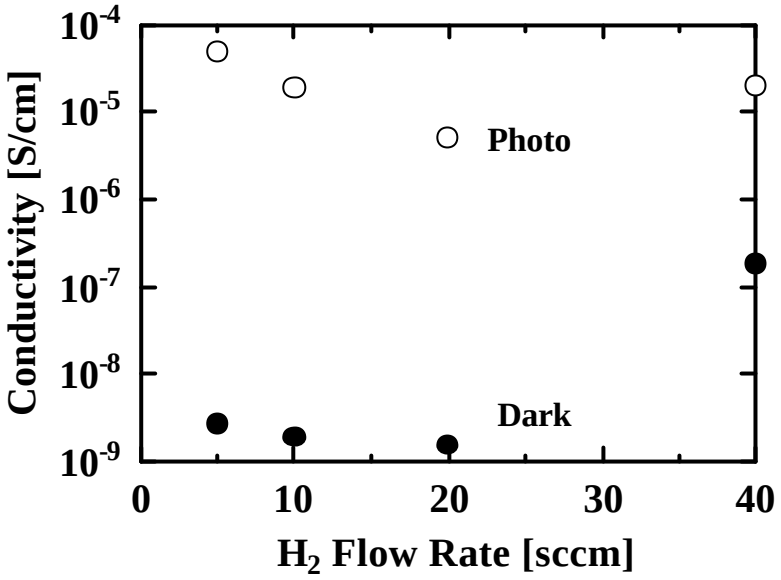

Fig. 5-8: Photo and dark conductivity as a function of H_2 flow rate

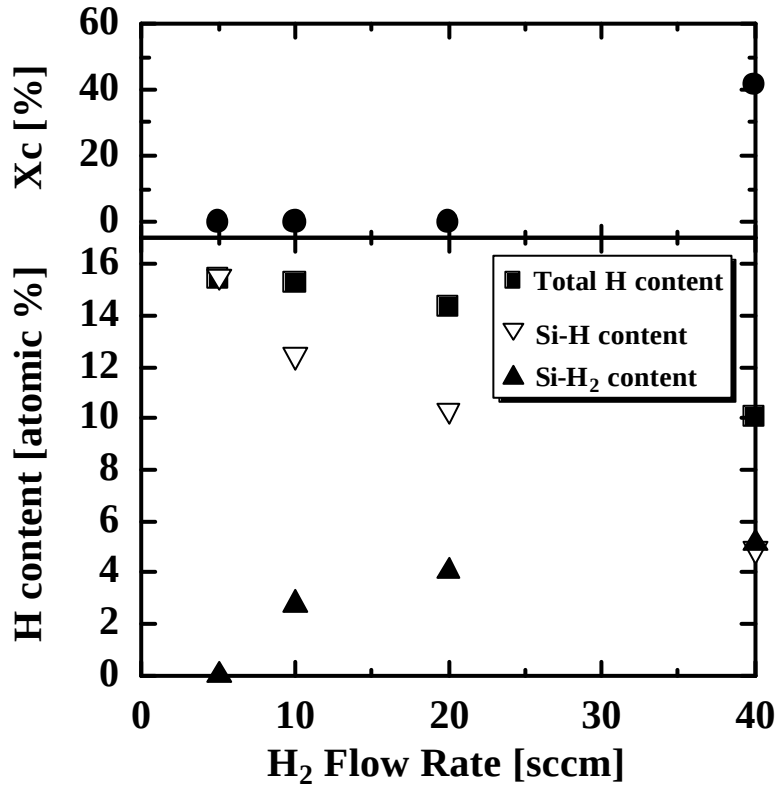

Fig. 5-9: X_c, total H, Si-H and Si-H_2 content as a function of H_2 flow rate

5-3-2 Dependence on Deposition Pressure

From the above results in 5-3-1, it was found that a film was crystallized at a H_2 flow rate of 40 sccm with adding hydrogen dilution to the deposition condition of high quality a-Si:H films. Next, H_2 flow rate was fixed 40 sccm, films were deposited by changing only SiH_4 partial pressure from 1 mTorr to 15 mTorr. The optimum SiH_4 partial pressure was around 10 mTorr for amorphous silicon, however we thought that in the case of μc-Si:H, total pressure increased because of hydrogen dilution, and decreasing the pressure was effective in further reduction of impurities due to the increase of gas evacuation speed. As shown in Fig. 5-10, Xc largely decreased at SiH_4 partial pressures of over 5 mTorr, the structure of the film became amorphous at a SiH_4 partial pressure of 15 mTorr. The atomic H plays an important role in the growth of μc-Si:H thin film. The concentration of atomic H in the deposition chamber decreased with increasing SiH_4 partial pressure, since gas phase reaction was promoted and atomic H was consumed at a high deposition pressure. Therefore, Xc decreased with increasing SiH_4 partial pressure. σ_d reflects the structural transition from amorphous to microcrystalline material, indicating a large increase from $\sigma_d = 10^{-10}$ S/cm for a-Si:H to $\sigma_d = 10^{-8}$-10^{-6} S/cm for μc-Si:H. On the other hand, σ_{ph} doesn't reflect such a structural transition from amorphous to microcrystalline material. When the SiH_4 partial pressure was 3 mTorr, σ_d and σ_{ph} showed the maximum with the values of 5.8×10^{-6} S/cm and 9.1×10^{-5} S/cm, respectively. In our previous works, σ_{ph} of μc-Si:H films deposited at a high pressure around 100 mTorr was in the order of 10^{-6}, however σ_{ph} was around 10^{-5}-10^{-4} S/cm in Fig. 5-10, indicating that film quality was improved, compared to the conventional films deposited at a high pressure. Fig. 5-11 shows oxygen (O) and carbon (C) SIMS depth

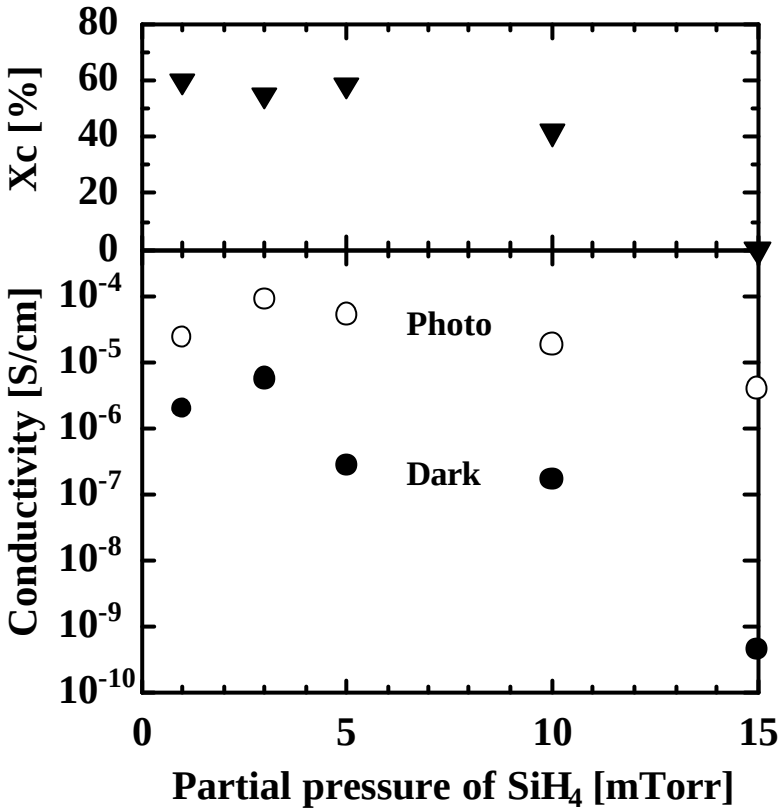

Fig. 5-10: X_c, photo and dark conductivity as a function of SiH_4 partial pressure

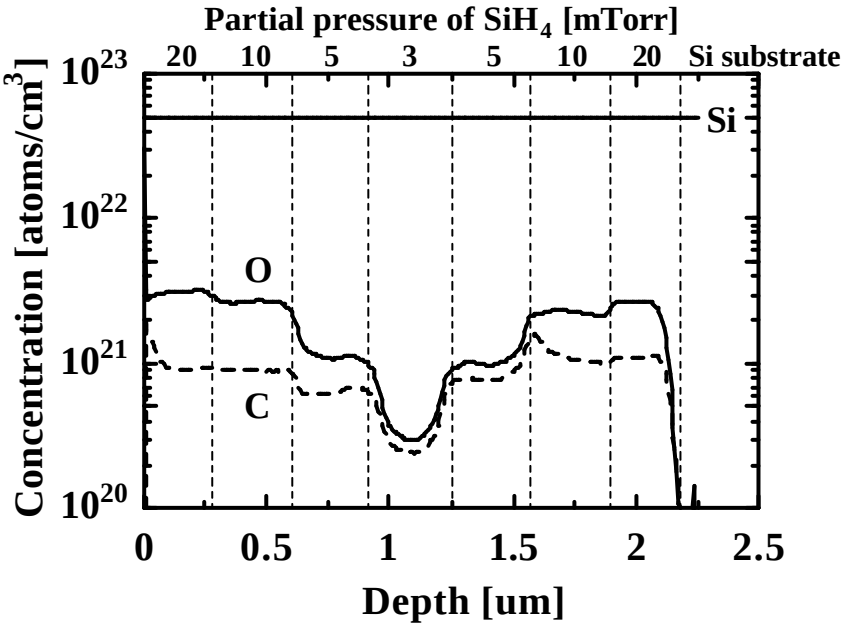

Fig. 5-11: SIMS depth profiles of μc-Si:H film as a function of SiH_4 partial pressure

profiles of μc-Si:H film as a function of SiH_4 partial pressure. For SIMS measurements, stacked thin film layers were deposited on a Si wafer as a function of SiH_4 partial pressure. The first layer was grown at a pressure of 20 mTorr and it was decreased step by step. The lowest deposition gas pressure was 3 mTorr and then it was again increased up to 20 mTorr. Each layer was deposited at a H_2 flow rate of 40sccm. The substrate and the filament temperature were 200°C and 1900°C, respectively. The dependence of O and C concentrations on the SiH_4 partial pressure was clearly indicated that the concentrations of O and C atoms could be reduced to the order of 10^{20} cm^{-3} by decreasing the partial pressure of SiH_4 down to 3mTorr. Since the evacuation speed is very high at a low deposition gas pressure, the concentrations of impurities such as O and C in the chamber are decreased. Furthermore, the generation of undesirable radicals such as SiH_2, Si_2H_6, Si_3H_8 and so on, are suppressed due to restraint of the gas phase reaction at a low deposition pressure. Thus, the incorporation of O and C during and/or after deposition can be suppressed. On the other hand, these impurity concentrations of $2x10^{20}$ is still high and a further reduction is required, however it might be thought that impurity concentrations could be further reduced by decreasing SiH_4 partial pressure less than 3 mTorr. Figs. 5-12(a) and (b) show cross-sectional SEM images of μc-Si;H films deposited at different pressures. Fig. 5-12(b) is a typical cross-sectional SEM image of μc-Si;H films deposited at a high pressure of 100mTorr by the HW-Cell method and the film has a columnar structure and many grain boundaries. On the other hand, no columnar structure can be seen in μc-Si;H film deposited at a low pressure of 3mTorr, as shown in Fig. 5-12(a). The film seems to be denser than that grown at the high pressure. Xc of μc-Si;H film shown in Figs. 5-12(a) and (b) was 60% and 90%, respectively. Therefore, these structural differences are attributed to the difference of Xc. From the SEM

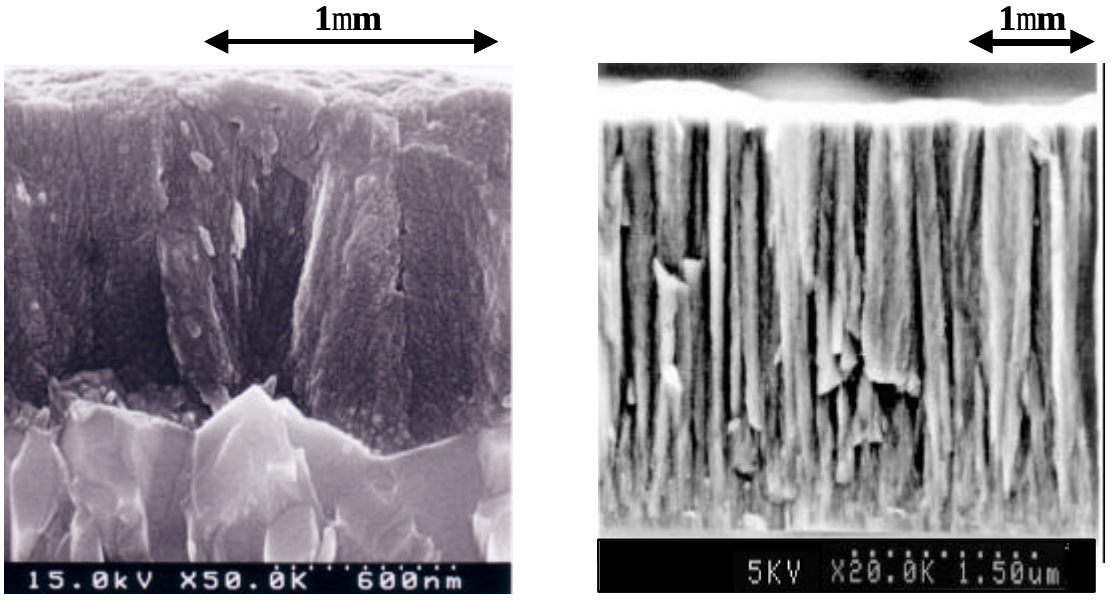

(a) (b)

Fig. 5-12: Cross-sectional SEM images of μc-Si:H films deposited at a low pressure of 3mTorr (a) and a high pressure of 100mTorr (b)

observation, it was shown that the other reason of high O and C concentrations in the μc-Si;H film deposited at a high pressure of 100mTorr is attributed to this columnar structure. The columnar structure has many grain boundaries, which have many dangling bonds and voids, therefore, impurity incorporation easily occurred during and/or after deposition.

Atomic H breaks the weak Si-Si bonds on the growing surface and chemically etches the surface through the formation of SiH_4,[18, 19] and it also terminates the dangling bonds on the growing surface and promotes the migration of SiH_3.[20] Furthermore, the generation of undesirable radicals are suppressed due to restraint of the gas phase reaction at a low deposition pressure. Thus, it is concluded that both sufficient atomic H and suppression of generation of undesirable radicals could reduce dangling bonds and voids in μc-Si:H film at a low pressure and σ_{ph} increased with decreasing SiH_4 partial pressure. According to these results, we adopted SiH_4 partial pressure of 3 mTorr for fabrication of μc-Si:H films and solar cells below mentioned.

5-3-3 Dependence on Substrate Temperature

From the results in 5-3-2, it was found that μc-Si:H films with better quality could be obtained at a SiH_4 partial pressure of 3 mTorr. Next, μc-Si:H films were deposited by changing substrate temperature. As shown in Fig. 5-13, X_c was almost constant with changing substrate temperature from 165°C to 250°C. No large differences could be observed in photo and dark conductivity, except that σ_{ph} and σ_d had a small increase at a substrate temperature of 200°C. As shown in Fig. 5-14, no large differences could be observed in H content. Total H content, Si-H bonding and $Si-H_2$ bonding were around 5-6%, 4% and 1-2%, respectively. Total H content and

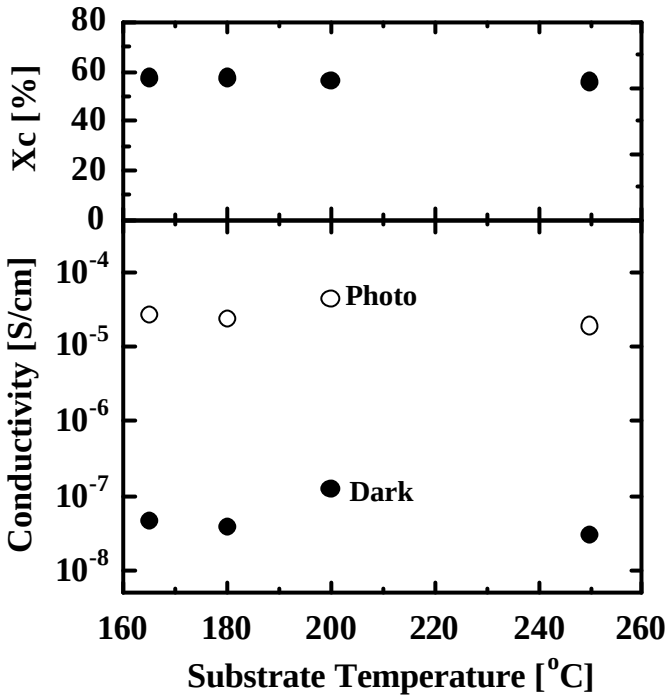

Fig. 5-13: X_c, photo and dark conductivity as a function of substrate temperature

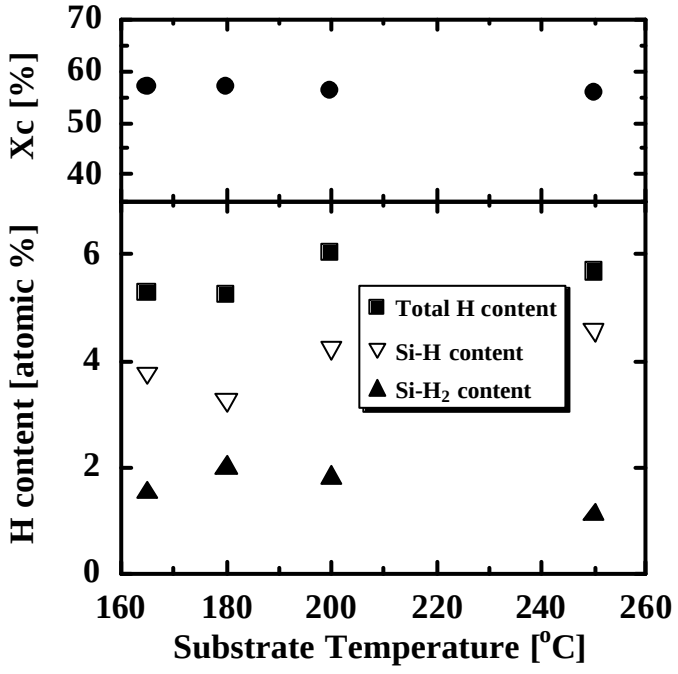

Fig. 5-14: X_c, total H, Si-H and Si-H_2 content as a function of substrate temperature

Si-H bonding had a small increase at a substrate temperature of 200°C, corresponding to the tendency of conductivities. Next, the substrate temperature was fixed 200°C, μc-Si:H films were deposited by changing filament temperature from 1800°C to 2100°C.

5-3-4 Dependence on Filament Temperature

It was demonstrated from the results in 5-3-2 that film quality largely changed with changing SiH_4 partial pressure. The film quality largely changed because pressure is a dominant deposition parameter that largely controls gas phase reactions. On the other hand, reactant gases are catalytically and pyrolitically decomposed on the surface of a filament, therefore dissociation efficiency of reactant gases has a large dependence on filament temperature. Thus, gas phase reactions might be largely changed by filament temperature. In this time, substrate temperature was fixed 200°C, films were deposited by changing filament temperature from 1800°C to 2100°C. As shown in Fig. 5-15, X_c largely increased from 48% to 63% with increasing a filament temperature from 1800°C to 2100°C, as a result, σ_d also largely increased from $1x10^{-8}$ S/cm to $2x10^{-6}$ S/cm. σ_{ph} had almost constant value of $2\text{-}4x10^{-5}$ S/cm. σ_{ph}/σ_d ratio largely increased at a filament temperature of 1800°C, indicating that film quality was improved. As shown in Fig. 5-16, total H content largely increased until 9% with decreasing a filament temperature down to 1800°C. The amorphous region ($100\%\text{-}X_c$) in μc-Si:H film decreased from 52% to 37%, total H content decreased from 9% to 4.2% with increasing filament temperature from 1800°C to 2100°C. Therefore, decreasing ratio of the amorphous region was 37/52=0.7 and decreasing ratio of total H content was 4.2/9=0.47, indicating that grain boundary was insufficiently passivated

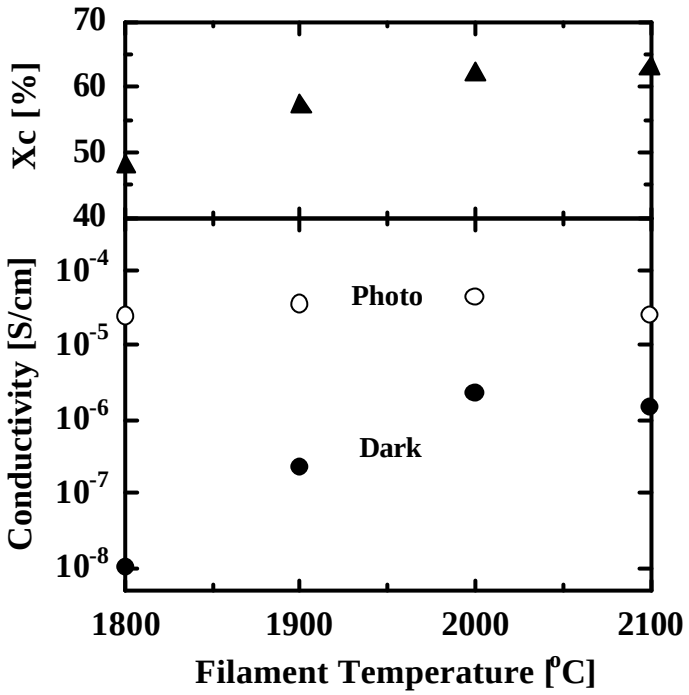

Fig. 5-15: X_c, photo and dark conductivity as a function of filament temperature

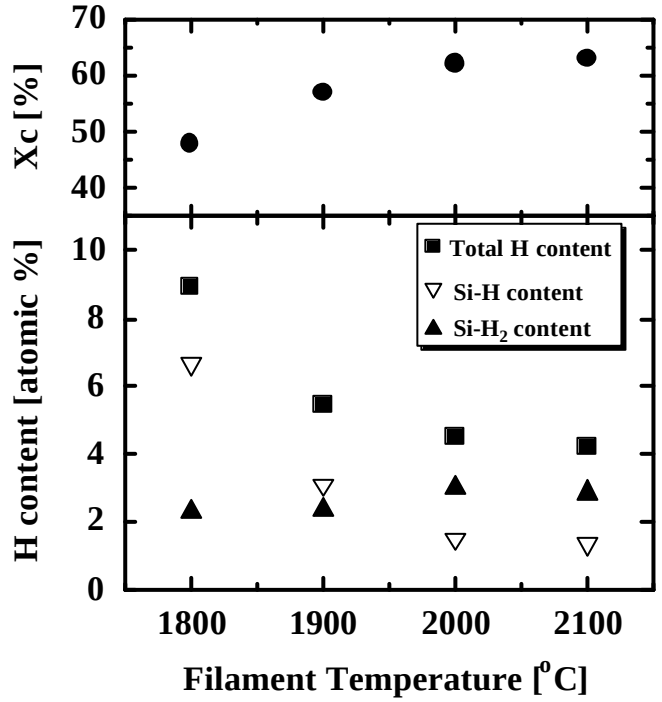

Fig. 5-16: X_c, total H, Si-H and Si-H_2 content as a function of filament temperature

by H atoms and defect densities increased at high filament temperatures. Si-H_2 bonding slightly decreased with decreasing filament temperature, however, Si-H bonding largely increased with decreasing a filament temperature down to 1800°C. From above results, it was found that total H content and Si-H/Si-H_2 ratio increased by decreasing a filament temperature down to 1800°C, indicating improvement of film quality. However, it is not clear yet that these results were derived from the decrease of gas dissociation efficiency or the decrease of heat radiation from the filament or the decrease of impurity contamination from the filament at a low filament temperature.

5-3-5 Fabrication and Characterization of Solar Cells

It was demonstrated from the results in 5-3-2 and 5-3-4 that impurity concentrations could be largely decreased by decreasing SiH_4 partial pressure down to 3 mTorr and film quality could be improved by decreasing filament temperature down to 1800°C. Therefore, in order to confirm the improvement of film quality, solar cells were fabricated and characterized.

First, solar cells were fabricated with using i-layer deposited at a substrate temperature of 200°C, a filament temperature of 1900°C, a SiH_4 partial pressure of 3 mTorr. In the conventional solar cells prepared at a filament temperature of 2100°C and a pressure of 100 mTorr, conversion efficiency of around 1% could be obtained and quantum efficiency had a very small spectrum response at a long wavelength of over 800nm, however, a conversion efficiency of 2.79% could be obtained and a relatively large spectrum response at a long wavelength of over 800nm could be observed in a quantum efficiency, as shown in Figs 5-17 and 5-18. Therefore, it was demonstrated from above results that film quality of μc-Si:H could be improved by

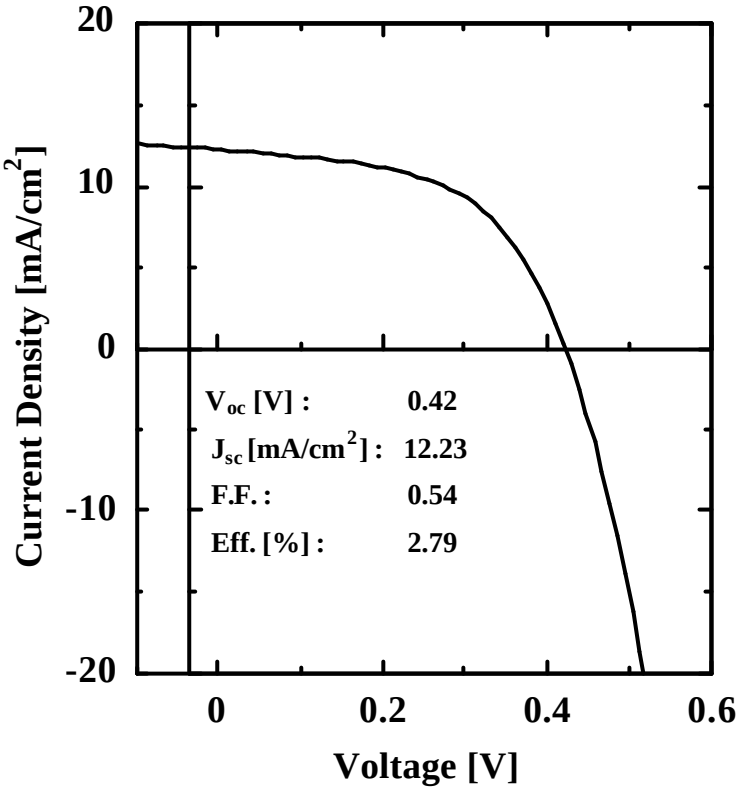

Fig. 5-17: I-V characteristics of μc-Si:H thin film solar cell

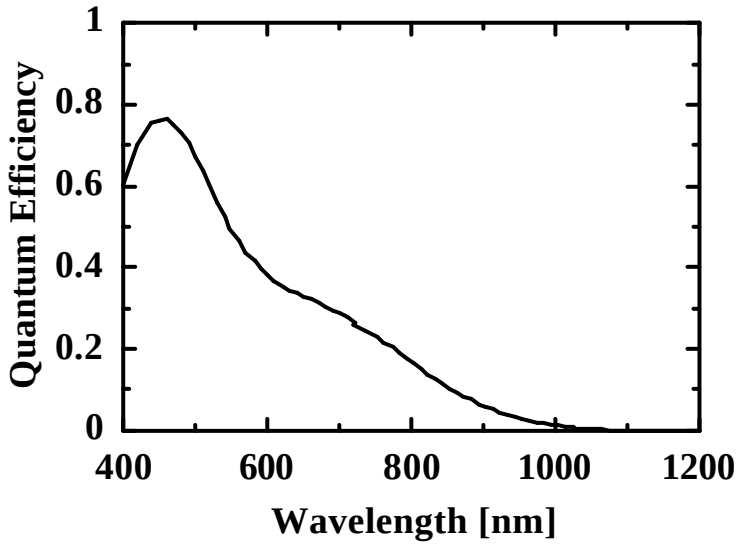

Fig. 5-18: Quantum efficiency spectrum of μc-Si:H thin film solar cell

decreasing filament temperature and SiH_4 partial pressure. Besides, as above mentioned, the other reason for the improvement of solar cell performances is that p-μc-Si:H film was used instead of p-a-SiC:H as a p-layer material.

Next, dependence of solar cell performances on substrate temperature and H_2 flow rate were investigated, respectively. No large differences could be observed in the film characterization, as shown in 5-3-3, in the solar cell performances, open circuit voltage (V_{oc}), short circuit current (J_{sc}) and conversion efficiency were almost constant at each substrate temperature, as shown in Fig. 5-19. However, fill factor (F.F.) obviously decreased with increasing substrate temperature. It might be thought that p-layer was thermally damaged at high substrate temperatures over 170°C thus the p/i interface was degraded by boron diffusion from p-layer to i-layer because the substrate temperature of the p-layer was around 170°C. Therefore, the optimum substrate temperature of the i-layer is around 150°C. As shown in Fig. 5-20, X_c largely increased from 53% to 63% with increasing H_2 flow rate from 25 sccm to 50 sccm and it was saturated at H_2 flow rates over 50 sccm. With increasing X_c, V_{oc} largely decreased from 0.4 V to 0.3 V, on the contrary F.F. largely increased from 0.4 to 0.5. J_{sc} had a peak value at a H_2 flow rate of 40 sccm. As a result, conversion efficiency increased with increasing H_2 flow rate from 25 sccm to 40 sccm, and then largely decreased at at H_2 flow rates over 50 sccm. It was found from these results that solar cell performances were largely degraded at X_c of over 60%. It was demonstrated in 5-3-1 that total H content largely decreased and Si-H/Si-H_2 ratio largely decreased with increasing H_2 flow rate, indicating degradation of film quality. Therefore, the results of solar cell performances correspond with that of film characterization, indicating that films were degraded by a large amount of H_2 dilution.

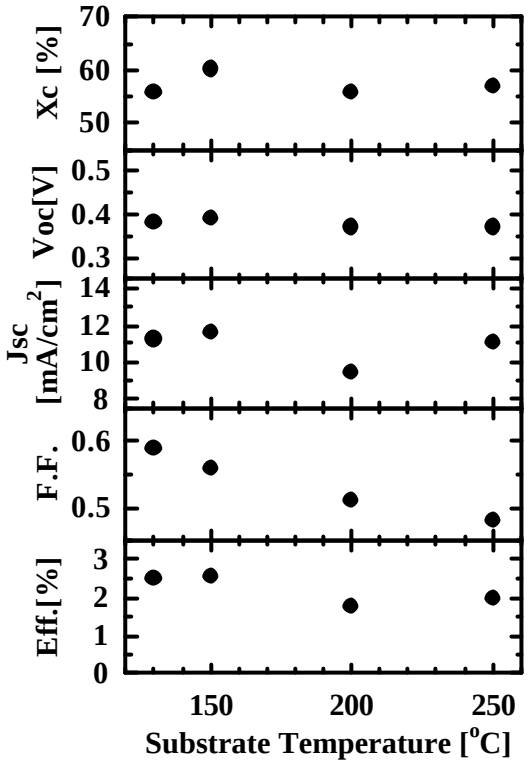

Fig. 5-19: Solar cell performances as a function of substrate temperature

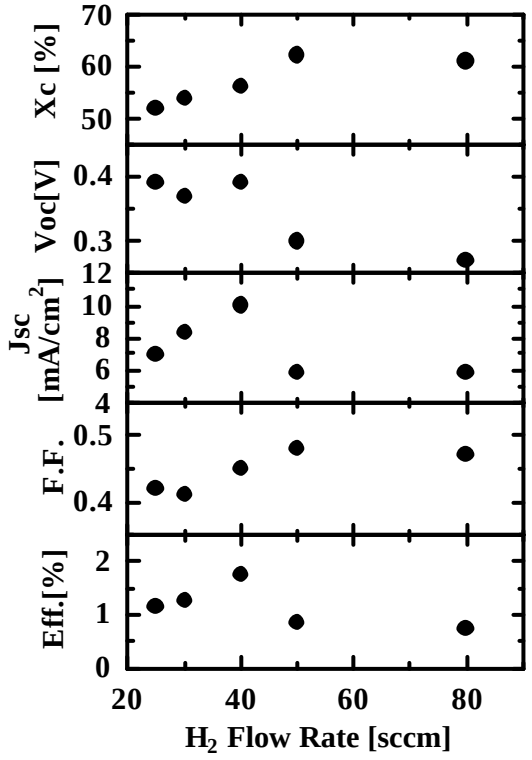

Fig. 5-20: Solar cell performances as a function of H_2 flow rate

Finally, dependence of solar cell performances on filament temperature was investigated. Substrate temperature, SiH_4 partial pressure and H_2 flow rate of the i-layer were 150°C, 3 mTorr and 40 sccm, respectively. As shown in Fig. 5-21, X_c largely increased from 48% to 62% with increasing filament temperature, as a result, V_{oc} largely decreased from 0.43 V to 0.34 V, on the contrary F.F. increased from 0.43 to 0.48. These results are the similar tendency to those of Fig. 5-19. J_{sc} largely increased with decreasing filament temperature down to 1800°C. And it had the maximum value of 14.5 mA/cm^2 in our previous works.

As shown in Fig. 5-22, the spectrum response in the long wavelength region was largely improved at a filament temperature of 1800°C, indicating the improvement of the i-layer. Therefore, the results in 5-3-4 were also supported by these results of solar cells. However, it has not been solved yet that the improvement of μc-Si:H films was derived from the decrease of impurity contaminations and/or heat radiation at the low filament temperature or the low crystal volume fraction. Therefore, next, our researches were intensively focused on these problems.

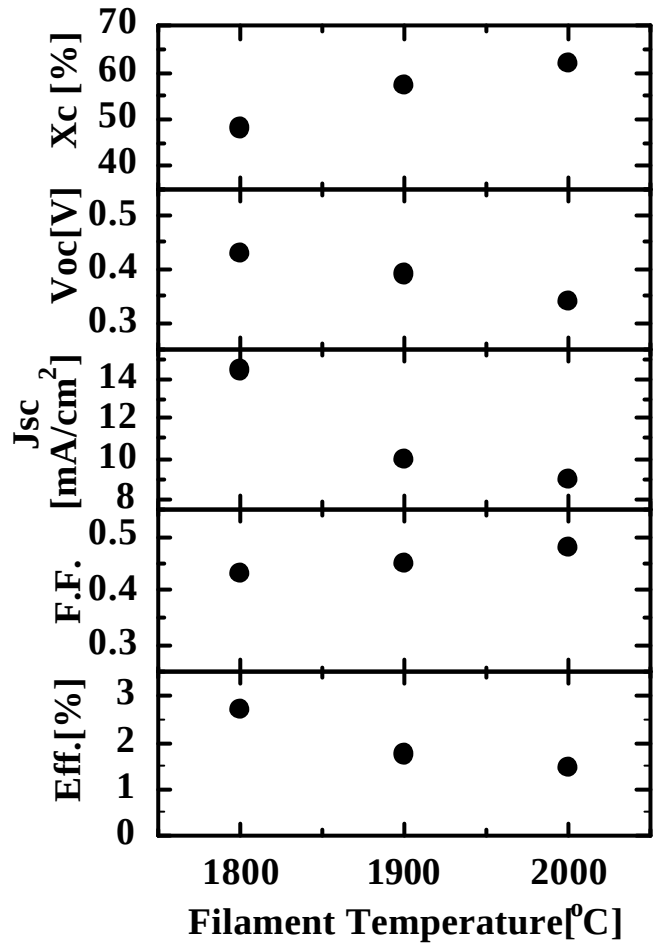

Fig. 5-21: Solar cell performances as a function of filament temperature

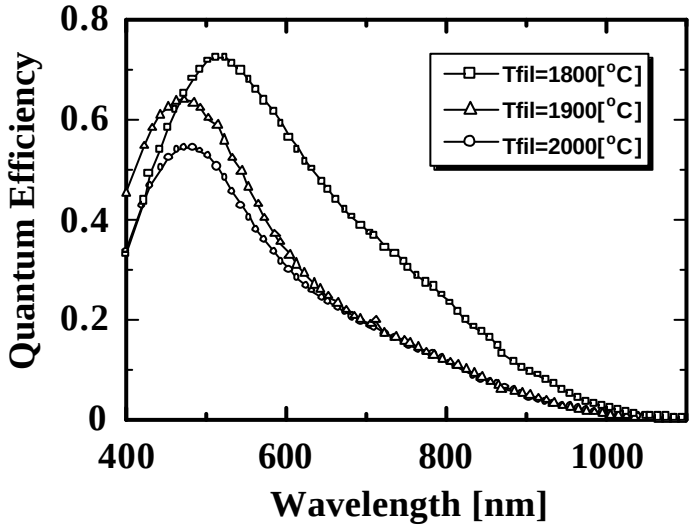

Fig. 5-22: Quantum efficiency spectrum as a function of filament temperature

5-4 Examination of Tantalum Filament and 2-Step Growth Method

5-4-1 Examination of Tantalum Filament

From the results of 5-3-5, it was found that solar cell performances were largely improved with decreasing filament temperature down to 1800°C. However, it has not been solved yet that the improvement of μc-Si:H films was derived from the decrease of impurity contaminations and/or heat radiation at the low filament temperature or the low crystal volume fraction. Therefore, in this time, μc-Si:H films were deposited at further low filament temperatures of less than 1800°C. However, when tungsten (W) is used as a filament material, there is a serious problem that W suffers from the silicide by SiH_4 gas. Since the silicide remarkably occurs at a filament temperature of less than 1800°C, a lifetime of a tungsten filament becomes extremely short at this low filament temperature. On the other hand, it is tantalum (Ta) that recently attracts much attention as a filament material that is silicide-free at filament temperatures of less than 1800°C. Therefore, in this time, μc-Si:H films and solar cells were fabricated by using a tantalum filament.

W filament has been used in the temperature region from 1800°C to 2100°C, however, we don't know the temperature region that Ta can be used. Therefore, first, the usable temperature region of Ta was investigated. In this study, a filament with a shape of coil was formed by using W or Ta wire, as a result, it was found that a filament temperature couldn't be increased over 1800°C because Ta wire is much softer than W wire and the shape of filament was largely changed by a heat at filament temperatures over 1800°C. Therefore, a Ta filament was used at filament temperatures

less than 1700°C. μc-Si:H films were deposited at a filament temperature from 1400°C to 1700°C, a substrate temperature of 190°C and a H_2 flow rate of 40 sccm and the films were characterized by photo and dark conductivity measurement, FT-IR measurement.

As shown in Fig. 5-23, a deposition rate largely decreased from 0.3 nm/s to 0.046 nm/s and X_c also largely decreased from 23% to 6% with decreasing a filament temperature from 1700°C to 1400°C, indicating that a dissociation efficiency of the reactant gases largely decreased at filament temperatures less than 1600°C. No large differences were observed in a deposition rate and X_c at a filament temperature of 1700°C, compared to W filament with filament temperatures from 1800°C to 2100°C. On the other hand, a tantalum filament didn't suffer from silicide at all even at a filament temperature of 1400°C. As shown in Fig. 5-24, photoconductivity increased in the order from 10^{-6} to 10^{-5}, on the contrary dark conductivity decreased in the order from 10^{-7} to 10^{-8} with increasing filament temperature from 1400°C to 1700°C. As a result, a photo response i.e. σ_{ph}/σ_d ratio had the maximum value at a filament temperature of 1600°C.

As shown in Fig. 5-25, X_c had a almost constant value of 6-9% at a filament temperature from 1400°C to 1600°C, it increased to 23% only at a filament temperature of 1700°C. Total H content had a almost constant large value of 9-10% at all the filament temperatures, since X_c was small value and films were almost amorphous. Besides, these total H contents were derived mainly from Si-H bonding, $Si-H_2$ content was very low and the value was 0% at filament temperatures from 1400°C to 1500°C, 0.8-1.2% at filament temperatures from 1600°C to 1700°C. As above mentioned in 5-3, in μc-Si:H films deposited at a filament temperature from 1900°C to 2100°C by using W filament, Si-H content largely decreased, on the

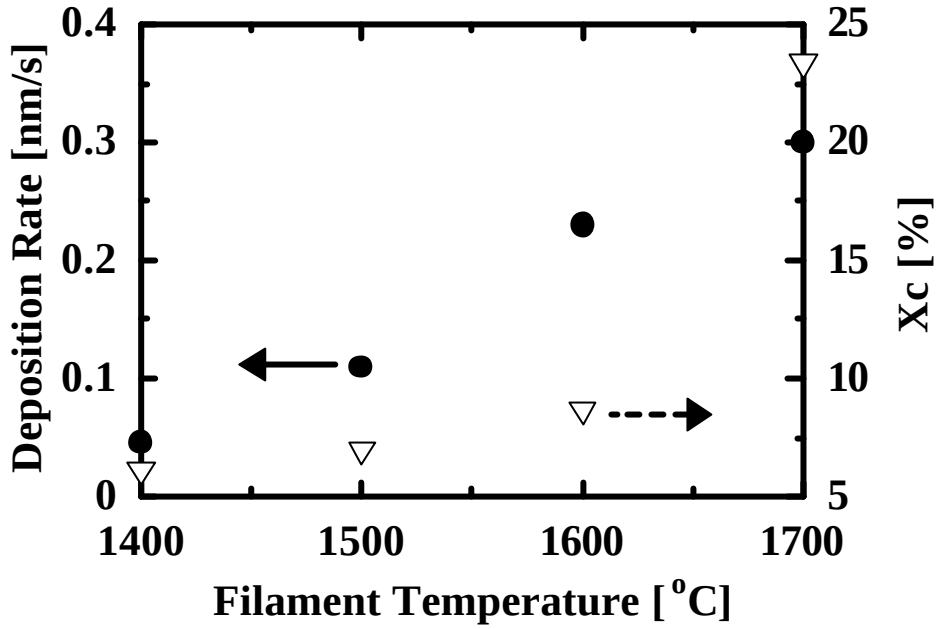

Fig. 5-23: Deposition rate and X_c as a function of filament temperature

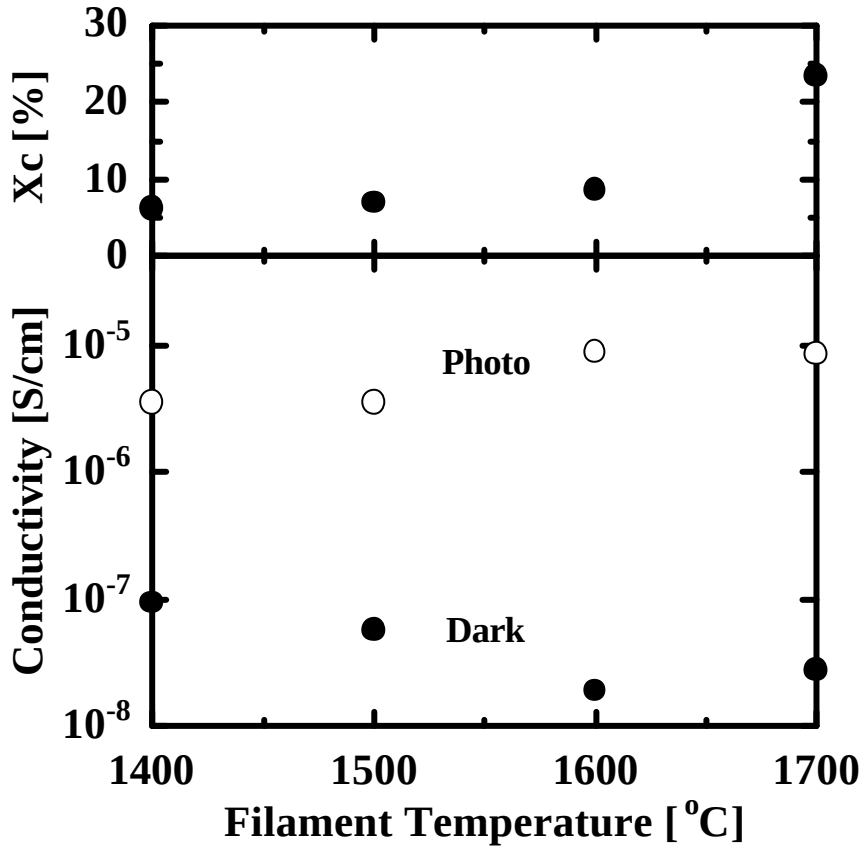

Fig. 5-24: X_c, photo and dark conductivity as a function of filament temperature

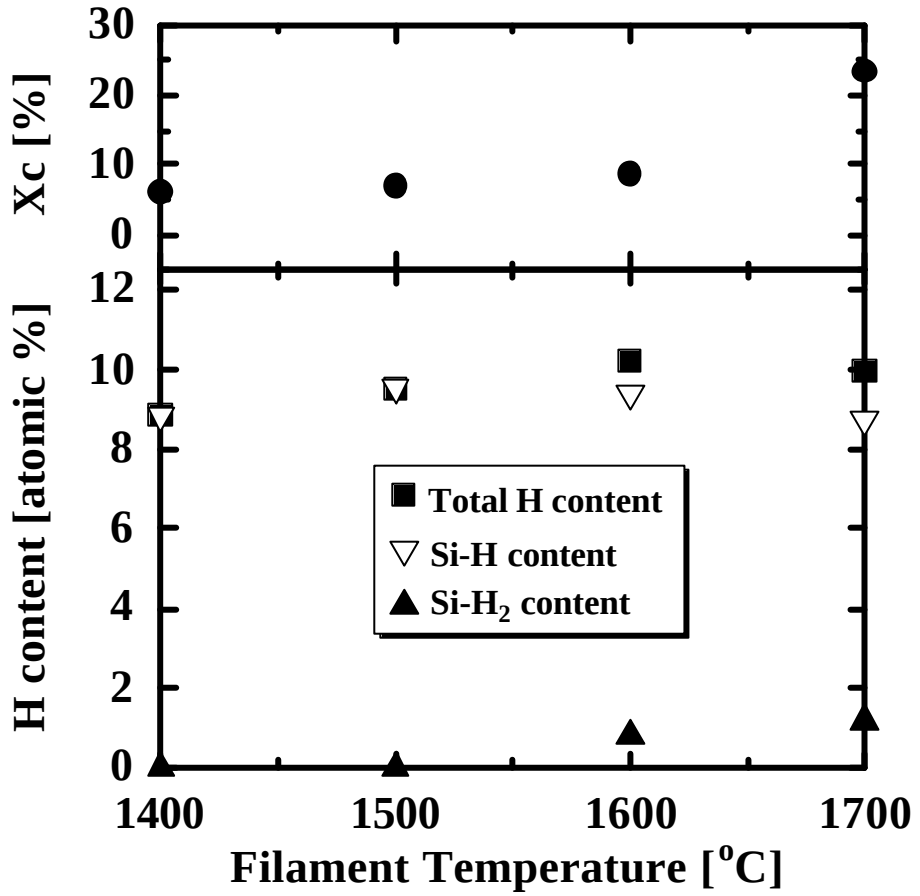

Fig. 5-25: X_c, Total H, Si-H and Si-H_2 content as a function of filament temperature

contrary Si-H_2 content largely increased with changing a film structure from amorphous to microcrystalline. Si-H bonding has never been dominant even at a low X_c. On the other hand, there was a tendency that Si-H content increased, Si-H_2 content decreased with decreasing filament temperature from 2100°C to 1800°C, therefore, following two reasons might be thought: Si-H bonding could be dominant because of the effect of Ta filament or the effect of low filament temperatures less than 1700°C.

From the above results, it was found that X_c and deposition rate largely decreased due to the decrease of gas dissociation efficiency at filament temperatures less than 1500°C, therefore, it was concluded that a practical filament temperature was from 1600°C to 1700°C. Thus, film properties as a function of H_2 flow rate was investigated at filament temperatures of 1600°C and 1700°C. A substrate temperature and SiH_4 partial pressure were 190°C and 3 mTorr, respectively. As shown in Fig. 5-26, at a filament temperature of 1600°C, X_c increased only from 8.5% to 27% with increasing H_2 flow rate from 40 sccm to 120 sccm, and decreased to 15% with increasing H_2 flow rate to 160 sccm. Therefore, filament temperature of 1600°C is insufficient for obtaining X_c of over 30%. There was a good correlation between X_c and conductivities. Both photo and dark conductivity increased with increasing X_c, they had a peak at a H_2 flow rate to 120 sccm. The values of photo and dark conductivities were around 10^{-5} S/cm and 10^{-8}-10^{-7} S/cm, respectively. Those values were similar to those of μc-Si:H films with a X_c of around 30% deposited by using a W filament. As shown in Fig. 5-27, at a filament temperature of 1700°C, X_c largely increased from 23% to 51% with increasing H_2 flow rate from 40 sccm to 60 sccm, then it was saturated at H_2 flow rates over 60 sccm. The conductivities had a good correlation with X_c, both photo and dark conductivity increased with increasing X_c. The values of photo and dark conductivities were around 10^{-5}-10^{-4} S/cm and 10^{-8}-10^{-6}

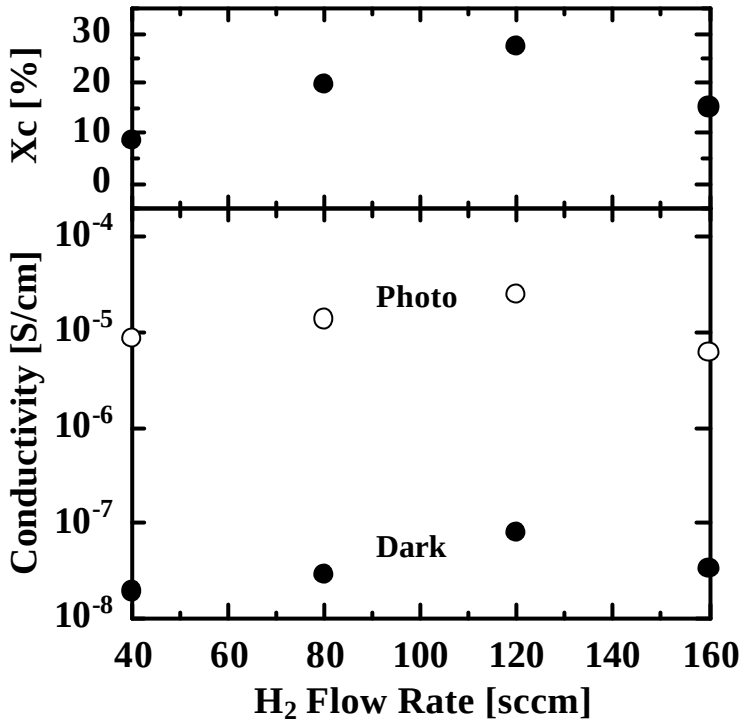

Fig. 5-26: X_c, photo and dark conductivity as a function of H_2 flow rate at T_{fil}=1600^{o}C

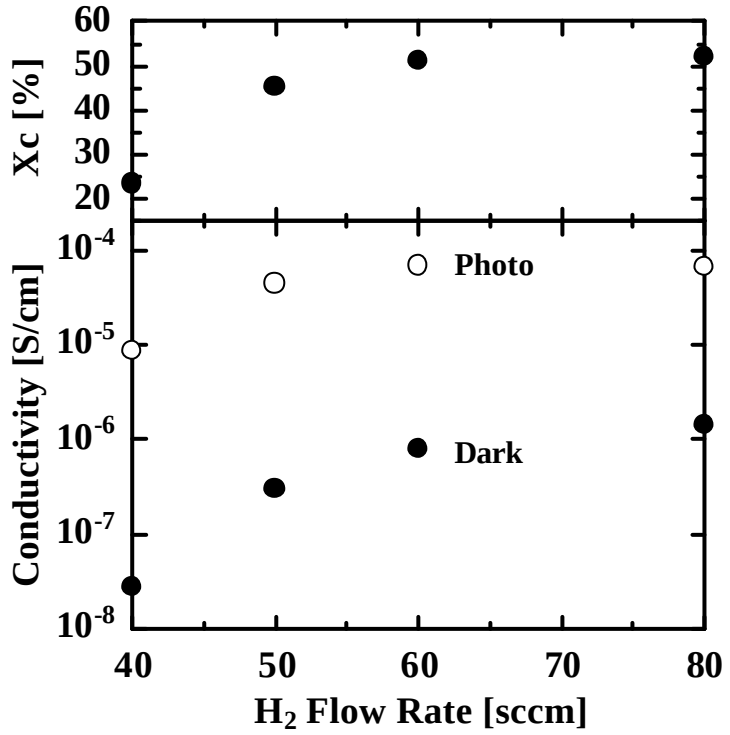

Fig. 5-27: X_c, photo and dark conductivity as a function of H_2 flow rate at T_{fil}=1700^{o}C

S/cm, respectively.

As shown in Fig. 5-28, total H and Si-H content decreased and $Si-H_2$ content increased with increasing H_2 flow rate. However those values had no large differences due to a small increase of X_c. As shown in Fig. 5-29, total H and Si-H content largely decreased and $Si-H_2$ content largely increased with increasing X_c. Compared to Fig. 5-28, those values had large changes due to a large increase of X_c. It can be thought that H atoms of μc-Si:H film exist mainly in the amorphous region. Thus, in the H_2 flow rate region from 40 sccm to 80 sccm, the amorphous region decreased from 77% to 48%, whose decrease ratio was 48/77=0.62, total H content decreased from 10% to 7%, whose decrease ratio was 7/10=0.7, indicating that total H content in the amorphous region was almost constant. On the other hand, Si-H bonding largely decreased, $Si-H_2$ bonding largely increased with increasing H_2 flow rate, indicating a degradation of quality of amorphous region due to the decrease of $Si-H/Si-H_2$ ratio.

From the above results, It was found that μc-Si:H films with a X_c less than 30% deposited at filament temperatures less than 1700°C by using a Ta filament had a extremely high $Si-H/Si-H_2$ ratio, compared to using a conventional W filament. Therefore, μc-Si:H solar cells were fabricated by using a Ta filament. A filament temperature was fixed 1700°C, because X_c could be largely varied at this temperature, a substrate temperature was 150°C and a H_2 flow rate was varied from 40 sccm to 80 sccm. A thickness of the i-layer was 1.5 μm. As shown in Fig. 5-30, X_c largely increased from 34% to 56% with increasing H_2 flow rate from 40 sccm to 80 sccm. V_{oc} decreased from 0.5 V to 0.4 V with increasing X_c. J_{sc} and F.F. had the maximum value at a H_2 flow rate of 60 sccm i.e. when a X_c was 50%, as a result a conversion efficiency of 3.5% was obtained. This conversion efficiency was the maximum value in our previous works, indicating that film quality could be improved at a low filament

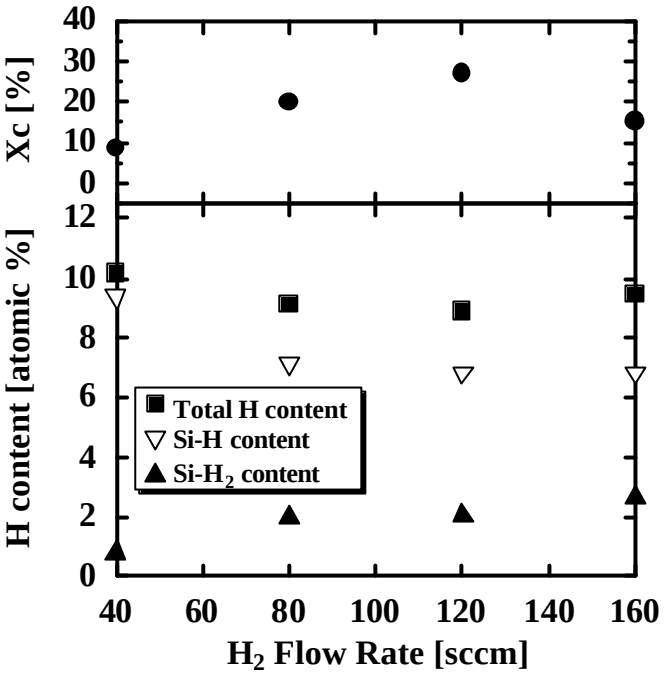

Fig. 5-28: X_c, Total H, Si-H and Si-H_2 content as a function of H_2 flow rate at T_{fil}=1600^{o}C

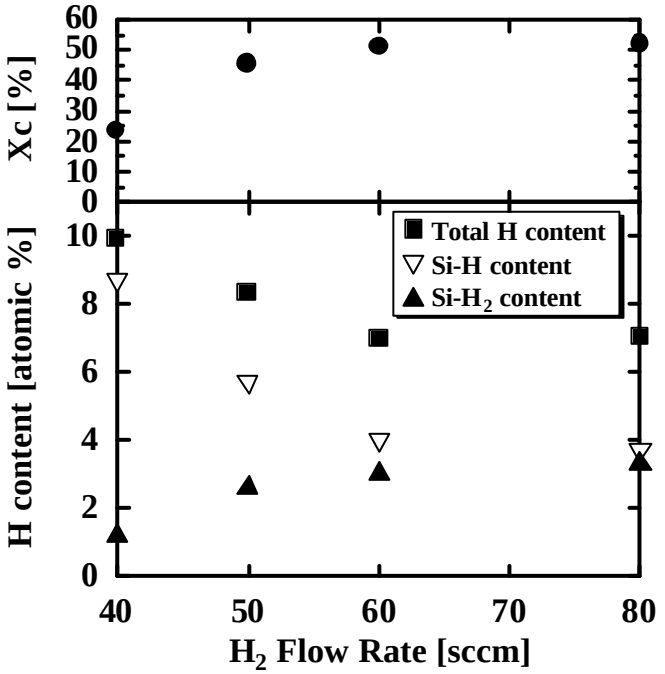

Fig. 5-29: X_c, Total H, Si-H and Si-H_2 content as a function of H_2 flow rate at T_{fil}=1700^{o}C

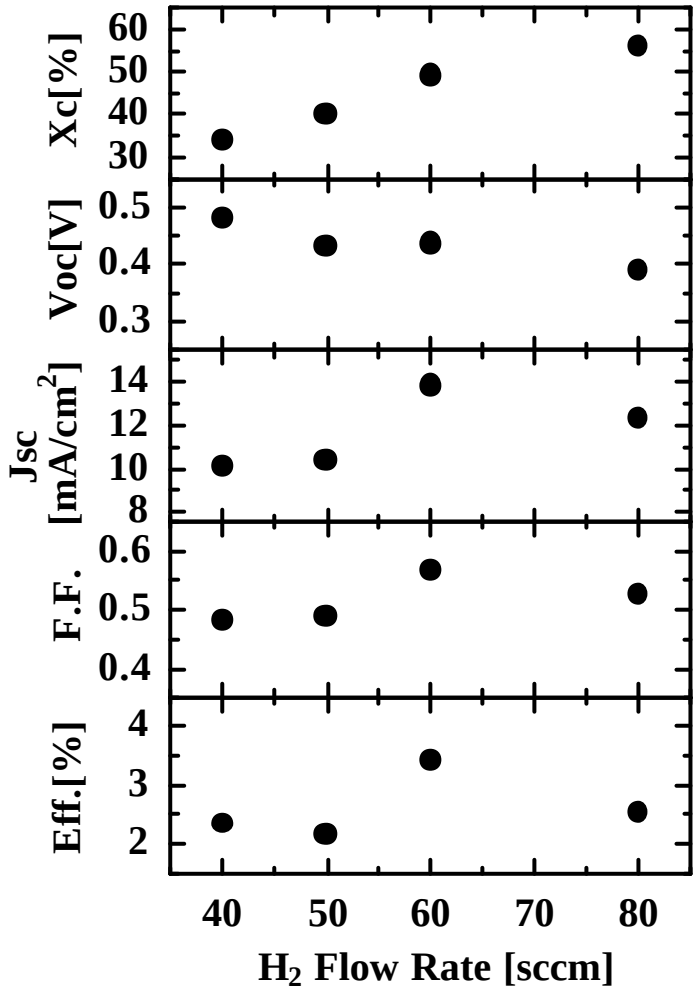

Fig. 5-30: Solar cell performances as a function of H_2 flow rate (Ta-filament:1700^{o}C)

temperature by using a tantalum filament. However, compared to the case of W filament, solar cell performances were not remarkably improved. Besides, the results such as σ_{ph}/σ_d and Si-H/Si-H_2 ratio in Figs. 5-27 and 5-29 suggests that μc-Si:H films with good quality can be obtained at H_2 flow rates less than 60 sccm. Therefore, we thought that other factors except the quality of the i-layer that lowered cell performances existed. For example, for the preparation of μc-Si:H thin films at high deposition rates and/or at a low crystallinity, the existence of an incubation (amorphous Si) layer in the initial growth was already reported.[21-23] The existence of an incubation layer at the p/i interface of a p-i-n solar cell might limit the solar cell performances. Therefore, it might be thought that the solar cell performances with low X_c of around 30-40% were unexpectedly low in the H_2 flow rate region from 40 sccm to 50 sccm because of incubation layer.

5-4-2 Study of Initial Growth of Films and 2-Step Growth Method

Next, the crystallinity of thin films was investigated as a function of H_2 flow rate to investigate the thickness of an incubation layer. As shown in Fig. 5-31, it was found that an amorphous layer with a thickness of around 80 nm was unintentionally deposited in the initial growth at the H_2 flow rate of 40 sccm (Xc: 34%). Since the i-layer was deposited on the p-μc-Si:H layer in the case of solar cells, it might be thought that the real thickness of the incubation layer was less than 80 nm. However, from these results, one of the factors that lowered the cell performances must be the incubation layer. The thickness of incubation layers could be reduced less than 10nm by increasing the H_2 flow rate up to 100sccm. In order to minimize the effect of the incubation layer on the cell performance, a novel 2-step growth method was proposed.

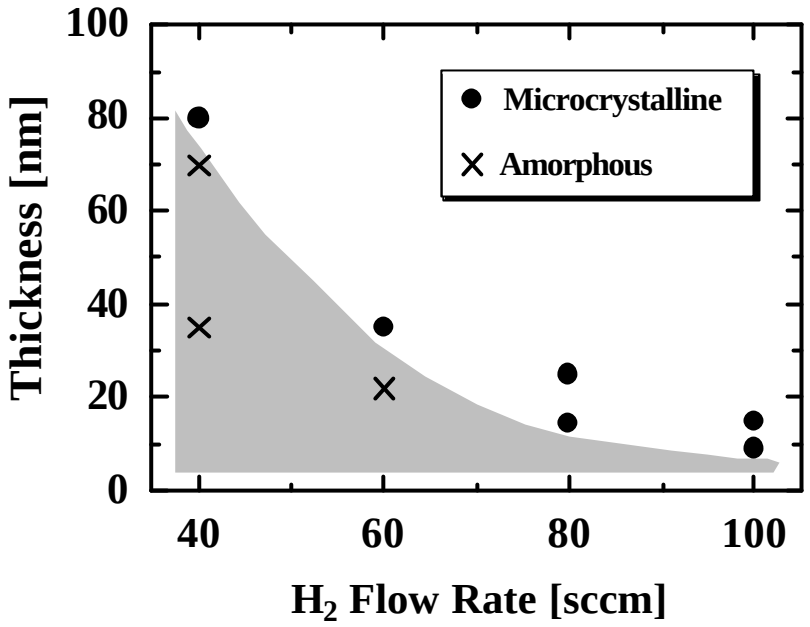

Fig. 5-31: Thickness of incubation layer as a function of H_2 flow rate

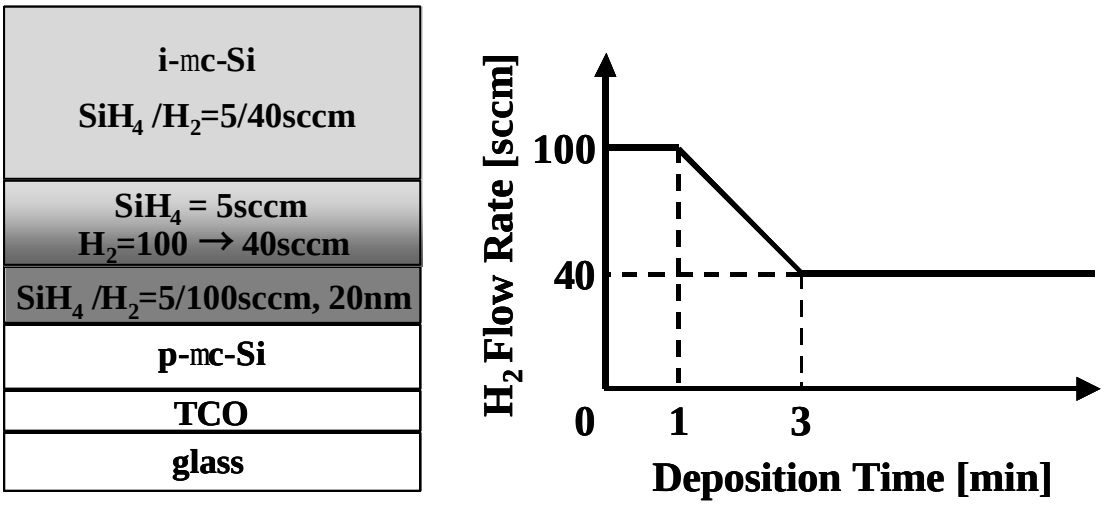

Fig. 5-32: Schematic view of the 2-step growth method

Figure 5-32 shows a schematic view of the 2-step growth method. The procedure of the 2-step growth method is as follows; after depositing μc-Si:H p-layer, a film with the thickness of 20nm was deposited at a H_2 flow rate of 100sccm that had an incubation layer thickness of less than 10nm, and then the H_2 flow rate was gradually decreased within 2 minutes down to 40sccm. All the procedures were carried out continuously.

5-4-3 Application of 2-Step Growth Method to Solar Cells

From the results in Figs. 5-30 and 5-31, there is a high probability that the incubation layer existing at the p/i interface lowered the cell performances at X_c of less than 50%. In order to investigate the influence of the incubation layer, solar cells were fabricated with using the 2-step growth method. The 2-step growth method was applied to the two solar cells with X_c of 34% (H_2 = 40 sccm) and 50% (H_2 = 60 sccm) in Fig. 5-30. A deposition rate of the i-layer was 0.3 nm/s. Figs.5-33 and 5-34 show the comparison of the solar cell performances and the I-V characteristics fabricated with and without the 2-step growth method, respectively. In the case of the solar cell with X_c of 34% (H_2 = 40 sccm), Jsc largely increased (10.11? 18.32 mA/cm^2), and a conversion efficiency of 3.9% (Voc: 0.44V, Jsc: 18.32mA/cm^2, F.F.: 0.48, active area: 0.086 cm^2, AM1.5) was achieved. On the other hand, no difference between the solar cell performances with and without the 2-step growth method was observed in solar cells with a high Xc of 50%. It implies that the reason of the low solar cell performances at the high Xc of 50% was due not to the incubation layer but to the film quality of i-layer. As shown in Fig. 5-35, the spectrum response was largely improved in the whole wavelength region from a short wavelength of 400 nm to a long

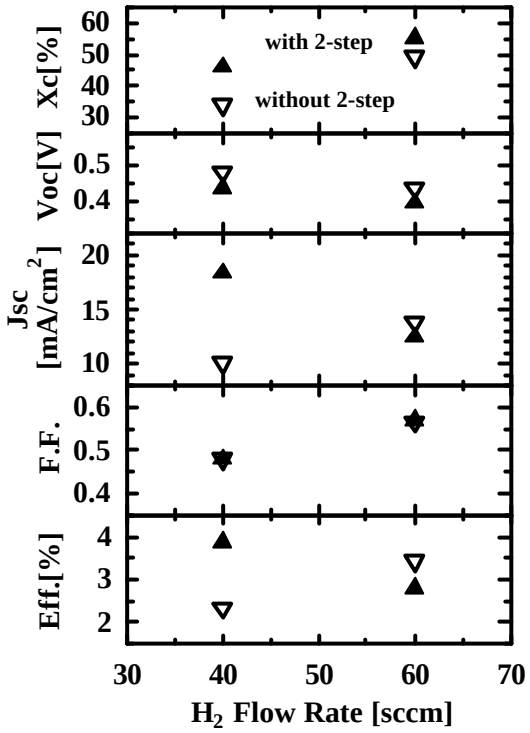

Fig. 5-33: Solar cell performances of μc-Si:H solar cells with and without the 2-step growth method at X_c of 34% and 50%

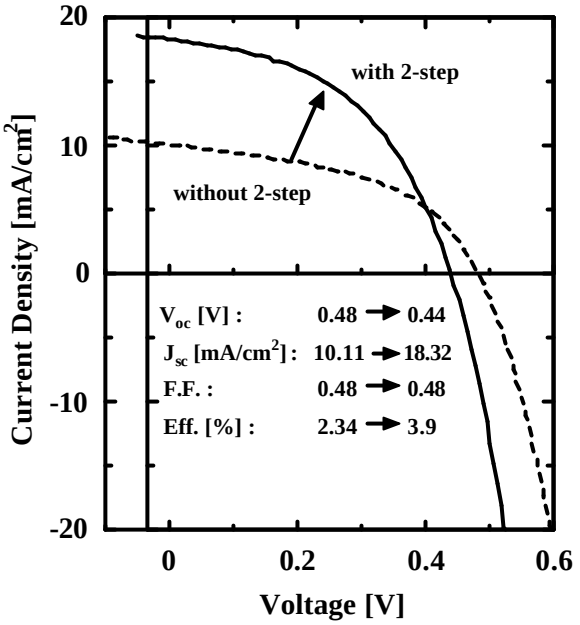

Fig. 5-34: I-V characteristics of μc-Si:H solar cells with and without the 2-step growth method at X_c of 34%

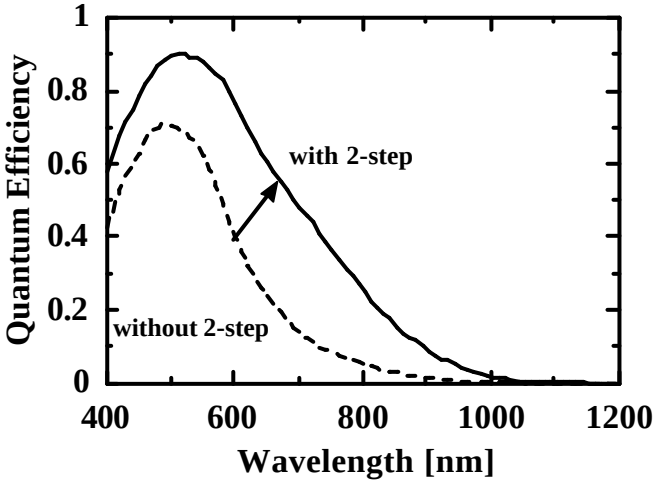

Fig. 5-35: Quantum efficiency of μc-Si:H solar cells with and without the 2-step growth method at X_c of 34%

wavelength of 1000 nm. From these results, it was found that an existence of the incubation layer at the p/i interface of p-i-n solar cells limited the solar cell performances and a good quality μc-Si:H film could be obtained at the low Xc of 30%. Furthermore, the 2-step growth method is very effective in reducing the incubation layer and the conversion efficiency of the solar cell could be successfully improved. In order to investigate the influence of incubation layer on solar cell performances, a numerical analysis was carried out using AMPS-1D BETA 1.00 (a one-dimensional device simulation program for the Analysis of Microelectronic and Photonic Structures). The material parameters used for AMPS-1D are shown in Table 5-4.

Table 5-4: Material parameters used for AMPS-1D

	p-layer (μc-Si:H)	Incubation-layer (a-Si:H)	i-layer (μc-Si:H)	n-layer (a-Si:H)
Thickness [μm]	0.02	0.06	1.2	0.02
Carrier concentration [cm^{-3}]	$1x10^{19}$	$1x10^{15}$	$1x10^{15}$	$5x10^{18}$
N_C [cm^{-3}]	$3x10^{19}$	$3x10^{19}$	$3x10^{19}$	$3x10^{19}$
N_V [cm^{-3}]	$2x10^{19}$	$2x10^{19}$	$2x10^{19}$	$2x10^{19}$
ϕ_b [eV]	1.0	-	-	0.2
g_A/g_D [$cm^{-3}eV^{-1}$]	$5x10^{19}/5x10^{19}$	$5x10^{19}/5x10^{19}$	$5x10^{19}/5x10^{19}$	$5x10^{19}/5x10^{19}$
E_A/E_D [eV]	0.01/0.02	0.03/0.04	0.01/0.02	0.03/0.04
D-state density [cm^{-3}]	$1x10^{16}$	$1x10^{16}$	$1x10^{15}$	$2x10^{17}$
D^+-level (above E_V) [eV]	0.5	0.5	0.5	0.5
D^--level (below E_C) [eV]	0.5	0.5	0.5	0.5
Capture cross section				
$D^++e^-=D^o$ [cm^2]	$1x10^{-14}$	$1x10^{-14}$	$1x10^{-14}$	$1x10^{-14}$
$D^o+h^+=D^+$ [cm^2]	$1x10^{-15}$	$1x10^{-15}$	$1x10^{-15}$	$1x10^{-15}$
$D^o+e^-=D^-$ [cm^2]	$1x10^{-15}$	$1x10^{-15}$	$1x10^{-15}$	$1x10^{-15}$
$D^-+h^+=D^o$ [cm^2]	$1x10^{-14}$	$1x10^{-14}$	$1x10^{-14}$	$1x10^{-14}$
σ_{AG} / σ_{DG} [eV]	0.13/0.13	0.09/0.09	0.13/0.13	0.09/0.09
Electron affinity χ [eV]	3.9	3.9	3.9	3.9
Dielectric constant	11.9	11.9	11.9	11.9
Mobility bandgap [eV]	1.1	1.7	1.1	1.7
Mobility μ_e/μ_h [$cm^2/V^{-1}/s^{-1}$]	50/5	20/3	50/5	10/1

Where N_C and N_V are effective density of states in the conduction band and valence band, respectively. ϕ_b is E_C-E_F at x=0 (front-surface/p-layer interface) or at x=L (n-layer/back-surface interface). g_A and g_D are prefactor in the following equations (2) and (3), respectively. E_A and E_D are the characteristic energy. σ_{AG} and σ_{DG} are the standard deviation of the acceptor-like and donor-like Gaussian dangling bond states, respectively. The equations (2) and (3) are the acceptor-like and donor-like band tail states, respectively.

$$g_A(E) = g_A \exp\{-(E_C-E)/E_A\} \quad (2)$$

$$g_D(E) = g_D \exp\{-(E-E_V)/E_D\} \quad (3)$$

From the result of the numerical analysis, it was found that conversion efficiencies largely decreased from 5.93% (Voc: 0.46V, Jsc: 20.28mA/cm^2, F.F.: 0.64) to 2.38% (Voc: 0.58V, Jsc: 7.29mA/cm^2, F.F.: 0.56) with insertion of the incubation (amorphous Si) layer at the p/i interface. This tendency of Voc and Jsc well corresponds to the result of Fig. 5-34. Fig. 5-36 shows calculated electric fields of p-i-n μc-Si solars cell with and without the incubation layer at the p/i interface. The homogeneous electric field was strongly formed in the whole i-layer region when the p/i interface had no incubation layer. A barrier was formed in the valence band at the p/i interface and the electric field became very weak in the whole i-layer region when the p/i interface had the incubation layer. Moreover, as shown in Fig. 5-37, it was revealed that when the p/i interface had the incubation layer, electron-hole recombination both at the p/i interface and in the i-layer largely increased from 4×10^{18} cm^{-3}s^{-1} to 3×10^{19} cm^{-3}s^{-1} and from 1×10^{20} cm^{-3}s^{-1} to 1×10^{21} cm^{-3}s^{-1}, respectively. As a result, short circuit current largely decreased.

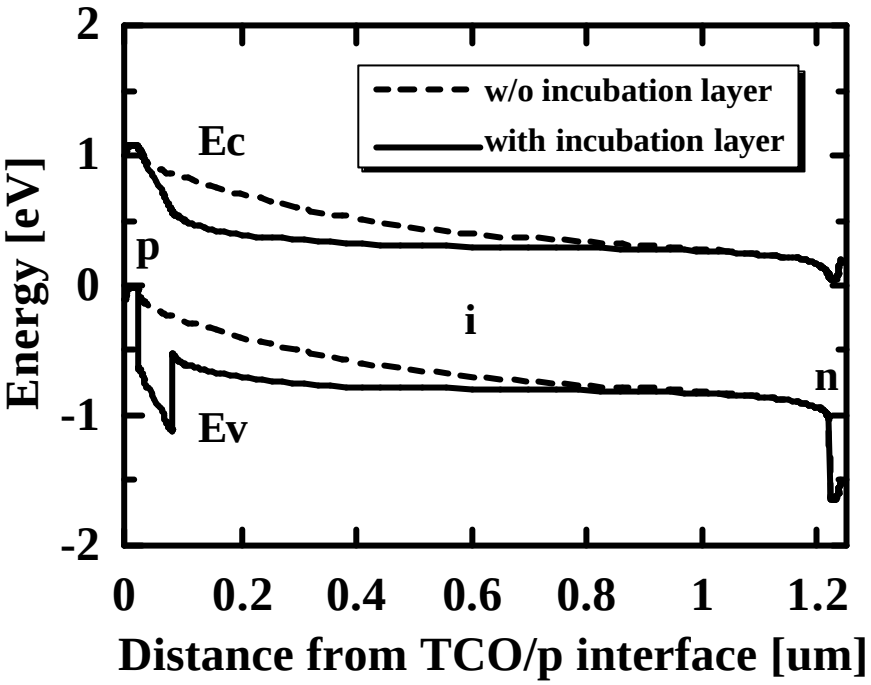

Fig. 5-36: Calculated electric field of p-i-n μc-Si:H solar cell with and without incubation layer at p/i interface

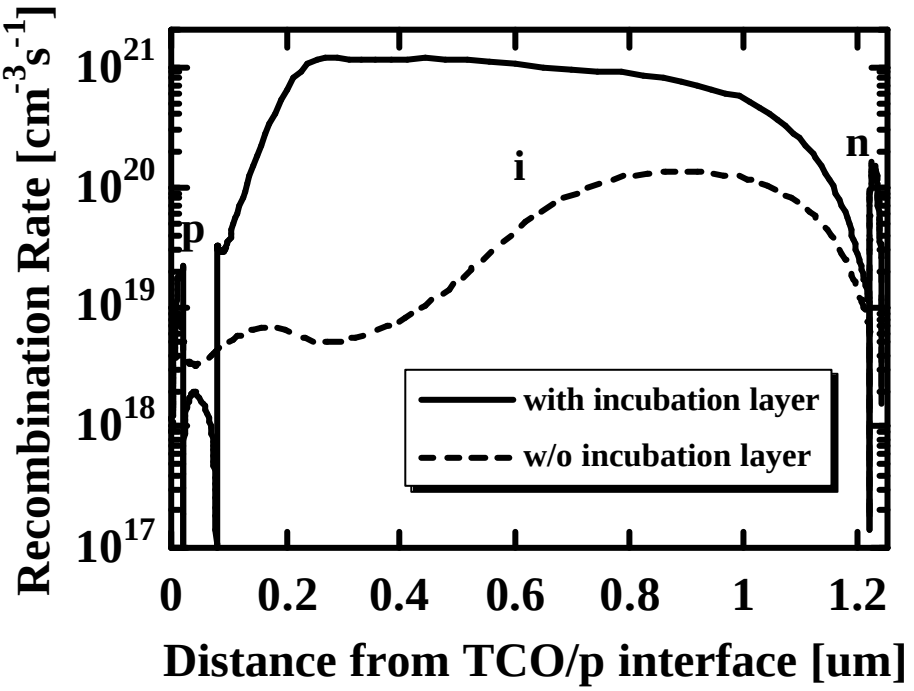

Fig. 5-37: Calculated recombination rate of p-i-n μc-Si:H solar cell with and without incubation layer at p/i interface

5-4-4 Comparison of Tungsten and Tantalum Filament in Solar Cell Performances

From the above results in 5-4, film quality of μc-Si:H was improved by decreasing filament temperature down to 1700°C using a Ta filament as a novel filament material, furthermore, the 2-step growth method was proposed and a large improvement could be successfully obtained for solar cell performances by reducing incubation layer. Therefore, in this time, W filament was again used and solar cells were fabricated with using 2-step growth method. Then, comparison of W and Ta filament in solar cell performances was investigated. Figure 5-38 shows solar cell performances as a function of filament temperature. In Fig. 5-38, the cell performances at a filament temperature of 1700°C show those of a solar cell prepared at a H_2 flow rate of 40 sccm with using Ta filament in 5-4-3, the cell performances at filament temperatures of from 1800°C to 2000°C show those of a solar cell prepared with using W filament, and X_c of those solar cells was maintained 30% by controlling H_2 flow rate from 20 sccm to 30 sccm for each filament temperature. The thickness of the i-layer of each solar cell was around 1.5 μm, the deposition rate was around 0.3 nm/s. The 2-step growth method was applied to each solar cell and the other deposition parameters were as same as those of the solar cell at a filament temperature of 1700°C in 5-4-3. V_{oc} was as high as 0.52 V only at a filament temperature of 1800°C and it was around 0.45 V at the other filament temperature. The reason of the high V_{oc} at a filament temperature of 1800°C was because X_c was 20% and lower than that of the other solar cells. J_{sc} had the maximum value of 18.32 mA/cm^2 at a filament temperature of 1700°C, although X_c was as high as 50%. Cell performances degraded at a high X_c, as shown in 5-3-5 and 5-4-3, therefore, it was indicated that film quality

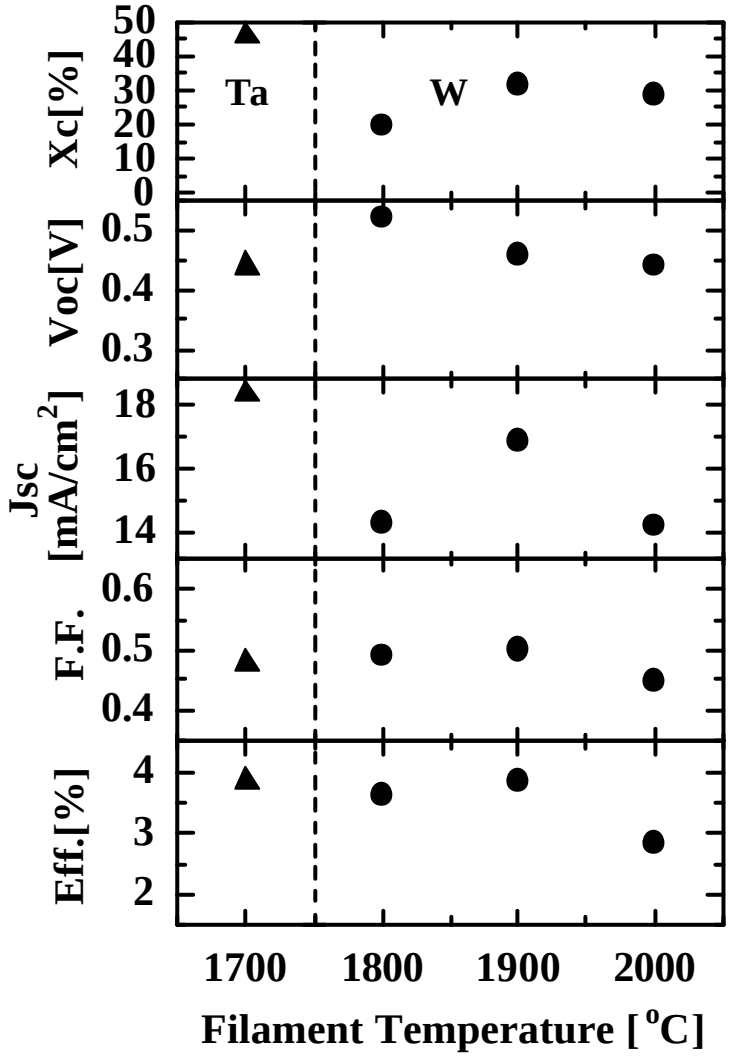

Fig. 5-38: Solar cell performances as a function of filament temperature

was improved at a low filament temperature of 1700°C. J_{sc} largely decreased at a filament temperature of 1800°C because X_c was as low as 20% and the film structure was similar to amorphous. J_{sc} at a filament temperature of 1900°C had the maximum value of around 17 mA/cm^2 in all the solar cells prepared by using W filament in our previous works, indicating the effects of a low X_c of 30% and 2-step growth method. On the other hand, although X_c was as low as 30%, J_{sc} largely decreased at a filament temperature of 2000°C, indicating a degradation of film quality of i-layer. F.F. had an almost constant value of 0.5 at each filament temperature. Conversion efficiency was around 4.0% at filament temperatures from 1700°C to 1900°C, however it decreased down to 3.0% at a filament temperature of 2000°C. Therefore, it is concluded that the filament temperature is very important for film quality and the optimum filament temperature region is from 1700°C to 1900°C. However, it is difficult to be concluded from above results if Ta filament is superior to W filament.

5-4-5 Optimization in Fabrication of Solar cells

From the results in 5-4-4, in the case of W filament as well as in the case of Ta filament with a temperature of 1700°C, a conversion efficiency of around 4.0% could be obtained by decreasing filament temperature less than 1900°C and using the 2-step growth method. Next, solar cells were optimized with using W filament, for further improvement of the solar cell performances. First, thickness of p-layer, i-layer and n-layer was optimized. Second, deposition time and H_2 flow rate in the first-step of the 2-step growth method was optimized in order to improve the p/i interface. In this time, the deposition parameters of i-layer of all the solar cells were the same as those of the solar cell with a conversion efficiency of 4.0% prepared at a filament

temperature of 1900°C in 5-4-4. As shown in Fig. 5-39, especially, J_{sc} had a large dependence on the p-layer thickness. V_{oc} and F.F. slightly increased with increasing the p-layer thickness. Conversion efficiency had the maximum value of 4.2% at a p-layer thickness of 25 nm, reflecting the change of J_{sc}. A thickness of i and n-layer were 1.5 μm and 40 nm, respectively. As shown in Fig. 5-40, spectral response in the short wavelength region largely decreased when the p-layer thickness was as thick as 35 nm, indicating the absorption of the incident light in the p-layer. On the other hand, spectral response in the long wavelength region increased at a p-layer thickness of 35 nm. Besides, V_{oc} and F.F. increased at this p-layer thickness, indicating that carrier recombination was restrained by a strong electric field in the i-layer due to a thick p-layer. On the contrary, spectral response in the short wavelength region largely increased at a p-layer thickness less than 25 nm, indicating the reduction of absorption of the incident light in the p-layer. However, V_{oc}, F.F. and spectral response in the long wavelength region decreased with decreasing p-layer thickness less than 25 nm. It might be thought that internal electric field in the i-layer became weak because of a thin p-layer. The cell performances had a peak at a p-layer thickness of 25 nm, therefore, next, p-layer thickness was fixed 25 nm and n-layer thickness was optimized. As shown in Fig. 5-41, J_{sc} largely decreased with decreasing the n-layer thickness from 40 nm to 15 nm. V_{oc} also slightly decreased with decreasing the n-layer thickness. On the other hand, F.F. increased with decreasing the n-layer thickness. As a result, conversion efficiency had the maximum value of 4.2% at a n-layer thickness of 40 nm. V_{oc} and J_{sc} decreased with decreasing n-layer thickness, probably because internal electric field in the i-layer became weak due to a thin n-layer. F.F. increased with decreasing n-layer thickness, probably because n-layer was amorphous and the series resistance was reduced when the n-layer thickness was thin. Next, a thickness of

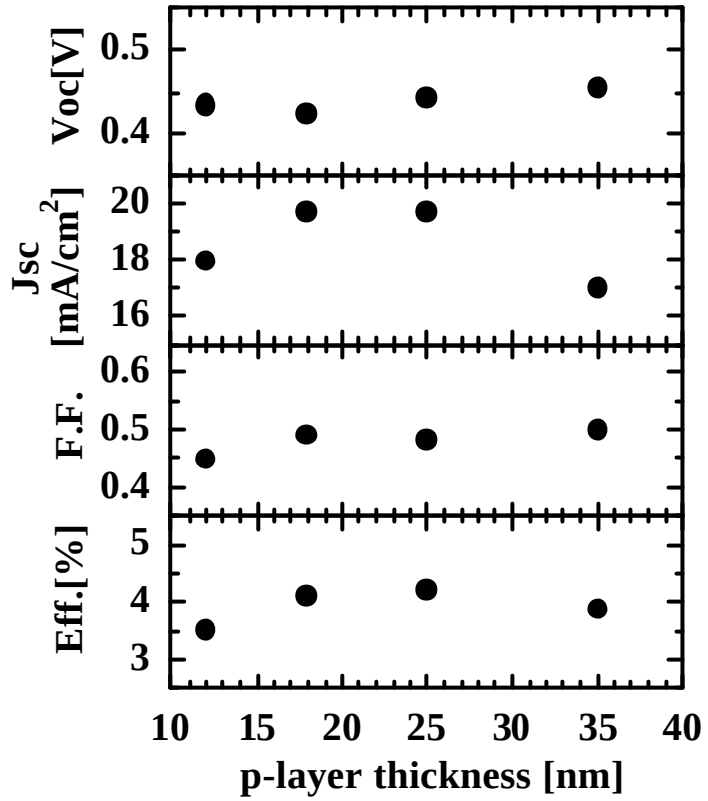

Fig. 5-39: Solar cell performances as a function of p-layer thickness

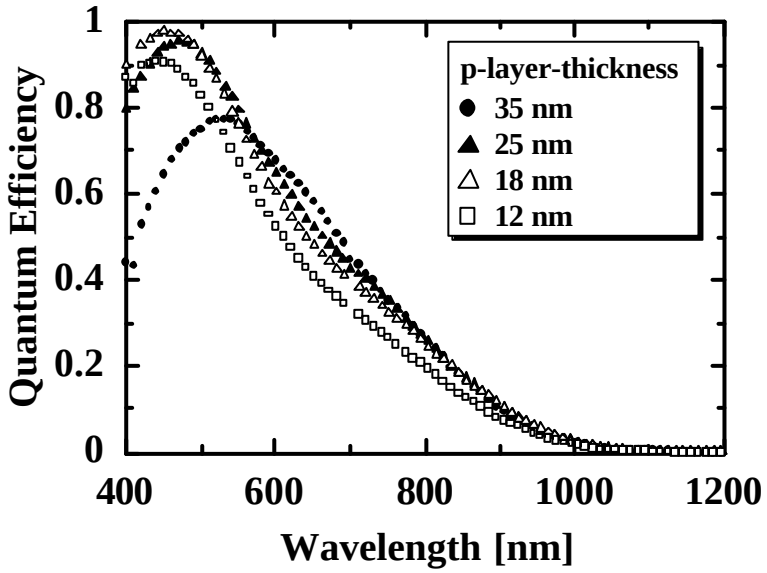

Fig. 5-40: Quantum efficiency of solar cell as a function of p-layer thickness

p and n-layer was fixed 25 nm and 40 nm, respectively. Then, the dependence on i-layer thickness was investigated. As shown in Fig. 5-42, all the parameters increased with decreasing the i-layer thickness from 2.25 μm to 0.75 μm. As a result, the solar cell performances were largely improved at i-layer thickness of 0.75 μm, the maximum conversion efficiency of 4.8% (Voc: 0.47V, Jsc: 17.44mA/cm^2, F.F.: 0.58, active area: 0.086 cm^2, AM1.5) was obtained. In this time, increase of J_{sc} was expected with increasing i-layer thickness, however J_{sc} decreased. For these results, following reasons can be thought: first, internal electric field in the i-layer became weak and carrier recombination increased with increasing i-layer thickness because of insufficient quality of the i-layer. Second, since the i-layer with a low X_c of 30% was almost amorphous and its optical properties were also similar to those of amorphous, a large light absorption could be obtained for a thin i-layer, however further light absorption couldn't be obtained with increasing i-layer thickness and cell performances decreased due to the increase of carrier recombination at a thick i-layer thickness. Third, if the p/i interface properties of our solar cells are bad, the cell performances are largely limited by carrier recombination at the p/i interface. Therefore, when i-layer thickness increased, carrier recombination increased and cell performances decreased because of the reduction of internal electric field in the i-layer. Next, in order to improve the p/i interface properties, deposition time and H_2 flow rate in the first-step of the 2-step growth method was optimized. The first layer has been deposited at a H_2 flow rate of 100 sccm for 1 minute. The incubation layer could be successfully reduced under this deposition condition, however the p-layer can be damaged by a large amount of atomic hydrogen. Therefore, first, H_2 flow rate in the first-step of the 2-step growth method was fixed 100 sccm, deposition time was varied from 0.5 minute to 3 minutes. Second, deposition time was fixed 1 minute and H_2 flow

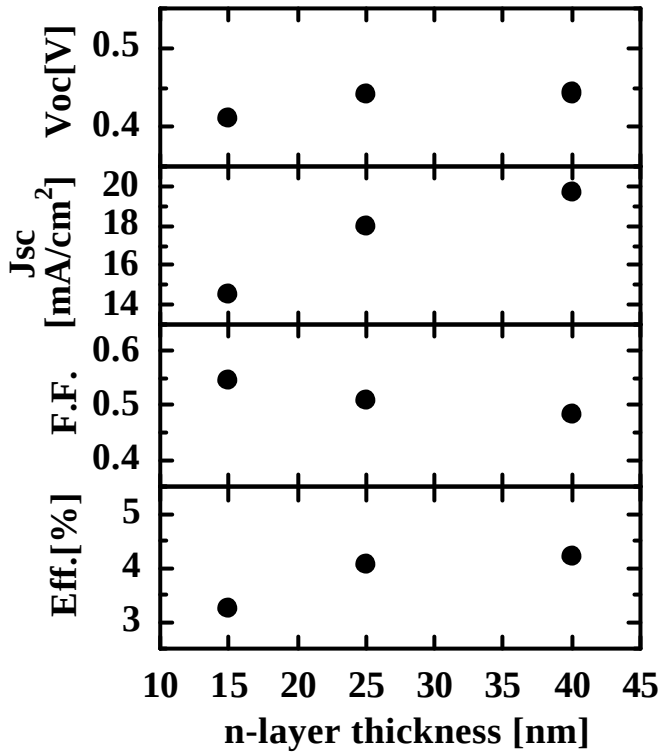

Fig. 5-41: Solar cell performances as a function of n-layer thickness

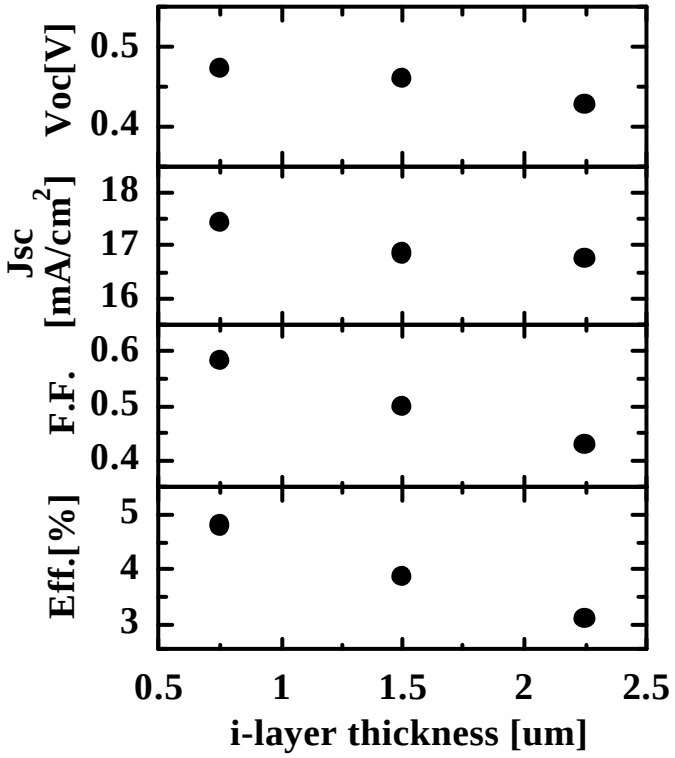

Fig. 5-42: Solar cell performances as a function of i-layer thickness

rate was varied from 25 sccm to 100 sccm. As shown in Fig. 5-43, no changes could be observed in the cell performances with changing deposition time from 0.5 minute to 3 minutes, except small differences in J_{sc}. It was already demonstrated that the film crystallization started within 0.5 minute at a H_2 flow rate of 100 sccm, therefore, a deposition time of 0.5 minute was sufficient for the reduction of the incubation layer. On the other hand, the p-layer can be damaged until the i-layer starts to grow. Therefore, there is no difference between 1 minute and 3 minute after the film grows. Thus, the cell performances were not varied with changing the deposition time in the first-step of the 2-step growth method from 0.5 minute to 3 minutes because of above reason. Therefore, we thought p-layer was damaged within several minutes in the initial growth of i-layer; next H_2 flow rate was varied. As shown in Fig. 5-44, the dependence of the cell performances on H_2 flow rate was clearly observed. V_{oc} was almost constant with a value of around 0.48 V, however J_{sc} largely changed, as a result, it was found that the optimum H_2 flow rate in the first-step of the 2-step growth method was 40 sccm. Besides, the maximum conversion efficiency of 5.3% was obtained at this H_2 flow rate. F.F. increased at a H_2 flow rate of 100 sccm because the i-layer thickness was 0.75 μm and thinner than 1 μm of the other solar cells. A H_2 flow rate of 25 sccm corresponds to the case without 2-step growth method. Therefore, the decrease of cell performances at a H_2 flow rate of 25 sccm because of an incubation layer. From the above results, it is concluded that the p-layer can be damaged by the deposition of the first-step of the 2-step growth method and the damage can be reduced by decreasing H_2 flow rate.

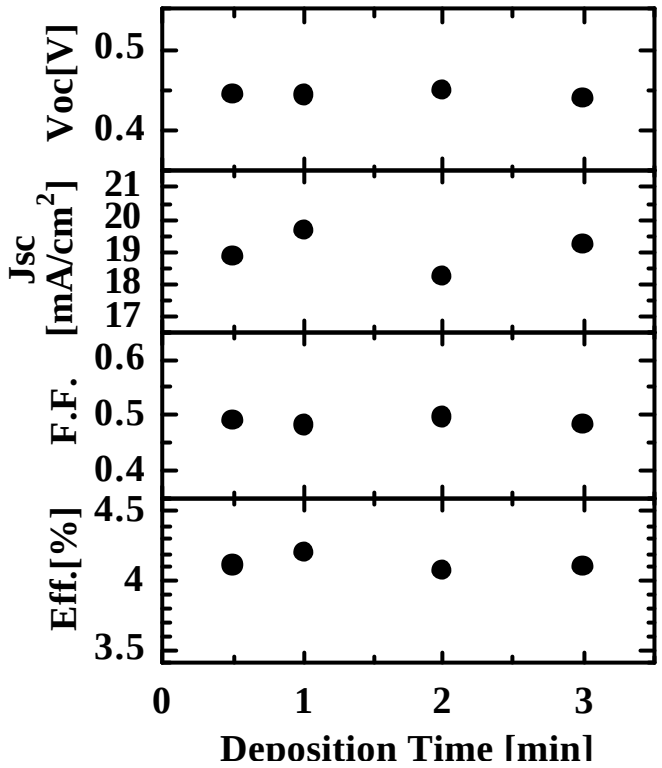

Fig. 5-43: Cell performances vs deposition time in the first-step of 2-step growth method

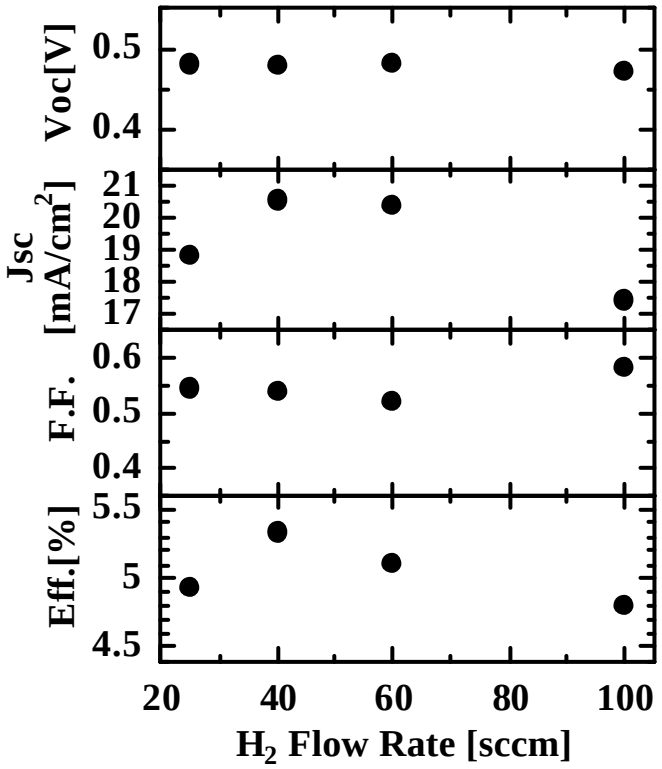

Fig. 5-44: Cell performances vs H_2 flow rate in the first-step of 2-step growth method

5-5 Optimization of Deposition Parameters and Degradation Properties of Microcrystalline Silicon Thin Films and Solar Cells

5-5-1 Optimization of Deposition Parameters

It is recently reported that high quality μc-Si:H films could be obtained at the amorphous-microcrystalline phase transition[24, 25] or at a relatively low X_c around 50%.[26] Besides, from the above results in 5-3 and 5-4, it was found that μc-Si:H films with good quality could be obtained at X_c of around 30%. Therefore, in this section, X_c was fixed around 30% and the influence of deposition parameters such as substrate temperature, H_2 flow rate, SiH_4 partial pressure and filament temperature on film properties and solar cell performances was investigated.

Substrate temperature is one of the significant parameters that largely influence film quality, especially defect density of a-Si:H and μc-Si:H films in CVD method. Therefore, μc-Si:H films and solar cells were prepared with varying substrate temperatures from 130°C to 250°C and these films were evaluated by photo and dark conductivity measurement, FT-IR measurement. Filament temperature of 1900°C, SiH_4 partial pressure of 3 mTorr and H_2 flow rate of 25 sccm were carried out. As shown in Fig. 5-45, X_c largely increased from 15% to 50% with increasing substrate temperatures from 130°C to 190°C, and it was saturated at substrate temperatures over 190°C. Both σ_{ph} and σ_d increased with increasing substrate temperatures from 130°C to 190°C, reflecting the increase of X_c and they decreased at substrate temperatures over 190°C. σ_{ph} had a peak value at substrate temperature around 165-190°C. As shown in Fig. 5-46, total H content largely decreased from 11% to 7% and Si-H/Si-H_2

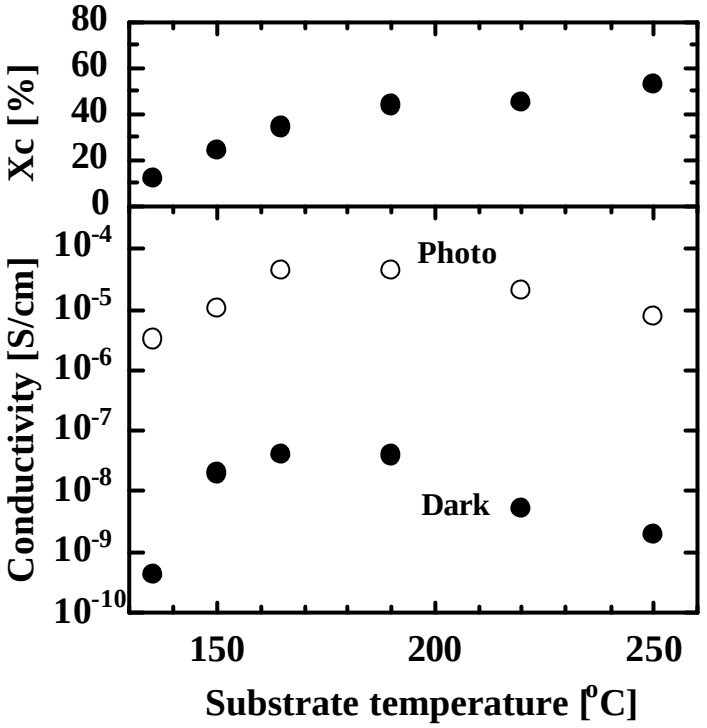

Fig. 5-45: X_c, photo and dark conductivity as a function of substrate temperature

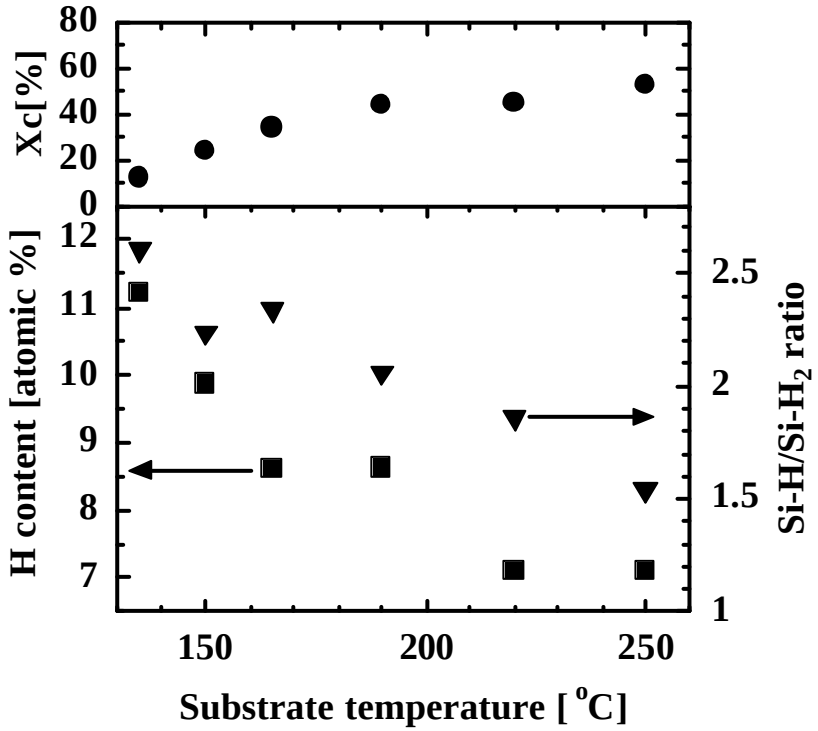

Fig. 5-46: X_c, total H content and Si-H/Si-H_2 ratio as a function of substrate temperature

ratio also largely decreased from 2.6 to 1.5 with increasing substrate temperatures from 130°C to 250°C. It can be thought that H atoms of μc-Si:H film exist mainly in the amorphous region. Thus, when substrate temperatures increased from 130°C to 190°C, the amorphous region decreased from 85% to 55%, whose decrease ratio was 55/85=0.65, total H content decreased from 11.21% to 8.63%, whose decrease ratio was 8.63/11.21=0.77, indicating that total H content in the amorphous tissue increased. Si-H/Si-H_2 ratio decreased from 2.5 to 2.0, indicating a slight degradation of amorphous region. On the other hand, although X_c was almost constant value of 50% at substrate temperatures from 190°C to 250°C, both total H content and Si-H/Si-H_2 ratio further decreased, indicating that the grain boundary was insufficiently passivated by H atoms and defect density increased and film quality of amorphous region was degraded. Figure 5-47 shows solar cell performances prepared by using these μc-Si:H films. A 2-step growth method was also used for the preparation of solar cells. V_{oc} monotonously decreased with increasing substrate temperature. On the other hand, J_{sc} and F.F. had peak values at substrate temperatures around 150-190°C. As a result, conversion efficiency had also peak values at substrate temperatures around 150-190°C. Therefore, it was found that the optimum substrate temperature was around 150-190°C. This result corresponds to the results in Figs. 5-45 and 5-46, indicating that film quality was improved at substrate temperatures around 150-190°C. As above mentioned in Fig 5-46, film quality was degraded at substrate temperatures over 190°C, besides, p-layer was damaged and boron diffused from p-layer to i-layer at substrate temperatures over 190°C because p-layer was prepared at a substrate temperature of 170°C. Therefore, they are also the factors of degradation of cell performances at substrate temperatures over 190°C.

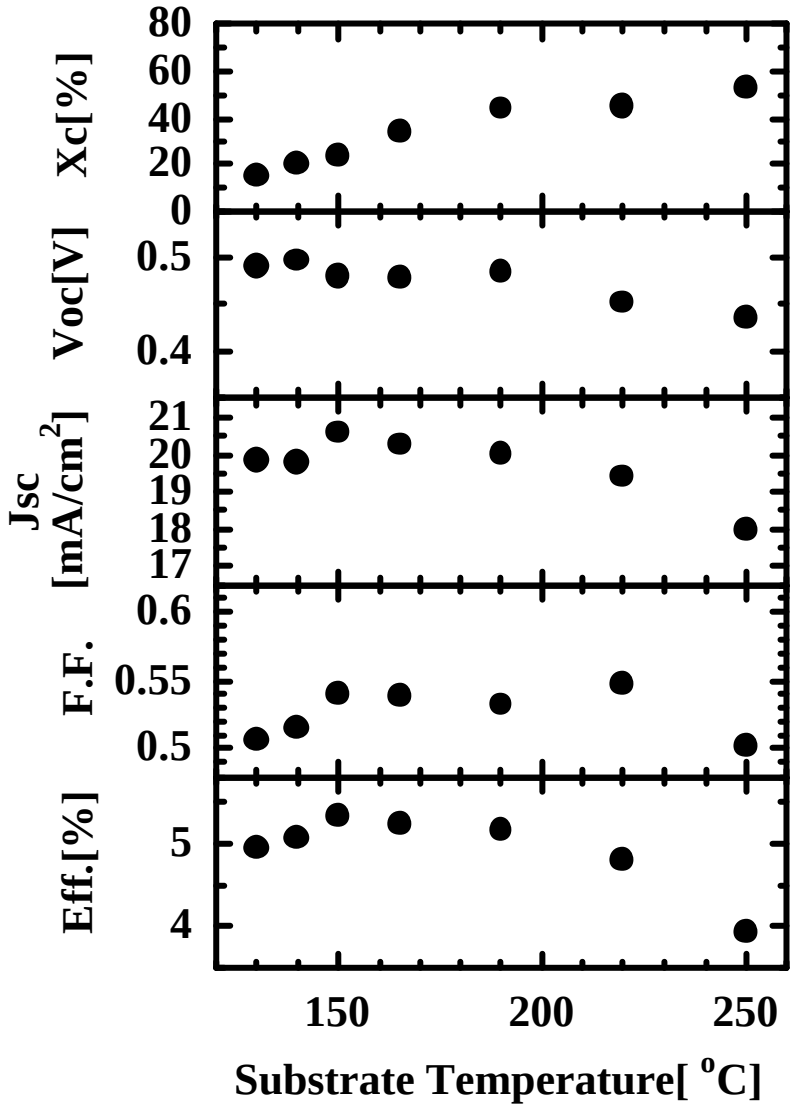

Fig. 5-47: Solar cell performances as a function of substrate temperature

H_2 flow rate is a deposition parameter that largely controls X_c. In our previous works, cell performances decreased and high conversion efficiencies were not obtained at high X_c. Therefore, in order to investigate the reason, μc-Si:H films were prepared with varying H_2 flow rate from 25 sccm to 100 sccm in the deposition conditions such as a substrate temperature of 150°C, a filament temperature of 1900°C, SiH_4 partial pressure of 3 mTorr and a H_2 flow rate of 25 sccm which the best cell performances could be obtained. These films were evaluated by photo and dark conductivity measurement, FT-IR measurement, ESR and SIMS measurement.

As shown in Fig. 5-48, X_c largely increased from 30% to 60% with increasing H_2 flow rate from 25 sccm to 40 sccm, and it was saturated at H_2 flow rate over 40 sccm. σ_d increased by one order of magnitude with increasing H_2 flow rate from 25 sccm to 40 sccm and it was saturated at H_2 flow rate over 40 sccm, reflecting X_c. On the other hand, σ_{ph} was almost constant. As shown in Fig. 5-49, total H content measured by FT-IR agreed with that measured by SIMS, and the value largely decreased from 10% to 5.5% with increasing H_2 flow rate from 25 sccm to 60 sccm, it was saturated at H_2 flow rate over 60 sccm. Si-H/Si-H_2 ratio largely decreased from 2.2 to 0.2 with increasing H_2 flow rate from 25 sccm to 60 sccm, it was saturated at H_2 flow rate over 60 sccm. These total H content and Si-H/Si-H_2 ratio had a good correlation with X_c. When H_2 flow rate increased from 25 sccm to 60 sccm, the amorphous region decreased from 70% to 40%, whose decrease ratio was 40/70=0.57, total H content decreased from 10% to 5.5%, whose decrease ratio was 5.5/10=0.55, indicating that total H content in the amorphous tissue was constant. On the other hand, Si-H/Si-H_2 ratio largely decreased from 2.2 to 0.2, i.e., the bonding between Si atom and H atom mainly became Si-H_2 bonding, indicating a large degradation of film quality.

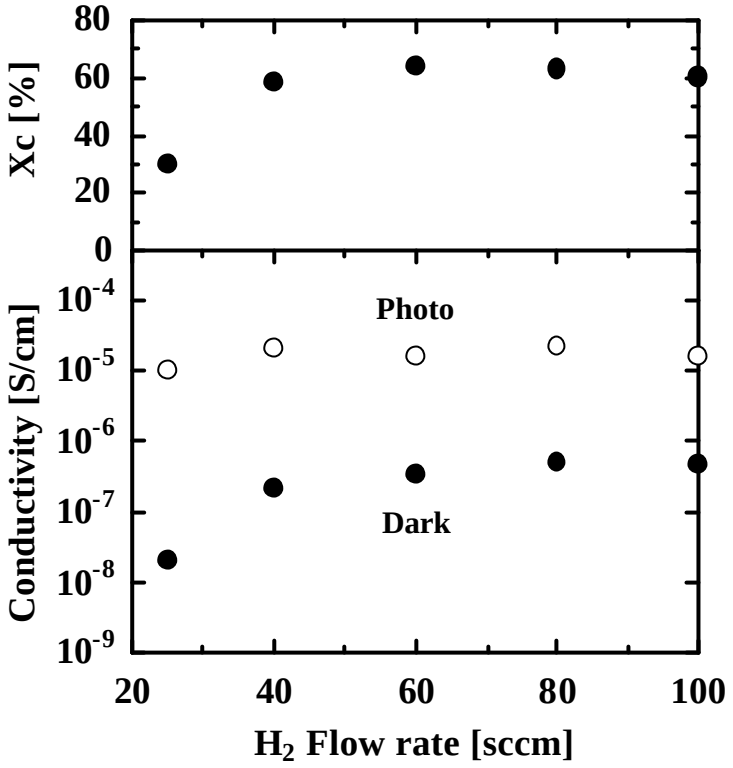

Fig. 5-48: X_c, photo and dark conductivity as a function of H_2 flow rate

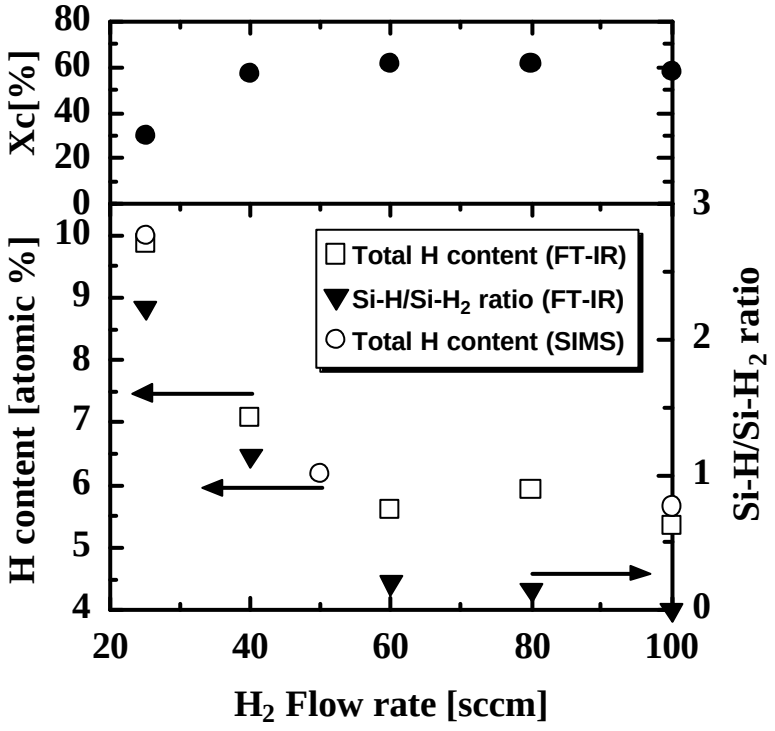

Fig. 5-49: X_c, total H content and Si-H/Si-H_2 ratio as a function of H_2 flow rate

As shown in Fig. 5-50, Ns largely increased from 1.0×10^{16} cm^{-3} to 8.9×10^{16} cm^{-3} with increasing H_2 flow rate from 25 sccm to 100 sccm. This result corresponds to that of Fig. 5-49, indicating that a-Si:H at grain boundaries for μc-Si:H was insufficiently passivated by small amount of H atoms at a large H_2 flow rate over 40 sccm, thus Ns largely increased at large H_2 flow rates over 40 sccm. Figure 5-51 shows Oxygen (O) and Carbon (C) SIMS depth profiles as a function of H_2 flow rate. For SIMS samples, μc-Si:H films were deposited on a low resistance Si wafer varying H_2 flow rate from 25 sccm to 100 sccm with using purifier, then μc-Si:H films were again deposited varying H_2 flow rate from 25 sccm to 100 sccm without using purifier, and finally a-Si:H cap layer was deposited. A thickness of each layer was about 200 nm. Effect of the purifier could not be observed. Beside the silicon substrate, O and C concentrations largely decreased. However, H content also largely decreased at the same time, indicating that an epitaxial layer was grown in the first layer with a thick ness of 200-400 nm. O and C concentrations showed a large dependence on H_2 flow rate. O and C concentrations increased in the order from 10^{20} to 10^{21} with increasing H_2 flow rate from 25 sccm to 100 sccm, indicating that impurity concentrations increased with increasing X_c. Therefore, it is concluded from these results that high quality μc-Si:H films could be obtained at low X_c around 30% in our HW-Cell system due to large Ns value, small Si-H/Si-H_2 ratio and large impurity concentrations at large X_c over 30%.

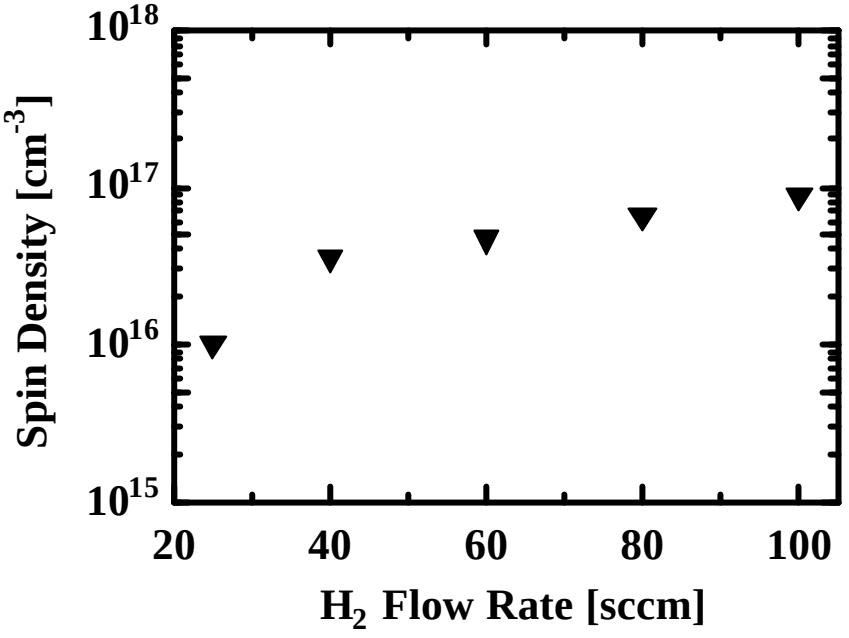

Fig. 5-50: Spin density (N_s) as a function of H_2 flow rate

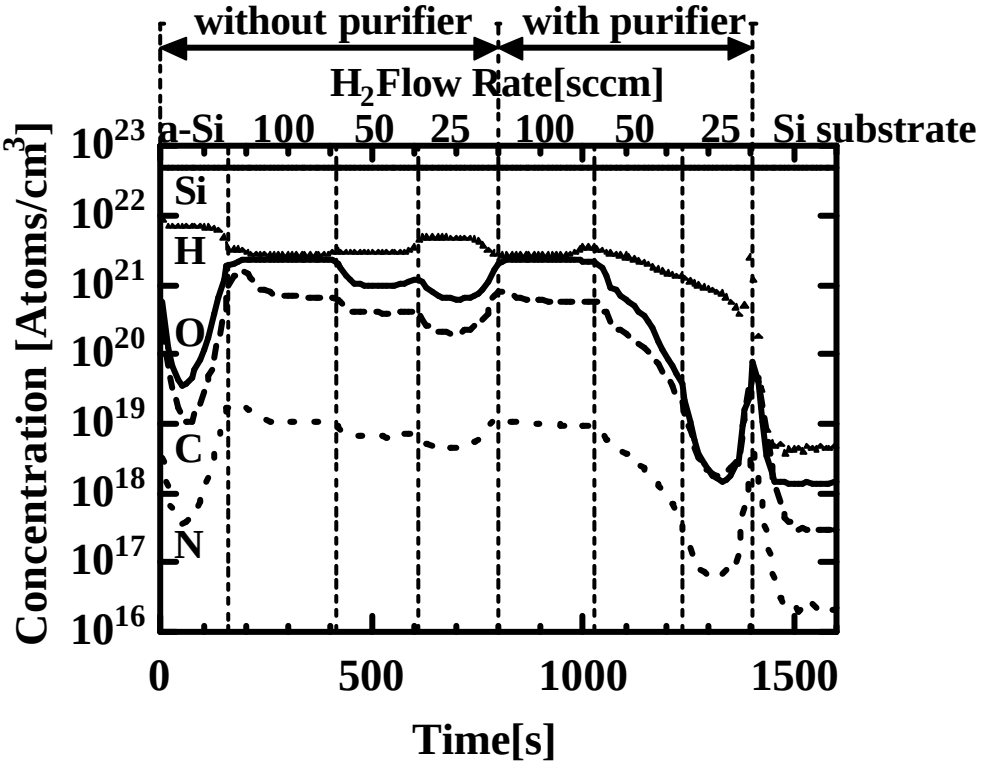

Fig. 5-51: Oxygen (O) and carbon (C) SIMS depth profiles as a function of H_2 flow rate

From the above results in 5-3, it was found that impurity concentrations could be reduced by decreasing SiH_4 partial pressure down to 3 mTorr. Therefore, in this section, μc-Si:H films were prepared with varying SiH_4 partial pressure from 1 mTorr to 5 mTorr, and these films were evaluated photo and dark conductivity measurement, FT-IR and SIMS measurement. Filament temperature and substrate temperature were 1900°C and 150°C, respectively. X_c was maintained around 30% by controlling H_2 flow rate from 20 sccm to 30 sccm, however, as shown in Fig. 5-52, X_c monotonously decreased from 50% to 20% with increasing SiH_4 partial pressure from 1 mTorr to 5 mTorr. But, both σ_{ph} and σ_d were almost constant. As shown in Fig. 5-53, total H content measured by FT-IR corresponded with that measured by SIMS. When SiH_4 partial pressure increased from 1 mTorr to 5 mTorr, X_c decreased from 51% to 20%, total H content and $Si-H/Si-H_2$ ratio increased from 8.3% to 11.6% and from 1.9 to 2.7, respectively. When SiH_4 partial pressure increased from 1 mTorr to 5 mTorr, the amorphous region increased from 49% to 80%, whose increase ratio was 80/49=1.6, total H content increased from 8.3% to 11.6%, whose increase ratio was 11.6/8.3=1.4, indicating that in the amorphous tissue, total H content at SiH_4 partial pressure of 1 mTorr was larger than that at SiH_4 partial pressure of 5 mTorr. $Si-H/Si-H_2$ ratio increased from 1.9 to 2.7 with decreasing X_c, indicating the similar tendency of the results in Figs 5-46 and 5-49. Figure 5-54 shows Oxygen (O) and Carbon (C) SIMS depth profiles as a function of SiH_4 partial pressure. For SIMS samples, μc-Si:H films were deposited on a low resistance Si wafer varying SiH_4 partial pressure from 1 mTorr to 5 mTorr with using purifier, then μc-Si:H films were again deposited varying SiH_4 partial pressure from 1 mTorr to 5 mTorr without using purifier, and finally a-Si:H cap layer was deposited. A thickness of each layer was about 150 nm. Effect of the purifier could not be observed.

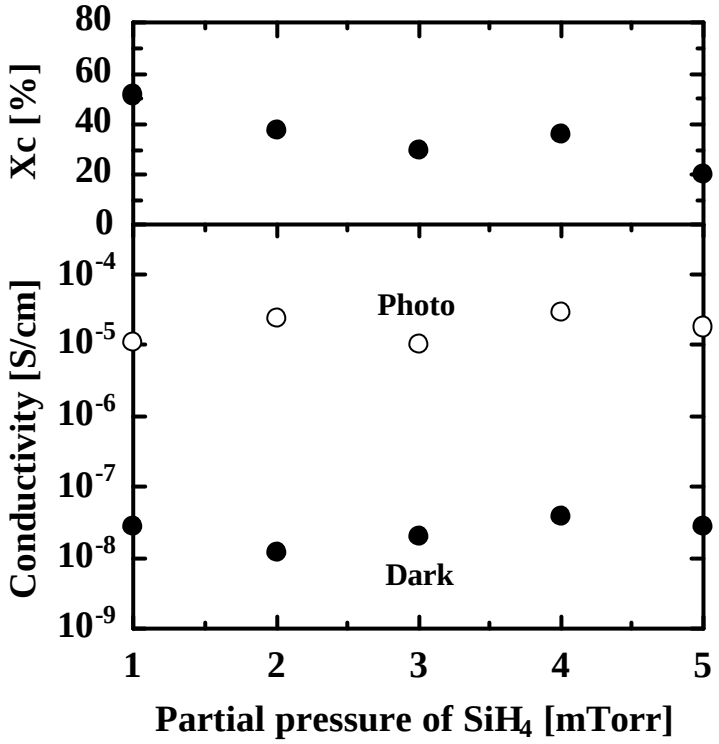

Fig. 5-52: X_c, photo and dark conductivity as a function of SiH_4 partial pressure

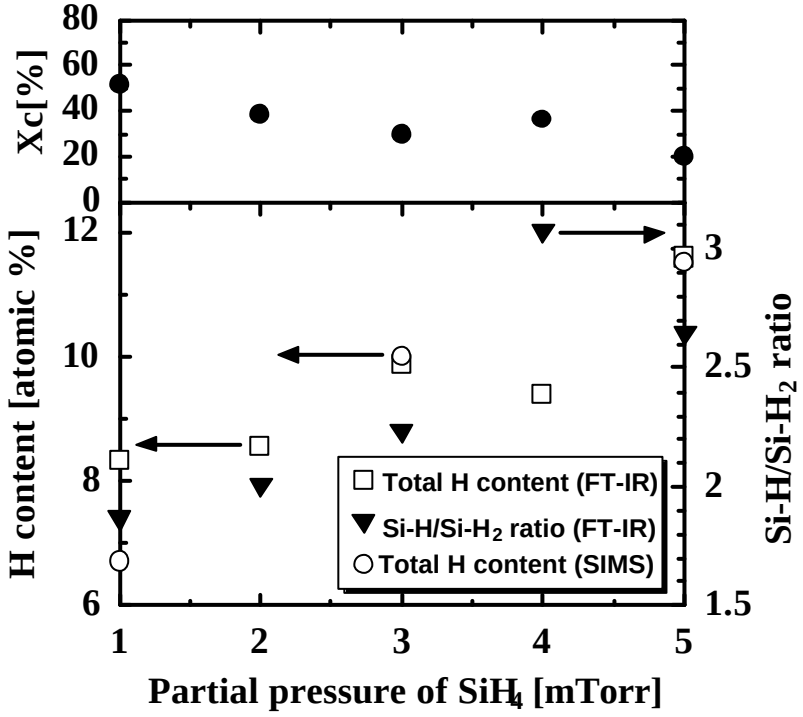

Fig. 5-53: X_c, total H content and Si-H/Si-H_2 ratio as a function of SiH_4 partial pressure

Beside the silicon substrate, O and C concentrations largely decreased. However, H content also largely decreased at the same time, indicating that an epitaxial layer was grown in the first layer with a thick ness of around 150 nm. O and C concentrations showed a large dependence on SiH_4 partial pressure. O and C concentrations largely decreased in the order from 10^{21} to 10^{19} with decreasing SiH_4 partial pressure from 5 mTorr to 1 mTorr. In 5-3, O and C concentrations could be reduced in the order of 10^{20} by decreasing SiH_4 partial pressure to 3 mTorr, however, as shown in Fig. 5-54, it was found that these impurities could be further reduced in the order of 10^{19} by decreasing SiH_4 partial pressure to 1 mTorr. Therefore, it is concluded that decreasing SiH_4 partial pressure is very effective in reducing O and C concentrations and the pressure should be decreased less than 1 mTorr.

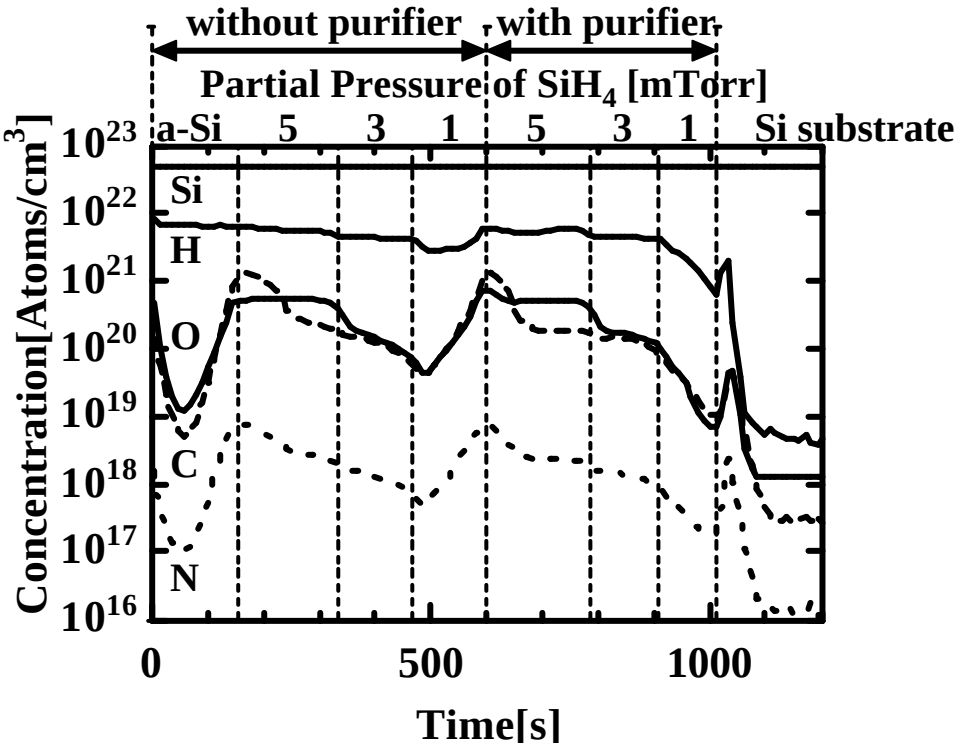

Fig. 5-54: Oxygen and carbon SIMS depth profiles as a function of SiH_4 partial pressure

Finally, μc-Si:H thin films and solar cells were deposited with changing filament temperature. SiH_4 partial pressure was fixed 3 mTorr. The filament temperature was varied from 1800°C to 2100°C and X_c was maintained around 30% by changing H_2 flow rate from 12 sccm to 35 sccm. The cell performances as a function of the filament temperature are summarized in Fig. 5-55. Open-circuit voltage (V_{oc}), short-circuit current density (J_{sc}) and fill factor (F.F.) largely increased with decreasing filament temperature, suggesting improvement of film quality. As a result, a conversion efficiency of 6.0% (Voc: 0.50 V, Jsc: 19.69 mA/cm^2, F.F.: 0.61, active area: 0.086 cm^2, AM1.5) was obtained at a filament temperature of 1800°C. X_c was maintained around 30-40%, therefore, following two reasons were considered in order to explain a large degradation of cell performances at high filament temperatures; one is heat radiation from the filament and the other is the increase of defect density and/or impurity concentration from the filament. Effects of the heat radiation were confirmed by fabricating solar cells at a filament temperature of 2100°C with substrate temperatures from 120°C to 150°C, as shown in Fig. 5-56. As a result, X_c decreased and cell performances couldn't be improved with decreasing substrate temperature. Therefore, heat radiation is not a critical reason for the degradation of cell performances.

Figure 5-57 shows X_c, σ_d, σ_{ph}, total H content and Si-H/Si-H_2 ratio as a function of filament temperature. σ_d and σ_{ph} largely increased and σ_{ph}/σ_d ratio decreased at a filament temperature of 2100°C, indicating the degradation of film quality of μc-Si:H. The total H content decreased from 11% to 7% with increasing filament temperature. Therefore, it indicates that a-Si:H at grain boundaries for μc-Si:H was insufficiently passivated by H atoms at high filament temperatures. Besides, Si-H/Si-H_2 ratio in μc-Si:H films also decreased from 2.6 to 1.9, indicating

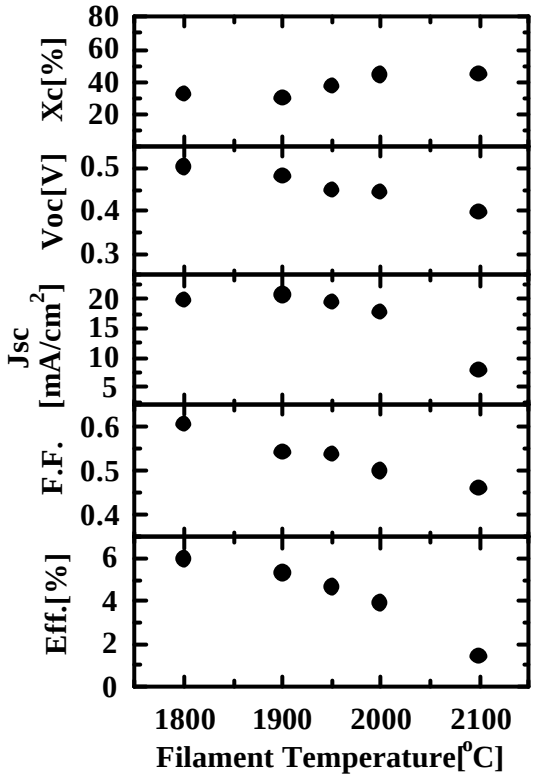

Fig. 5-55 Solar cell performances as a function of filament temperature

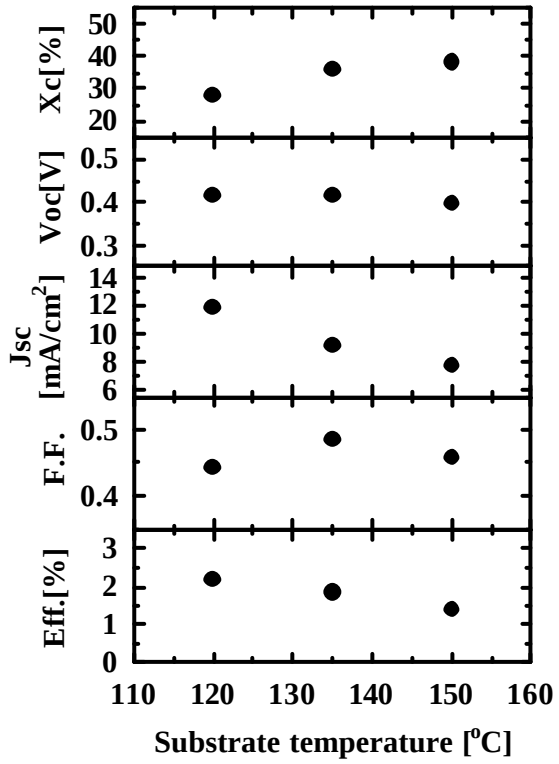

Fig. 5-56 Solar cell performances as a function of substrate temperature at T_{fil}=2100^{o}C

the degradation of film quality of a-Si:H tissue in μc-Si:H film. From these results, the quality of μc-Si:H film degraded at high filament temperatures. Figure 5-58 shows infrared absorption coefficient spectra as a function of filament temperature. In the case of 2100°C, the sample was prepared at a filament temperature of 2100°C and a SiH_4 partial pressure of 50 mTorr without hydrogen dilution. The three spectra have very different shapes each other. At a filament temperature of 2100°C, the spectrum has a large split peak at around 2100 cm^{-1}. This split peak at around 2100 cm^{-1} is derived from SiHO and/or SiH_2O bonding[27] and it was typically observed in μc-Si:H films with columnar structure that were deposited at a filament temperature of 2100°C and a SiH_4 partial pressure of over 50 mTorr without hydrogen dilution in our previous works. However, it was not observed in μc-Si:H films deposited at a filament temperature of 2100°C and a SiH_4 partial pressure of less than 10 mTorr. On the other hand, in the μc-Si:H films deposited at a filament temperature of 1700°C and 1800°C, a split peak at around 2100 cm^{-1} was not observed, a peak at 2100 cm^{-1} decreased and on the contrary, a peak at 2000 cm^{-1} increased with decreasing filament temperature. From these results, it is concluded that film quality can be improved by decreasing filament temperature.

Figure 5-59 shows dependence of E_a, N_s and ambipolar diffusion length on the filament temperature. E_a was almost constant with a value of 0.5 eV, indicating intrinsic characteristics in entire filament temperature range. N_s was found to be as low as about 1.0×10^{16} cm^{-3} at filament temperatures from 1800°C to 2100°C and it slightly decreased with decreasing filament temperature. The lowest N_s of 7.5×10^{15} cm^{-3} was obtained at a filament temperature of 1800°C, which corresponds to the solar cell results. However, the difference of N_s is small, therefore this small difference cannot be a critical reason for a large degradation of solar cell performances at high

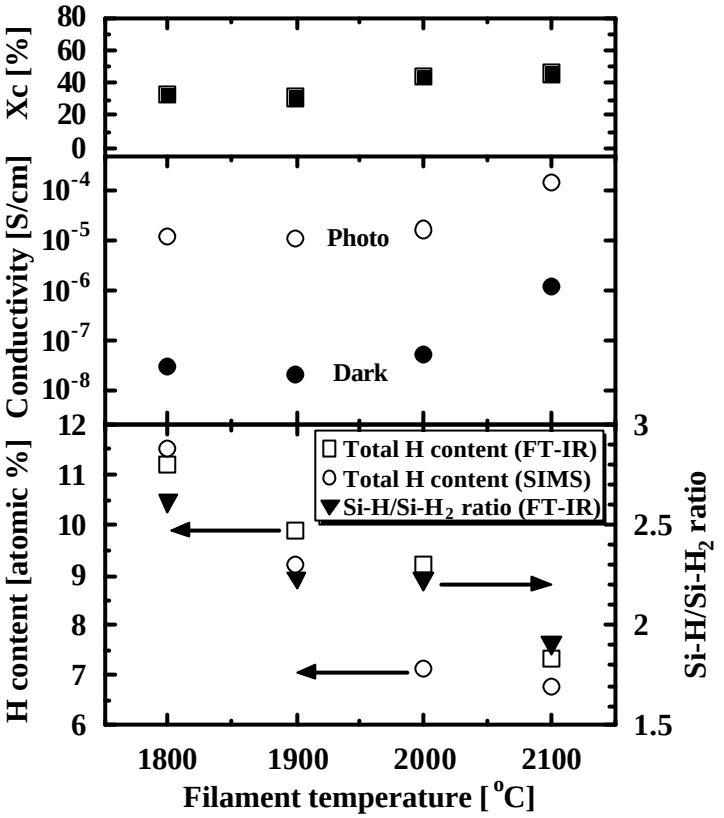

Fig. 5-57: X_c, photo and dark conductivity, total H content and Si-H/Si-H_2 ratio as a function of filament temperature

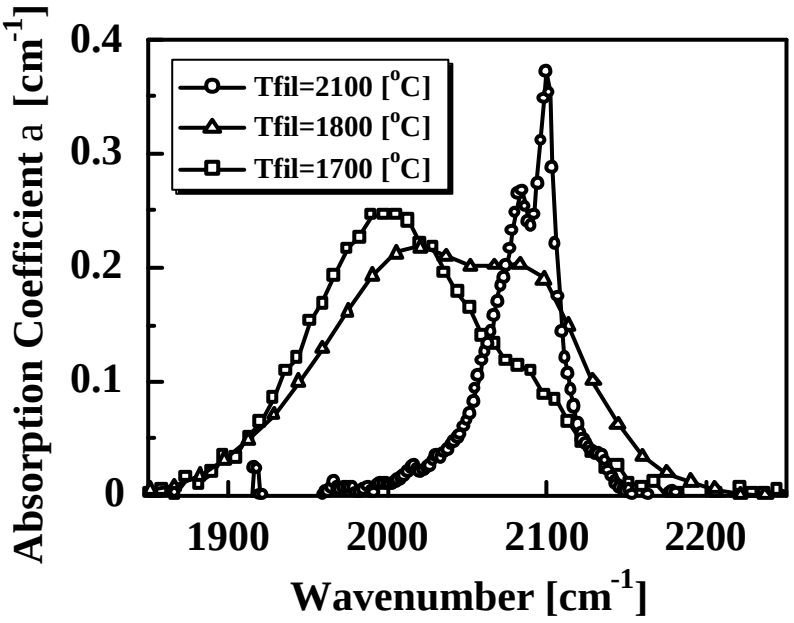

Fig. 5-58: Infrared absorption coefficient spectra as a function of filament temperature

filament temperatures. $L_{\parallel}$ and $L_{\perp}$ were around 100 nm, and these values increased with decreasing filament temperature and this result also corresponds to the solar cell results. There was no difference between the values of $L_{\parallel}$ and $L_{\perp}$, indicating that there is electrically isotropic properties.[8, 10, 28)]

For further investigation of impurity contaminations, SIMS profile for metal elements such as Fe, Co, Ni, Mo, W and Al was investigated. W and Al concentrations showed very clear dependence on the filament temperature, and they largely increased with increasing filament temperature, as shown in Fig. 5-60. W and Al atoms in μc-Si:H film could originate from W filament and Al_2O_3 insulators used in the hot wire unit, respectively. Thus, we concluded that the contamination of W and Al was one of the critical factors for large degradation of cell performances at high filament temperatures. Therefore, filament temperature must be decreased less than 1800^{o}C for further improvement of cell performances.

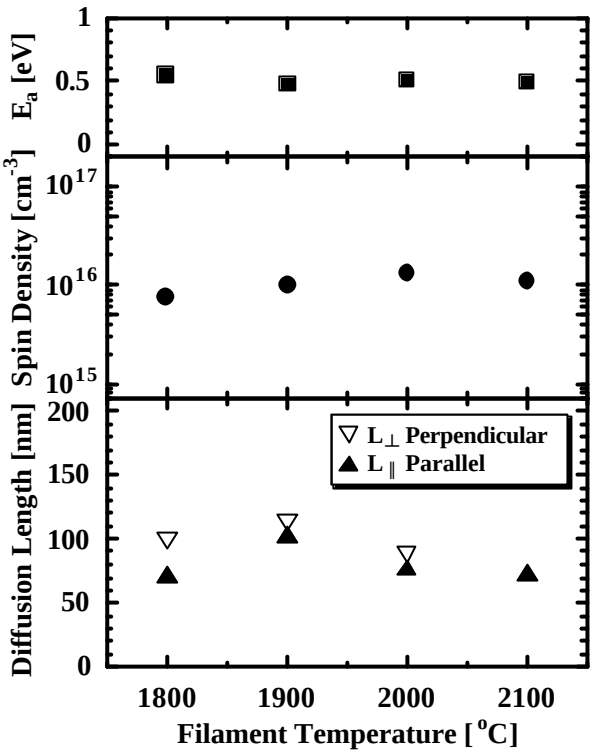

Fig. 5-59: Activation energy (E_a), spin density (N_s), perpendicular ($L_\perp$) and parallel ($L_\parallel$) ambipolar diffusion length as a function of filament temperature

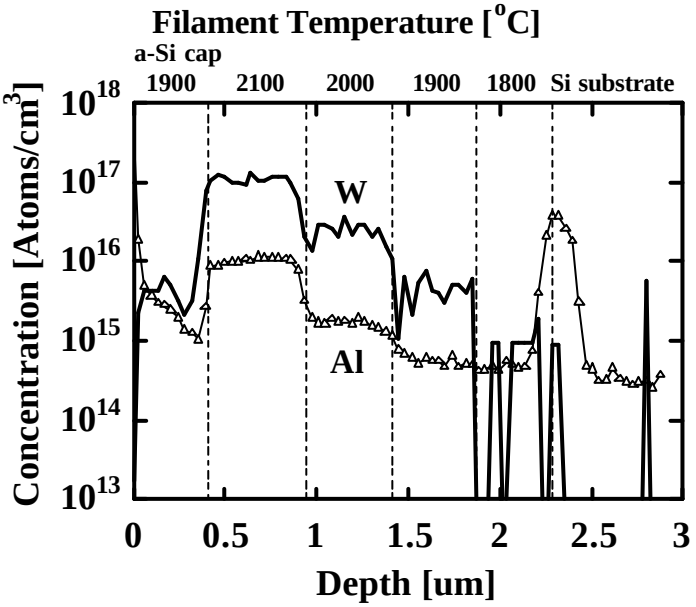

Fig. 5-60: Tungsten (W) and Aluminum (Al) SIMS depth profiles of μc-Si:H film as a function of filament temperature

5-5-2 Degradation Properties of Films and Solar Cells

In this section, we will describe aging of films and solar cells. Figure 5-61 shows initial and degraded solar cell performances as a function of the filament temperature. The solar cells were preserved in air without any light exposure for 4 months. The cell performances largely degraded for solar cells grown at filament temperatures from 1900°C to 2000°C, while such a large degradation was not observed in the solar cells prepared at a filament temperature of 1800°C and 2100°C, respectively. In the filament temperature region from 1900°C to 2100°C, V_{oc} and J_{sc} largely degraded down to 0.25 V and 10 mA/cm^2, respectively. Thus, the conversion efficiencies degraded to 1.0-1.5%, indicating the degradation of intrinsic μc-Si:H absorber layer. In order to confirm the degradation by aging, the degradation of μc-Si:H films was investigated. Figure 5-62 shows initial and degraded N_s of μc-Si:H films as a function of filament temperature. The N_s was measured 2 months after fabrication. N_s largely increased from about 1.0×10^{16} cm^{-3} to about 4.0×10^{16} cm^{-3} by aging. Figure 5-63 shows initial state and degraded state of FT-IR spectra of μc-Si:H films as a function of filament temperature. No difference between initial state and degraded state of FT-IR spectra was observed in the peaks at 2000 cm^{-1} and 2100 cm^{-1} originated from Si-H and Si-H_2 bonding, respectively. However, when the films were grown at filament temperatures less than 1900°C, the peak at 1000-1100 cm^{-1} originated from Si-O-Si bonding[27,29,30] largely increased after 2 months, indicating the post-oxidation of μc-Si:H films. The post-oxidation mechanism is as follows; break of Si-Si and/or Si-H bonding and creation of new dangling bonds were caused by an invasion of oxygen atoms in air, and spontaneous break of weak Si-Si and/or Si-H bonding was induced by stress and it caused the further invasion of impurity atoms.

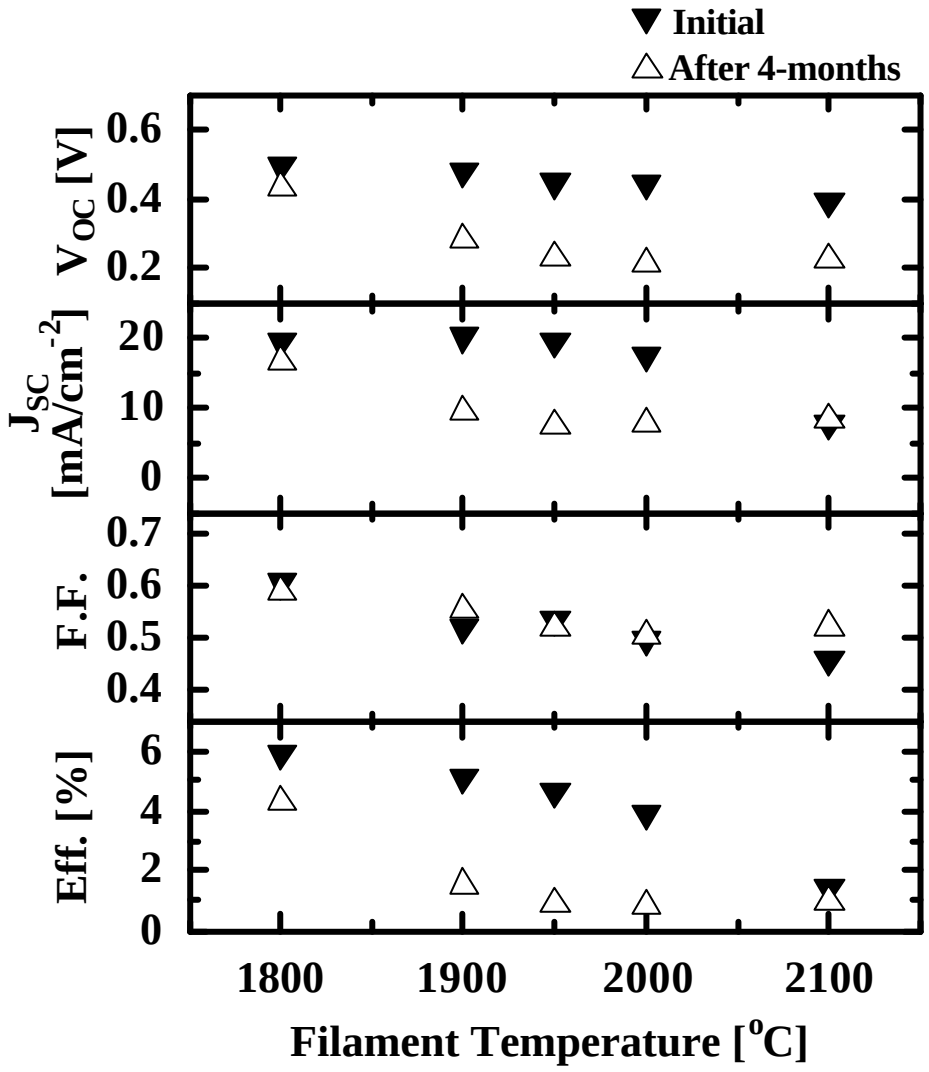

Fig. 5-61: Initial and degraded (after 4 months) solar cell performances of p-i-n μc-Si:H solar cells as a function of filament temperature

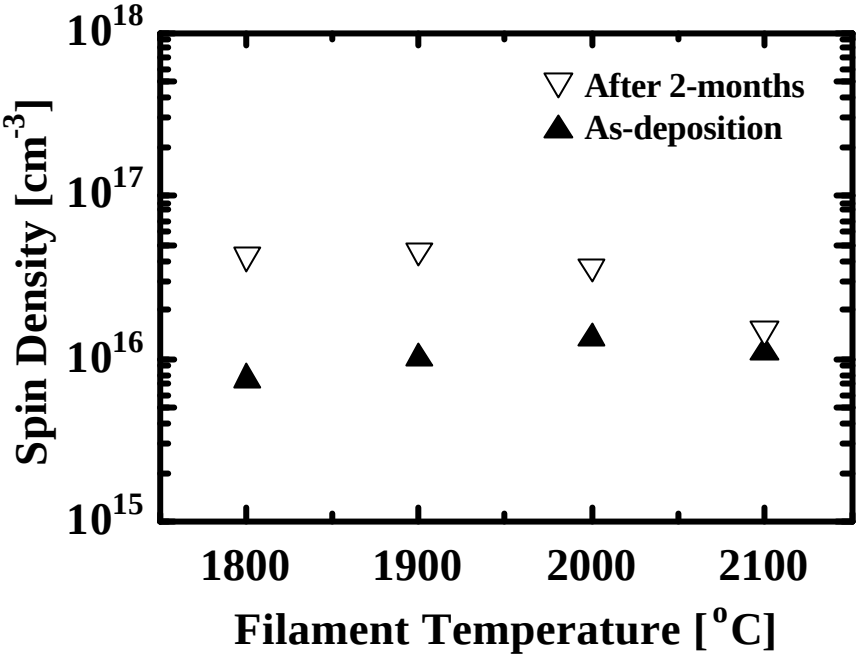

Fig. 5-62: Initial (as deposition) and degraded (after 2 months) spin density (N_s) of μc-Si:H films as a function of filament temperature

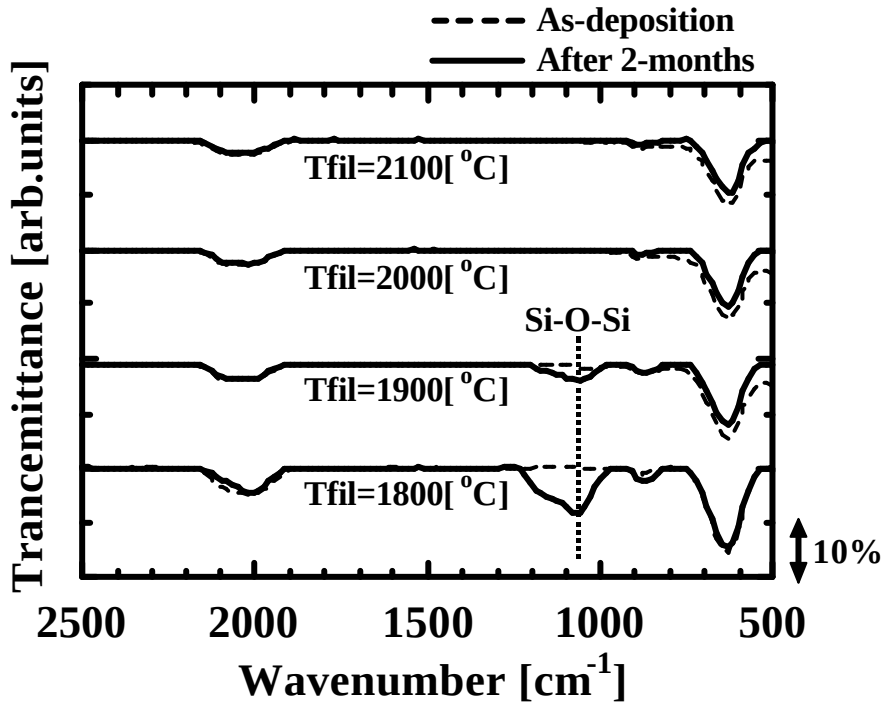

Fig. 5-63: Initial state (as deposition) and degraded state (after 2 months) of FT-IR spectra of μc-Si:H films as a function of filament temperature

The increase of the peak increased with decreasing filament temperature. These results correspond with those of Fig. 5-62, concluding that the μc-Si:H films deposited at a low filament temperature have low spin densities and impurity concentrations in the initial state, however it is structurally unstable for ageing. In order to investigate the influence of substrate temperature on the stability of μc-Si:H film, μc-Si:H films were deposited at various substrate temperatures from 130°C to 300°C. Filament temperature was fixed 1800°C, because the stability of μc-Si:H film was lowest at this filament temperature. Figures 5-64 and 5-65 show N_s of μc-Si:H films as a function of substrate temperature (? : as-deposition, ? : after 1.5 months, ? : after 2 months) and initial state and degraded state of FT-IR spectra of μc-Si:H films as a function of substrate temperature, respectively. The filament temperature was fixed 1800°C. N_s measured after 1.5 months had the minimum value at a substrate temperature around 200°C, indicating the similar trend of substrate temperature dependence on N_s of general μc-Si:H film.[31, 32] Even after 1.5 months, N_s at a substrate temperature of 190°C was still as low as the initial N_s at a substrate temperature of 150°C. Besides, N_s at substrate temperatures over 165°C were lower than the degraded N_s at a substrate temperature of 150°C. Therefore, μc-Si:H films deposited at substrate temperatures over 165°C has a high stability for aging. The peak at 1000-1100 cm^{-1} largely increased after 2 months at substrate temperatures less than 165°C, indicating the post-oxidation of μc-Si:H films. The increase of the peak increased with decreasing substrate temperature. These results correspond with those of N_s, indicating that μc-Si:H films deposited at a low substrate temperature less than 165°C was unstable and the instability has relationship with the post-oxidation. Therefore, it is concluded that the instability of μc-Si:H film is derived from a growth at low substrate temperatures. In Figs. 5-62 and 5-63, the substrate temperature was fixed 150°C at

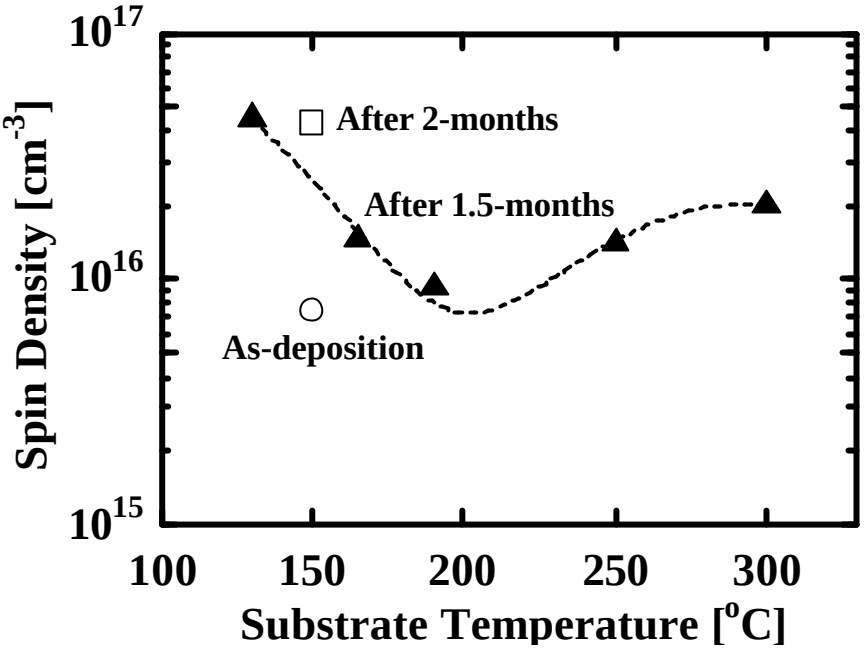

Fig. 5-64: Spin density (N_s) of μc-Si:H films as a function of substrate temperature (? : as-deposition, ? : after 1.5 months, ? : after 2 months)

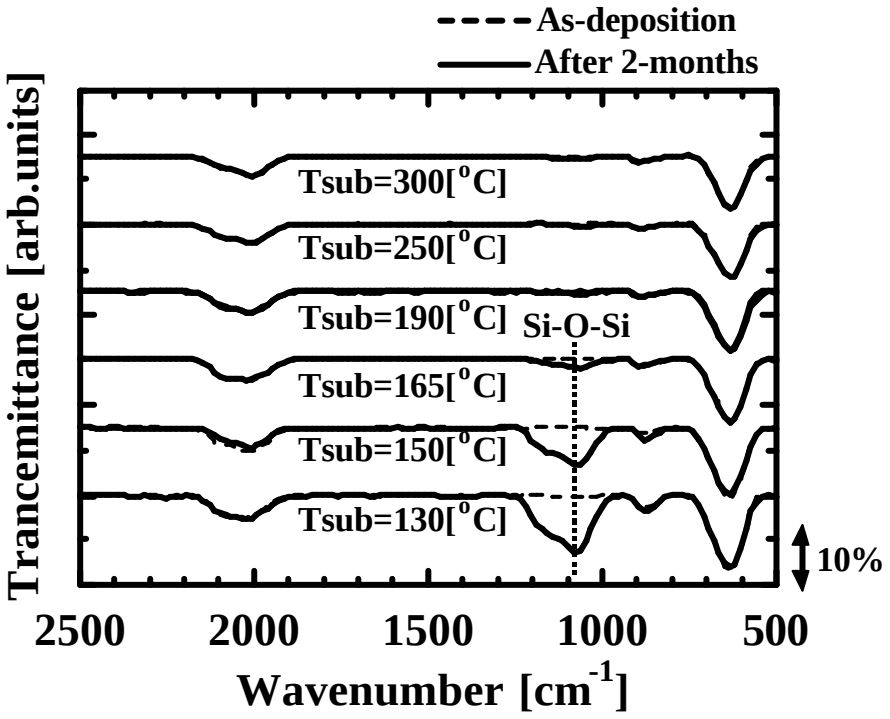

Fig. 5-65: Initial state (as deposition) and degraded state (after 2 months) of FT-IR spectra of μc-Si:H films as a function of substrate temperature

each filament temperature, however, this substrate temperature was estimated value and it was really measured and calibrated only at a filament temperature of 1900^{o}C in our previous works. Therefore, the real substrate temperature shifted and it was lower than 150^{o}C at filament temperatures less than 1800^{o}C because of low heat radiation from filament to substrate at a lower filament temperature. Thus, it is concluded that the instability of μc-Si:H film originates not from filament temperatures but from the deposition at low substrate temperature less than 150^{o}C and therefore these unstable μc-Si:H film deposited at a low substrate temperature cannot prevent from the post-oxidation.

5-5-3 Post-oxidation of Microcrystalline Silicon Thin Films

It was already found in 5-3 that the deposition at a low pressure was very effective in reduction of impurities such as oxygen and carbon atoms in μc-Si:H film, these impurity concentrations could be reduced down to $2x10^{20}$ cm^{-3} by decreasing the partial pressure of SiH_4 to 3 mTorr. It was also found from above results that μc-Si:H films deposited by HW-Cell method could easily suffer from the post-oxidation. Therefore, in order to investigate the initial impurity concentrations, the location of the film where impurity atoms came from and the way how to prevent from the post-oxidation, μc-Si:H films were investigated by SIMS measurement. For SIMS measurement, 3 samples were prepared as shown in Fig. 5-66. Sample "A" is μc-Si:H film without a-Si:H cap layer, sample "B" has an a-Si:H cap layer and sample "C" has a-Si:H layer surrounding μc-Si:H film. The thickness of the cap layers was about 3 μm. Samples "B" and "C" suffered from air-break for 10 minutes and 40minutes, respectively. The each edge of the four sides of sample "C" was etched until the

silicon substrate by CF_4 etching after depositing μc-Si:H first layer. SIMS measurement was carried out 1.5 months later after these samples were prepared. Fig. 5-67 shows oxygen (O) and carbon (C) SIMS depth profiles of these samples. These results showed that O and C atoms diffused from the film surface rather than from the side. The diffusion length was as long as 2-2.5 μm. It was found for the first time that initial O and C concentrations in μc-Si:H film was as low as $2x10^{18}$ cm^{-3}, indicating μc-Si:H film deposited by our HW-Cell method has good quality. The large increase of O and C concentrations was observed at the interface between a cap layer and a μc-Si:H layer. Furthermore, the peak value and width of O and C concentrations for sample "C" were quite larger than those of sample "B", indicating that the post-oxidation easily and quickly occurred in a short time of 10-40 minutes. It was also shown that a thick cap layer could completely prevent the impurity diffusion.

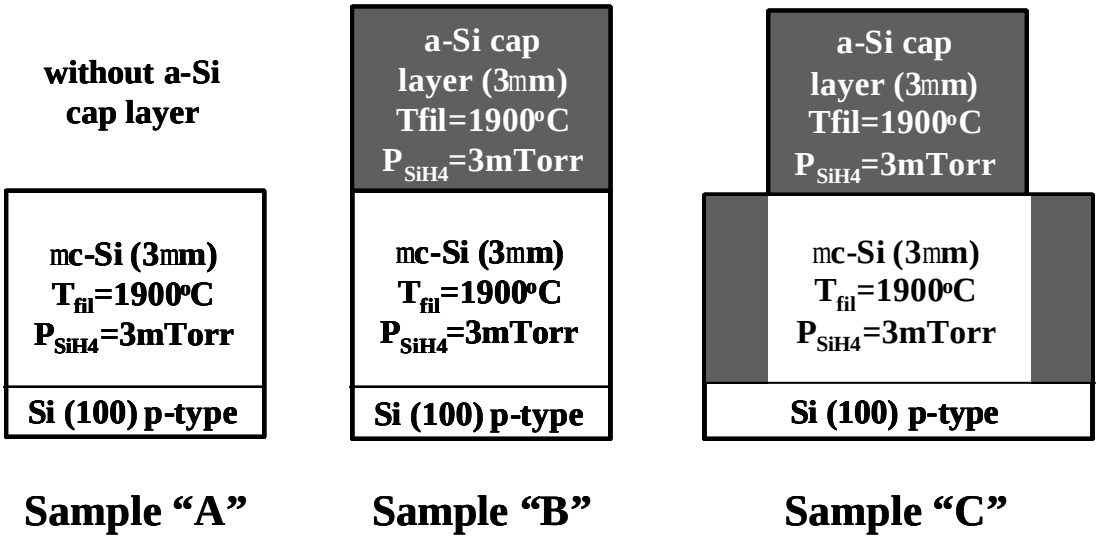

Fig. 5-66: Schematic view of SIMS samples without a-Si:H cap layer (Sample "A"), with a-Si:H cap layer (Sample "B") and with a-Si:H layer surrounding μc-Si:H film

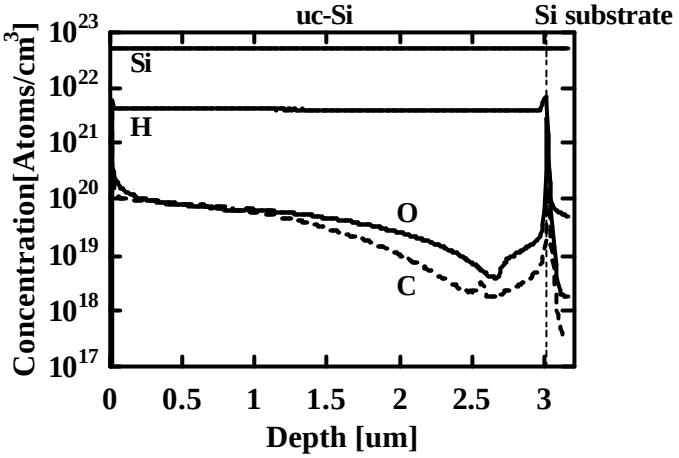

(a)

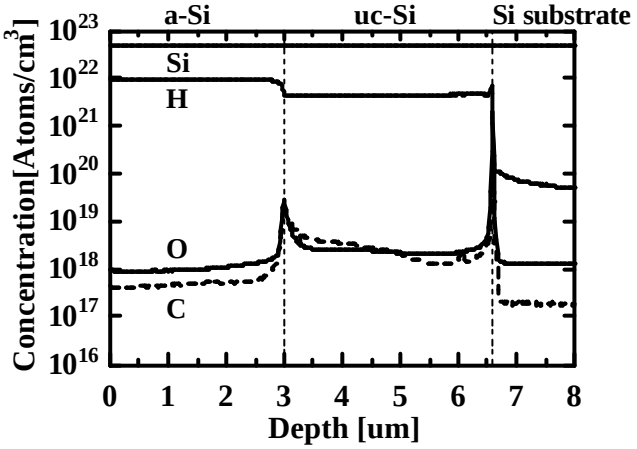

(b)

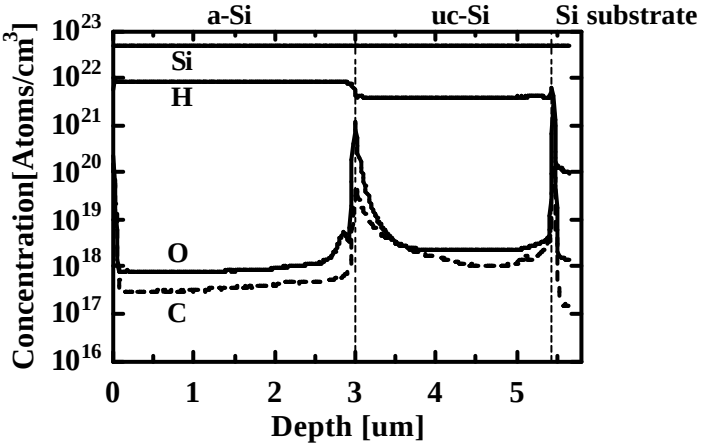

(c)

Fig. 5-67: Oxygen and carbon SIMS depth profiles of μc-Si:H film without a-Si:H cap layer (a), with a-Si:H cap layer (b) and with a-Si:H layer surrounding μc-Si:H film (c)

This post-oxidation is the other factor for lowering the cell performances. Even our best solar cells that have highest efficiency of 6% probably suffer from the post-oxidation. In order to investigate how to prevent from the post-oxidation, the influence of SiH_4 partial pressure on the stability of μc-Si:H film was investigated.

Figure 5-68 shows O and C SIMS depth profiles of μc-Si:H film as a function of SiH_4 partial pressure. The sample has an a-Si:H cap layer with a thickness of 0.5 μm. O and C concentrations largely decreased from$1.0x10^{20}$ cm^{-3} to $2.0x10^{18}$ cm^{-3} with decreasing SiH_4 partial pressure from 5 mTorr to 1 mTorr. In the case of SiH_4 partial pressure of 3 mTorr in Fig. 5-68, all the deposition parameters were as same as those of μc-Si:H layer in Fig. 5-67, and initial O and C concentrations was $2x10^{18}$ cm^{-3}, as shown in Fig. 5-67. Therefore, it was found from the result of Figs. 5-67 and 5-68 that a thin (0.5 μm) a-Si:H cap layer was not enough for preventing the impurity diffusion, and furthermore, the μc-Si:H layer deposited at SiH_4 partial pressure of 1 mTorr was difficult to suffer from the post-oxidation. Figure 5-69 shows spin density (N_s) of μc-Si:H films as a function of SiH_4 partial pressure. N_s measured after 1.5 months decreased with decreasing SiH_4 partial pressure, and it had the minimum value at a SiH_4 partial pressure of 1 mTorr. Even after 1.5 months, N_s at a SiH_4 partial pressure of 1 mTorr was still as low as the initial N_s at a SiH_4 partial pressure of 3 mTorr. Therefore, μc-Si:H films deposited at a SiH_4 partial pressure of 1 mTorr has a high stability for aging.

Thus, from these results, it is concluded that a deposition at a low SiH_4 partial pressure less than 1 mTorr is also effective in the reduction of the post-oxidation.

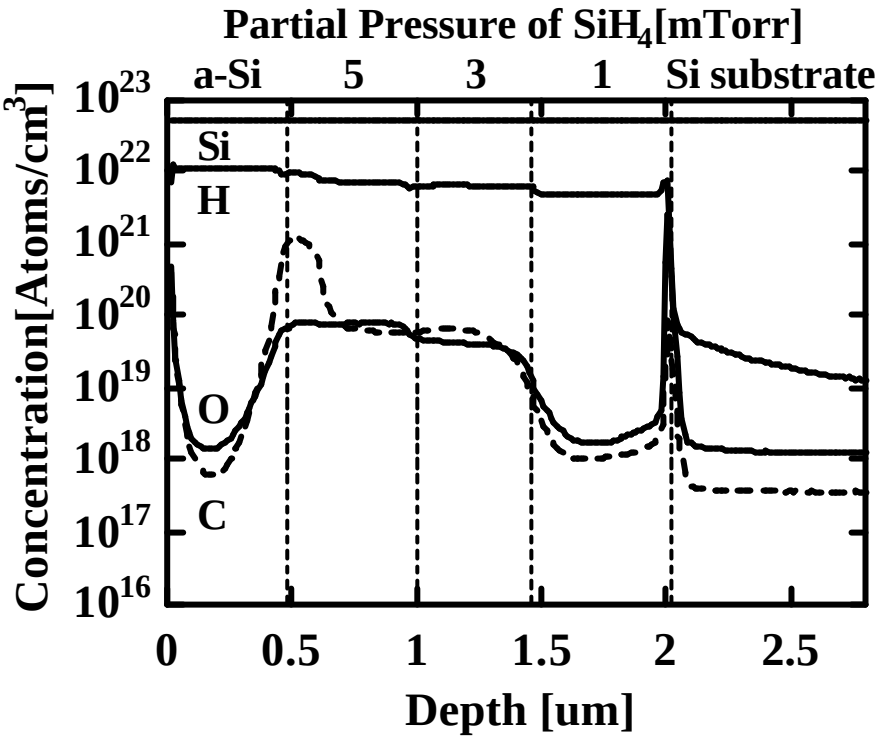

Fig. 5-68: Oxygen (O) and Carbon (C) SIMS depth profiles of μc-Si:H film as a function of SiH_4 partial pressure

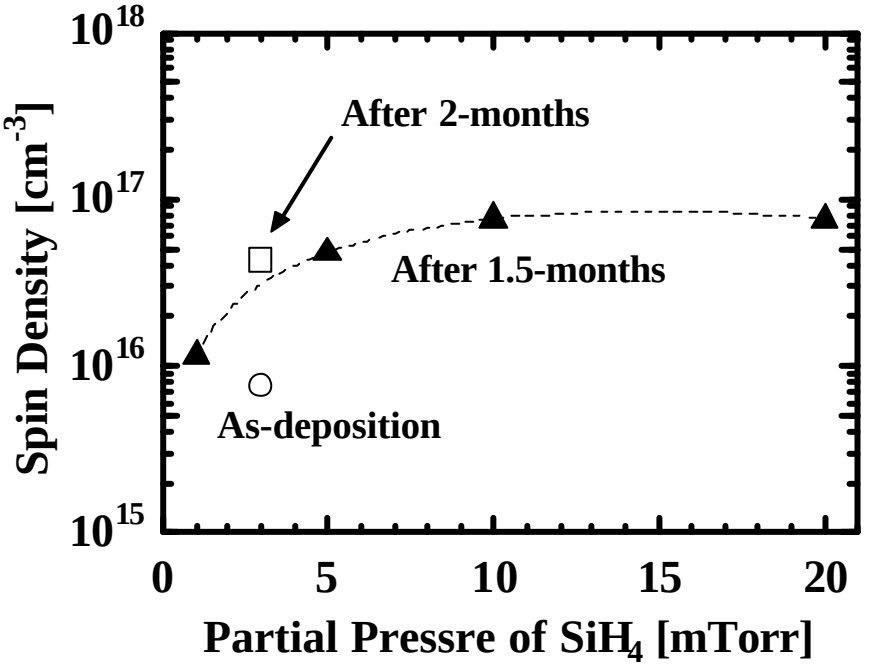

Fig. 5-69: Spin density (N_s) of μc-Si:H films as a function of SiH_4 partial pressure (? : as-deposition, ? : after 1.5 months, ? : after 2 months)

5-6 Theoretical Analysis and Fabrication of Amorphous Silicon/Microcrystalline Silicon Tandem Solar Cells

In order to obtain further high conversion efficiency of over 15% for silicon based thin film solar cells, fabrication of hybrid type solar cells such as amorphous silicon/microcrystalline silicon tandem solar cells are required. Up to now, the maximum stabilized conversion efficiencies of amorphous silicon and microcrystalline silicon single solar cells are 9.0%[33] and 10.7%,[34] respectively. However, it has been reported that the maximum conversion efficiency of 14.5% could be obtained for amorphous silicon/microcrystalline silicon tandem solar cells.[34] Therefore, recently, many researchers are intensively investigating amorphous silicon/microcrystalline silicon tandem solar cells worldwide.[35-39] In this section, first, theoretical analysis of amorphous silicon/microcrystalline silicon tandem solar cells was investigated by using AMPS-1D for the current matching between the top cell and the bottom cell, and the expected conversion efficiency. Then, amorphous silicon/microcrystalline silicon tandem solar cells were actually fabricated and they were also theoretically analyzed. The material parameters of the top cell and the bottom cell used for AMPS-1D are summarized in Tables 7-1 and 7-2. General parameters[40-44] were used for AMPS-1D.

Table 5-5: Material parameters of a-Si:H top cell used for AMPS-1D

	p-layer (a-SiC:H)	i-layer (a-Si:H)	n-layer (a-Si:H)
Thickness [nm]	20	100-500	20
Carrier concentration [cm^{-3}]	$5x10^{17}$-$1x10^{18}$	$1x10^{10}$-$1x10^{15}$	$5x10^{18}$
N_C [cm^{-3}]	$3x10^{19}$	$3x10^{19}$	$3x10^{19}$
N_V [cm^{-3}]	$2x10^{19}$	$2x10^{19}$	$2x10^{19}$
ϕ_b [eV]	1.3-1.4	-	0.1
g_A/g_D [$cm^{-3}eV^{-1}$]	$5x10^{19}/5x10^{19}$	$5x10^{19}/5x10^{19}$	$5x10^{19}/5x10^{19}$
E_A/E_D [eV]	0.03/0.04	0.03/0.04	0.03/0.04
D-state density [cm^{-3}]	$1x10^{18}$	$5x10^{15}$-$4x10^{16}$	$4x10^{17}$
D^+-level (above E_V) [eV]	0.5	0.5	0.5
D^--level (below E_C) [eV]	0.5	0.5	0.5
Capture cross section			
$D^+ + e^- = D^o$ [cm^2]	$1x10^{-14}$	$1x10^{-14}$	$1x10^{-14}$
$D^o + h^+ = D^+$ [cm^2]	$1x10^{-15}$	$1x10^{-15}$	$1x10^{-15}$
$D^o + e^- = D^-$ [cm^2]	$1x10^{-15}$	$1x10^{-15}$	$1x10^{-15}$
$D^- + h^+ = D^o$ [cm^2]	$1x10^{-14}$	$1x10^{-14}$	$1x10^{-14}$
σ_{AG} / σ_{DG} [eV]	0.09/0.09	0.09/0.09	0.09/0.09
Electron affinity χ [eV]	3.9	3.9	3.9
Dielectric constant	11.9	11.9	11.9
Mobility bandgap [eV]	1.95	1.75	1.75
Mobility μ_e/μ_h [$cm^2/V^{-1}/s^{-1}$]	5/0.5	20/3	10/1

Table 5-6: Material parameters of µc-Si:H top cell used for AMPS-1D

	p-layer (µc-Si:H)	i-layer (µc-Si:H)	n-layer (µc-Si:H)
Thickness [µm]	0.02	1.2-3.0	0.02
Carrier concentration [cm^{-3}]	$1x10^{19}$	$1x10^{10}$-$6x10^{15}$	$1x10^{19}$
N_C [cm^{-3}]	$3x10^{19}$	$3x10^{19}$	$3x10^{19}$
N_V [cm^{-3}]	$2x10^{19}$	$2x10^{19}$	$2x10^{19}$
ϕ_b [eV]	1.05	-	0.02
g_A/g_D [$cm^{-3}eV^{-1}$]	$5x10^{19}/5x10^{19}$	$5x10^{19}/5x10^{19}$	$5x10^{19}/5x10^{19}$
E_A/E_D [eV]	0.01/0.02	0.01/0.02	0.01/0.02
D-state density [cm^{-3}]	$1x10^{16}$	$1x10^{15}$-$5x10^{16}$	$1x10^{16}$
D^+-level (above E_V) [eV]	0.3	0.3	0.3
D^--level (below E_C) [eV]	0.3	0.3	0.3
Capture cross section			
$D^+ + e^- = D^o$ [cm^2]	$1x10^{-15}$	$1x10^{-15}$	$1x10^{-15}$
$D^o + h^+ = D^+$ [cm^2]	$1x10^{-16}$	$1x10^{-16}$	$1x10^{-16}$
$D^o + e^- = D^-$ [cm^2]	$1x10^{-16}$	$1x10^{-16}$	$1x10^{-16}$
$D^- + h^+ = D^o$ [cm^2]	$1x10^{-15}$	$1x10^{-15}$	$1x10^{-15}$
σ_{AG} / σ_{DG} [eV]	0.13/0.13	0.13/0.13	0.13/0.13
Electron affinity χ [eV]	3.9	3.9	3.9
Dielectric constant	11.9	11.9	11.9
Mobility bandgap [eV]	1.1	1.1	1.1
Mobility μ_e/μ_h [$cm^2/V^{-1}/s^{-1}$]	50/5	50/5	50/5

5-6-1 Theoretical Analysis of Amorphous Silicon/Microcrystalline-silicon Tandem Solar Cells

In the fabrication of tandem solar cells, the current matching between the top cell and the bottom cell is very important for obtaining high conversion efficiency. With increasing the top cell thickness, the light absorption of the top cell increases, however, that of the bottom cell decreases. When the current generated in the top cell is larger than that in the bottom cell, the total current of the tandem solar cell is limited the smaller current of the bottom cell, and vice versa, since the top cell and the bottom cell are connected in series. Therefore, in order to obtain high conversion efficiency, equalizing the current of the top and the bottom cell is required, i.e., adjusting the thickness of the top and bottom cell is necessary. Thus, two kinds of bottom cells (μc-Si:H) with conversion efficiencies of 6% and 10% were prepared, the current density (J_{sc}) of the top cell and the bottom cell was investigated by changing the top cell thickness from 0 nm to 500 nm. The thickness of the two bottom cells with conversion efficiencies of 6% and 10% were fixed 1.2 μm and 3.0 μm, respectively. The defect density of the two bottom cells with conversion efficiencies of 6% and 10% were $1x10^{15}$ cm^{-3} and $1x10^{13}$ cm^{-3}, respectively. As shown in Fig. 5-70, with increasing the top cell thickness from 0 nm to 500 nm, J_{sc} of the top cell increased from 10 mA/cm^2 to 15 mA/cm^2, and it had saturation with a value of 15 mA/cm^2, on the other hand, J_{sc} of the two bottom cells largely decreased. The J_{sc} value that is equal in both top and bottom cells were around 12 mA/cm^2 and 14 mA/cm^2, respectively for the two bottom cells with conversion efficiencies of 6% and 10%. Besides, the top cell thickness at the current matching point between the top cell and the bottom cell were 170 nm and 300 nm, respectively for the two bottom cells with conversion efficiencies

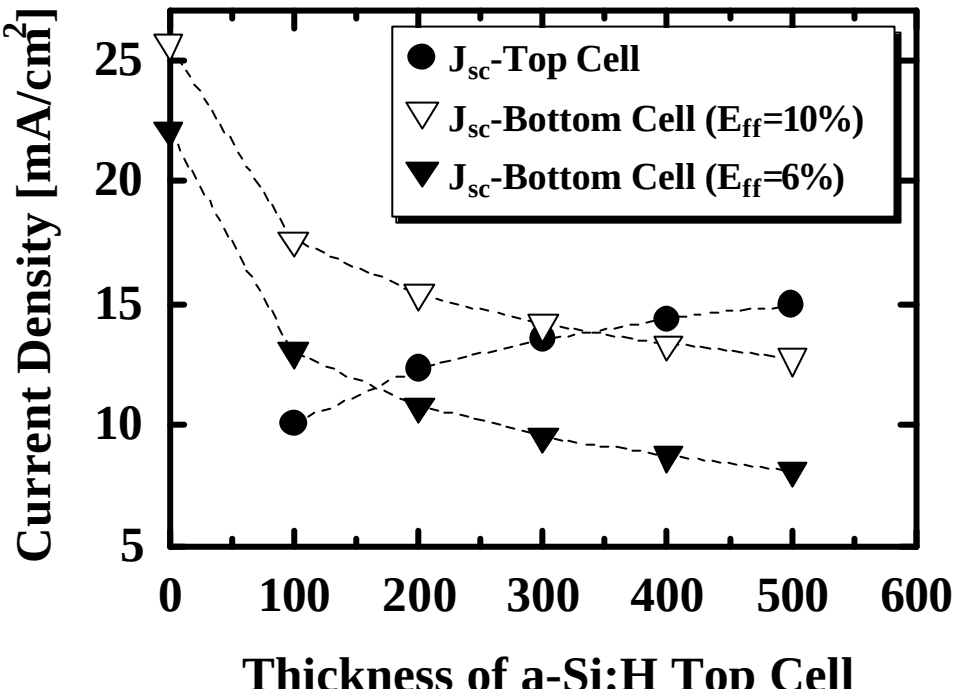

Fig. 5-70: J_{sc} of a-Si:H top cell and μc-Si:H bottom cell as a function of top cell thickness

of 6% and 10%. Therefore, it was found that the optimum thickness of the top cell and bottom cell in a tandem solar cell largely depend on the ability of the bottom cell.

Next, conversion efficiencies of tandem solar cells were predicted by theoretical analysis. First, a tandem solar cell using a-Si:H top cell with a conversion efficiency of 10.1% and μc-Si:H bottom cell with a conversion efficiency of 10.6% was investigated. From the above results in Fig. 5-70, the thickness of the top cell and the bottom cell were fixed 300 nm and 3 μm, respectively. As a result, a conversion efficiency of 15.1% (Voc: 1.48 V, Jsc: 13.7 mA/cm^2, F.F.: 0.75, AM1.5) was obtained, as shown in Fig. 5-71. This result corresponds with that of the best a-Si:H/μc-Si:H tandem solar cell of Kaneka Corp. with a conversion efficiency of 14.5% (Voc: 1.41 V, Jsc: 14.4 mA/cm^2, F.F.: 0.719, AM1.5).[34)] Therefore, it was found that a conversion efficiency of over 15% could be expected for a-Si:H/μc-Si:H tandem solar cells. Second, a tandem solar cell using our a-Si:H top cell with a conversion efficiency of 7.4% and μc-Si:H bottom cell with a conversion efficiency of 6% was investigated. From the above results in Fig. 5-70, the thickness of the top cell and the bottom cell were fixed 170 nm and 1.2 μm, respectively. As a result, a conversion efficiency of 9.0% (Voc: 1.26 V, Jsc: 11.39 mA/cm^2, F.F.: 0.63, AM1.5) was obtained, as shown in Fig. 5-72. It was found that a relatively high conversion efficiency of 9.0% could be expected for a tandem solar cell using our a-Si:H top cell and μc-Si:H bottom cell, therefore, next, a-Si:H/μc-Si:H tandem solar cell was actually fabricated and characterized.

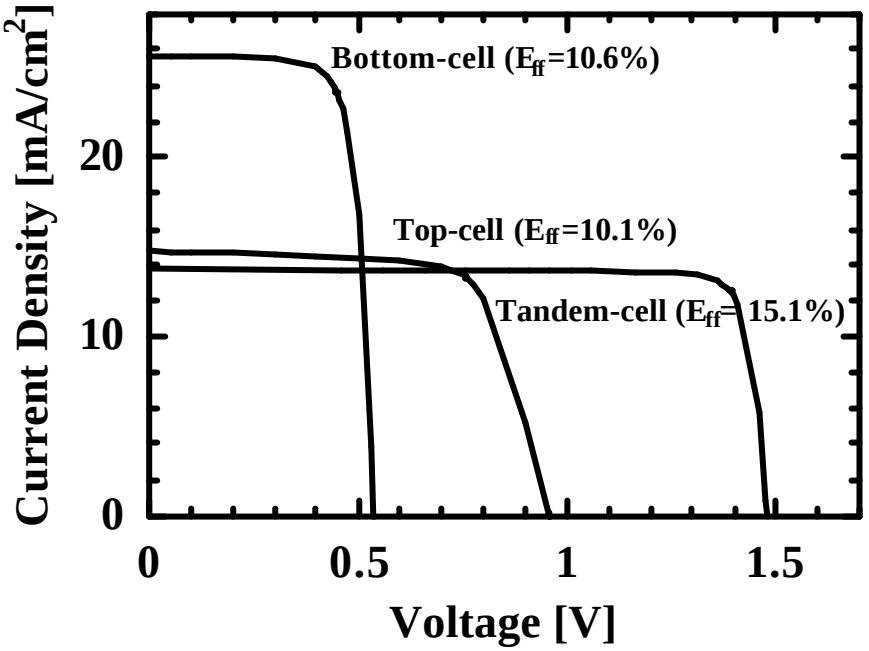

Fig. 5-71: Calculated I-V characteristics of tandem solar cell using a-Si:H top cell (E_{ff} =10.1%) and μc-Si:H bottom cell (E_{ff} =10.6%)

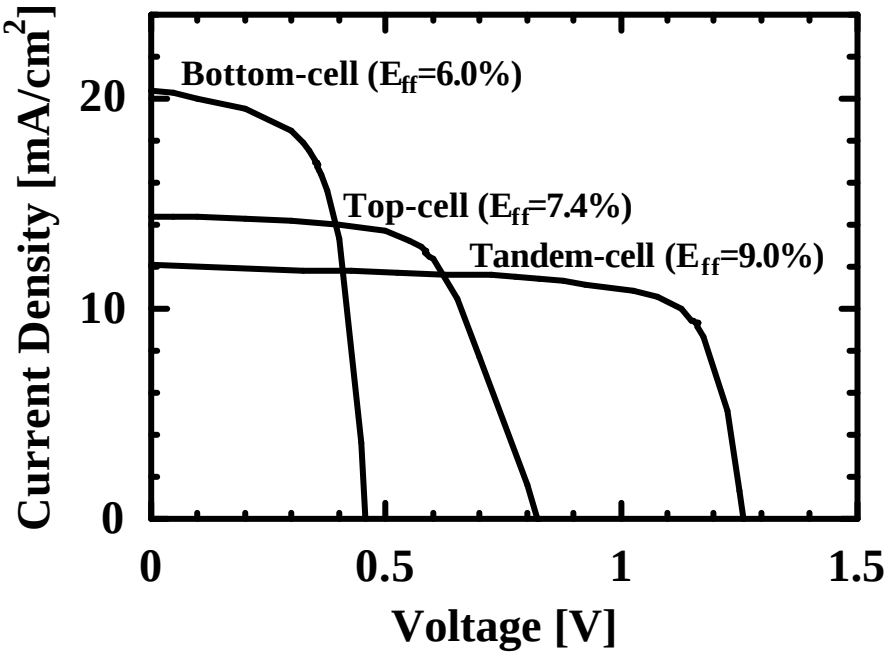

Fig. 5-72: Calculated I-V characteristics of tandem solar cell using our a-Si:H top cell (E_{ff} =7.4%) and μc-Si:H bottom cell (E_{ff} =6%)

5-6-2 Fabrication and Characterization of Amorphous Silicon/ Microcrystalline silicon Tandem Solar Cells

In this section, amorphous silicon/microcrystalline silicon tandem solar cell was actually fabricated by the Hot Wire Cell method and characterized. The tandem solar cell structure fabricated has a following configuration. Glass/TCO(SnO_2)/p-a-Si:H/i-a-Si:H/n-a-Si:H/p-a-Si:H/i-μc-Si:H/n-μc-Si:H/ZnO/Ag/Al. The all silicon layers of the top and the bottom cells were prepared by Hot Wire Cell method. The thickness of the top and bottom cell was 170 nm and 1.2 μm, respectively. As shown in Fig. 5-73, a conversion efficiency of 3.8% (Voc: 1.20 V, Jsc: 6.83 mA/cm^2, F.F.: 0.46, active area: 0.086 cm^2, AM1.5) was obtained. Contrary to the prospects of theoretical analysis, the conversion efficiency was as low as 3.8%. In order to investigate the reason, the performances of each top cell and bottom cell was characterized. As a result, it was found that a conversion efficiency of the top cell was 5.4% (Voc: 0.74 V, Jsc: 12.14 mA/cm^2, F.F.: 0.60, active area: 0.086 cm^2, AM1.5) and a conversion efficiency of the bottom cell was 3.9% (Voc: 0.51 V, Jsc: 16.00 mA/cm^2, F.F.: 0.49, active area: 0.086 cm^2, AM1.5). One of the reasons of the low conversion efficiency of the top cell is the p-layer. In the previous a-Si:H solar cell with a conversion efficiency of 7.5%, p-a-SiC:H and graded a-SiC:H buffer layer were used, however, p-a-Si:H layer was used for the p-layer of this a-Si:H top cell. A conversion efficiency of the bottom cell was also very low probably because the deposition condition was not optimized. In order to investigate the other factors of the low conversion efficiency, a theoretical analysis was carried out. Figure 5-74 shows calculated I-V characteristics of a tandem cell using a-Si:H top cell with a conversion efficiency of 5.33% and μc-Si:H bottom cell with a conversion efficiency of 3.97%. The calculation results show a conversion

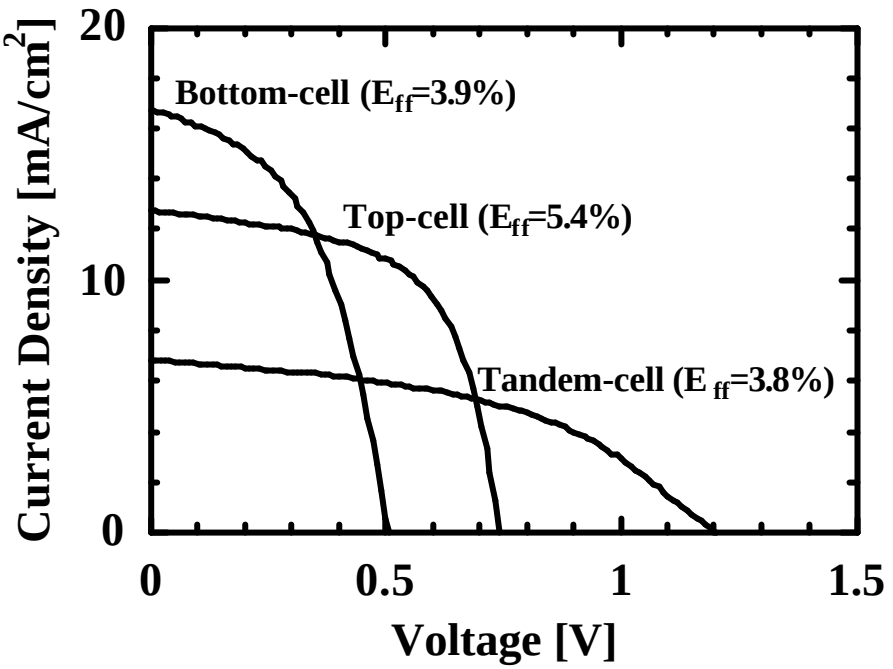

Fig. 5-73: I-V characteristics of a-Si:H top cell, μc-Si:H bottom cell and tandem

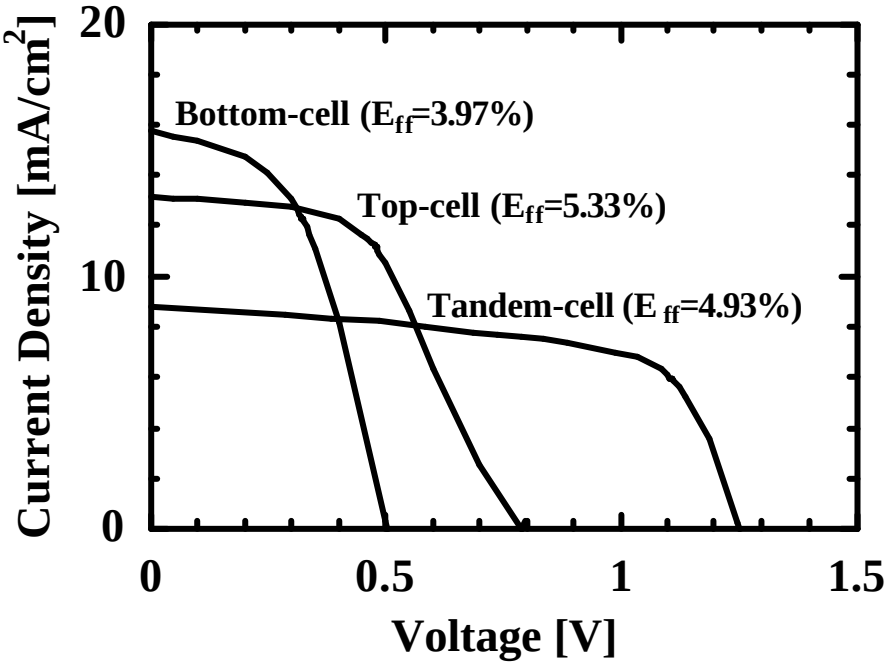

Fig. 5-74: Calculated I-V characteristics of tandem solar cell using a-Si:H top cell (E_{ff} =5.33%) and μc-Si:H bottom cell (E_{ff} =3.97%)

efficiency of 4.93% (Voc: 1.25 V, Jsc: 8.57 mA/cm^2, F.F.: 0.46, AM1.5). This theoretical result corresponds with the result of the real tandem cell. Therefore, the low conversion efficiency of the tandem cell fabricated was mainly derived from the bad cell performances of each top and bottom cell. Jsc of the tandem cell fabricated was lower than that of theoretical value, a loss at the junction between the top cell and the bottom cell and/or a low absorption at long wavelengths over 800 nm due to a low X_c (30%) of the bottom cell might be thought. For obtaining higher conversion efficiency of tandem solar cells, the cell performances of each top and bottom cell must be further improved.

5-7 Summary

Hot Wire Cell (HW-Cell) method has been developed in order to grow microcrystalline silicon (μc-Si:H) thin films. The influence of various deposition parameters on the structural and electrical properties of the films was investigated to improve film quality. As the result, it was found that the concentrations of O and C atoms in μc-Si:H films could be reduced from the order of 10^{21} cm^{-3} to the order of 10^{20} cm^{-3} by decreasing the partial pressure of SiH_4 from 100 mTorr to 3 mTorr. Then, a novel 2-step growth method was proposed in order to reduce an incubation layer in the initial growth of μc-Si:H i-layer. By using this method, Jsc largely increased (10.11 ? 18.32 mA/cm^2), as the result, a conversion efficiency of 3.9% could be achieved. The influence of the incubation layer on solar cell performances was also investigated by a numerical analysis. Then, a conversion efficiency of 5.3% (Voc: 0.48 V, Jsc: 20.56 mA/cm^2, F.F.: 0.54, active area: 0.086 cm^2, AM1.5) was obtained for μc-Si:H solar cells with an i-layer thickness of 1.0μm by optimizing deposition

parameters. Finally, solar cell performances were dramatically improved by decreasing filament temperature from 2100°C to 1800°C, the maximum conversion efficiency of 6.0% (Voc: 0.50 V, Jsc: 19.69 mA/cm^2, F.F.: 0.61, active area: 0.086 cm^2, AM1.5) was obtained for μc-Si:H solar cells with an i-layer thickness of 0.8μm at a low filament temperature of 1800°C. The influence of the filament temperature on μc-Si:H film properties was intensively investigated. As the result, it was found from SIMS results that W and Al concentrations largely increased with increasing the filament temperature from 1800°C to 2100°C and this metal contamination was one of the factors for large degradation of cell performances at a high filament temperatures. Next, we found that a large degradation of solar cell performances occurred by aging. FT-IR and ESR measurement were carried out in order to investigate the influence of ageing on μc-Si:H film properties. The results showed that the peak at 1000-1100 cm^{-1} originated from Si-O-Si bonding and spin density largely increased by aging. SIMS results also showed that O and C atoms in our μc-Si:H films were as low as 2x10^{18} cm^{-3} in the initial state and a large amount of O and C atoms diffused from the surface of μc-Si:H film, and that the diffusion length was as long as 2-2.5 μm. However, it was found that a deposition at a high substrate temperature over 165°C was very effective in high stability of the μc-Si:H film, and it was also shown that a thick (3 μm) a-Si:H cap layer and/or a deposition at a low SiH_4 partial pressure less than 1 mTorr could completely prevent the impurity diffusion. Finally, theoretical analysis and fabrication of amorphous silicon/microcrystalline silicon tandem solar cells were carried out. From the results of theoretical analysis using AMPS-1D BETA 1.00, a conversion efficiency of 15.1% (Voc: 1.48 V, Jsc: 13.7 mA/cm^2, F.F.: 0.75, AM1.5) could be expected for a tandem solar cell using a-Si:H top cell with a conversion efficiency of 10.1% and μc-Si:H bottom cell with a conversion efficiency of 10.6%.

Besides, it was found that a relatively high conversion efficiency of 9.0% could be expected for a tandem solar cell using our a-Si:H top cell with a conversion efficiency of 7.4% and μc-Si:H bottom cell with a conversion efficiency of 6%. Then, amorphous silicon/microcrystalline silicon tandem solar cell was actually fabricated by the Hot Wire Cell method. As a result, a conversion efficiency of 3.8% (Voc: 1.20 V, Jsc: 6.83 mA/cm^2, F.F.: 0.46, active area: 0.086 cm^2, AM1.5) was obtained. It was found that a conversion efficiency of the top cell was 5.4% and a conversion efficiency of the bottom cell was 3.9%. The theoretical analysis showed that the low conversion efficiency of the tandem cell fabricated was mainly derived from the bad cell performances of each top and bottom cell.

References

[1] H. Matsumura and H. Tachibana: Appl. Phys. Lett. **47** (1985) 833.

[2] A. H. Mahan, J. Carapella, B. P. Nelson, R. S. Crandall and I. Balberg: J. Appl. Phys. **69** (1991) 6728.

[3] M. Ichikawa, J. Takeshita, A. Yamada and M. Konagai: Jpn. J. Appl. Phys. **38** (1999) L24.

[4] M. Ichikawa, T. Tsushima, A. Yamada and M. Konagai: Sol. Energy. Mater. & Sol. Cells **66** (2001) 225.

[5] M. Konagai, T. Tsushima, M. K. Kim, K. Asakusa, A. Yamada, Y. Kudriavtsev, A. Villegas and R. Asomoza: Thin Solid Films **395** (2001) 152.

[6] H. Matsumura: Jpn. J. Appl. Phys. **30** (1991) L1552.

[7] T. Mates, A. Fejfar, I. Drobohlav, B. Rezek, P. Fojtik, K. Luterova, J. Kocka, C. Koch, M.B. Schubert, M. Ito, K. Ro and H. Uyama: J. Non-Cryst. Solids **299-302** (2002) 767.

[8] K. Nakahata, T. Kamiya, C.M. Fortmann, I. Shimizu, H. Stuchlikova, A. Fejfar and J. Kocka: J. Non-Cryst. Solids **266-269** (2000) 341.

[9] J. Kocka, A. Fejfar, P. Fojtik, K. Luterova, I. Pelant, B. Rezek, H. Stuchlikova, J. Stuchlik and V. Svrcek: Sol. Energy. Mater. & Sol. Cells **66** (2001) 61.

[10] V. Svrcek, A. Fejfar, P. Fojtik, T. Mates, A. Poruba, H. Stuchlikova, I. Pelant, J. Kocka, Y. Nasuno, M. Kondo and A. Matsuda: J. Non-Cryst. Solids **299-302** (2002) 395.

[11] V. Svrcek, I. Pelant, P. Fojtik, J. Kocka, A. Fejfar, J. Tousek, M. Kondo and A. Matsuda: J. Appl. Phys. **92** (2002) 2323.

[12] T. Kaneko, M. Wakagi, K. Onisawa and T. Minemura: Appl. Phys. Lett. **64** (1994)

1865.

[13] S. Miyajima, A. Yamada and M. Konagai: Thin Solid Films **430** (2003) 274.

[14] S. Miyajima, M. Kim, Y. Ide, A. Yamada and M. Konagai: Jpn. J. Appl. Phys. **42** (2003) 3328.

[15] T. Oshima, A. Yamada and M. Konagai: Jpn. J. Appl. Phys. **36** (1997) 6481.

[16] K. Abe, T. Watahiki, A. Yamada and M. Konagai: Jpn. J. Appl. Phys. **37** (1998) 1202.

[17] K. Higuchi, K. Tabuchi, K. S. Lim, M. Konagai and K. Takahashi: Jpn. J. Appl. Phys. **30** (1991) 1635.

[18] H. Shirai: Jpn. J. Appl. Phys. **34** (1995) 450.

[19] K. Nakamura, K. Yoshina, S. Takeoka and I. Shimizu: Jpn. J. Appl. Phys. **34** (1995) 442.

[20] A. Matsuda: J. Non-Cryst. Solids **59&60** (1987) 767.

[21] J. Koh, A. S. Ferlauto, P. I. Rovira, R. J. Koval, C. R. Wronski and R. W. Collins: J. Non-Cryst. Solids **266-269** (2000) 43.

[22] H. Fujiwara, Y. Toyoshima, M. Kondo and A. Matsuda: J. Non-Cryst. Solids **266-269** (2000) 38.

[23] H. Fujiwara, M. Kondo and A. Matsuda: Surf. Sci. **497** (2002) 333.

[24] C. Niikura, Y. Poissant, M. E. Gueunier, J. P. Kleider and J. E. Bouree: J. Non-Cryst. Solids **299-302** (2002) 1179.

[25] A. Shah, J. Meier, E. Vallat-Sauvain, C. Droz, U. Kroll, N. Wyrsch, J. Guillet and U. Graf: Thin Solid Films **403-404** (2002) 179.

[26] T. Matsui, R. Muhida, T. Kawamura, T. Toyama, H. Okamoto, T. Yamazaki, S. Honda, H. Takakura and Y. Hamakawa: Appl. Phys. Lett. **81** (2002) 4752.

[27] G. Lucovsky, S.S. Chao, J.E. Tyler and W. Czubatyj: Phys. Rev. **B28** (1983) 3225.

[28] J. Kocka, H. Stuchlikova, J. Stuchlik, B. Rezek, T. Mates, V. Svrcek, P. Fojtik, I. Pelant and A. Fejfar: J. Non-Cryst. Solids **299-302** (2002) 355.

[29] E.C. Freeman and W.B. Paul: Phys. Rev. **B18** (1978) 4288.

[30] S. Klein, F. Finger, R. Carius, H. Wagner and M. Stutzmann: Thin Solid Films **395** (2001) 305.

[31] Y. Nasuno, M. Kondo and A. Matsuda: Sol. Energy. Mater. & Sol. Cells **74** (2002) 497.

[32] S. Klein, F. Finger, R. Carius, T. Dylla, B. Rech, M. Grimm, L. Houben, M. Stutzmann: Thin Solid Films **430** (2003) 202.

[33] K. Dairiki, A. Yamada and M. Konagai: Jpn. J. Appl. Phys. **38** (1999) 4007.

[34] Y. Tawada, H. Yamagishi and K. Yamamoto: Solar Energy Materials & Solar Cells **78** (2003) 647.

[35] J. K. Rath, F. A. Rubinelli and R. E. I. Schropp: J. Non-Cryst. Solids **266-269** (2000) 1129.

[36] J. K. Rath, F. A. Rubinelli and R. E. I. Schropp: J. Non-Cryst. Solids **227-230** (1998) 1282.

[37] A. Nakajima, T. Suzuki, M. Yoshimi and K. Yamamoto: Solar Energy Materials & Solar Cells **48** (1997) 287.

[38] B. Rech, T. Roschek, T. Repmann, J. Muller, R. Schmitz and W. Appenzeller: Thin Solid Films **427** (2003) 157.

[39] A. Shah, J. Meier, E. Vallat-Sauvain, C. Droz, U. Kroll, N. Wyrsch, J. Guillet and U. Graf: Thin Solid Films **403-404** (2002) 179.

[40] J. P. R. Bakker, B. J. van der Horst and J. I. Dijkhuis: J. Non-Cryst. Solids **299-302** (2002) 1256.

[41] H. Liu, L. Jiao, S. Semoushkina and C. R. Wronski: J. Non-Cryst. Solids **198-200**

(1996) 1168.

[42] H. Takakura and Y. Hamakawa: Solar Energy Materials & Solar Cells **74** (2002) 479.

[43] S. Yamanaka, M. Konagai and K. Takahashi: Jpn. J. Appl. Phys. **28** (1989) 1178.

[44] H. Tasaki, W. Y. Kim, M. Hallerdt, M. Konagai and K. Takahashi: J. Appl. Phys. **63** (1988) 550.

Chapter6

Approaches for High Rate Deposition of Microcrystalline Silicon Thin Films

6-1 Introduction

The technology for high rate deposition of microcrystalline silicon thin films with small hydrogen dilution ratio was developed. In our previous works, it was already found that high deposition rates of 2-3 nm/s could be obtained at low substrate temperatures of 200-300^{o}C. As above-mentioned, for the cost reduction of solar cells, high deposition rate of 2-5 nm/s is highly required, many researches for high rate depositions have been done, up to now.[1-10)] Therefore, further high rate deposition was attempted. In order to obtain high deposition rate, deposition parameters such as SiH_4 flow rate and filament-substrate distance was changed. The film properties such as dark conductivity, photoconductivity and crystal volume fraction were investigated for the films deposited by changing those deposition parameters. Then, microcrystalline silicon thin film solar cells were also fabricated with high deposition rates. On the other hands, it was already demonstrated in Chapter 5 that the filament temperature must be decreased to less than 1800^{o}C for obtaining high quality microcrystalline films and high efficiency solar cells. However, gas dissociation efficiency decreased with increasing reactant gases at a low filament temperature less than 1900^{o}C, as a

result, the film couldn't be crystallized. Therefore, in order to increase gas dissociation efficiency with maintaining the filament temperature of 1900^{o}C, instead of ordinary 18-turn filament with a length of 1.5 cm, 36-turn long filament with a length of 3 cm was used and examined.

6-2 Experimental Details

Intrinsic μc-Si:H thin films were deposited on Corning7059 glass and Asahi U-type TCO glass by Hot Wire Cell method in a hybrid multichamber system (Hot Wire Cell method and photo-CVD). The chamber was evacuated by a turbomolecular pump, and the base pressure was around $2x10^{-7}$ Torr. A mixture of SiH_4 and H_2 gases was used for intrinsic μc-Si:H film deposition. The filament in the shape of a coil that had a diameter of 4 mm and a length of 1.5 cm or 3.0 cm was used and it was placed parallel to the gas inlet. The filament temperature was monitored by an infrared pyrometer through a quartz window.

The deposition conditions are shown in Table 6-1. In order to characterize μc-Si:H thin films, Fourier transform infrared absorption spectroscopy (FT-IR) measurement, dark (σ_d) and photoconductivity (σ_{ph}) measurements were carried out. In order to investigate the application of these a-Si:H films to Si-based thin film solar cells, superstrate pin solar cells were prepared with the deposition rate of 0.4-1.5 nm/s. The structure of the superstrate pin solar cell was as follows: glass/TCO(SnO_2)/p-a-SiC:H/buffer-a-SiC:H/i-a-Si:H/n-a-Si:H/ZnO/Ag/Al. The p-type, buffer and n-type layers were prepared by the photo-CVD method. 2-step growth method was also carried out for the fabrication of solar cells.

Table 6-1: Deposition parameters.

Filament temperature	1900-2100^{o}C
Substrate temperature	100-215^{o}C
SiH_4 partial pressure	3-4.2 mTorr
SiH_4 gas flow rate	5-25 sccm
H_2 gas flow rate	15-200 sccm
Filament-substrate distance	1.5-10 cm
Filament length	1.5 cm (18-turn) or 3.0 cm (36-turn)

6-3 High Rate Deposition and Solar Cell Properties

6-3-1 Dependence on Mono-silane Flow Rate

In our previous works, the dominant deposition parameters that largely control the deposition rate are SiH_4 flow rate and filament-substrate distance. Therefore, in order to largely increase the deposition rate, it can be simply thought that SiH_4 flow rate should be increased at a near filament-substrate distance. Thus, first, in order to know the effects of SiH_4 flow rate, the dependence of deposition rate on SiH_4 flow rate was investigated. The deposition conditions are as follows: substrate temperature of 150°C, filament temperature of 1900°C, SiH_4 partial pressure of 3 mTorr, SiH_4 flow rate of 5-15 sccm, H_2 flow rate of 25-120 sccm and filament-substrate distance of 5 cm. As shown in Fig. 6-3-1, it was found that the deposition rate largely increased from 0.3 nm/s to 1.4 nm/s with increasing SiH_4 flow rate of from 5 sccm to 15 sccm. When SiH_4 flow rate was 5 sccm, H_2 flow rate was 25 sccm, i.e. H_2/SiH_4 ratio of 5, and crystal volume fraction of the film was around 30% in this case. In case of SiH_4 flow rate of 15 sccm, H_2 flow rate was increased to 120 sccm, i.e. H_2/SiH_4 ratio of 8, because H_2/SiH_4 ratio required for the same crystal volume fraction increased with increasing SiH_4 flow rate. However, as shown in Fig. 6-3-2, although H_2 flow rate largely increased, the crystal volume fraction of the film largely decreased with increasing SiH_4 flow rate over 10 sccm, and the film completely became amorphous at SiH_4 flow rate of 15 sccm. The film couldn't be crystallized at SiH_4 flow rate of 15 sccm even when H_2 flow rate was increased to 150 sccm. Therefore, that is because the gas dissociation efficiency at the filament was reduced by the large increase of total reactant gas flow rate. Besides, deposition rate

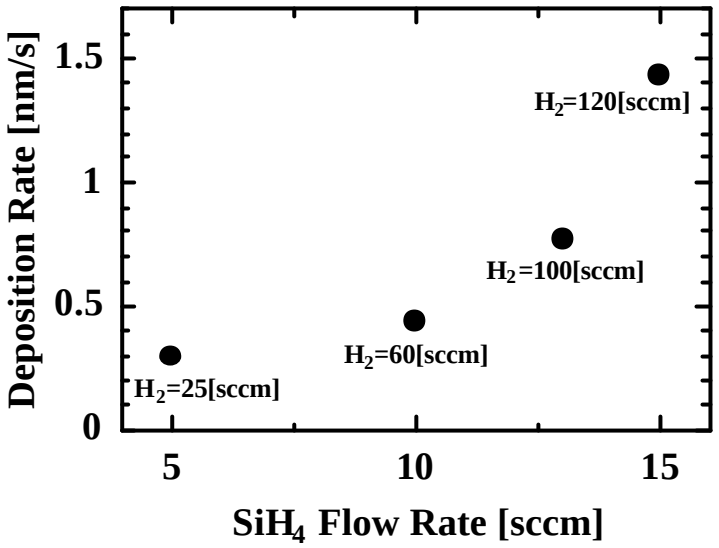

Fig. 6-3-1: Deposition rate as a function of SiH_4 flow rate

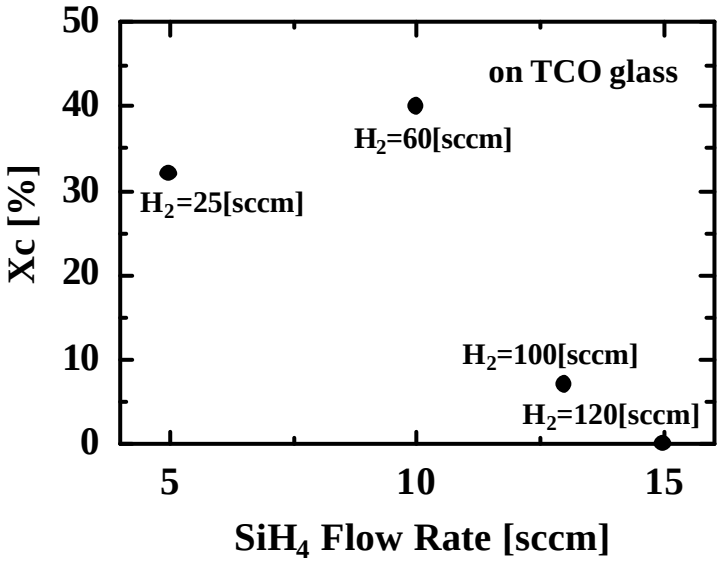

Fig. 6-3-2: Crystal volume fraction of a film as a function of SiH_4 flow rate

didn't increase in proportion to SiH_4 flow rate. That is because SiH_4 partial pressure was constant of 3 mTorr in this case, thus the total gas pressure increased with largely increasing H_2 flow rate.

6-3-2 Dependence on Filament-Substrate Distance

Next, in order to check the effects of filament-substrate distance, deposition rate as a function of SiH_4 flow rate was investigated. The deposition conditions are as follows: substrate temperature of 165^oC, filament temperature of 1900^oC, SiH_4 partial pressure of 3 mTorr, SiH_4 flow rate of 5 sccm, H_2 flow rate of 40 sccm and filament-substrate distance of 1.5-10 cm.

As shown in Fig. 6-3-3, deposition rate largely increased from 0.16 nm/s to 1.24 nm/s with decreasing filament-substrate distance from 10 cm to 1.5 cm. Deposition rate largely increased, especially in the region of filament-substrate distance from 6 cm to 1.5 cm. As shown in Fig. 6-3-4, crystal volume fraction of the films kept almost constant value of 50-60% in the region of filament-substrate distance from 6 cm to 1.5 cm, while crystal volume fraction largely decreased with increasing filament-substrate distance over 8 cm, and it decreased to 13.5% at filament-substrate distance of 10 cm. That is because consume of atomic hydrogen produced at the filament is promoted by gas phase reaction with increasing filament-substrate distance, thus the quantity of atomic hydrogen which arrive on the substrate reduces. Next, for these films, dark conductivity, photoconductivity measurement were carried out and H content and Si-H/Si-H_2 ratio was also measured by FT-IR measurement. The results of them are shown in Figs. 6-3-5 and 6-3-6, respectively.

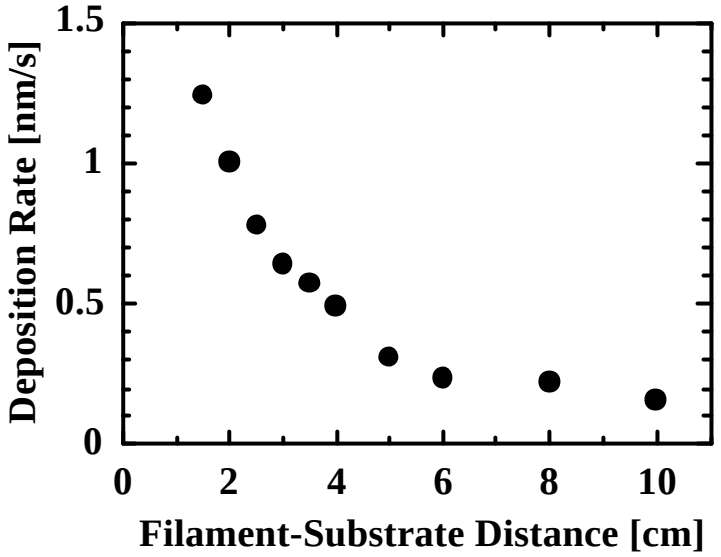

Fig. 6-3-3: Deposition rate as a function of filament-substrate distance

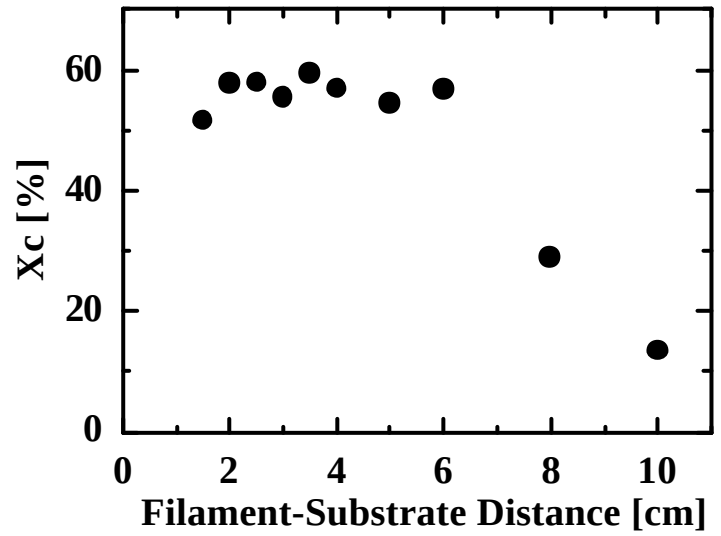

Fig. 6-3-4: Crystal volume fraction of a film as a function of filament-substrate distance

As shown in Fig. 6-3-5, in the region of filament-substrate distance from 6 cm to 1.5 cm, photoconductivity and dark conductivity had some variations, however those values were the order of 10^{-4}-10^{-5}, 10^{-6}, respectively. On the other hand, dark conductivity decreased to 1x10 with increasing filament-substrate distance over 6 cm, reflecting the decrease of crystal volume fraction. The photoconductivity/dark conductivity ratio had a large value of 10^{-2}-10^{-3} at a long filament-substrate distance over 6 cm. As shown in Fig. 6-3-6, although crystal volume fraction kept constant value of around 60% in the region of filament-substrate distance from 6 cm to 1.5 cm, total H content in the film decreased from 5.6% to 4.4% with decreasing filament-substrate temperature. Although crystal volume fraction was constant, total H content decreased, therefore, the grain boundary of the film was insufficiently passivated by H atoms, indicating degradation of film quality. On the other hand, Si-H/Si-H_2 ratio kept an almost constant value of around 1.0 in the region of filament-substrate distance from 6 cm to 2 cm, while it largely decreased with increasing filament-substrate distance to 1.5 cm. This tendency is similar to that of the films deposited with high hydrogen dilution as demonstrated in Chapter 5, indicating the existence of large amount of atomic hydrogen around the filament. Besides, the real substrate temperature increased with decreasing filament-substrate distance because thermal radiation from the filament largely increased in a short distance, implying that H atoms emitted from the film. FT-IR measurement couldn't be carried out successfully in the cases of filament-substrate distance of 8 cm and 10 cm probably because the films were grown epitaxicially.

Based on these results of the dependence on SiH_4 flow rate and filament-substrate distance, further high rate deposition was attempted by combining these two deposition parameters. In above results, a degradation of film properties was

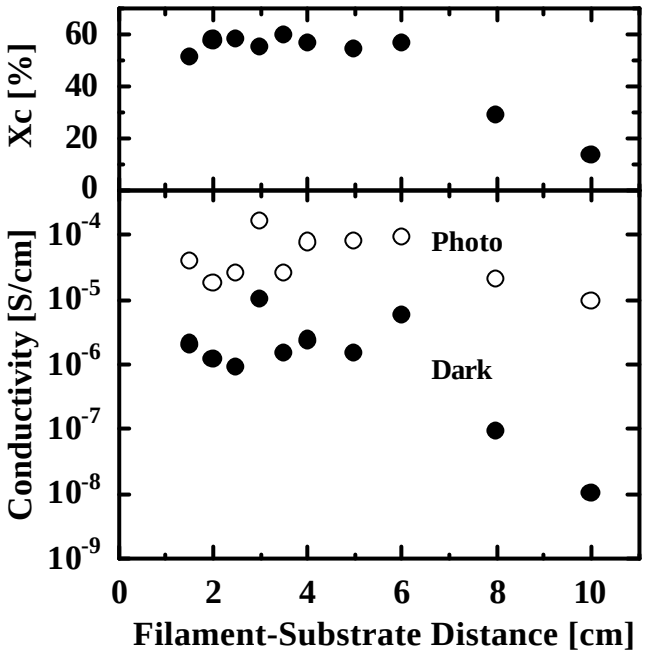

Fig. 6-3-5: Crystal volume fraction and dark, photoconductivity as a function of filament-substrate distance

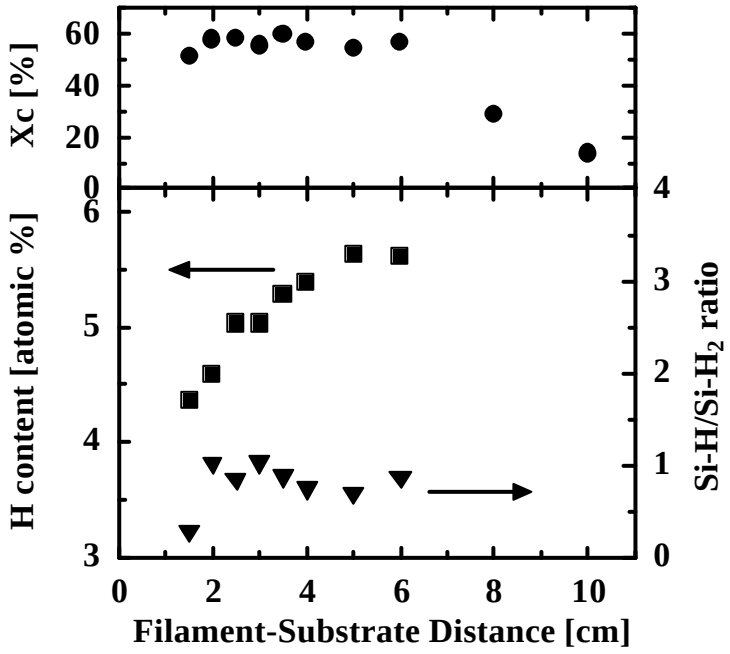

Fig. 6-3-6: Crystal volume fraction, total H content and Si-H/Si-H_2 ratio as a function of filament-substrate distance

not seen in the region of filament-substrate distance from 6 cm to 2 cm, therefore, next, filament-substrate distance was fixed 2 cm and SiH_4 flow rate was varied 5 sccm to 25 sccm. As shown in Fig. 6-3-2, crystal volume fraction largely decreased with increasing SiH_4 flow rate over 10 sccm at a filament temperature of 1900^oC, therefore filament temperature was fixed 2050^oC. Substrate temperature was 190^oC, SiH_4 partial pressure was 4.2 mTorr and H_2/SiH_4 dilution ratio was fixed 8. Deposition rate and crystal volume fraction as a function of SiH_4 flow rate and dark and photoconductivity as a function of SiH_4 flow rate were shown in Figs. 6-3-7 and 6-3-8, respectively.

As shown in Figs. 6-3-7, deposition rate extremely largely increased from 0.8 nm/s to 11.5 nm/s with increasing SiH_4 flow rate from 5 sccm to 25 sccm. Crystal volume fraction was maintained a constant value of around 60% until SiH_4 flow rate of 15 sccm, i.e. deposition rate of 3.7 nm/s, while it largely decreased to 11% with further increasing SiH_4 flow rate to 25 sccm. That is because dissociation efficiency of reactant gases at the filament was reduced with increasing gas flow rate, and also probably because in general, higher substrate temperatures are required for crystallinity and restrain of defect density at a high deposition rate compared to moderate deposition rate less than 0.5 nm/s, therefore substrate temperature of 190^oC was not enough for high rate deposition in this case. As shown in Fig. 6-3-8, both of photo and dark conductivity decreased with increasing SiH_4 flow rate. Dark conductivity largely decreased at SiH_4 flow rate of over 15 sccm, because crystal volume fraction of the film decreased as shown in Fig. 6-3-7. Besides, compared to other photoconductivity, it largely decreased to the order of 10^{-7} at SiH_4 flow rate of 25 sccm, indicating a degradation of the film quality.

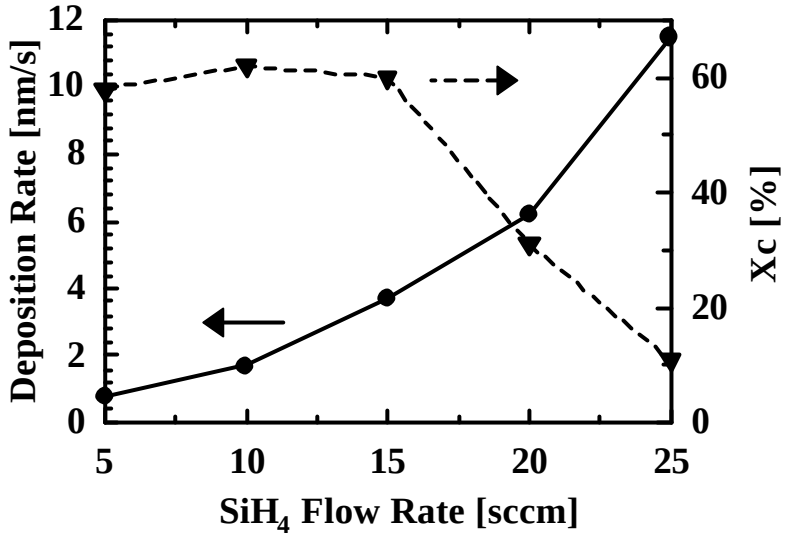

Fig. 6-3-7: Deposition rate and crystal volume fraction as a function of filament-substrate distance

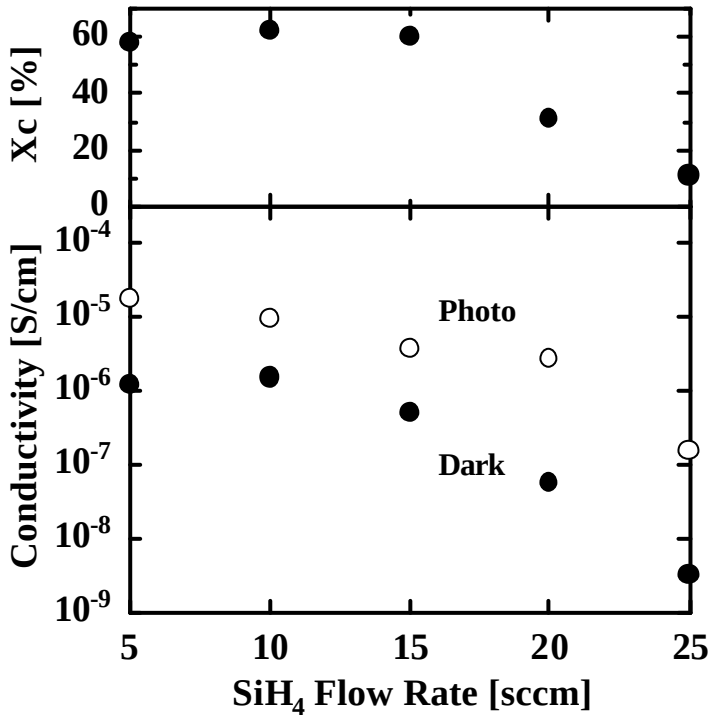

Fig. 6-3-8: Crystal volume fraction, photo and dark conductivity as a function of filament-substrate distance

6-3-3 Effects of Filament Length on Film Properties

From the results in 6-3-1 and 6-3-2, it was found that high deposition rate could be easily obtained by increasing reactant gas flow rate, however, filament temperature was required to increase up to around 2050-2100^{o}C, because dissociation efficiency of reactant gases at the filament was reduced by increase of gas flow rate. On the other hand, from the results in Chapter 5, solar cell performances largely degraded at filament temperatures of over 2000^{o}C, high conversion efficiencies have not been obtained at this high filament temperature region. Therefore, in this study, in order to increase the dissociation efficiency of reactant gases with maintaining a filament temperature of 1900^{o}C, instead of conventional tungsten filament with a length of 1.5 cm (18-turn), a novel long tungsten filament with a length of 3 cm (36-turn) was attempted to use for deposition of microcrystalline silicon thin films.

First, in order to confirm if dissociation efficiency really increases by using a long filament, the relationship between crystal volume fraction and H_2 flow rate was investigated for both of ordinary filament (1.5 cm) and long filament (3 cm), respectively. The deposition conditions are as follows: substrate temperature of 150^{o}C, filament temperature of 1900^{o}C, SiH_4 partial pressure of 3 mTorr, SiH_4 flow rate of 5 sccm, H_2 flow rate of 15-100 sccm and filament-substrate distance of 5 cm. As shown in Fig. 6-3-9, the obvious differences in crystal volume fraction were observed between 18-turn filament and 36-turn filament in the region of H_2 flow rate from 10 sccm to 60 sccm. H_2 flow rate of 25 sccm was required for crystal volume fraction of 30% in the case of 18-turn filament, however H_2 flow rate of only 10 sccm was needed for the same crystal volume fraction in the case of 36-turn filament. In the region of H_2 flow rate from 10 sccm to 60 sccm, H_2 flow rate required for the same crystal

volume fraction shifts to a low H_2 flow rate side in the case of 36-turn filament. Therefore, it is concluded that dissociation efficiency of SiH_4 and H_2 gases increased by increasing filament length, thus the quantity of atomic hydrogen supplied to the substrate largely increased. On the other hand, in the region of H_2 flow rate over 60 sccm, crystal volume fraction was saturated with a value of around 60% in case of both filament. Raman spectra were deconvoluted in their integrated crystalline, I_c (520 cm^{-1}), amorphous, I_a (480 cm^{-1}) and intermediate, I_m (510 cm^{-1}) peaks, then crystal volume fraction, X_c, was calculated from these values. The problem of this method for evaluating X_c is that value of X_c is saturated with a value of around 60% at a high X_c of over 60%. Therefore, X_c seems to be saturated in the region of H_2 flow rate over 60 sccm. Besides, it is also one factor of this saturation that the substrate temperature was as low as 150^{o}C, thus, the crystallinity of the films were limited by this low substrate temperature.

From the above results, it was confirmed that dissociation efficiency of reactant gases increased and H_2 flow rate required for crystallization could be reduced by using a long filament. It was also indicated that crystallinity of films might be limited by substrate temperature. Therefore, next, the relationship between crystallinity and substrate temperature was investigated for SiH_4 flow rate of both 5 sccm and 15 sccm. The deposition conditions are as follows: filament length of 3 cm (36-turn), filament temperature of 1900^{o}C, substrate temperatures of 100-215^{o}C, SiH_4 partial pressure of 3 mTorr, filament-substrate distance of 5 cm and SiH_4/H_2 flow rates of 5 sccm/15 sccm and 15 sccm/ 75 sccm. Deposition rate for SiH_4 flow rates of 5 sccm and 15 sccm was 0.4 nm/s and 1.3 nm/s, respectively.

As shown in Fig. 6-3-10, films were crystallized even at SiH_4 flow rate of 15 sccm. Until now, films couldn't be crystallized at a filament temperature of 1900^{o}C in

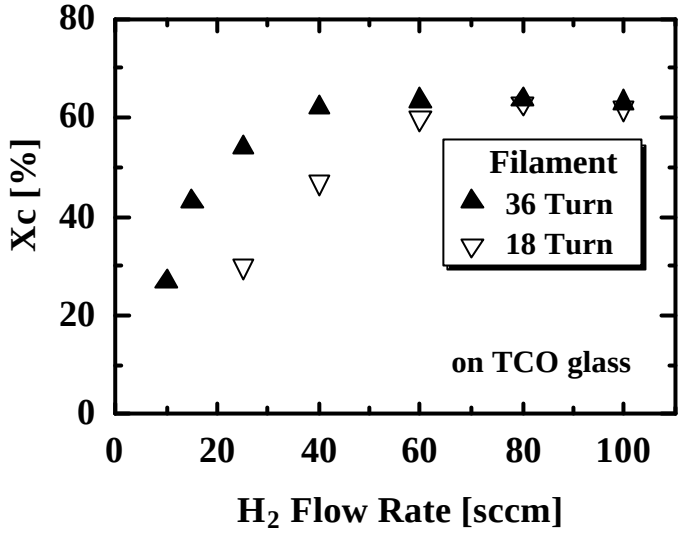

Fig. 6-3-9: Crystal volume fraction as a function of H_2 flow rate

-comparison between 36-turn and 18-turn filament-

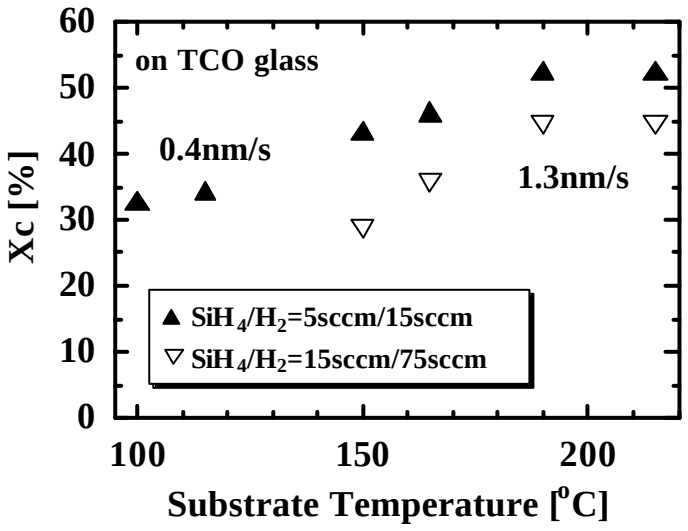

Fig. 6-3-10: Crystal volume fraction as a function of substrate temperature

case of 18-turn filament, filament temperature required to be increased to 2100°C, however, microcrystalline silicon films could be obtained at 1900°C by using 36-turn filament. From these results, it was also confirmed that dissociation efficiency of reactant gases increased by increasing filament length. Crystal volume fraction largely increased with increasing substrate temperature from 100°C to 215°C at deposition rates of both 0.4 nm/s and 1.3 nm/s. In case of deposition rate of 1.3 nm/s, crystal volume fraction largely decreased at substrate temperature of lower than 200°C, and the substrate temperature required for the same crystal volume fraction shifted to high temperature side, compared to the case of deposition rate of 0.4 nm/s. Therefore, compared to at low deposition rate, the substrate temperature is required to be increased at high deposition rate. However, a substrate temperature of i-layer cannot be increased more than that of p-layer in p-i-n superstrate type solar cell, thus some measures against these problems are required.

From above results, it was found that a long filament (3 cm, 36-turn) was very effective and useful in crystallinity and high rate deposition. Therefore, it is necessary to investigate the application of these films prepared by a long filament to solar cells. On the other hand, in this study, our solar cells need 2-step growth method, thus, initial growth of films was investigated by using a long filament before the preparation of solar cells. The deposition conditions are as follows: filament temperature of 1900°C, substrate temperature of 150°C, SiH_4 partial pressure of 3 mTorr, SiH_4 flow rates of 5 sccm and filament-substrate distance of 5 cm.

Figures 6-3-11 and 6-3-12 show film crystallinity in the initial growth as a function of H_2 flow rate in case of 18-turn filament and 36-turn filament, respectively. H_2 flow rate required for film crystallization shifted to a low H_2 flow rate side using 36-turn filament, compared to using 18-turn filament. Crystal volume fraction was

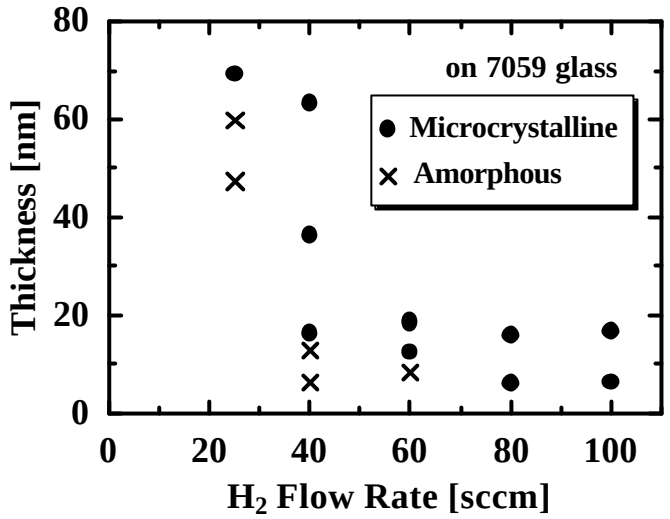

Fig. 6-3-11: Crystallinity of films in the initial growth as a function of H_2 flow rate using 18-turn filament

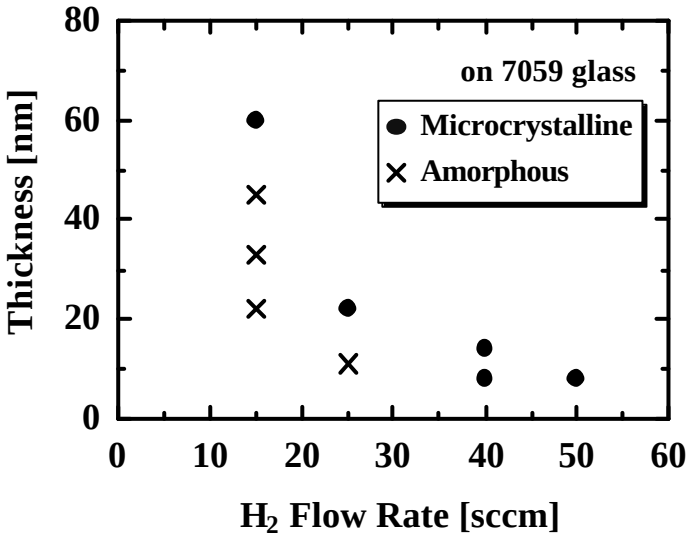

Fig. 6-3-12: Crystallinity of films in the initial growth as a function of H_2 flow rate using 18-turn filament

around 30% at H_2 flow rate of 25 sccm and 15 sccm using 18-turn filament and 36-turn filament, respectively. Besides, the thickness of the films which crystallization started was around 60-70 nm and corresponded well in both cases, as shown in Figs. 6-3-11 and 6-3-12. In both cases, the thickness of the films which crystallization started largely decreased with increasing H_2 flow rate. Therefore, it is concluded that the thickness of a film which crystallization starts mainly depends on crystal volume fraction of a thick film when the deposition rate is almost same. H_2 flow rate required for crystallization in case of 36-turn filament was almost half of that in case of 18-turn filament.

6-3-4 Fabrication and Characterization of Solar Cells

From the results in 6-3-2, it was found that microcrystalline silicon thin films could be obtained at the maximum deposition rate of 11.5nm/s using our current Hot Wire Cell system. Solar cells were fabricated with increasing deposition rate from 0.3-0.4 nm/s to 1-2 nm/s. First, filament-substrate distance was fixed 5 cm and solar cells were fabricated by changing SiH_4 flow rate from 5sccm to 15 sccm in a similar way to 6-3-1, then their performances were characterized. The other deposition conditions were completely same as those of 6-3-1. However, the film couldn't be crystallized at a SiH_4 flow rate of 15 sccm and at a filament temperature of 1900^{o}C, as shown in 6-3-1, therefore, in this time, filament temperature was increased to 2100^{o}C only at a SiH_4 flow rate of 15 sccm. Besides, all the solar cells were fabricated using 2-step growth method and thickness of i-layer was around 1.5μm.

As shown in Fig. 6-3-13, although deposition rate was increased from 0.3 nm/s to 0.5 nm/s by increasing SiH_4 flow rate from 5 sccm to 10 sccm, no degradation

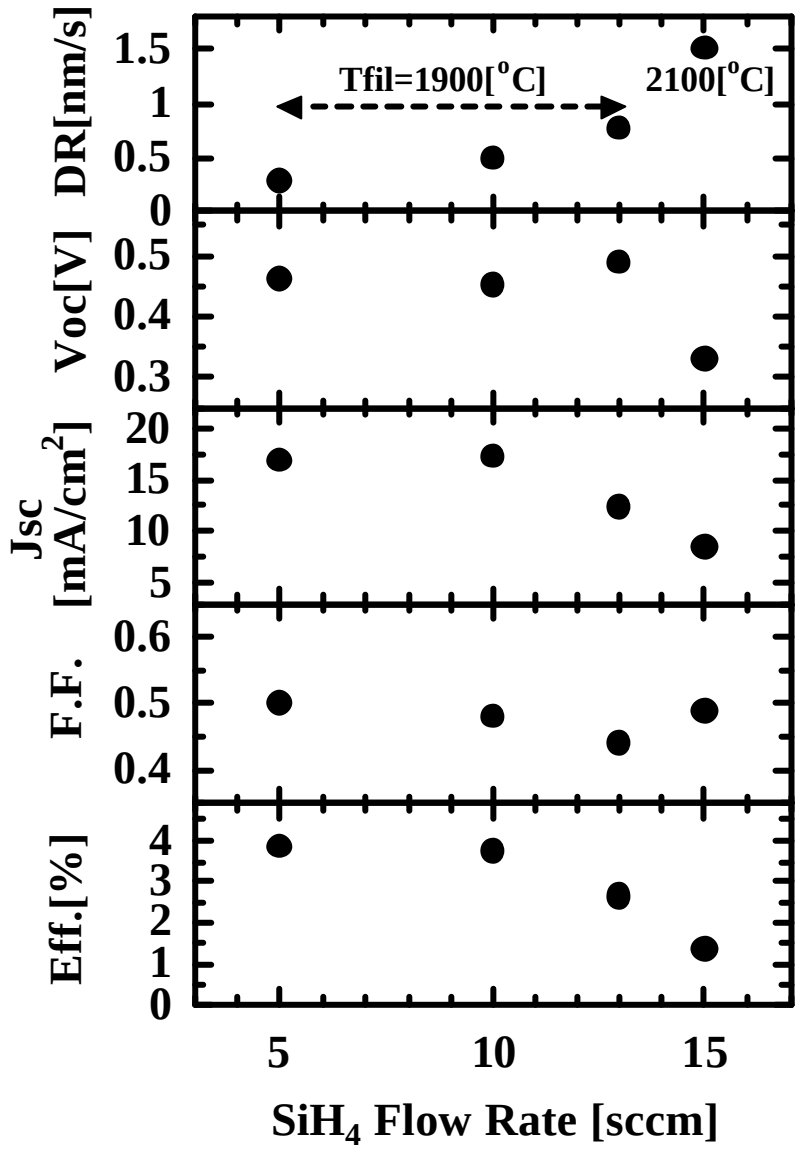

Fig. 6-3-13: Solar cell performances as a function of SiH_4 flow rate

was observed in the solar cell performances and a conversion efficiency of around 4.0% was obtained. V_{oc} increased to around 0.5 V but J_{sc}, F.F. decreased and a conversion efficiency decreased to 2.5% with increasing SiH_4 flow rate to 13 sccm. This is because crystal volume fraction largely decreased to 7% and the film structure became almost amorphous. Therefore, crystal volume fraction was controlled around 30% at a SiH_4 flow rate of 15 sccm and at a filament temperature of 2100°C. As a result, deposition rate increased up to 1.5 nm/s, however V_{oc} and J_{sc} largely decreased and conversion efficiency largely decreased to 1.4%. It is one of the reasons that film quality was degraded by a high deposition rate of 1.5 nm/s, however that is mainly because of the metal contamination from the filament at a high filament temperature of 2100°C as demonstrated in Chapter 5. Therefore, instead of increasing filament temperature, some deposition techniques that maintain crystal volume fraction of films at a large amount of SiH_4 flow rate are highly required.

Solar cell performances were no influenced when SiH_4 flow rate increased until 10 sccm, as shown in Fig. 6-3-13, therefore, next, SiH_4 flow rate was fixed 10 sccm and solar cells were fabricated by changing filament-substrate distance from 5 cm to 2 cm in a similar way to 6-3-2, then their performances were characterized. The deposition conditions are as follows: substrate temperature of 150°C, filament temperature of 1900°C, SiH_4 partial pressure of 3 mTorr, H_2 flow rate of 50-60 sccm. As shown in Fig. 6-3-14, deposition rate largely increased from 0.5 nm/s to 1.5 nm/s with decreasing filament-substrate distance from 5 cm to 2 cm. No large degradation of solar cell performances was observed at filament-substrate distance until 3.5 cm probably because deposition rate didn't increase largely. When filament-substrate distance was decreased to 2 cm, V_{oc} was almost constant, but J_{sc} largely decreased, and conversion efficiency decreased to 2.8%. Although deposition rate was as same as

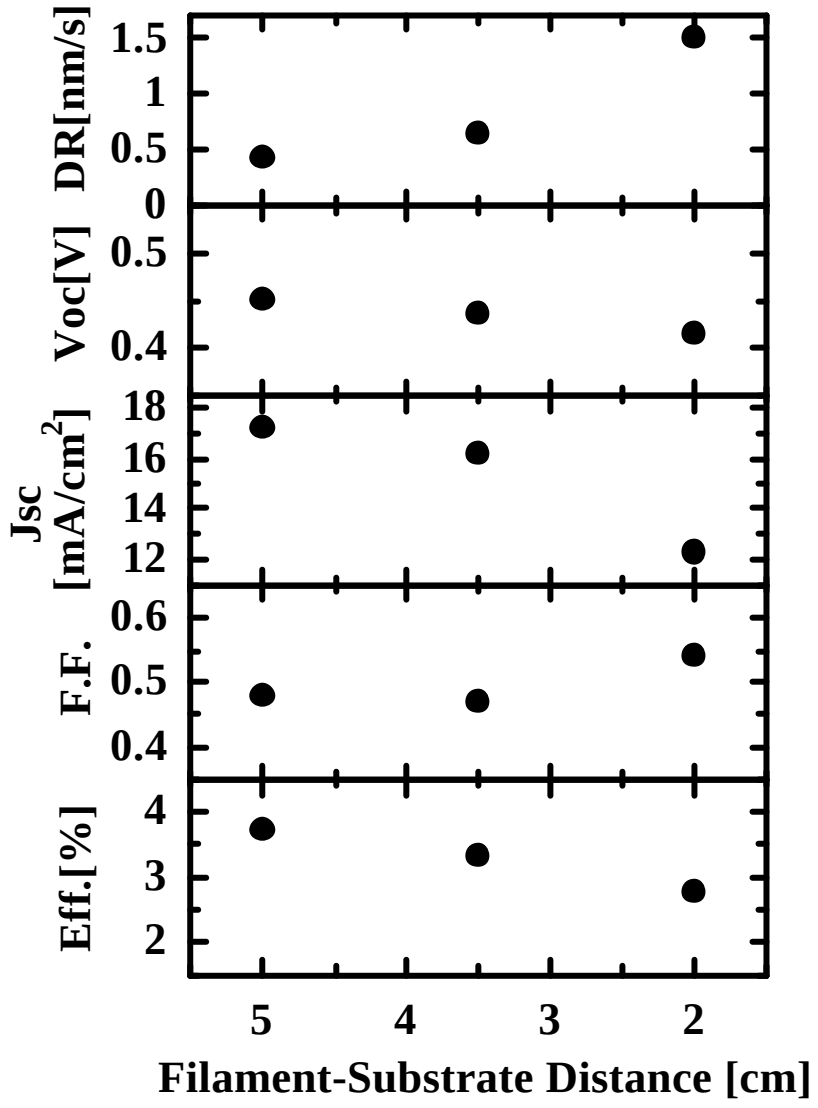

Fig. 6-3-14: Solar cell performances as a function of filament-substrate distance

1.5 nm/s, compared to the case of Fig. 3-6-13, such a large degradation was not observed. Therefore, such a large degradation as shown in Fig. 3-6-13 mainly derived from metal contamination from filament. The reasons of the degradation in Fig. 3-6-14 are as follows: increase of defect density due to high deposition rate, increase of heat radiation from the filament due to a short filament-substrate distance, the influence of incubation layer because 2-step growth method was not established for high rate deposition yet.

Next, solar cells were fabricated by using 36-turn filament. In 6-3-3, it was demonstrated that 36-turn filament was effective in high rate deposition, therefore, the application of 36-turn filament to solar cells was investigated. First, solar cells were fabricated at a SiH_4 flow rate of 5 sccm. The other deposition conditions of the i-layer are as follows: filament length of 3 cm, filament temperature of 1900^oC, substrate temperature of 150^oC, SiH_4 partial pressure of 3 mTorr, filament-substrate distance of 5 cm, H_2 flow rate of 15 sccm, thickness of 1 μm and deposition rate of 0.4 nm/s. H_2 flow rate in the 1st layer of the 2-step growth method was 100 sccm. As shown in Fig. 6-3-15, a conversion efficiency of 3.4% was obtained. The maximum conversion efficiency of the solar cells fabricated by using 18-turn filament at the same deposition conditions was 4.8% (Voc: 0.47 V, Jsc: 17.44 mA/cm^2, F.F.: 0.58, active area: 0.086 cm^2, AM1.5) on that time. Compared to the solar cell with 18-turn filament, especially Voc and F.F. decreased. Xc of this solar cell was 43% and it's higher than 30% of the solar cell that has a conversion efficiency of 4.8%. In this study, as demonstrated in Chapter 5, the maximum conversion efficiency was obtained at a low Xc of around 30%. Therefore, a high Xc of the solar cell is one of the reasons of the decrease of sell performances. Besides, in this time, the solar cells were fabricated at a H_2 flow rate in the 1st layer of the 2-step growth method of 100 sccm. As demonstrated in 6-3-3, H_2

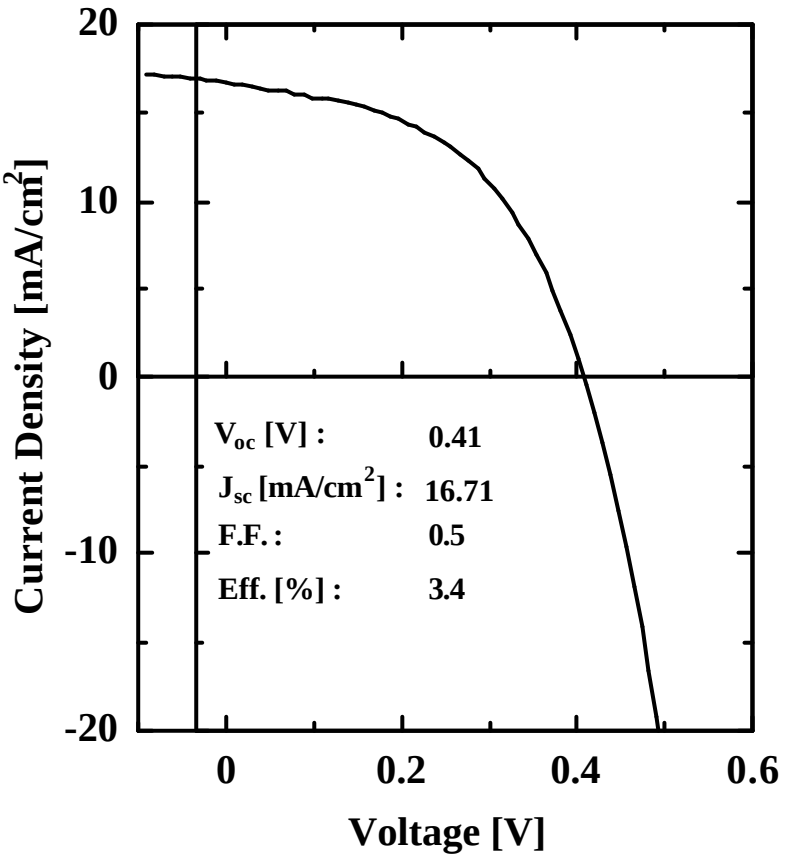

Fig. 6-3-15: I-V characteristics of a solar cell fabricated by using 36-turn filament

flow rate of 50sccm is enough for the crystallization due to high dissociation efficiency of reactant gases in the case of 36-turn filament. Therefore, p-layer might be damaged by a great deal of atomic hydrogen at H_2 flow rate of 100sccm. On the other hand, a relatively high Jsc of 16.71 mA/cm^2 was obtained. Until now, the 18-turn filament with a temperature of 2100^{o}C has a serious problem of a large decrease of Jsc and conversion efficiency due to a large degradation of film quality. However, such degradations were not observed in the case of 36-turn filament, therefore, it was demonstrated that the 36-turn filament with a low temperature of 1900^{o}C could increase a dissociation efficiency of reactant gases as high as that of 18-turn filament with a temperature of 2100^{o}C maintaining the film quality. Next, for further improvement of cell performances, solar cells were fabricated by changing H_2 flow rate in the 1st layer of the 2-step growth method. As shown in Fig. 6-3-16, Voc, Jsc and F.F. increased with decreasing H_2 flow rate from 100 sccm to 25 sccm, as a result, conversion efficiency was improved to 4%. This result indicates that p-layer can be easily damaged and the property of p/i interface is degraded by a large amount of H_2 flow rate in the 1st layer of the 2-step growth method. Fig 6-3-12 shows that incubation layer with a thickness of 20 nm was deposited at a H_2 flow rate of 25 sccm, however this result was demonstrated for corning 7059 glasses, indicating that H_2 flow rate can be reduced less than 25 sccm for solar cells because i-layer can be easily crystallized on μc-Si:H p-layer, compared to corning 7059 glass. Solar cell performances might be further improved by decreasing H_2 flow rate less than 25 sccm.

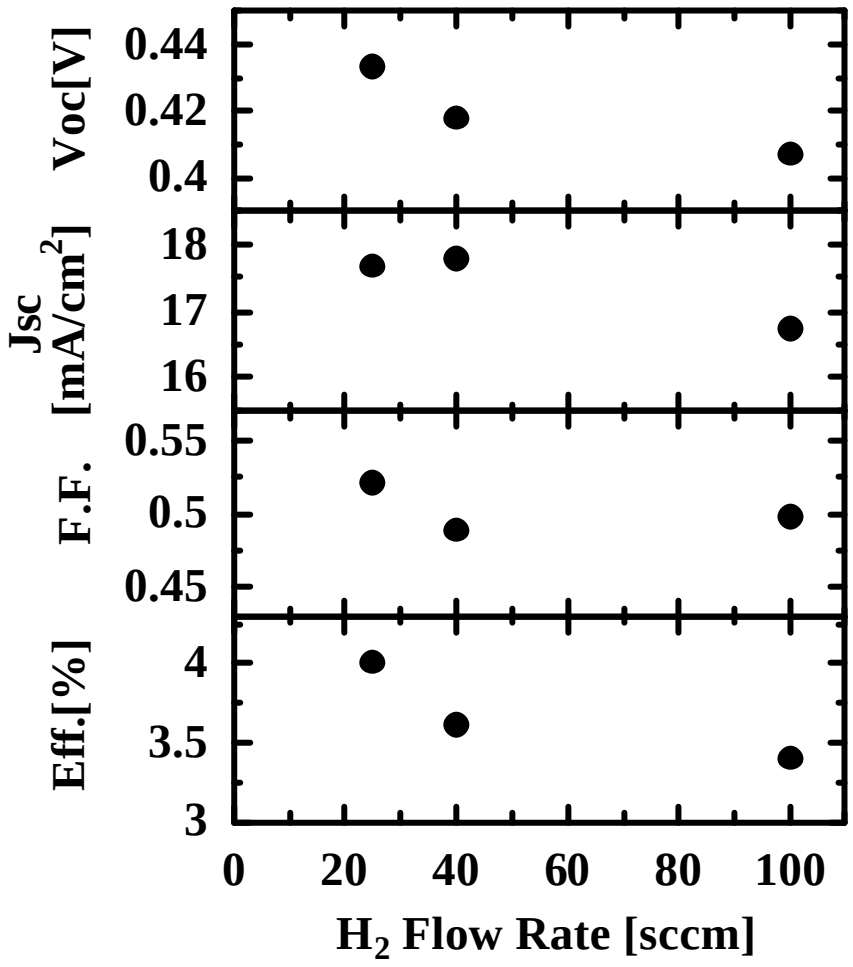

Fig. 6-3-16: Solar cell performances as a function of H2 flow rate in the first-step of the 2-step growth method

6-4 Summary

It was demonstrated that SiH_4 flow rate and filament-substrate distance are most dominant parameters that largely control deposition rate. Filament-substrate distance was decreased from 5 cm to 2 cm, SiH_4 flow rate was increased to 25 sccm, as a result, μc-Si:H films with the maximum deposition rate of 11.5 nm/s could be obtained. μc-Si:H solar cells fabricated at a high deposition rate of 1.5nm/s showed a conversion efficiency of 2.8% (Voc: 0.42 V, Jsc: 12.31 mA/cm^2, F.F.: 0.54, active area: 0.086 cm^2, AM1.5).

It was found that following two serious problems occurred in high rate deposition. 1. At a filament temperature less than 1900^{o}C, films with good quality could be obtained, however film crystallization was difficult for a large SiH_4 flow rate due to the decrease of dissociation efficiency at a filament. 2. At a filament temperature over 2100^{o}C, films could be easily crystallized, however film quality largely degraded due to metal contaminations. In order to solve these problems, 36-turn long filament was proposed and used for μc-Si:H films and solar cells. As a result, it was demonstrated that dissociation efficiency of reactant gases could be increased, high rate deposition could be obtained and H_2 flow rate required for film crystallization could be reduced even at a filament temperature of 1900^{o}C. a conversion efficiency of 4.0% was obtained at a deposition rate of 0.4 nm/s, indicating that quality of μc-Si:H films deposited by using 36-turn filament was as good as that of μc-Si:H films deposited by using ordinary 18-turn filament.

References

[1] Y. Nasuno, M. Kondo and A. Matsuda: Solar Energy Materials & Solar Cells **74** (2002) 497.

[2] A. H. Mahan: Solar Energy Materials & Solar Cells **78** (2003) 299.

[3] E. Iwaniczko, Y. Xu, R. E. I. Schropp and A. H. Mahan: Thin Solid Films **430** (2003) 212.

[4] A. Matsuda, M. Takai, T. Nishimoto, M. Kondo: Solar Energy Materials & Solar Cells **78** (2003) 3.

[5] M. Kondo and A. Matsuda: Current Opinion in Solid State and Materials Science **6** (2002) 445.

[6] T. Nishimoto, M. Takai, H. Miyahara, M. Kondo and A. Matsuda: J. Non-Cryst. Solids **299-302** (2002) 1116.

[7] J. K. Rath, A. J. Hardeman, C. H. M. van der Werf, P. A. T. T. van Veenendaal, M. Y. S. Rusche and R. E. I. Schropp: Thin Solid Films **430** (2003) 67.

[8] C. H. M. van der Werf, A. J. Hardeman, P. A. T. T. van Veenendaal, M. K. van Veen, J. K. Rath and R. E. I. Schropp: Thin Solid Films **427** (2003) 41.

[9] T. Takagi, R. Hayashi, G. Ganguly, M. Kondo and A. Matsuda: Thin Solid Films **345** (1999) 75.

[10] M. Itoh, Y. Ishibashi, A. Masuda and H. Matsumura: Thin Solid Films **395** (2001) 138.

Chapter7

General Conclusions and Future Prospects

7-1 General Conclusions

As environmental and energy resource concerns have increased, greater stress has been placed on development of renewable energy resources such as photovoltaic electric generators. In order to attain the expected breakthrough of photovoltaic technology as a competitive energy source against fossil fuels, further improvement of efficiency and significant reduction of production costs are required.

In recent years, the development of thin-film photovoltaic devices based on microcrystalline semiconductor materials from the standpoint of high-efficiency and low-cost is the main focus of considerable research worldwide. Microcrystalline silicon thin film solar cells are currently one of the most promising technologies because they have a great potential to attain high conversion efficiency and high stability compared to amorphous silicon solar cells. To achieve mass production of solar cells, new deposition techniques that have simple apparatus and high deposition rate on cheap substrates such as glass substrates are required. In this study, Hot Wire Cell method is developed as a novel technique for the growth of microcrystalline silicon thin films, film properties, the improvement of film quality and high rate depositions were investigated. In this method, the reactant gases are decomposed on

the surface of a heated tungsten filament. The resulting fragments act as precursors of possible gas phase reactions and thin film deposition. Deposition of silicon films using mono-silane gas and hydrogen gas as reactant gases was investigated at various deposition parameters for achieving high quality microcrystalline silicon thin films and high rate depositions. Furthermore, high efficiency microcrystalline silicon thin film solar cells were investigated.

In chapter 3, a-Si:H films were deposited by the Hot Wire Cell method and it was found that the deposition at a low pressure was effective in improvement of the quality of a-Si:H films. We could succeed in reducing $Si-H_2$ bonding and the concentrations of O and C atoms to the order of 10^{18} cm^{-3} at the deposition pressures of 1-10 mTorr, and the photoconductivity of $6.5x10^{-5}$ S/cm could be obtained. The initial and stabilized conversion efficiency of 7.5% and 6.3% with the deposition rate of 0.4 nm/s were achieved for superstrate pin a-Si:H solar cell. It was also found that the short filament-substrate distance was effective for the high deposition rate with maintaining film quality. We could succeed in obtaining the high photoconductivity and the dominant peak at 2000 cm^{-1} in FT-IR spectra with a high deposition rate of 1 nm/s at a pressure of 5 mTorr and a filament-substrate distance of 3 cm. The initial conversion efficiency of 5.5% with the deposition rate of 1 nm/s was achieved for superstrate pin a-Si:H solar cell.

In chapter 4, it was investigated if p-layer and n-layer materials such as p-a-SiC:H, p-a-Si:H, p-μc-Si:H, n-a-Si:H and n-μc-Si:H were suitable for μc-Si:H thin film solar cells by theoretical analysis using AMPS-1D BETA 1.00. First, effects of p-layer materials on solar cell performances were examined. As a result, it was found that the most suitable p-layer material for μc-Si:H thin film solar cells is p-μc-Si:H. Next, n-a-Si:H and n-μc-Si:H were investigated in order to confirm if they were

suitable n-layer materials for μc-Si:H thin film solar cells. As a result, it was found that both n-a-Si:H and n-μc-Si:H can be used for μc-Si:H thin film solar cells. Finally, effects of i-layer film properties such as defect density, impurity concentration and film thickness on solar cell performances were investigated. Defect density was varied from $1x10^{15}$ cm^{-3} to $1x10^{18}$ cm^{-3}, as a result, it was found that defect density is very effective in solar cell performances, and for obtaining high conversion efficiencies, defect density must be reduced less than $1x10^{16}$ cm^{-3}. Impurity concentrations were varied from $1x10^{10}$ cm^{-3} to $1x10^{18}$ cm^{-3}, as a result, it was found that for obtaining high conversion efficiency, impurity concentration must be decreased less than $1x10^{15}$ cm^{-3}. The thickness of the i-layer was varied from 0.5 μm to 5.0 μm for the defect densities of $1x10^{15}$ cm^{-3} and $1x10^{16}$ cm^{-3}, respectively, as the results, when a defect density was $1x10^{15}$ cm^{-3}, a conversion efficiency largely increased with increasing i-layer thickness and it had the maximum value of 11% at a thickness of 5.0 μm. On the other hand, when a defect density was $1x10^{16}$ cm^{-3}, the optimum i-layer thickness was around 1.0-2.0 μm and the maximum conversion efficiency was 6% at that thickness.

In chapter 5, Hot Wire Cell (HW-Cell) method has been developed in order to grow microcrystalline silicon (μc-Si:H) thin films. The influence of various deposition parameters on the structural and electrical properties of the films was investigated to improve film quality. As the result, it was found that the concentrations of O and C atoms in μc-Si:H films could be reduced from the order of 10^{21} cm^{-3} to the order of 10^{20} cm^{-3} by decreasing the partial pressure of SiH_4 from 100 mTorr to 3 mTorr. Then, a novel 2-step growth method was proposed in order to reduce an incubation layer in the initial growth of μc-Si:H i-layer. By using this method, Jsc largely increased (10.11 ? 18.32 mA/cm^2), as the result, a conversion efficiency of 3.9% could be achieved. The influence of the incubation layer on solar cell performances was also

investigated by a numerical analysis. Then, a conversion efficiency of 5.3% (Voc: 0.48 V, Jsc: 20.56 mA/cm^2, F.F.: 0.54, active area: 0.086 cm^2, AM1.5) was obtained for μc-Si:H solar cells with an i-layer thickness of 1.0μm by optimizing deposition parameters. Finally, solar cell performances were dramatically improved by decreasing filament temperature from 2100^{o}C to 1800^{o}C, the maximum conversion efficiency of 6.0% (Voc: 0.50 V, Jsc: 19.69 mA/cm^2, F.F.: 0.61, active area: 0.086 cm^2, AM1.5) was obtained for μc-Si:H solar cells with an i-layer thickness of 0.8μm at a low filament temperature of 1800^{o}C. The influence of the filament temperature on μc-Si:H film properties was intensively investigated. As the result, it was found from SIMS results that W and Al concentrations largely increased with increasing the filament temperature from 1800^{o}C to 2100^{o}C and this metal contamination was one of the factors for large degradation of cell performances at a high filament temperatures. Next, we found that a large degradation of solar cell performances occurred by aging. FT-IR and ESR measurement were carried out in order to investigate the influence of ageing on μc-Si:H film properties. The results showed that the peak at 1000-1100 cm^{-1} originated from Si-O-Si bonding and spin density largely increased by aging. SIMS results also showed that O and C atoms in our μc-Si:H films were as low as 2x10^{18} cm^{-3} in the initial state and a large amount of O and C atoms diffused from the surface of μc-Si:H film, and that the diffusion length was as long as 2-2.5 μm. However, it was found that a deposition at a high substrate temperature over 165^{o}C was very effective in high stability of the μc-Si:H film, and it was also shown that a thick (3 μm) a-Si:H cap layer and/or a deposition at a low SiH_4 partial pressure less than 1 mTorr could completely prevent the impurity diffusion. Finally, theoretical analysis and fabrication of amorphous silicon/microcrystalline silicon tandem solar cells were carried out. From the results of theoretical analysis using AMPS-1D BETA 1.00, a

conversion efficiency of 15.1% (Voc: 1.48 V, Jsc: 13.7 mA/cm^2, F.F.: 0.75, AM1.5) could be expected for a tandem solar cell using a-Si:H top cell with a conversion efficiency of 10.1% and μc-Si:H bottom cell with a conversion efficiency of 10.6%. Besides, it was found that a relatively high conversion efficiency of 9.0% could be expected for a tandem solar cell using our a-Si:H top cell with a conversion efficiency of 7.4% and μc-Si:H bottom cell with a conversion efficiency of 6%. Then, amorphous silicon/microcrystalline silicon tandem solar cell was actually fabricated by the Hot Wire Cell method. As a result, a conversion efficiency of 3.8% (Voc: 1.20 V, Jsc: 6.83 mA/cm^2, F.F.: 0.46, active area: 0.086 cm^2, AM1.5) was obtained. The cell performances of each top and bottom cell was investigated, it was found that a conversion efficiency of the top cell was 5.4% and a conversion efficiency of the bottom cell was 3.9%. The theoretical analysis showed that the low conversion efficiency of the tandem cell fabricated was mainly derived from the bad cell performances of each top and bottom cell.

In chapter 6, it was demonstrated that SiH_4 flow rate and filament-substrate distance are most dominant parameters that largely control deposition rate. Filament-substrate distance was decreased from 5 cm to 2 cm, SiH_4 flow rate was increased to 25 sccm, as a result, μc-Si:H films with the maximum deposition rate of 11.5 nm/s could be obtained. μc-Si:H solar cells fabricated at a high deposition rate of 1.5nm/s showed a conversion efficiency of 2.8% (Voc: 0.42 V, Jsc: 12.31 mA/cm^2, F.F.: 0.54, active area: 0.086 cm^2, AM1.5).

It was found that following two serious problems occurred in high rate deposition. 1. At a filament temperature less than 1900^{o}C, films with good quality could be obtained, however film crystallization was difficult for a large SiH_4 flow rate due to the decrease of dissociation efficiency at a filament. 2. At a filament

temperature over 2100°C, films could be easily crystallized, however film quality largely degraded due to metal contaminations. In order to solve these problems, 36-turn long filament was proposed and used for μc-Si:H films and solar cells. As a result, it was demonstrated that dissociation efficiency of reactant gases could be increased, high rate deposition could be obtained and H_2 flow rate required for film crystallization could be reduced even at a filament temperature of 1900°C. a conversion efficiency of 4.0% was obtained at a deposition rate of 0.4 nm/s, indicating that quality of μc-Si:H films deposited by using 36-turn filament was as good as that of μc-Si:H films deposited by using ordinary 18-turn filament.

Consequently, it is concluded that Hot Wire Cell method is very promising technique for depositing microcrystalline silicon thin films for photovoltaic applications. The main emphasis for achieving high efficiency microcrystalline silicon thin film solar cells and the industrialization of Hot Wire Cell method is to pursue the simple fabrication techniques and the characterization of the structural, chemical, electrical and optical properties of each layer and their interfaces in the solar cells. It is expected that the high conversion efficiency microcrystalline silicon thin film solar cells can be obtained by reduction of defect density and impurity concentration, and improvement of interfaces. The process of achieving a conversion efficiency of 6% by HW-Cell method is summarized in Fig. 7-1.

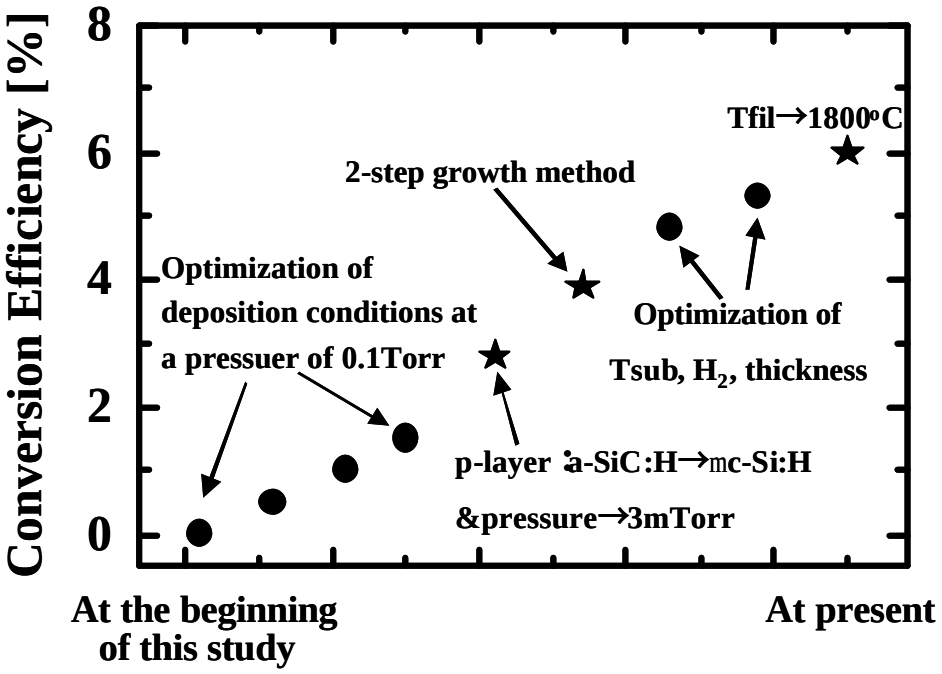

Fig. 7-1: Process of achieving a conversion efficiency of 6% by HW-Cell method.

7-2 Future Prospects

For mass production of silicon based thin film solar cells, microcrystalline silicon solar cells with a high conversion efficiency of 9-10% prepared at a high deposition rate of 2-5 nm/s are highly required. Theoretical analysis demonstrates that higher conversion efficiency can be expected for amorphous silicon/microcrystalline silicon tandem solar cells compared to amorphous silicon and microcrystalline silicon single solar cells. However, the conversion efficiency of tandem solar cells largely depends on that of both amorphous top cell and microcrystalline bottom cell. Therefore, higher conversion efficiency is required for Hot Wire Cell method. It is theoretically demonstrated that the increase of defect density and impurity concentration in the i-layer of p-i-n type solar cells largely degrades the solar cell performances. Therefore, for higher conversion efficiency, the reduction of defect density and impurity concentration in the intrinsic microcrystalline silicon layer is the key issue. The experimental results demonstrate that a low SiH_4 partial pressure of less than 1 mTorr is very effective in the reduction of O and C impurity atoms in μc-Si:H films and the film stability, besides a low filament temperature of less than 1800^{o}C is also very effective in the reduction of W atoms in μc-Si:H films. Therefore, higher conversion efficiency can be expected by decreasing SiH_4 partial pressure of less than 1 mTorr and using tantalum filament that can be used at a filament temperature of less than 1700^{o}C. Furthermore, in our Hot Wire system, high quality μc-Si:H films are currently obtained at low X_c of 30%, however, for obtaining high current density of 25-30mA/cm^2, large increase of absorption at long wavelengths is required. Thus, high quality μc-Si:H films must be obtained at high X_c of over 50%.

Acknowledgements

The author is indebted to Professor Makoto Konagai for providing such an interesting theme and for their continuous guidance and warm encouragement through the author's post-graduate course.

The author wishes to express to his sincere appreciation to Associated Professor Akira Yamada for their constructive advises, critical comments throughout this study.

The author would like to express special gratitude to Professors Shunri Oda and Mitsumasa Iwamoto, Associated Professor Adarsh Sandhu and Professor Jürgen H. Werner (Stuttgart Univ. Germany), and also Professors Toyosaka Moriizumi, Masanori Abe, and Associated Professors Osamu Sugiura, Takamichi Nakamoto, Shigeki Nakagawa and Yutaka Majima for their critical comments and encouraging remarks.

The author wishes to thank Drs. Tamotsu Okamoto, Katsuya Abe, Koji Dairiki, Mitsuru Ichikawa and Tatsuro Watahiki for their technical and warm advices and their practical instruction. The author is also grateful to Professor Rene Asomoza (Mexico) for SIMS measurement and Professor Jan Kocka (Czech) for activation energy, SPV and SSPG measurements.

The author would like to thank Messrs. Dr. Zhao Ying (Nankai Univ. Chaina), Yuichi Wakita, Yusuke Sumita, Yutaka Kobayashi, Koichi Asakusa, Tomoya Fujisaki, Shinsuke Miyajima, Kazuki Oki, Yuji Saito, Shuichi Hiza and Isao Shoukaku as a co-worker, and also thank Drs. Tomohiko Otsuka, Nowshad Amin, Sutichai Chaisitsak, Messrs. Yuichi Matsuzaki, Shuhei Yagi and Takeshi Tsushima for valuable comments and suggestions of this study.

The author wishes to thank all members of the Konagai Lab. and Yamada Lab., who participated in the interesting discussions and made suggestions for improving the research activity. Thanks are extended to the secretaries for their kind assistance: Ms. Kimiko Furukawa, Ms. Yuko Yoshida, Ms. Manami Kawauchi and Ms. Miharu Takakuwa.

List of Publications

Papers

1. Yoshinori IDE, Yuji SAITO, Akira YAMADA and Makoto KONAGAI "Intrinsic Microcrystalline Silicon Thin Films Prepared by Hot Wire Cell Method and Its Application to Solar Cells" Jpn. J. Appl. Phys. (submitted)

2. Yoshinori IDE, Yuji SAITO, Akira YAMADA and Makoto KONAGAI "2-Step Growth Method and Microcrystalline Silicon Thin Film Solar Cells Prepared by Hot Wire Cell Method" Jpn. J. Appl. Phys. (accepted)

3. Shinsuke MIYAJIMA, Mingyu KIM, Yoshinori IDE, Akira YAMADA and Makoto KONAGAI "Highly Conductive Boron Doped Microcrystalline Si Films Deposited by Hot Wire Cell Method and Its Application to Solar Cells" Jpn. J. Appl. Phys., 42 (2003) 3328.

4. Yoshinori IDE, Koichi ASAKUSA, Akira YAMADA and Makoto KONAGAI "Amorphous Silicon Thin Films Prepared by Hot Wire Cell Method and Its Application to Solar Cells" Jpn. J. Appl. Phys., 42 (2003) 1521.

5. Ying ZHAO, Shinsuke MIYAJIMA, Yoshinori IDE, Akira YAMADA and Makoto KONAGAI "Microcrystalline Silicon Films and Solar Cells Prepared by Photochemical Vapor Deposition on Textured SnO_2 with High Haze Factors" Jpn. J. Appl. Phys., 41 (2002) 6417.

International Conferences

1. Yoshinori IDE, Yuji SAITO, Shuichi HIZA, Akira YAMADA and Makoto KONAGAI "μc-Si Thin Films Prepared by Hot Wire Cell Method and Its Application to Solar Cells" 14th International Photovoltaic Science and Engineering Conference, January 26-30, 2004, Bangkok, Thailand

2. Yoshinori IDE, Yuji SAITO, Akira YAMADA and Makoto KONAGAI "Microcrystalline Silicon Thin Film Solar Cells Prepared by Hot Wire Cell Method" 3rd World Conference on Photovoltaic Energy Conversion, May 11-18, 2003, Osaka, Japan.

3. Yoshinori IDE, Koichi ASAKUSA, Ying ZHAO, Akira YAMADA and Makoto KONAGAI "Amorphous and Microcrystalline Silicon Films Deposited by Hot Wire Cell Method: Application to Silicon Based Thin Film Solar Cells" 29th IEEE Photovoltaic Specialists Conference, May 20-24, 2002, New Orleans, Louisiana.

4. Makoto KONAGAI, Takeshi TSUSHIMA, Yoshinori IDE, Koichi ASAKUSA, Tomoya FUJISAKI, Myong-Kyu KIM, Yuichi WAKITA and Akira YAMADA "High Rate Deposition of Silicon Thin Films by Hot Wire Cell Method for Solar Cell Applications" 28th IEEE Photovoltaic Specialists Conference, September 15-22, 2000, Anchorage, AK, USA

5. Yoshinori IDE, Yuichi WAKITA, Akira YAMADA and Makoto KONAGAI "Fabrication of Polycrystalline Silicon Thin Film Solar Cells by Hot Wire Cell Method" 11th International Photovoltaic Science and Engineering Conference, September 20-24, 1999, Hokkaido, Japan, pp775-776.

Domestic Conferences

1. **井出吉紀、斉藤雄二、檜座秀一、山田明、小長井誠**
「ホットワイヤーセル法及び光 CVD 法による微結晶 Si 薄膜の作製と評価」
第 64 回応用物理学会学術講演会(2003 年秋季),福岡大学(福岡),2a-YE-1/II

2. **井出吉紀、斉藤雄二、山田明、小長井誠**
「ホットワイヤーセル法による微結晶 Si 薄膜太陽電池」
第 50 回応用物理学会学術講演会(2003 年春季),神奈川大学
(神奈川),30p-M-7/II

3. **井出吉紀、斉藤雄二、山田明、小長井誠**
「ホットワイヤーセル法による微結晶 Si 薄膜太陽電池」
第 10 回「高効率太陽電池および太陽光発電システム」ワークショップ
(2002), **岐阜**

4. **井出吉紀、斉藤雄二、山田明、小長井誠**
「ホットワイヤーセル法による微結晶 Si 薄膜の高速製膜」
第 63 回応用物理学会学術講演会(2002 年秋季), 新潟大学(新潟),
25a-ZM-4/II

5. 井出吉紀、趙　穎、宮島晋介、斉藤雄二、山田明、小長井誠
「光 CVD 法によるμc-Si:H 薄膜太陽電池の作製」
第 49 回応用物理学会学術講演会(2002 年春季),東海大学(神奈川),29a-X-9

6. 小長井誠、井出吉紀、浅草剛一、大木和樹、宮島晋介、山田明
「ホットワイヤーセル法による Si 系薄膜太陽電池」
第 9 回「高効率太陽電池および太陽光発電システム」ワークショップ
(2001), 東京

7. 井出吉紀、脇田雄一、宮島晋介、趙　穎、山田明、小長井誠
「ホットワイヤーセル法による p 形微結晶 Si 薄膜を用いた a-Si 太陽電池」
第 62 回応用物理学会学術講演会(2001 年秋季),愛知工業大学(愛知),
12p-ZA-11

8. 井出吉紀、浅草剛一、脇田雄一、山田明、小長井誠
「ホットワイヤーセル法によるシリコン系薄膜太陽電池の作製」
第 47 回応用物理学会学術講演会(2000 年春季),青山学院大学(東京),
31a-ZF-8